TABLE OF CONTENTS

Western Canada Sedimentary Basin

Interior Basins

Coalbed Gas

THE POTENTIAL FOR GEOLOGICAL STORAGE OF CARBON DIOXIDE IN NORTHEASTERN BRITISH COLUMBIA

Stefan Bachu[1]

ABSTRACT

Carbon dioxide capture and storage in geological media is a technologically feasible mitigation measure for the reduction of emissions of anthropogenic CO_2 from large stationary sources. Carbon dioxide can be sequestered underground in oil and gas reservoirs, deep saline aquifers, uneconomic coal beds, and salt caverns. The sedimentary succession in northeastern British Columbia has significant potential for CO_2 storage in gas reservoirs and deep saline aquifers because this region is located in a tectonically stable area and has significant, large gas reservoirs and deep saline aquifers that are confined by thick, regional-scale shaly aquitards. In addition, there is significant infrastructure in place, there are several large CO_2 sources in the area, including high-purity sources (gas plants), and there is operational and regulatory experience with acid-gas disposal in both depleted hydrocarbon reservoirs and deep saline aquifers. The CO_2 storage capacity in gas reservoirs is very large (more than 1900 Mt CO_2), of which approximately 1350 Mt CO_2 is in the largest 80 reservoirs. This capacity alone is likely sufficient to cover BC's needs for this century. The CO_2 storage capacity in oil reservoirs is practically negligible at 5 Mt CO_2, and the only reason that this capacity would ever be realized is that additional oil may be produced in CO_2-EOR operations. Storage of CO_2 in coal beds does not have potential unless used in conjunction with coal gas recovery (technology that has yet to be proven), and even then it is questionable given the depth of the coal beds. Besides gas reservoirs, northeastern BC has significant potential for CO_2 storage in deep saline aquifers. Carbon dioxide can be injected into almost all of the deep saline aquifers in the sedimentary succession. The only aquifers that are not suitable for CO_2 storage are the shallower Upper Cretaceous Dunvegan and Cardium Formations, which crop out at river valleys as a result of Tertiary to Recent erosion. Cambrian to Lower Cretaceous aquifers are well confined by intervening and overlying shales. Geographically, Carboniferous to Triassic aquifers are the best targets for CO_2 storage in the southern part of northeastern BC, while Devonian aquifers should be used for CO_2 storage in the northern part. Although there is great capacity and potential infrastructure for CO_2 storage in gas reservoirs, they will become available for CO_2 storage only after depletion, which, at current production rates, will occur in the next few decades. Until these gas reservoirs become available, deep saline aquifers can be safely used for CO_2 storage in northeastern BC.

KEYWORDS: Carbon dioxide, CO_2, CO_2 sequestration, CO_2 storage, anthropogenic CO_2, oil and gas pools, hydrocarbon reservoirs, enhanced oil recovery, storage capacity, deep saline aquifers, coal beds, northeastern British Columbia, Devonian, Carboniferous, Jurassic, Jean Marie, Permian, Montney, Halfway, Lower Mannville, Upper Mannville, Paddy, acid-gas injection sites

INTRODUCTION

Human activity since the industrial revolution has increased atmospheric concentrations of greenhouse gases such as carbon dioxide (CO_2) and methane (CH_4). For example, atmospheric concentrations of CO_2 have risen from pre-industrial levels of 280 ppm to the current level of more than 370 ppm, primarily as a consequence of fossil-fuel combustion for energy production. Circumstantial evidence suggests that the increase in greenhouse gas concentrations in the atmosphere leads to climate warming and weather changes, a fact that by now is generally accepted in the scientific community and by policy makers. Because of its relative abundance compared with the other greenhouse gases, CO_2 is responsible for about 64% of the enhanced greenhouse effect. To address the effects of global climate change, scientific and policy efforts are focused in three major directions: 1) understanding better the science of climate change, 2) adaptation to predicted climate changes, and 3) mitigating the effects of climate change. As a result, reducing atmospheric emissions of anthropogenic CO_2 and methane is one of the main mitigating measures considered by the society, with most efforts being focused on reducing CO_2 emissions.

The 1992 United Nations Framework Convention on Climate Change (UNFCCC) states as an objective the "stabilization of greenhouse gas concentrations in the atmosphere at a level that would prevent dangerous anthropogenic interference with the climate system". The Kyoto Protocol, signed in 1997 and ratified in February 2005, set targets and timetables for emission reductions for Annex I

[1]Alberta Geological Survey, Alberta Energy and Utilities Board

Parties (developed and transition economies) at a level on average 5% below 1990 levels by 2008–2012 (the "Kyoto period"). Canada has committed to reduce CO_2 emissions to 6% below 1990 levels; however, economic development, population increase, and lack of a clear policy have resulted so far in an increase of approximately 24% over 1990 greenhouse gas emissions. Thus, in order to meet Canada's Kyoto commitments, the federal and provincial governments need to implement a very aggressive policy for reducing atmospheric emissions of anthropogenic greenhouse gases.

Reducing anthropogenic CO_2 emissions into the atmosphere involves three approaches: 1) lowering the energy intensity of the economy (i.e., increasing the conservation and efficiency of primary energy conversion and end use)[1]; 2) lowering the carbon intensity of the energy system by substituting lower-carbon or carbon-free energy sources for the current sources[2]; and 3) artificially increasing the capacity and capture rate of CO_2 sinks. Short of revolutionary, large-scale new technological advances and major expenditures, the energy intensity of the economy will continue to decrease at a lower rate than the rate of GDP increase, and mitigation strategies will have a limited impact (Turkenburg, 1997). Similarly, fossil fuels, which currently provide more than 80% of the world's energy, will likely remain a major component of the world's energy supply for at least the first half of this century (IEA, 2004) because of their inherent advantages, such as availability, competitive cost, ease of transport and storage, and large resources. Other forms of energy production are either insufficient or not acceptable to the public. Thus, the carbon intensity of the energy system is not likely to decrease significantly in the medium term. On the other hand, increasing carbon sinks and their capture rate is the single major means of reducing net carbon emissions into the atmosphere in the short to medium term, although it is recognized that no single category of mitigation measures is sufficient (Turkenburg, 1997; IEA, 2004).

Large, natural CO_2 sinks are terrestrial ecosystems (soils and vegetation) and oceans, with retention times of the order of tens and thousands of years, respectively. Terrestrial ecosystems and the ocean surface represent diffuse natural carbon sinks that capture CO_2 from the atmosphere after release from various sources. The capacity, but not the capture rate, of terrestrial ecosystems can be increased by changing forestry and agricultural practices[3]. On the other hand, CO_2 capture and storage (CCS) in geological media presents the opportunity to significantly reduce atmospheric CO_2 emissions from large, stationary sources such as thermal power plants (IEA, 2004; IPCC, 2005) by capturing the CO_2 prior to its release into the atmosphere and injecting it deep into geological formations that have a retention time of centuries to millions of years.

Geological storage of CO_2 is achieved through a combination of physical and chemical trapping mechanisms (IPCC, 2005). Physical trapping occurs when CO_2 is immobilized in free phase (static trapping and residual-gas trapping) or migrates in the subsurface with extremely low velocities such that it would take time on a geological scale to reach the surface (hydrodynamic trapping), by which time usually it is trapped by other mechanisms. Chemical trapping occurs when CO_2 dissolves in subsurface fluids (solubility and ionic trapping) and either undergoes chemical reactions (geochemical trapping) or is adsorbed onto the rock surface (adsorption trapping). In some cases, more than one trapping mechanism is active, although they usually act on different time scales.

The physico-chemical mechanisms for CO_2 storage in underground geological media translate into the following means of trapping:

- Volumetric, whereby pure-phase, undissolved CO_2 is trapped in a rock volume and cannot rise to the surface due to physical and/or hydrodynamic barriers. The storage volume can be provided by
  - large man-made cavities, such as caverns and abandoned mines (cavern trapping); or
  - the pore space present in geological media. If trapped in the pore space, CO_2 can be at saturations less or greater than the irreducible saturation; if the former, the interfacial tension keeps the residual gas in place; if the latter, pure CO_2 can be trapped

    - in static accumulations in stratigraphic and structural traps in depleted oil and gas reservoirs and in deep saline aquifers, or

    - as a migrating plume in large-scale flow systems in deep aquifers.
- Dissolution, whereby CO_2 is dissolved into fluids that saturate the pore space in geological media, such as formation water and reservoir oil.
- Adsorption onto organic material in coal and shales rich in organic content.
- Chemical reaction to form a mineral precipitate.

---

[1]The Government of British Columbia adopted in December 2004 a 40-point action plan to address climate change that promotes Sustainable Energy Production and Efficient Use, and Efficient Infrastructure, namely: energy conservation, energy efficiency; alternative energy (hydroelectric, wind and landfill gas); development of hydrogen and fuel cell technology; and use of alternative and hybrid fuels in transportation (Weather, Climate and the Future: B.C.'s Plan @ http://wlapwww.gov.bc.ca/air/climate/).

[2] Ibid.

[3] Similarly, in its climate change action plan (Weather, Climate and the Future: B.C.'s Plan @ http://wlapwww.gov.bc.ca/air/climate/), the Government of British Columbia has adopted measures for Sustainable Forest and Carbon Sink Management.

These means of CO_2 storage can occur in the following geological media (IPCC, 2005):

- oil and gas reservoirs;
- deep saline aquifers, saturated with brackish water or brine;
- coal seams (sorption is the only potentially practical technique in coal seams and is not a significant storage mechanism in the other classes of geological media);
- man-made underground cavities (i.e., salt caverns, in CO_2).

Any geological site for CO_2 storage must possess the following characteristics:

- capacity—for accepting the volumes of CO_2 that need to be stored;
- injectivity—to allow introduction of CO_2 into the subsurface at the desired rates; and
- confining ability—to retain the CO_2 for the desired period of time (i.e., avoidance of leakage).

These characteristics are largely met by geological media in sedimentary basins, where oil and gas reservoirs, coal beds, and salt beds and domes are found. Igneous and metamorphic rocks are generally not suitable for CO_2 storage because they lack the permeability and porosity needed for CO_2 injection and storage and/or because of their lack of confining properties due to their fractured nature. Volcanic areas and orogenic belts (mountains) are also unsuitable for CO_2 storage mainly because they lack capacity and are unsafe.

BC's landmass includes nine sedimentary basins and two geological troughs (Figure 1) that may have, to various degrees, potential for geological CO_2 storage. A previous analysis (Bachu, 2005) has identified the portion of the Western Canada Sedimentary Basin (WCSB) in northeastern BC (Figure 1) as the sedimentary basin in BC most suitable for geological CO_2 storage and likely with the largest capacity. Most of the "large" stationary CO_2 sources have emissions less than 500 kt CO_2/yr, and very few sources emit more than 1 Mt CO_2/yr (Figure 1). The CO_2 sources are distributed according to the major industrial and population centers along the Pacific coast, in the BC interior, and in northeastern BC, where gas plants produce a stream of high-purity CO_2 and where a pipeline system is more developed locally.

The portion of the WCSB in northeastern BC is the best suited and most immediately accessible basin for geological CO_2 storage in BC . It meets all the general suitability criteria for geological CO_2 storage (Bachu and Stewart, 2002; Bachu, 2003). It

- is located in a tectonically stable region;
- has regional-scale groundwater flow systems confined by thick aquitards;
- has significant oil and gas reservoirs;
- has coal beds;
- has significant infrastructure in place;

and:

- there are CO_2 sources in the area, including high-purity sources (gas plants); and
- there is experience with acid-gas injection operations.

Northeastern BC has significant CO_2 storage capacity in oil and gas reservoirs, in deep saline aquifers, and possibly in coal beds if the technology proves successful. The purpose of the work reported here is to evaluate the potential and capacity for geological CO_2 storage in northeastern BC.

CAPACITY FOR CO_2 STORAGE IN OIL AND GAS RESERVOIRS

Worldwide, the largest CO_2 storage capacity is likely in deep saline aquifers, while the smallest is in coal beds (IPCC, 2005), and this is probably true of northeastern BC. On the other hand, it is recognized that, generally, CO_2 storage in geological media will occur first in oil and gas reservoirs for the following reasons (IPCC, 2005): 1) their geology and trapping characteristics are better known as a result of hydrocarbon exploration and production, 2) there is already infrastructure in place (pipelines and wells), and 3) in the case of oil reservoirs that are suitable for CO_2-flood enhanced oil recovery (EOR), additional oil production will lower the cost of CO_2 storage, in some cases even realizing a profit, and will increase the stability and security of energy supplies. For this reason, this assessment starts with examining the CO_2 storage capacity in oil and gas reservoirs.

Methodology

The capacity for CO_2 storage in hydrocarbon reservoirs in a region is the sum of the capacities of all reservoirs in that region; capacity is calculated on the basis of reservoir properties, such as original oil or gas in place, recovery factor, temperature, pressure, rock volume and porosity, as well as in situ CO_2 characteristics, such as phase behaviour and density.

The assumption made in these calculations is that the volume previously occupied by the hydrocarbons becomes available for CO_2 storage. This assumption is generally valid for reservoirs that are not in contact with an aquifer or that are not flooded during secondary and tertiary oil recovery. In reservoirs that are in contact with an underlying aquifer, formation water invades the reservoir as the pressure declines because of production. However, CO_2 injection can

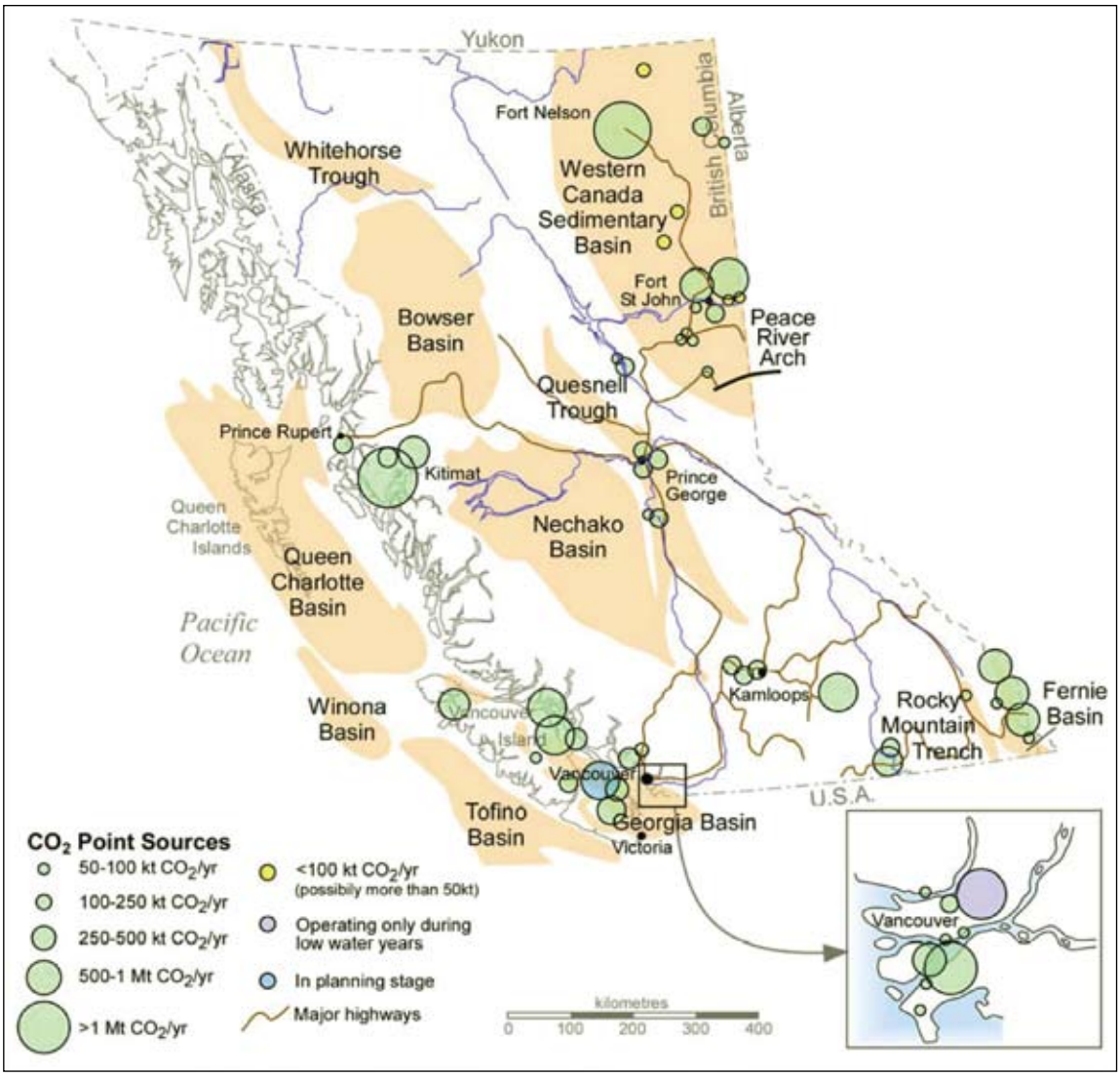

Figure 1. Location of sedimentary basins and major stationary CO_2 sources in British Columbia.

reverse the aquifer influx, thus making pore space available for CO_2. Not all the previously hydrocarbon-saturated pore space will become available for CO_2 because some residual water may be trapped in the pore space due to capillarity, viscous fingering, and gravity effects (Stevens *et al.*, 2001). Another important assumption is that CO_2 will be injected into depleted oil and gas reservoirs until the reservoir pressure is brought back to the original, or virgin, reservoir pressure.

The results thus obtained represent a conservative estimate of capacity because the pressure can generally be raised beyond the original reservoir pressure as long as it remains safely below the threshold rock-fracturing pressure. In this case, the CO_2 storage capacity would be higher due to CO_2 compression. However, the risk of raising the storage pressure beyond the original reservoir pressure requires a case-by-case reservoir analysis that is not practical for basin-scale evaluations.

Several capacity definitions are being introduced to clarify the meaning of and relationships between various types of estimates. The theoretical capacity assumes that all the pore space (volume) freed up by the production of all recoverable reserves will be replaced by CO_2 at in situ conditions. The effective capacity is the more realistic estimate obtained after water invasion, displacement, gravity, heterogeneity, and water-saturation effects have been taken into account. Practical capacity is the storage capacity after consideration of technological limitations, safety, CO_2 sources, reservoir distributions, and current infrastructure, regulatory, and economic factors. In the end, all the issues and factors relating to CO_2 capture, delivery, and storage contribute to a reduction in the real capacity for CO_2 storage in hydrocarbon reservoirs. However, none of these capacity estimates is final, in the sense that these values evolve in time, most likely increasing as new oil and gas discoveries take place or as better production technologies are developed.

Theoretical CO_2 Storage Capacity

Only non-associated and associated gas reservoirs are considered in CO_2 sequestration capacity calculations because solution gas is taken into account in oil reservoirs through the oil shrinkage factor. Since reserves databases indicate the volume of original gas in place (OGIP) at surface conditions, the mass-capacity for CO_2 storage in a reservoir at in situ conditions, MCO_2, is given by:

$$\mathbf{M_{CO2} = \rho_{CO2r} \cdot R_f \cdot (1 - F_{IG}) \cdot OGIP \cdot [(P_s \cdot Z_r \cdot T_r) / (P_r \cdot Z_s \cdot T_s)]} \quad (1)$$

In the above equation, ρCO_2 is CO_2 density, R_f is the recovery factor, F_{IG} is the fraction of injected gas, P, T, and Z denote pressure, temperature, and the compressibility factor, and the subscripts 'r' and 's' denote reservoir and surface conditions, respectively. The CO_2 density at reservoir conditions is calculated from equations of state (e.g., Span and Wagner, 1996).

The CO_2 storage capacity of single-drive oil reservoirs is calculated similarly to gas reservoirs on the basis of reservoir rock volume (area [A] times thickness [h]), porosity (φ), and oil saturation ($1 - S_w$), where S_w is the water saturation. For reservoirs flooded with or invaded by water, the volume available for CO_2 storage is reduced by the volume of injected and/or invading water (V_{iw}). If water is produced with oil, then the volume available for CO_2 storage is augmented by the volume of produced water (V_{pw}). The same mass balance applies in the case of miscible flooding with solvent or gas. Thus:

$$\mathbf{M_{CO2} = \rho_{CO2res} \cdot [R_f \cdot A \cdot h \cdot \varphi \cdot (1 - S_w) - V_{iw} + V_{pw}]} \quad (2)$$

The volumes of injected and/or produced water, solvent, or gas can be calculated from production records. However, the pore volume invaded by water from underlying aquifers cannot be estimated without detailed monitoring of the oil-water interface and detailed knowledge of reservoir characteristics.

Effective CO_2 Storage Capacity

In the case of reservoirs underlain by aquifers, the reservoir fluid (oil and/or gas) was originally in hydrodynamic equilibrium with the aquifer water. As hydrocarbons are produced and the pressure in the reservoir declines, a pressure differential is created that drives aquifer water up into the reservoir. The amount and rate of water influx is controlled by 1) reservoir permeability and heterogeneity; 2) water expansion in the aquifer; 3) pore volume contraction due to the increase in effective stress caused by the pressure drop in the reservoir; 4) expansion of hydrocarbon accumulations linked to the common aquifer; and 5) artesian flow where the aquifer is recharged by surface water. As hydrocarbons are produced, some portions of the reservoir may be invaded by aquifer water, in addition to the initial water saturation. If CO_2 is then injected into the reservoir, the pore space invaded by water may not become available for CO_2 storage, resulting in a net reduction of reservoir capacity. The reduced storage volume may eventually become available if the reservoir pressure caused by CO_2 injection is allowed to increase beyond the original reservoir pressure, which may not always be allowed or possible. Furthermore, the hysteresis effect caused by various mechanisms may also prevent complete withdrawal of invaded water, leading to a permanent loss of storage space.

Analysis of the production history of close to 300 oil and gas pools in western Canada led to the establishment of a set of criteria for determining if an oil or gas reservoir has strong or weak aquifer support (Bachu and Shaw, 2003, 2005; Bachu *et al.*, 2004) on the basis of pressure history, water production, and cumulative water-gas ratio (WGR) or water-oil ratio (WOR). For oil reservoirs, the gas-oil ratio (GOR) was also included in the analysis because, typically, an oil pool with strong aquifer support tends to have a slow pressure decline and flat GOR profile close to solution GOR, and vice-versa. In addition, the production decline versus reservoir pressure was analyzed for these pools. For gas pools, P/Z plots were used to identify the presence of aquifer support or lack thereof. The criteria and threshold values for identification of the strength of underlying aquifers are presented in Table 1.

The effect of the underlying aquifers was assessed using the Petroleum Expert's MBALTM (Material BALance) software for a limited number of oil and gas pools distributed across the Western Canada Sedimentary Basin that were considered to be reasonably representative for the range of conditions found in the basin (Bachu and Shaw, 2003; Bachu *et al.*, 2004). Injection of CO_2 was assumed to start immediately after reservoir depletion and to continue until the pool pressure exceeded the original pressure. Although the material balance reservoir model simulated by MBALTM is a tank model and does not account for reservoir geometry, drainage area, and well locations, it is a very useful tool in matching the production history by determining the presence, type, and size of an aquifer and predicting reservoir pressure and performance for given production and/or injection scenarios.

Table 1 shows the reduction in CO_2 storage capacity for reservoirs with strong aquifer support. The storage capacity of reservoirs with weak or no aquifer support is not affected by the presence of the underlying aquifer. However, a very small effect needs to be considered in light of the fact that water is a wetting phase while oil and gas are non-wetting, hence it should be expected that some irreducible water would be left behind in the pore space by the receding aquifer. To account for this effect, it is assumed that the theoretical CO_2 storage capacity in oil and gas reservoirs with weak aquifer support is reduced by approximately 3%.

Notwithstanding the effect of an underlying aquifer, three factors in particular control the effectiveness of the

TABLE 1. CRITERIA FOR ESTABLISHING THE STRENGTH AND EFFECT OF UNDERLYING AQUIFERS ON THE CO_2 STORAGE CAPACITY IN DEPLETED OIL AND GAS RESERVOIRS IN THE WESTERN CANADA SEDIMENTARY BASIN AND THE CORRESPONDING COEFFICIENT OF REDUCTION IN CO_2 STORAGE CAPACITY.

Reservoir Type	WOR (m^3/m^3) or WGR (bbl/MMcf)	GOR (m^3/m^3)	Aquifer Strength	Capacity Reduction Coefficient
Oil	≥0.25		Strong	0.50
	≥0.15 and <0.25	<1000		
	≥0.15 and <0.25	≥1000	Weak	0.97
	<0.15			
Gas	≥5.6		Strong	0.70
	<5.6		Weak	0.97

CO_2 storage process: CO_2 mobility with respect to oil and water; the density contrast between CO_2 and reservoir oil and water, which leads to gravity segregation; and reservoir heterogeneity. Because of the very low CO_2 viscosity in liquid or supercritical phase, on the order of 10-5 Pa·s, the CO_2/oil and CO_2/water mobility ratios at reservoir conditions are on the order of 20 and higher. As a result, viscous fingering will develop and the CO_2 will tend to bypass the oil/water system in place in the reservoir, leading to a very unfavourable displacement process (Bondor, 1992).

Depending on reservoir temperature and pressure, the density of supercritical or liquid CO_2 may range between approximately 200 and 800 kg/m^3. The density difference (buoyancy) between the lighter CO_2 and the reservoir oil and water leads to gravity override at the top of the reservoir, particularly if the reservoir is relatively homogeneous and has high permeability (Bondor, 1992; Stephenson *et al.*, 1993; Doughty and Preuss, 2004). This negatively affects the CO_2 storage and, in the case of EOR, the oil recovery.

If the reservoir is heterogeneous, the injected CO_2 will flow along the path of less resistance, namely through regions of high permeability, bypassing regions of lesser permeability. This has a negative effect for oil recovery because whole regions of the reservoir may be left unswept by CO_2 before it breaks at the production well, thereby reducing the economic benefit. On the other hand, reservoir heterogeneity may have a positive effect because it may counteract the buoyancy effect by slowing down the rise of CO_2 to the top of the reservoir and forcing it to spread laterally, resulting in better vertical sweep efficiency (Doughty and Preuss, 2004).

The presence of water in the reservoir also has the effect of reducing the CO_2 storage capacity, as discussed previously. Water may be present because of initial water saturation, because of water invasion as the reservoir is depleted, or because it was introduced during secondary and/or tertiary recovery. As a result of capillary forces, irreducible water saturation (Swirr) will remain in the reservoir even if the water is 'pushed back' by the injected CO_2.

All the processes and reservoir characteristics that reduce the actual volume available for CO_2 storage can be expressed by capacity coefficients ($C < 1$) in the form (Doughty and Preuss, 2004):

$$\mathbf{M_{CO2eff} = C_m \cdot C_b \cdot C_h \cdot C_w \cdot C_a \cdot M_{CO2res}} \quad \textbf{(3)}$$

where MCO_{2eff} is the effective reservoir capacity for CO_2 storage, and the subscripts m, b, h, w, and a stand for mobility, buoyancy, heterogeneity, water saturation, and aquifer strength, respectively, and refer to the phenomena discussed previously. These capacity coefficients likely vary over a wide range, depending on reservoir characteristics, and this explains the wide range of incremental oil recovery (7 to 23% of original oil in place) and CO_2 utilization (0.7 to 4.7 m^3 CO_2 / m^3 recovered oil at reservoir conditions) observed for 25 CO_2-flood EOR operations in Texas (Holt *et al.*, 1995). Unfortunately, there are very few studies of and methodologies for estimating, mostly on the basis of numerical simulations, the values of these capacity coefficients, and generally there are no data nor studies for the specific case of CO_2 storage in depleted hydrocarbon reservoirs. The first four capacity coefficients can be captured in a single 'effective' coefficient:

$$\mathbf{C_{eff} = C_m \cdot C_b \cdot C_h \cdot C_w} \quad \textbf{(4)}$$

which can be estimated on the basis of experience with CO_2-flood EOR. A review of capacity coefficients for CO_2 storage in aquifers suggests that $C_{eff} < 0.3$. Conditions are more favourable in the case of oil reservoirs (for example, the buoyancy contrast is much reduced), and a value of $C_{eff} = 0.5$ was considered in this study. For gas reservoirs, $C_m \approx 1$ because fingering effects are very small to negligible. Because CO_2 density is greater than that of methane at reservoir conditions, the CO_2 injected in gas reservoirs will fill the reservoir from its bottom. Thus, it can be assumed that $C_b \approx 1$ as well. The effect of initial water saturation was already implicit in the estimates of theoretical ultimate CO_2 storage capacity, such that $C_w \approx 1$ too. Although reservoir heterogeneity may reduce the CO_2 storage capacity by leaving pockets of original gas in place, C_h is probably

high, approaching values close to unity. Thus, the reduction in CO_2 storage capacity for gas reservoirs is much less by comparison with oil reservoirs and a value of $C_{eff} = 0.9$ was used in this study.

CO_2 Storage Capacity in Enhanced Oil Recovery

Carbon dioxide can be used in tertiary enhanced oil recovery in miscible floods, if high purity CO_2 is available. To date, except for the Weyburn oil field in Saskatchewan, operated by Encana, and the Joffre Viking A oil reservoir in Alberta, currently operated by Penn West, no CO_2-EOR operations were implemented in western Canada because of the high cost of CO_2 capture and lack of pipeline infrastructure for CO_2 delivery at the well head. However, this situation may change rapidly if incentives for geological CO_2 storage are introduced and a market for carbon credits is created. For example, in 2004 the Alberta Government introduced a Royalty Credit Program to encourage the development of a CO_2-EOR industry in the province, and as a result, four pilot operations started in Alberta in 2005. In a future carbon-constrained environment and with sustained high oil prices, CO_2 flooding will probably become the preferred EOR option, leading to both geological CO_2 storage and additional oil recovery. In fact, it is most likely that this option will be implemented before any other. Thus, identification of reservoirs suitable for CO_2 flooding and estimation of their CO_2 storage capacity becomes essential.

Based on the experience gained in the United States where CO_2-EOR has been practiced for more than 30 years at close to 70 oil fields in the Permian Basin of west Texas, a series of technical criteria were developed for assessing the suitability of oil reservoirs for CO_2-EOR, reviewed and summarized in several publications (Taber *et al.*, 1997; Kovscek, 2002; Shaw and Bachu, 2002). In assessing the suitability of oil reservoirs in northeastern BC for CO_2-EOR, the following criteria were used (Shaw and Bachu, 2002):

- Oil gravity between 27 and 48 ºAPI
- Initial reservoir pressure greater than 7580 kPa
- Reservoir temperature less than 121 ºC (250 ºF)
- Ratio of initial pressure to minimum miscibility pressure (MMP) greater than 0.95

An additional, quasi-economic criterion was also used in the screening, namely that the reservoir be sufficiently large to warrant the cost of implementing CO_2-EOR. Reservoir size was expressed either by original oil in place (OOIP) of at least 1 Mmbl (159,000 m^3), or by area, with the requirement that it has to be at least one section in size (256 ha) to allow for a 5-spot pattern with current well spacing regulations.

The minimum miscibility pressure (MMP) was calculated with the relation (Mungan, 1981):

$$MMP = -329.558 + (7.727 \times MW \times 1.005T) - (4.377 \times MW) \quad (5)$$

where T is temperature (ºF) and MW is the molecular weight of the oil C5+ components. In the absence of information in databases about oil composition, the following relation was used to estimate the molecular weight of the C5+ components as a function of oil gravity, G, expressed in ºAPI (Lasater, 1958):

$$MW = \left(\frac{7864.9}{G}\right)^{1/1.0386} \quad (6)$$

Prediction of reservoir performance and incremental oil recovery on the basis of information contained in reserves databases was performed using an analytical model developed for this purpose (Shaw and Bachu, 2002). The CO_2 storage capacity in EOR operations at CO_2 breakthrough is a direct result of that model for predicting reservoir performance. Considering that, on average, 40% of the injected CO_2 is recovered at the surface after breakthrough (Hadlow, 1992) and assuming that it will be re-injected back into the reservoir, the CO_2 storage capacity for any fraction, Fi, of hydrocarbon pore volume (HCPV) of injected CO_2 was calculated using the following relations:

- At breakthrough (BT),

$$M_{CO2} = \rho_{CO2res} \cdot RF_{BT} \cdot OOIP/Sh \quad (7)$$

- At any HCPV injection,

$$M_{CO2} = \rho_{CO2res} \cdot [RF_{BT} + 0.6 \times (RF_{\%HCPV} - RF_{BT})] \cdot OOIP/Sh \quad (8)$$

where RF_{BT} and $RF_{\%HCPV}$ are, respectively, the recovery factor at breakthrough and at the assumed percentage of hydrocarbon pore volume (HCPV) of injected CO_2; OOIP is the volume of the original oil in place; Sh is the oil shrinkage factor (the inverse of the formation volume factor B0); and ρCO_{2res} is CO_2 density calculated at reservoir temperature and pressure conditions (Span and Wagner, 1996).

Practical CO_2 Storage Capacity

The theoretical CO_2 storage capacity represents the mass of CO_2 that can be stored in hydrocarbon reservoirs assuming that the volume occupied previously by the produced oil or gas will be occupied in its entirety by the injected CO_2. The effective CO_2 storage capacity represents the mass of CO_2 that can be stored in hydrocarbon reservoirs after taking into account intrinsic reservoir characteristics and flow processes, such as heterogeneity, aquifer support, sweep efficiency, gravity override, and CO_2 mobility. However, there are also extrinsic criteria, discussed in the following, which need consideration when implementing CO_2 storage in oil and gas reservoirs on a large scale and that further reduce the CO_2 storage capacity in oil and gas reservoirs to practical levels.

The storage capacity of oil reservoirs undergoing water flooding is significantly reduced, making it very difficult to assess their CO_2 storage capacity in the absence of detailed, specific numerical simulations of reservoir performance. It is very unlikely that these oil pools, and generally commingled pools, will be used for CO_2 storage, at least in the near future.

The low capacity of shallow reservoirs, where CO_2 would be in the gas phase, makes them uneconomic because of storage inefficiency (Winter and Bergman, 1993). On the other hand, CO_2 storage in very deep reservoirs could also become highly uneconomic because of the high cost of well drilling and of CO_2 compression and the low 'net' CO_2 storage (CO_2 sequestered minus CO_2 produced during compression). Thus, the pressure window of 9 to 34.5 MPa is considered economic for CO_2 storage in depleted hydrocarbon reservoirs (Winter and Bergman, 1993), which roughly translates to a depth interval of 900 to 3500 m.

In terms of CO_2 storage capacity, most reservoirs are relatively small in volume and have a low capacity for CO_2 storage, rendering them uneconomic. On the other hand, associated oil and gas reservoirs (oil reservoirs with a gas cap) have a CO_2 storage capacity that is equal to the sum of the individual capacities of each reservoir. Considering the size of the major stationary CO_2 sources, it is most likely that only reservoirs with large CO_2 storage capacity will be considered in the short and medium term. Building the infrastructure for CO_2 capture, transportation, and injection is less costly if the size of the sink is large enough and if its lifespan is long enough to justify the investment and reduce the cost per ton of sequestered CO_2. Thus, only reservoirs with individual CO_2 storage capacity greater than 1 Mt CO_2/year were selected at the end of the capacity assessment process. More detailed analysis, based on economic criteria, should be applied for the selection of top oil and gas reservoirs for CO_2 storage, but this is beyond the scope and resources of this study.

CAPACITY FOR CO_2 STORAGE IN HYDROCARBON RESERVOIRS IN NORTHEASTERN BRITISH COLUMBIA

The methodology described previously was applied to the 2004 BC oil and gas reserves databases to estimate the CO_2 storage capacity in oil and gas reservoirs and identify the pools with sufficiently large capacity to warrant further examination. The process consisted of three steps:

- checking for the existence of critical data needed in calculations,
- calculating the CO_2 storage capacity on a reservoir by reservoir basis, and
- identifying the oil pools with an associated gas cap.

Data Analysis

The BC oil reserves database contains 474 entries differentiated on the basis of field, pool, sequence, and project unit. However, only the first three categories identify a physically distinct oil pool, the last one indicating only an administrative unit based on production type. The number of actual oil pools is 414, of which only 380 have all the data necessary to perform the calculations for determination of CO_2 storage capacity. A breakdown of these pools by production type and data existence is given in Table 2. All oil pools in northeastern BC contain light-medium oil (°API > 25).

Of the 34 oil reservoirs that lack critical data, 18 lack area (of these 8 lack thickness, 5 lack water saturation, 5 lack porosity, 2 lack the shrinkage factor, and 2 lack oil density), and 16 lack just the shrinkage factor. The list of oil reservoirs lacking critical data for calculating the CO_2 storage capacity is given in Appendix A. The 34 oil pools that are lacking critical data are generally quite small (16 have OOIP less than 1 Mmbl, 12 have OOIP between 1 and 2 Mmbl, 4 have OOIP between 4 and 7 Mmbl) and very likely have negligible CO_2 storage capacity, considering also the low recovery factor of oil reservoirs. Only 2 pools, Eagle Belloy-Kiskatinaw and Eagle West Belloy, have sufficient OOIP (approximately 54 and 149 Mmbl, respectively) to be worth considering for potential CO_2 storage calculations, and the missing data for these pools should be retrieved in the future.

There are 1832 gas pools in the 2004 reserves database, differentiated by field, pool, and sequence, but only 1743 of them have the data needed for calculation of CO_2 storage capacity, as shown in Table 3. The list of gas reservoirs lacking critical data for calculating the CO_2 storage capacity is given in Appendix B. It is worth noting that all the gas reservoirs classified as "associated" are lacking fundamental data such as original gas in place (OGIP), pressure, and temperature. The two non-associated gas reservoirs that are missing depth could not be located, but they are very small with likely corresponding negligible CO_2 storage capacity.

Table 4 shows the range of variability in the data needed for calculating the CO_2 storage capacity for the 380 oil reservoirs and 1732 gas reservoirs in northeastern BC that have the whole suite of required data. It is worth noting that 97 of the gas reservoirs have a recovery factor greater than unity, which means that these reservoirs have produced more gas than they were originally estimated to contain. Also, 49 gas reservoirs have a compressibility factor (Z) greater than unity, which is an artifact due to the way Z is calculated for reservoirs that contain gas mixtures with a significant fraction of heavier gases.

Only 118 oil reservoirs are suitable for CO_2-EOR according to the criteria presented previously. These 118 reservoirs were selected through a process of successive

screening in the order presented here; if a reservoir did not meet a particular criterion, it was eliminated without checking it against the remaining criteria. Of the 262 rejected oil reservoirs, 18 are either too heavy (API < 27º) or too light (API > 48º), 13 have inadequate pressure (< 7580 kPa), 38 have initial pressure less than the minimum miscibility pressure, and 136 are too small (OOIP < 1 Mmbl or 159,000 m^3) for consideration. The list of oil pools that are suitable for CO_2-EOR is given in Appendix C.

Where oil and gas occur in the same pool, data analysis by field, pool, and sequence codes (or names) revealed 220 pairs of oil-gas pools among the initial 414 oil pools and 1832 gas pools. However, both the oil and corresponding gas reservoir are lacking critical data in the case of 7 pairs; in another 79 cases the oil reservoir has data, but the corresponding gas reservoir does not (the gas pools are among the associated gas pools with no data— see Table 3); and in another 10 cases the oil reservoir is lacking critical data, while the gas reservoir has them. Thus, in these 96 cases the combined CO_2 storage capacity in both the oil and corresponding gas reservoir could not be evaluated, leaving only 124 such pairs for which the calculations could be performed.

CO_2 Storage Capacity

The theoretical CO_2 storage capacity at depletion was calculated according to relation (1) for all the 1743 gas reservoirs with data and according to relation (2) for all the 380 oil reservoirs in single drive with data. The effective storage capacity was then calculated for all of them according to relation (3) on the basis of aquifer support as determined according to the criteria presented in Table 1. Of the 49 water-flooded oil reservoirs, only 29 have storage capacity left, and this is negligible for a total of approximately 1 Mt CO_2.

The additional CO_2 storage capacity in CO_2-EOR was calculated for the 118 oil reservoirs that are suitable according to the methodology presented previously for 50% HCPV (hydrocarbon pore volume) of injected CO_2. Generally the additional storage capacity is not large, varying between 13.5 and 800 kt CO_2, except for 2 reservoirs, Buick Creek Lower Halfway and Stoddart West Belloy, whose additional CO_2 storage capacity is approximately 1.5 and 1.8 Mt CO_2, respectively. The cumulative additional CO_2 storage capacity in these 118 oil reservoirs is approximately 16.2 Mt CO_2. The incremental oil recovered through CO_2-EOR at these reservoirs varies between approximately 12,000 and 515,000 m^3, except again for the Buick Creek Lower Halfway and Stoddart West Belloy reservoirs, whose estimated incremental oil production would be approximately 1,050,000 and 1,345,000 m^3 respectively (6.6 Mmbl and 8.46 Mmbl). The total incremental oil recovery from these 118 oil pools is estimated to be approximately 12,192,000 m^3 (76.68 Mmbl). Of course, these figures are only estimates, obtained with the methodology presented previously and on the basis of the data currently in the BC reserves database. However, they show the potential for CO_2-EOR in northeastern BC and identify the oil reservoirs with the largest potential. These reservoirs (e.g., Buick Creek Lower Halfway and Stoddart West Belloy) should be studied in more detail using specific reservoir simulations and production strategies to identify their real potential and economic value. The complete list of these reservoirs and their CO_2 storage capacity and incremental oil recovery is given in Appendix C.

For oil reservoirs, the total CO_2 storage capacity is the sum of the effective storage capacity at depletion and the additional storage capacity in CO_2-EOR if the oil reservoir is suitable for enhanced oil recovery. For the 124 pairs of oil and gas reservoirs in the same pool that both have data, the combined CO_2 storage capacity is the sum of the respective oil and gas capacities. The individual CO_2 storage capacity for the oil and gas pools in northeastern BC is listed in the CD associated with this report. The totals amount to 5.46 Mt CO_2 in 256 oil reservoirs, 2162.53 Mt CO_2 in 1619 gas reservoirs, and 151.37 Mt CO_2 in the 124 pairs of oil and gas reservoirs (1999 different pools in total). The 79 oil pools for which the corresponding gas pool lacks critical data all

TABLE 2. TYPE AND NUMBER OF OIL RESERVOIRS IN NORTHEASTERN BRITISH COLUMBIA AS PER BC 2004 RESERVES DATABASE, SHOWING ALSO THE AVAILABILITY OF CRITICAL DATA.

Recovery	Production Type	Number	Number of Oil Pools with Data
Primary (single drive)	Depletion	255	229
	Gas Cap Expansion	97	93
	Gas Injection	6	6
	Gravity	1	1
	Combination	6	5
Secondary	Waterflood	44	43
	Waterflood and Gas Cap Expansion	5	3
	Total	**414**	**380**

TABLE 3. TYPE AND NUMBER OF GAS RESERVOIRS IN NORTHEASTERN BRITISH COLUMBIA AS PER BC 2004 RESERVES DATABASE, SHOWING ALSO THE AVAILABILITY OF CRITICAL DATA.

Type of Gas Reservoir	Number	Number of Gas Pools with Data	Type of Missing Data
Non-associated	1618	1616	Depth
Gas Cap	127	127	-
Associated	87	87	OGIP, pressure, temperature
Total	**1832**	**1743**	

TABLE 4. RANGE OF CHARACTERISTICS OF OIL AND GAS POOLS IN NORTHEASTERN BRITISH COLUMBIA THAT HAVE THE WHOLE SUITE OF DATA NEEDED FOR CO_2 CAPACITY CALCULATIONS.

Reservoir Type	Parameter	Minimum	Maximum
Oil	OOIP (10^3 m^3)	1.6	82,090
	Recovery Factor	0.001	0.629
	Depth (m)	407	3088
	Area (ha)	2.4	9728
	Net Pay (m)	0.3	28.0
	Water Saturation	0.026	0.617
	Porosity	0.02	0.28
	Shrinkage Factor	0.494	0.961
	Initial Pressure (kPa)	3481	39,580
	Temperature (°C)	25	119
	Oil Density (kg/m^3)	699	926
	Oil Gravity (°API)		
Gas	OGIP (10^6 m^3)	3	101,000
	Recovery Factor	0.008	43.17
	Depth (m)	340	4897
	Initial Pressure (kPa)	1,452	64,430
	Temperature (°C)	13	175
	Compressibility (Z factor)	0.563	1.312
	CO_2 Content	0	0.3

have individual storage capacity of less than 0.5 Mt CO_2, hence likely are of little or no significance. Similarly, of the 10 gas pools for which the corresponding oil pool is missing data, only Eagle West Belloy A has capacity of 1.8 Mt CO_2; all the others have capacity less than 1 Mt CO_2. However, the corresponding oil pool for the Eagle West Belloy A gas pool is water-flooded with no CO_2 storage capacity, hence no error is introduced in the assessment and selection of oil and gas pools with large capacity.

The practical CO_2 storage capacity in oil and gas reservoirs in northeastern BC was determined by applying the screening criteria of size (> 1 Mt CO_2) and depth (between 900 and 3500 m) discussed previously. It should be mentioned here that 25 of the 1743 gas pools have no location given, but all except one have an effective CO_2 storage capacity less than 0.5 Mt CO_2, and only the Cutbank Falher B gas pool has a storage capacity of 830 kt CO_2. These are small gas pools that likely are not producing and are of no further interest anyway. Of the 1999 individual oil and gas pools in northeastern BC, only 353 pools meet the criteria of size and depth, for a total CO_2 storage capacity of 1935 Mt CO_2. The list of these reservoirs is given in Appendix D. Although these oil and gas pools represent 17.65% of the oil and gas pools in northeastern BC that were assessed, they possess 83.43% of the estimated CO_2 storage capacity in these oil and gas reservoirs.

Further analysis of these pools shows that the CO_2 storage capacity of approximately 5.3 Mt CO_2 in 31 oil reservoirs is negligible when compared to that in 352 gas reservoirs (approximately 1930 Mt CO_2). Note that 30 gas reservoirs have a corresponding oil reservoir. Of the 5.3 Mt CO_2 capacity in oil reservoirs, approximately 4.4 Mt CO_2 storage capacity will become available at reservoir depletion, and another 0.91 Mt CO_2 will be added through CO_2-EOR that will also produce close to four million cubic metres of additional oil (25 Mmbl) at 50% HCPV flooding. There is only one oil reservoir, Brassey Artex B, that has no corresponding gas reservoir and that, by itself, has a storage capacity of 1.26 Mt CO_2 at depletion (as it happens, this reservoir is not suitable for CO_2-EOR). All other 30 oil reservoirs in Appendix D have individual storage capacity of less than 1 Mt CO_2, but all are associated with a corresponding gas reservoir with large capacity. Five water-flooded oil reservoirs have no CO_2 storage capacity. Fourteen oil reservoirs that are not suitable for CO_2-EOR, excluding the Brassey Artex B, have a cumulative CO_2 storage capacity at depletion of 1.67 Mt CO_2. Eleven oil reservoirs are suitable for CO_2-EOR, with an estimated cumulative storage capacity of 2.39 Mt CO_2, of which 1.48 Mt CO_2 at depletion and 0.91 Mt CO_2 in CO_2-EOR.

The CO_2 storage capacity in gas reservoirs ranges between 1 Mt CO_2 (Laprise Creek Baldonnel/Upper Charlie Lake F) and 118 Mt CO_2 (Helmet Jean Marie A), with an average of 5.47 Mt CO_2. Figure 2 is a histogram of the CO_2 storage capacity in these gas pools. It is worth noting that 80 gas reservoirs have storage capacity greater than 5 Mt CO_2 each, but cumulatively they have a capacity of 1355 Mt CO_2. Although they represent 3.6% of the oil and gas reservoirs in northeastern BC, these reservoirs, whose location is shown in Figure 3 and that are listed in Table 5, should be the target of further studies because they constitute 58.42% of the CO_2 storage capacity in northeastern BC. Furthermore, 21 of these 80 gas reservoirs are in the Foothills (Figure 3), with likely difficult access and maybe great depth and structural complexity. The other 59 large gas reservoirs in the undisturbed part of the basin, with a total capacity of 1135 Mt CO_2 (approximately 49% of the total), are much more accessible and likely have infrastructure in place; these should form the object of further, detailed studies.

POTENTIAL FOR CO2 STORAGE IN DEEP SALINE AQUIFERS AND COAL BEDS

Deep saline aquifers and uneconomic coal beds are other geological media that can be used for storing CO_2. However, estimating their CO_2 storage capacity is much more difficult than it is for hydrocarbon reservoirs.

CHALLENGES IN ESTIMATING CO_2 STORAGE CAPACITY IN DEEP SALINE AQUIFERS AND UNECONOMIC COAL BEDS

The challenges in estimating the CO_2 storage capacity in deep saline aquifers and uneconomic coal beds fall into three categories:

- knowledge and scientific gaps;
- lack of a consistent and widely accepted methodology; and
- lack of data.

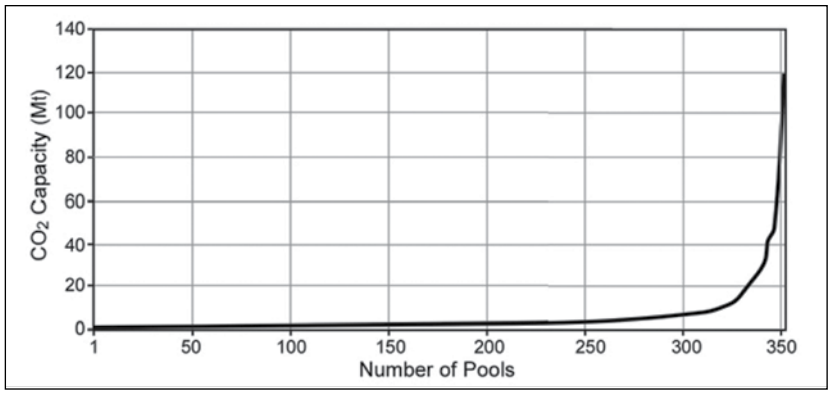

Figure 2. Histogram of the oil and gas pools in northeastern British Columbia with individual storage capacity greater than 1 Mt CO_2.

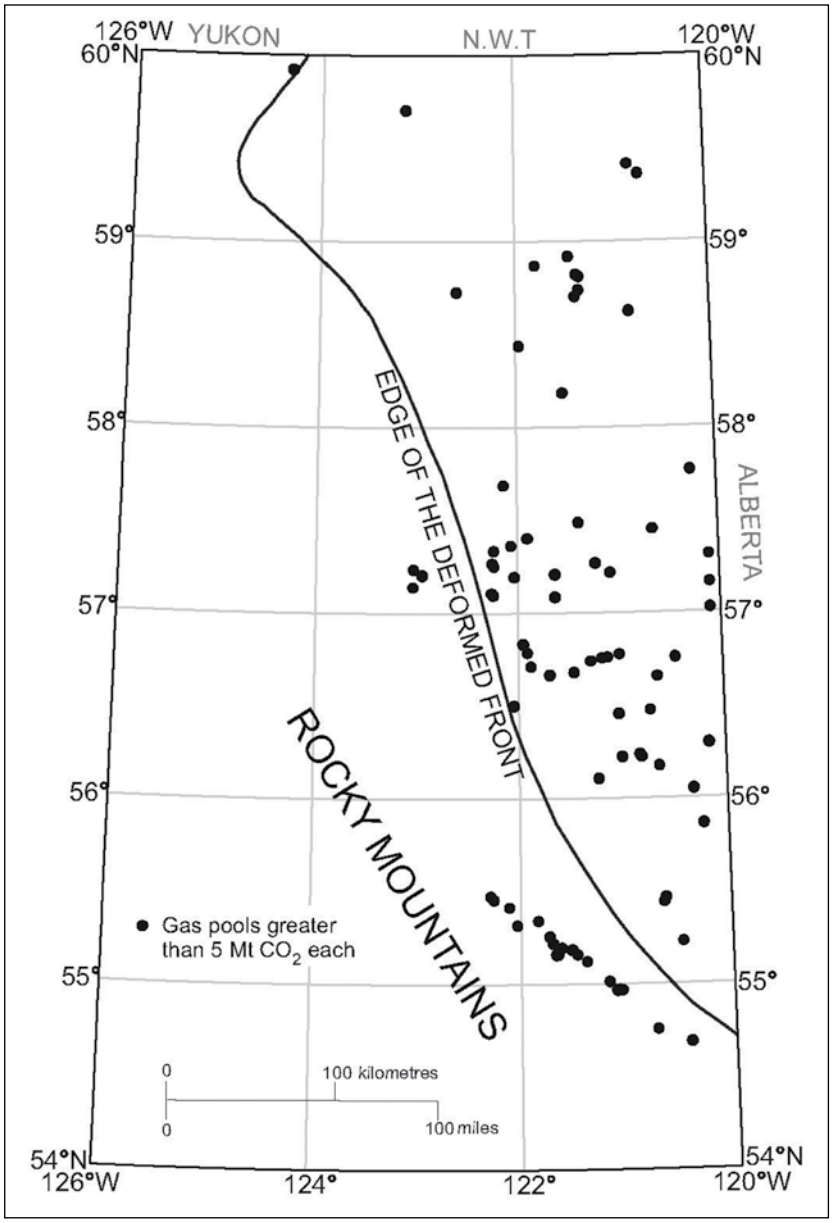

Figure 3. Location of the 80 gas pools in northeastern BC with the largest CO_2-storage capacity (greater than 5 Mt CO_2 each).

Field Code	Pool Code	Field Name	Pool Name	Pool Sequence	Mass CO2 @ EOR	Effective Mass CO2 (ton)	Oil CO2 Capacity	Gas CO2 Capacity	Combined Pool Capacity
740	8580	BEAVER RIVER	NAHANNI	A				8251410.437	8251410.437
800	4100	BEG	BALDONNEL	A				5903633.467	5903633.467
800	4800	BEG	HALFWAY	A				17898669.67	17898669.67
1400	2900	BLUEBERRY	DUNLEVY	A				11151657.46	11151657.46
1400	2900	BLUEBERRY	DUNLEVY	B				7307110.976	7307110.976
1400	4800	BLUEBERRY	HALFWAY	B				6326076.485	6326076.485
1950	4060	BOULDER	PARDONET-BALDONNEL	A				9776675.331	9776675.331
1950	4060	BOULDER	PARDONET-BALDONNEL	B				5592540.546	5592540.546
2000	6200	BOUNDARY LAKE	BELLOY	J				11671670.29	11671670.29
2150	4060	BRAZION	PARDONET-BALDONNEL	B				7525995.648	7525995.648
2200	4100	BUBBLES	BALDONNEL	A				7890510.267	7890510.267
2240	4150	BUBBLES NORTH	BALDONNEL/UPPER CHARLIE LAKE	A				7575459.584	7575459.584
2400	2600	BUICK CREEK	BLUESKY	C				10130019.19	10130019.19
2400	2900	BUICK CREEK	DUNLEVY	A	4122.442407	2014.671628	6137.114035	8464520.959	8470658.073
2400	2900	BUICK CREEK	DUNLEVY	B	0	786.3356989	786.3356989	7666411.534	7667197.869
2400	2900	BUICK CREEK	DUNLEVY	C	0	2133.676103	2133.676103	11072131.76	11074265.44
2800	2900	BUICK CREEK WEST	DUNLEVY	A	0	49.62855484	49.62855484	5351543.186	5351592.815
2860	4100	BULLMOOSE	BALDONNEL	A				7921424.741	7921424.741
2860	4100	BULLMOOSE	BALDONNEL	B				6807463.566	6807463.566
2860	4100	BULLMOOSE	BALDONNEL	C				6758089.11	6758089.11
2865	4060	BULLMOOSE WEST	PARDONET-BALDONNEL	C				6593968.151	6593968.151
2865	4060	BULLMOOSE WEST	PARDONET-BALDONNEL	D				6593251.452	6593251.452
2850	4060	BURNT RIVER	PARDONET-BALDONNEL	A				6946824.489	6946824.489
2920	4800	CACHE CREEK	HALFWAY	A				6238586.098	6238586.098
2985	4995	CHINCHAGA RIVER	LOWER CHARLIE LAKE/MONTNEY	A				6020139.021	6020139.021
3200	8400	CLARKE LAKE	SLAVE POINT	A				88553247.14	88553247.14
3380	2630	DAHL	BLUESKY-GETHING	A				16995537.11	16995537.11
3400	5000	DAWSON CREEK	MONTNEY	A				8513386.532	8513386.532
3430	2400	DRAKE	NOTIKEWIN	A				7232951.629	7232951.629
3450	8200	EKWAN	JEAN MARIE	A				5281233.359	5281233.359
3455	8200	ELLEH	JEAN MARIE	B				6802218.267	6802218.267
3600	4100	FORT ST JOHN	BALDONNEL	A				11773356.41	11773356.41
3600	4800	FORT ST JOHN	HALFWAY	A				6133278.104	6133278.104
4000	6200	FORT ST JOHN SOUTHEAST	BELLOY	A				7179477.321	7179477.321
4385	4100	GRIZZLY SOUTH	BALDONNEL	B				24894212.11	24894212.11
4470	8200	GUNNELL CREEK	JEAN MARIE	A				25631699.36	25631699.36
4700	8200	HELMET	JEAN MARIE	A				118066403.4	118066403.4
4700	8400	HELMET	SLAVE POINT	A				7501139.679	7501139.679

TABLE 5. LIST AND CO_2 STORAGE CAPACITY OF THE LARGEST 80 OIL AND GAS RESERVOIRS IN NORTHEASTERN BRITISH COLUMBIA WITH INDIVIDUAL CAPACITY GREATER THAN 5 MT CO_2 EACH. FOR OIL RESERVOIRS, THE STORAGE CAPACITY IN EOR AT DEPLETION AND IN TOTAL IS GIVEN. IF AN OIL POOL IS ASSOCIATED WITH A GAS POOL, THEN THE TOTAL CAPACITY IS THE SUM OF THE TWO, OTHERWISE THE TOTAL CAPACITY IS EQUAL TO THE CAPACITY OF THE RESPECTIVE OIL OR GAS POOL.

Field Code	Pool Code	Field Name	Pool Name	Pool Sequence	Mass CO2 @ EOR	Effective Mass CO2 (ton)	Oil CO2 Capacity	Gas CO2 Capacity	Combined Pool Capacity
4900	4575	INGA	INGA	A	0	0	0	12691634.91	12691634.91
5000	4150	JEDNEY	BALDONNEL/UPPER CHARLIE LAKE	A				36962850.42	36962850.42
5000	4800	JEDNEY	HALFWAY	A				16323309.44	16323309.44
5200	4800	KOBES	HALFWAY	A				11410651.73	11410651.73
5500	8400	LADYFERN	SLAVE POINT	A				30540369.15	30540369.15
5600	4150	LAPRISE CREEK	BALDONNEL/UPPER CHARLIE LAKE	A				59792495.42	59792495.42
5600	4150	LAPRISE CREEK	BALDONNEL/UPPER CHARLIE LAKE	B				12019955.53	12019955.53
5852	2805	MAXHAMISH LAKE	CHINKEH	A				22981632.25	22981632.25
6140	4800	MONIAS	HALFWAY	N/A				42853184.9	42853184.9
6220	4100	MURRAY	BALDONNEL	A				5143467.026	5143467.026
6220	4100	MURRAY	BALDONNEL	B				5813993.234	5813993.234
6220	4100	MURRAY	BALDONNEL	E				7766167.426	7766167.426
6220	4150	MURRAY	BALDONNEL/UPPER CHARLIE LAKE	A				21503666.81	21503666.81
6400	4100	NIG CREEK	BALDONNEL	A	1495.581537	2198.729638	3694.311176	27490336.92	27494031.23
6410	2600	NIG CREEK	BLUESKY	A				6963812.547	6963812.547
6430	2510	NOEL	FALHER B	C				5725211.813	5725211.813
6460	4800	OAK	HALFWAY	A	0	3192.63434	3192.63434	6374381.17	6377573.805
6480	4100	OJAY	BALDONNEL	A				22516110.32	22516110.32
9000	7400	OTHER AREAS	DEBOLT	C-053-J/094-G-03				5790890.102	5790890.102
6600	8100	PARKLAND	WABAMUN	A				14298530.01	14298530.01
7250	2400	PICKELL	NOTIKEWIN	A				6757579.467	6757579.467
7600	2900	RIGEL	DUNLEVY	F				41132614.98	41132614.98
7660	4990	RING	BLUESKY-GETHING-MONTNEY	A				45359322.45	45359322.45
7770	8200	SIERRA	JEAN MARIE	A				6162646.462	6162646.462
7770	8600	SIERRA	PINE POINT	A				58041889.53	58041889.53
7770	8600	SIERRA	PINE POINT	B				23953639.73	23953639.73
7770	8600	SIERRA	PINE POINT	D				8205766.58	8205766.58
7775	7400	SIKANNI	DEBOLT	C				9553961.083	9553961.083
7775	7400	SIKANNI	DEBOLT	G				5723020.652	5723020.652
7775	7400	SIKANNI	DEBOLT	H				10917177.69	10917177.69
7780	2600	SILVER	BLUESKY	A				7091702.016	7091702.016
8000	6200	STODDART	BELLOY	A				29214894.28	29214894.28
8110	4060	SUKUNKA	PARDONET-BALDONNEL	E				22431633.55	22431633.55
8110	4060	SUKUNKA	PARDONET-BALDONNEL	L				6049712.369	6049712.369
8110	4060	SUKUNKA	PARDONET-BALDONNEL	M				7171135.592	7171135.592
8110	4060	SUKUNKA	PARDONET-BALDONNEL	P				5739363.488	5739363.488
8115	2800	SUNDOWN	CADOMIN	B				12097243.51	12097243.51
8115	2200	SUNDOWN	CADOTTE	A				5797026.039	5797026.039
8150	4800	TOMMY LAKES	HALFWAY	A				46167148.17	46167148.17
8260	4100	WARGEN	BALDONNEL	B				6883745.846	6883745.846
8360	4800	WILDER	HALFWAY	A				5231576.855	5231576.855
8800	8600	YOYO	PINE POINT	A				72748677.05	72748677.05

TABLE 5. CONTINUED.

Knowledge and Scientific Gaps

The processes leading to CO_2 storage in deep saline aquifers are more complex than in the case of either hydrocarbon reservoirs or coal beds. This is because in deep saline aquifers, several processes may act simultaneously but on different time scales; these include static trapping in stratigraphic and structural traps similarly to hydrocarbon reservoirs, hydrodynamic trapping in long-range flow systems, residual-gas trapping, dissolution and ionic trapping in formation water, and mineral precipitation. Not only do these processes act on different time scales, but also they interact with and affect each other. Figure 4 shows diagrammatically the relationship between various CO_2 storage processes in deep saline aquifers.

A significant gap in knowledge is the geochemistry of CO_2-brine-rock systems at elevated pressures and temperatures and the speed of geochemical reactions. Most studies indicate that dissolution and geochemical reactions operate on time scales of centuries to millennia (Figure 4a; e.g., Xu *et al.*, 2003; Perkins *et al.*, 2005). Thus, to meet the CO_2 storage needs of this century, one can argue that these storage mechanisms should be disregarded—they would only add to the security of storage as time passes (Figure 4b) but do not contribute to capacity. On the other hand, some geochemists argue that some reactions occur very quickly and alter the mineral composition of the formation water and rock matrix.

Similarly, there is no quantitative understanding of the effect of mineral geochemical changes (dissolution and precipitation) on the flow characteristics (porosity and permeability) of the rock matrix. These in turn affect the spread and flow of the injected CO_2 (hence hydrodynamic trapping, dissolution, and mineral precipitation), since a plume of CO_2 that travels faster will encounter more undersaturated brine and new rock. The residual-gas trapping process is activated only when the plume of injected CO_2 flows away, updip, from the injection site, and formation water invades the pore space previously occupied by CO_2 (Kumar *et al.*, 2005). This process too is affected by the hydrodynamics of CO_2 flow and by the displacement characteristics of CO_2-brine systems.

Finally, there are currently no comprehensive numerical models to simulate all the physico-chemical processes that take place when CO_2 is injected and stored in deep saline aquifers, neither is there computational power to solve such a complex system at the needed resolution.

In regard to CO_2 storage in uneconomic coal beds, there is disagreement in the scientific community about the effect of supercritical CO_2 on coal and about the storage process for liquid and supercritical CO_2. Is it adsorption, as in the case of gaseous CO_2, or is it absorption? It seems that adsorption is replaced by absorption and the CO_2 diffuses ("dissolves"; Larsen, 2003) in coal. The transition from one process to the other is not sharp but gradual. Carbon dioxide is a "plasticizer" for coal, lowering the temperature required to cause the transition from a glassy, brittle structure to a rubbery, plastic structure ("coal softening"; Larsen, 2003). The transition temperature may drop from approximately 400 °C at 3 MPa to less than 30 °C at 5.5 MPa (Larsen, 2003). Coal plasticization destroys any permeability that would allow CO_2 injection. In addition, some studies suggest that the injected CO_2 may react with the coal. However, CO_2 was successfully injected in coal beds in the San Juan Basin and in Alberta at depths that correspond to supercritical CO_2 phase.

Another issue relating to CO_2 storage in coal beds is coal permeability and how it is affected by CO_2. It is known that coal permeability decreases with increasing depth as a result of increasing stress, which closes the cleats, but this relationship has not been quantified and it is highly dependent on local coal characteristics and depositional setting. Furthermore, coal swells as CO_2 is adsorbed and/or absorbed, which reduces permeability and injectivity (Clarkson and Bustin, 1997; Larsen, 2003). Also, the effect of other gases (either present in the coal matrix or injected in an impure stream of CO_2) on CO_2 adsorption onto the coal matrix is not well understood nor quantified. The lack of understanding regarding CO_2 effects on coal and the effect of other gases affects the ability to estimate the CO_2 capacity in coal beds.

Lack of Consistent Methodology

As pointed out in the IPCC Special Report on CO_2 Capture and Storage (IPCC, 2005), currently there is no consistent and accepted methodology for estimating the CO_2 storage capacity in deep saline aquifers. One school of thought considers that only stratigraphic and structural enclosures at the top of deep saline aquifers should be considered, these being similar to hydrocarbon reservoirs overlying an aquifer but being saturated with formation water rather than charged with oil and/or gas (e.g., Holloway *et al.*, 2006), all other trapping mechanisms being neglected. These estimates represent indeed a lower bound of storage capacity in deep saline aquifers. At the other end of the spectrum, dissolution and mineral precipitation are included in capacity estimates (e.g., Xu *et al.*, 2003), but these estimates do not consider the different time scales involved and the need for storage capacity this century rather than several centuries or thousand years from now.

Yet other methods, used in the past particularly, estimate the CO_2 storage capacity for an aquifer or a basin based on area and pore space (e.g., Koide *et al.*, 1993), while others are based on numerical simulations (e.g., van der Meer, 1993; Kumar *et al.*, 2005). Each methodology has different data requirements and is based on different assumptions. The first method has been shown to be errone-

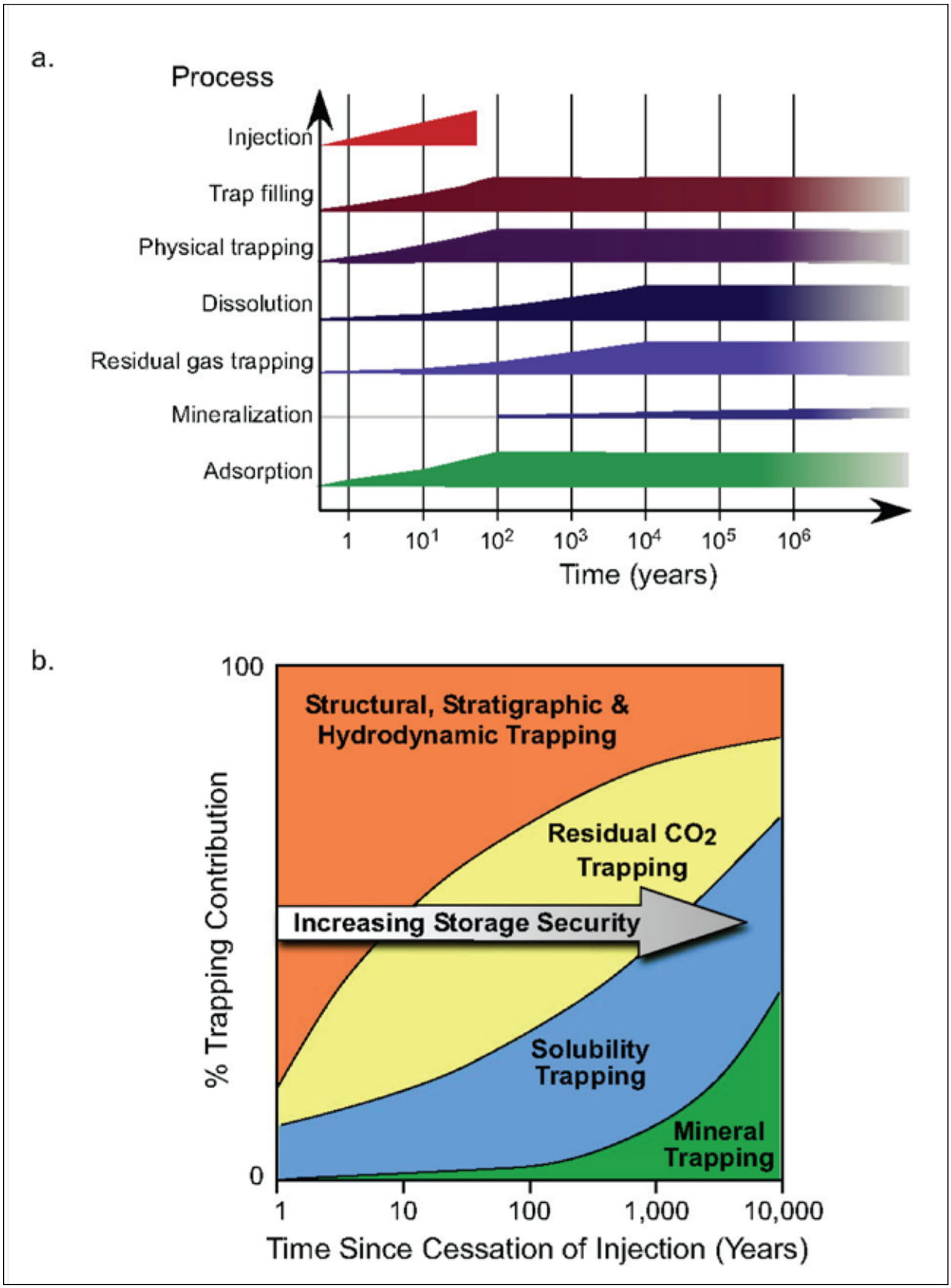

Figure 4. Relationship between various CO_2 storage processes in deep saline aquifers: a) time scales and b) storage security.

ous (Bradshaw and Dance, 2005), and the second one can produce estimates only at the local, site-specific scale, and it is not suitable for the whole of a sedimentary basin or at regional scale.

The lack of knowledge about the limits of applicability (permeability-wise or from the point of view of CO_2 phase) to CO_2 storage in coal beds shows only that it is very difficult to establish the deep depth-limit of a coal bed being considered for CO_2 storage. Is it the depth at which the very low permeability does not allow CO_2 injection unless the coal is fractured, jeopardizing the integrity of the storage site, or is it the depth that corresponds to the phase change of CO_2 from gaseous to liquid or supercritical? At the other end, the shallow depth-limit is equally difficult to establish, but for different reasons—the main criterion being protection from contamination of potable groundwater resources.

In addition, the definition of "uneconomic coal beds" is debatable and likely will evolve as technology advances and the need for stable and secure energy supplies increases. Shallow coal seams that are uneconomic to be mined today may be mined underground in the future, at which time any stored CO_2 will be released back into the atmosphere, notwithstanding that it may pose a safety hazard. Or, currently uneconomic coal seams may produce coal gas in the future or may be gasified in situ as the price of gas increases. Finally, for any particular coal bed, the well density and recovery and completion factors will affect the CO_2 storage capacity estimates.

Lack of Data

In the case of deep saline aquifers, there is a need to know their geometry and internal architecture, pressure, and temperature as well as the composition, properties, and characteristics of formation water and rocks. However, much less is known about these, and at a poorer, coarser resolution than in the case of oil and gas reservoirs because of the lack of an economic interest in obtaining, collecting, and storing this information. Whatever is known is the result of drilling and testing when exploring for oil and gas (i.e., from dry holes). Furthermore, there are no data about the displacement characteristics of CO_2-brine systems (as opposed to CO_2-oil systems), and only very recently have a few laboratory measurements been performed to quantify these (Bennion and Bachu, 2005).

In the case of uneconomic coal beds, there is a need to know their geometry, thickness, composition, rank, ash and moisture content, adsorbed gases, and adsorption capacity for CO_2 at various temperatures and pressures and in the presence of other gases. This information is not collected usually, and when it is collected, it is generally at a very coarse resolution. The definition of "uneconomic coal bed" precludes data collection since this represents a cost with no return on investment. Lately, with growing interest in producing coalbed methane (or coalbed gas), more data are being collected by industry to define and characterize this resource and associated reserves. Since CO_2 storage in coal beds may enhance coalbed methane recovery, additional relevant data are collected in places but nowhere are sufficient for estimating CO_2 storage capacity.

To conclude, the CO_2 storage capacity in deep saline aquifers and coal beds in northeastern BC currently cannot be estimated with any confidence with the existing knowledge and data. However, an evaluation of the potential for CO_2 storage and identification of strata and areas where this technology can be used are possible, and these will be addressed in the following discussion.

THE POTENTIAL FOR CO_2 STORAGE IN DEEP SALINE AQUIFERS AND COAL BEDS IN NORTHEASTERN BRITISH COLUMBIA

Because the capacity for CO_2 storage in deep saline aquifers currently cannot be accurately estimated, the potential for CO_2 storage will be assessed indirectly on the basis of proxy characteristics. Deep saline aquifers posses the porosity and permeability needed for CO_2 storage and injectivity, respectively. If fluids cannot be produced from or injected into a geological formation, then that formation is either an aquitard (e.g., shales) or an aquiclude (e.g., salt beds), otherwise it is an aquifer. Thus, the potential for CO_2 storage in deep saline aquifers is assessed here on the basis of the existence of a confining unit above each aquifer (a condition that is met by all but the shallowest drift aquifers in northeastern BC) and by the pressure and temperature conditions at which CO_2 is a dense fluid (liquid or supercritical), to maximize storage efficiency. To illustrate this point, Figure 5 shows the dependence of CO_2 density on temperature and pressure, and Figure 6 shows the variation of CO_2 density with depth assuming a hydrostatic pressure gradient and various geothermal regimes. The geological space (defined by geological and lithological units, pressure, and temperature) is transformed into the CO_2-phase space using the methodology described by Bachu (2002), and the region of CO_2 storage applicability is defined for each aquifer on the basis of the domain where the injected CO_2 will be in a dense phase.

Geology and Hydrostratigraphy

Only a very brief geological description is provided here for the sedimentary succession in northeastern BC; for more detail the interested reader could consult the Geological Atlas of the Western Canada Sedimentary Basin (Mossop and Shetsen, 1994). The Cambrian to Lower Jurassic succession was deposited during the passive-margin stage of basin evolution and consists mainly of carbonate and

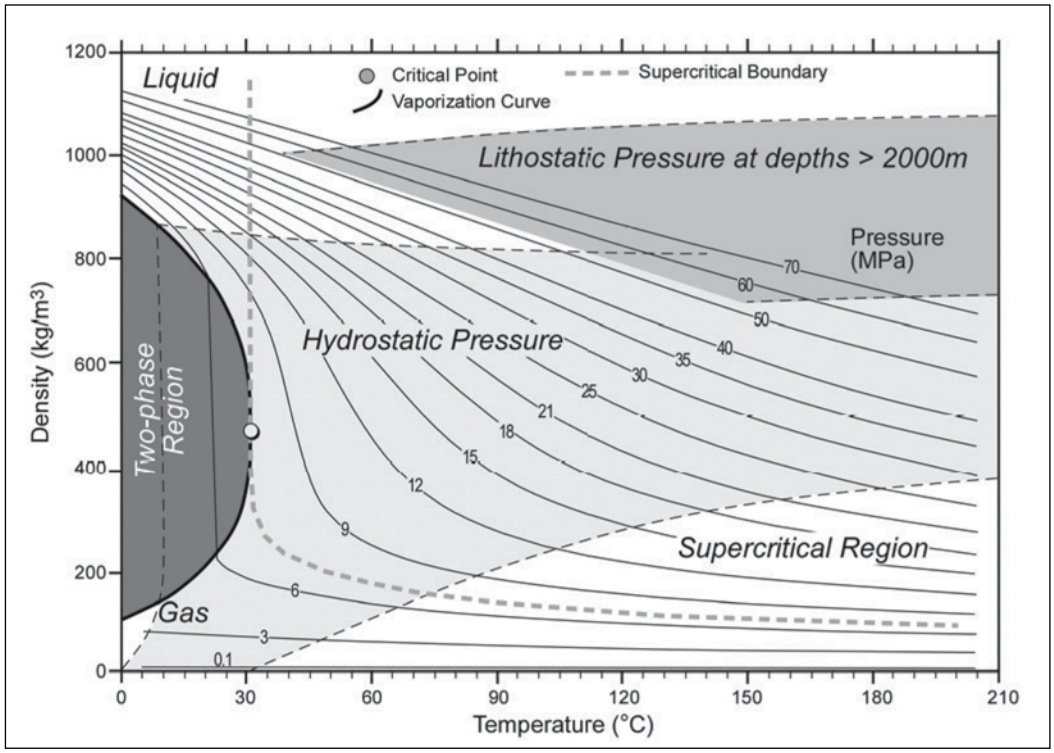

Figure 5. Variation of CO_2 density with temperature and pressure, and expected range of variation in sedimentary basins.

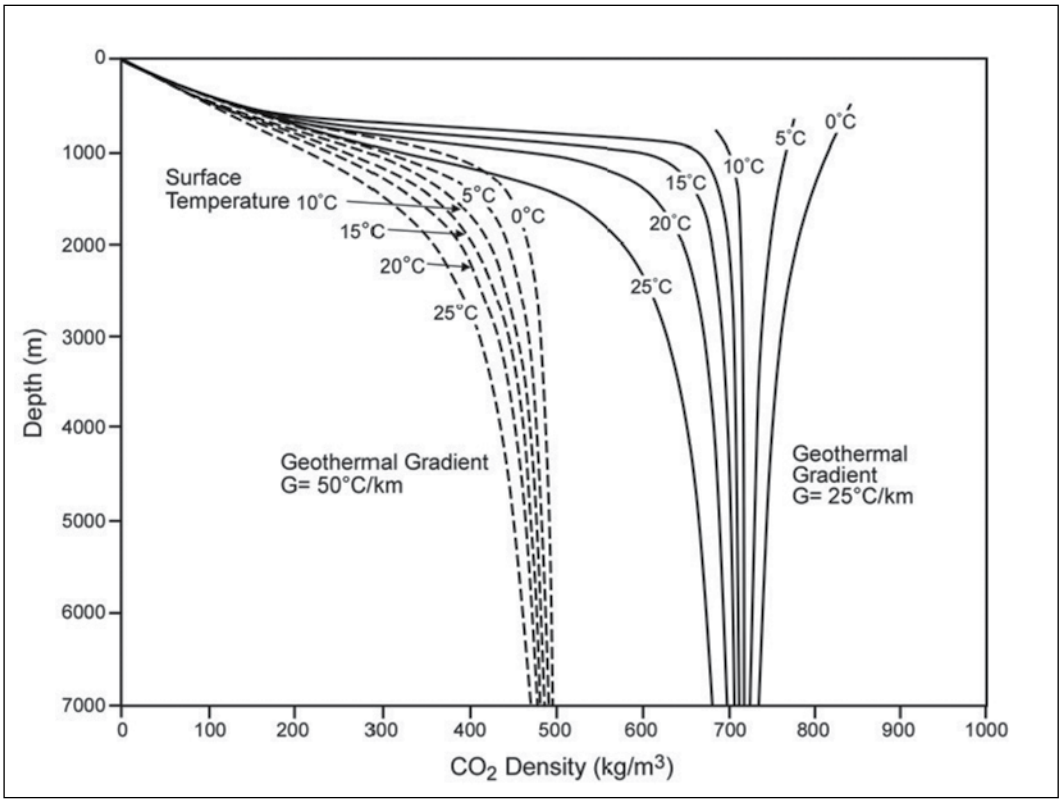

Figure 6. Variation with depth of CO_2 density assuming a hydrostatic pressure gradient and various geothermal conditions in a sedimentary basin (after Bachu, 2003).

evaporitic strata with a few intervening shale units. The Upper Jurassic to Cretaceous strata consist of a succession of regional-scale thin sandstone and thick shale units deposited during the foreland stage of basin evolution. The stratigraphic and hydrostratigraphic nomenclature of the sedimentary succession in northeastern BCis presented in Figure 7.

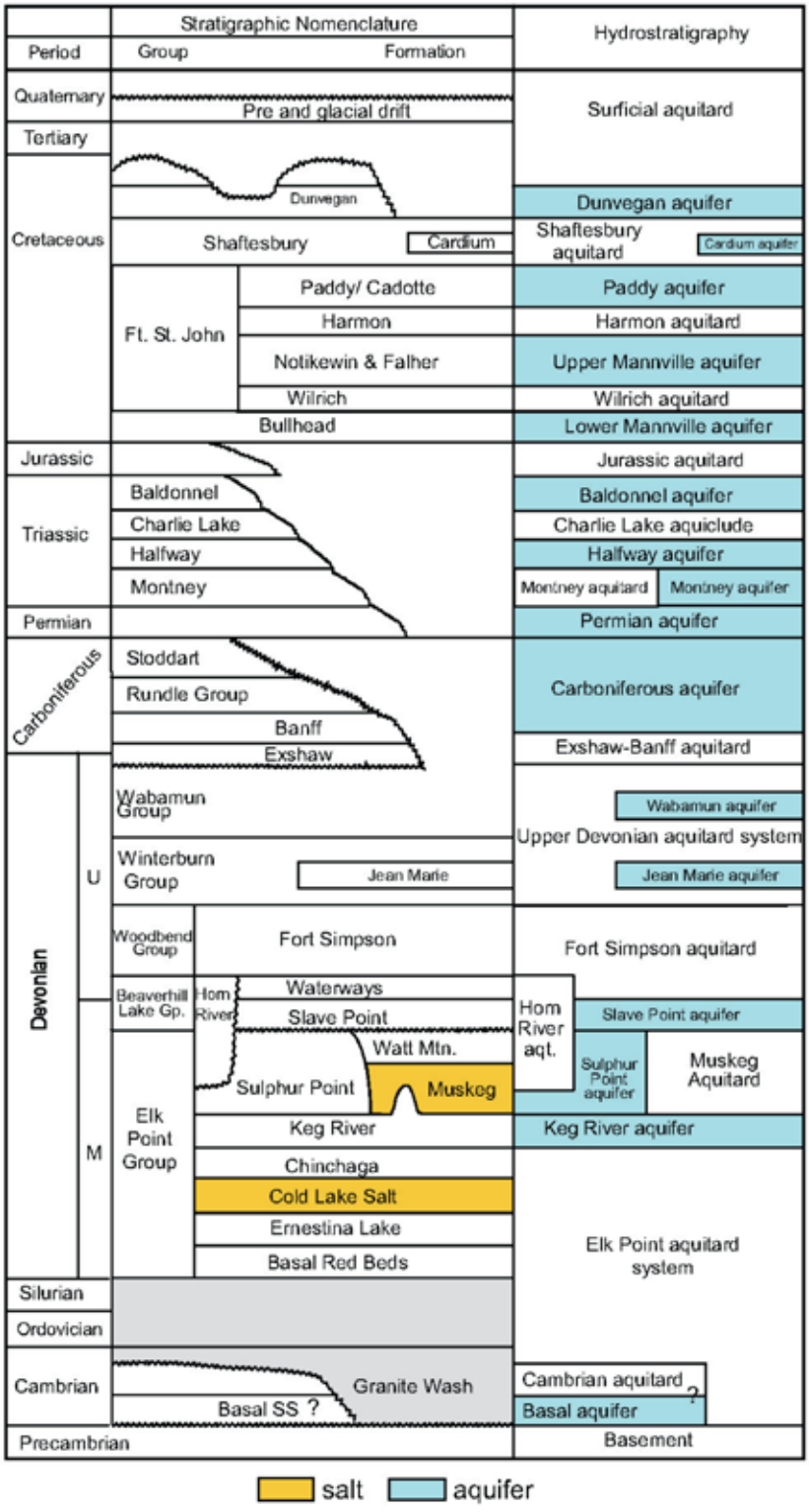

Figure 7. Stratigraphic and hydrostratigraphic nomenclature of the sedimentary succession in northeastern British Columbia.

The basin was initiated during the Proterozoic by rifting of the North American craton. Due to extensive erosion in the Middle Ordovician and especially in the Early Devonian, only a small remnant of Cambrian strata is present in northeastern BC. This succession, up to 200 m thick, comprises a thin basal sandstone unit, which forms an aquifer, overlain by dominantly silty shale, which forms an aquitard. During most of the Devonian, the Peace River Arch was a land feature that slowly submerged in the surrounding sea. As a result, depositional boundaries of successively younger Middle and Late Devonian units advance southward against the Peace River landmass until its complete submersion during Late Devonian, when it was covered by the carbonate rocks of the Wabamun Group (Figure 8a). A Middle Devonian interbedded succession of low-permeability anhydritic red beds and carbonate, halite, and argillaceous carbonate (Basal Red Beds and the Ernestina Lake, Cold Lake, and Chinchaga Formations) overlies the Cambrian or Granite Wash detritus at the top of the Precambrian and forms the Elk Point aquitard system (Bachu, 1997). The location of the thin Cold Lake salt beds in the northern part of the area is also shown in Figure 8a. The succession at the base of the Middle Devonian is overlain by the platform and reefal carbonate rocks of the Keg River Formation, which form an aquifer.

A major feature in northeastern BC is the Presqu'ile Reef Barrier (Figure 8a), deposited during the late Middle Devonian. Shales of the Horn River Formation were deposited west of the barrier reef. The barrier limited the southward flow of seawater and led to deposition in the southern part of the area (toward the Peace River Arch landmass) of the evaporitic beds of the anhydrite-dominated Muskeg Formation, which forms an aquitard. Toward the Peace River Arch in the south, the evaporite beds of the Muskeg Formation change facies into the sandstone of the Gilwood Member, which is derived from clastic sediments eroded from the Peace River landmass. Subsequent reef growth along the seaward (northwest) edge of the Presqu'ile barrier reef formed the Sulphur Point Formation. Inside the barrier reef complex, the small inter-reef Cordova sub-basin was filled with shale coeval with the Horn River Formation. This complex lithological structure is disconformably overlain by the thin shale of the Watt Mountain Formation. Thus, the Keg River aquifer is overlain by a laterally complex, interlaced hydrostratigraphic structure consisting of the Horn River aquitard, the Sulphur Point aquifer, and the Muskeg aquiclude (Figure 7). In the northern part of northeastern BC, the Keg River and Sulphur Point aquifers are in contact, forming the Elk Point aquifer system (Bachu, 1997). In the south, abutting the Peace River Arch, the carbonate of the Keg River Formation and the overlying sandstone of the Gilwood Member also form the Elk Point aquifer system.

The Elk Point Group is overlain by the Beaverhill Lake Group, which can be subdivided into the open-marine platform carbonate of the Slave Point Formation and the shale and argillaceous carbonate of the Waterways Formation. The seaward depositional margin of the Beaverhill Lake Group is roughly coincident with the underlying Elk Point Group Reef Barrier, with coeval shales of the Horn River Formation being deposited seaward. The Beaverhill Lake Group is overlain by the Woodbend Group, which consists mostly of a thick succession of shale-dominated strata (Fort Simpson Formation). Thus, the Slave Point aquifer is overlain by the Fort Simpson aquitard system (comprising the Waterways and Fort Simpson Formations). The Woodbend Group is overlain by the Winterburn and Wabamun Groups, which are dominated in northeastern BC by shales, except for the carbonates of the Jean Marie Member in the Winterburn Group to the northeast and carbonates of the Wabamun Group to the southeast.

Carboniferous strata in northeastern BC conformably overlie the Devonian rocks and consist of two major lithofacies associations. The lower one comprises the thin but competent shale of the Exshaw Formation and the overlying thick, shale-dominated Banff Formation, which together form the Exshaw–Banff aquitard. The top part of the Carboniferous succession consists of the carbonate rocks of the Rundle and Stoddart Groups that form the Carboniferous aquifer (Bachu, 1997). A thin layer of Permian (Belloy Formation) interbedded siliciclastic and carbonate unconformably overlies the Carboniferous strata and is overlain in turn by a Triassic succession that consists, in ascending order, of the shale and the sandstone of the Montney Formation, the sandstone-dominated Halfway Formation, the evaporites (halite) of the Charlie Lake Formation, and the sandstone of the Baldonnel Formation (Figure 7). The Permian and Triassic strata form a succession of aquifers (Belloy, Montney, Halfway, and Baldonnel) separated by intervening aquitards and aquicludes (Montney and Charlie Lake).

As a result of accretion of allochthonous terranes to the western margin of the North American protocontinent during the Columbian and Laramide orogenies of the Late Jurassic to Early Cretaceous and the Early Tertiary, respectively, the sedimentary strata were pushed eastward, being thrusted and folded into the Rocky Mountains and the foreland Thrust and Fold Belt, which today constitute the western boundary of the undeformed part of the basin. Because of lithostatic loading and isostatic flexure, the Precambrian basement tilted westward, such that progressively older Jurassic to Carboniferous strata subcrop in northeastern BC at the sub-Cretaceous unconformity as a result of basement tilting and pre-Cretaceous erosion (Figure 8b). The foreland basin filled with synorogenic clastic sediments derived from the Cordillera.

The Upper Jurassic sandstone and shale strata of the Fernie Group represent the first influx of siliciclastic sediments from the west. The entire area is unconformably overlain by the Lower Cretaceous sediments of the Mines and Bullhead Groups. As a result of peat deposition in a fluvial environment, these strata are rich in coal. The overlying

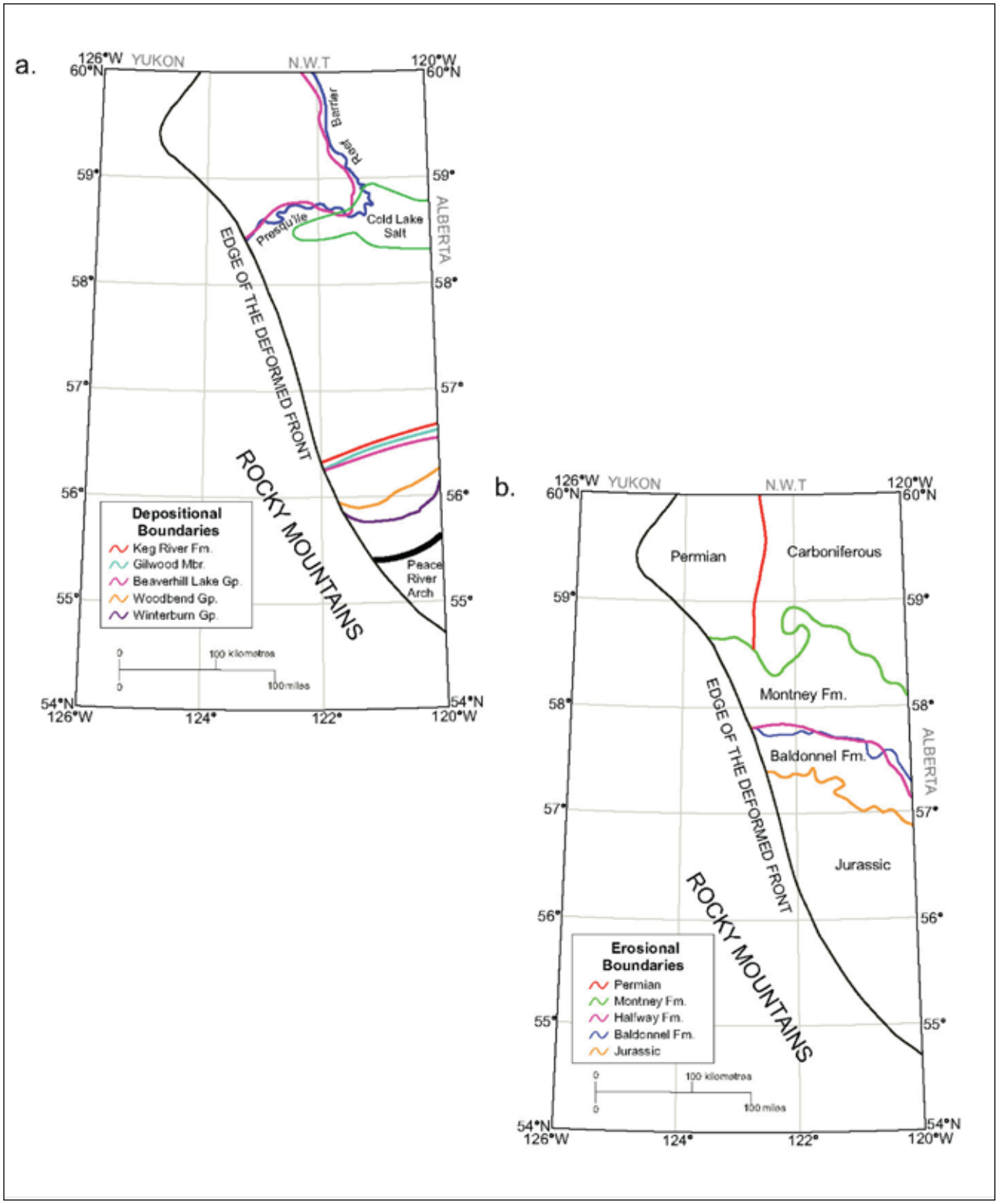

Figure 8. Depositional features in northeastern British Columbia: a) Devonian strata, and b) Carboniferous to Jurassic strata.

Lower Cretaceous Fort St. John Group consists of a succession of sandstone-dominated strata (Falher, Notikewin, and Paddy Formations) deposited in a mainly fluvial and estuarine environment, alternating with shale-dominated strata deposited in a mainly marine environment (Wilrich, Harmon and Shaftsbury Formations). The deposition of the post-Notikewin strata corresponds to the post-Columbian orogeny lull in plate convergence, which was characterized by a widespread marine transgression. By analogy with the hydrostratigraphic succession in northern Alberta (Bachu, 1997), the entire Jurassic–Lower Cretaceous succession can be divided (Figure 7) into a succession of aquifers (Bullhead, Falher, and Paddy) separated by intervening aquitards (Wilrich, Harmon, and Shaftsbury). The entire succession becomes shaly northward, such that the aquifers are present mostly in the southern part of northeastern BC, whereas a single aquitard (Fort St. John) is present in the northern part.

Most of the Upper Cretaceous strata are eroded in northeastern BC. The sandstone Dunvegan Formation, overlying the Fort St. John Group, is present in the subsurface in the south (south of latitude 56°N) and at the top of the bedrock further to the north, until it almost disappears north of 58°N. The sandstone Cardium Formation, isolated by underlying and overlying shale units, is present only at the southern tip of northeastern BC. Finally, the sandstone-dominated Wapiti Group is similarly present at the top of the bedrock only at the southern tip. The Cretaceous strata that crop out at the top of the bedrock, with increasing age from south to north (Wapiti Group to Fort St. John Group), are covered by unconsolidated Quaternary sediments of pre- and postglacial origin.

Geothermal, Flow, and Pressure Regimes

The multiyear ground-surface temperature in northeastern BC is around 4 °C, and geothermal gradients increase from slightly less than 30 °C/km in the south to more than 45 °C/km in the north (Bachu and Burwash, 1991). With respect to geothermal effects on CO_2 storage, northeastern BC displays the characteristics of a cold basin in the south and a warm basin in the north (Bachu, 2003). Carbon dioxide migrating upward will change phase from supercritical to liquid and then to gas in the south but will undergo a direct phase change from supercritical to gas in the north. Also, CO_2 will reach higher density in the south than in the north, resulting in greater storage capacity for the same pore space.

The flow of formation waters in pre-Cretaceous strata in the northern part of northeastern BC is driven by topography in a regional-scale system that flows from recharge areas at the Thrust and Fold Belt to discharge areas in the northeast at the Slave River and Great Slave Lake (Bachu, 1997). In the south, toward the Peace River arch, flow in deep Devonian strata is driven in a regional-scale flow system by past tectonic compression (Hitchon *et al.*, 1989; Bachu, 1995). The flow in the Lower and Upper Mannville aquifers is generally driven by topography in an intermediate-scale flow system (Hitchon *et al.*, 1989). However, the Lower Cretaceous strata near the Thrust and Fold Belt at the southern tip of northeastern BC are mostly saturated with gas and are abnormally pressured as a result of gas generation (Hitchon *et al.*, 1989; Michael and Bachu, 2001). The flow in Carboniferous to Triassic aquifers in the south is also driven in regional-scale systems. Finally, the flow in the shallow Paddy, Dunvegan, and Cardium aquifers is driven by topography in local-scale flow systems that discharge at outcrop along river valleys throughout northeastern BC or to the east in Alberta.

The sedimentary strata in northeastern BC are normally pressured or slightly subhydrostatic. At these conditions, CO_2 will always be lighter than formation waters (Figure 5) and lighter than reservoir oil in most cases. Carbon dioxide injected into aquifers in the sedimentary succession of northeastern BC will migrate updip to the northeast, driven by buoyancy. Its migration will be enhanced by the concurrent, northeastward flow of formation waters. Because the flow in the shallow post-Mannville aquifers is in local-scale systems, CO_2 storage in these strata should generally not be considered because of the high buoyancy of the CO_2, unless depleted oil or gas reservoirs are being used for storage (stratigraphic trapping).

Suitability of Deep Saline Aquifers for CO2 Storage

The Middle Devonian and Cambrian strata in northeastern BC are found at depths greater than 1500 m, with corresponding pressures and temperatures greater than 14 MPa and 50 ºC, respectively. This means that CO_2 injected into and stored in the Cambrian Basal Sandstone aquifer, if present, and in the carbonate Keg River, Sulphur Point, and Slave Point aquifers (Figure 7) will always be in dense supercritical phase. These aquifers underlie most of northeastern BC, except for its northwest corner (Figure 8a) and are overlain by the thick Fort Simpson aquitard. Thus, there is likely good potential for CO_2 storage in these aquifers in both stratigraphic and structural traps that have to be identified and hydrodynamically in the regional-scale flow system that operates below the Ft. Simpson aquitard (Bachu, 1997). Carbon dioxide dissolution probably will be limited because of the high salinity of formation water in these aquifers. The Jean Marie aquifer in the Winterburn Group, of limited areal extent, is the lowermost aquifer in the succession where, depending on location, the injected CO_2 will be in gaseous phase or in a dense, liquid, or supercritical phase (Figure 9a). This is because pressures in the northeast are below the CO_2 critical pressure of 7.38 MPa. Because most of the Wabamun Group consists of shale over most

of the area (particularly in the north), and carbonate rocks, which form an aquifer, are present only in the south, where temperatures and pressures are greater than 80 ºC and 20 MPa, respectively, CO_2 injected into the Wabamun aquifer in the south will be in dense supercritical phase.

The lower part of the Carboniferous, comprising the shales and shale-dominated Exshaw and Lower Banff Formations, forms a strong aquitard that separates the overlying Carboniferous aquifer (Rundle and Stoddart Groups) from the underlying Devonian units. Depths to the top of the aquifer vary from less than 400 m in the north to more than 4400 m in the south, with temperatures and pressures varying accordingly from less than 20 °C in the northeast to approximately 160 °C in the south, and from less than 4 MPa in the northeast to greater than 26 MPa in the south, respectively. Thus, depending on location, CO_2 injected into the Carboniferous aquifer will be in all three phases, from supercritical in the south to gaseous in the north and northeast (Figure 9b). This pattern reoccurs for all shallower, stratigraphically younger aquifers in the sedimentary succession, and its distribution is either limited by aquifer extent or is uncertain due to lack of data.

The Permian (Belloy Formation) is present only in the southern part of northeastern BC and in the Liard subbasin in the northwest, having been eroded during the Late Jurassic and Early Cretaceous. Depths range from less than 200 m to more than 3200 m in the northwest (Liard subbasin), and from less than 600 m in the northeast to more than 4200 m in the south. Temperatures vary accordingly from less than 10 °C to approximately 150 °C in the south. There are no pressure data for the northern and southwestern parts of the Permian, but the existing data indicate that pressures vary from less than 8 MPa to greater than 26 MPa. As in the case of the underlying Carboniferous aquifer, CO_2 injected into the Permian will be in all three phases, depending on location (Figure 9c), although one can only speculate about the Liard subbasin.

Like the underlying Permian and Carboniferous strata, the Triassic has been eroded by late Jurassic to early Cretaceous erosion, and is present only in the southern two thirds of northeastern BC. Successively younger formations (the Montney, Halfway, Charlie Lake, and Baldonnel) subcrop from south to north (Figure 8b). The oldest Triassic unit, the Montney Formation, is dominated by shale in the western part and by sandstone in the eastern part; it is therefore an aquitard in the west and an aquifer in the east. Depths to the Montney Formation vary between approximately 600 m at its northern end to more than 4000 m at its southern end. Temperatures vary from less than 30 °C to approximately 150 °C. The very few existing pressure data for the Montney aquifer indicate that pressures vary from less than 4 MPa to more than 12 MPa. Therefore, CO_2 injected in the Montney aquifer would be in all three phases, depending on location (Figure 9d).

The overlying Halfway aquifer is found at depths varying from less than 1000 m in the north to 4000 m in the south. Temperatures range from approximately 40 °C in the north to approximately 140 °C in the south. Pressures in this aquifer vary from less than 6 MPa to greater than 34 MPa; consequently, CO_2 injected into the Halfway aquifer will be in all three phases but mostly in supercritical phase, depending on location (Figure 9e). The Baldonnel aquifer is separated from the underlying Halfway aquifer by the evaporitic rocks of the Charlie Lake Formation. Depths to the top of the Baldonnel aquifer vary from approximately 1000 m in the north to approximately 3700 m in the south. Temperatures at the top of the aquifer vary from less than 40 °C in the northeast to approximately 130 °C in the south. Although there are no pressure data in the north and southwest, pressures vary likely from less than 8 MPa in the north to greater than 14 MPa in the south. Thus, CO_2 injected into this aquifer will be in supercritical phase in the southern area and likely in liquid and gas phase in the northern part.

The Triassic strata are partially overlain by Jurassic siliciclastic rocks (Figure 8b), which are dominated by shale in northeastern BC. Thus the Jurassic, where present, forms an aquitard between the underlying Baldonnel aquifer and the overlying Lower Cretaceous Bullhead aquifer, which disconformably overlies the Carboniferous to Jurassic strata that subcrop at the sub-Cretaceous unconformity (Figure 8b). The entire succession becomes shaly in the northern part of northeastern BC, such that the Bullhead and Falher aquifers are present only in the southern part. Both aquifers are gas-saturated at their southern tip (Figures 9f and 9g), where gas generation probably still takes place (Masters, 1979). Thus, this region should not be used for CO_2 storage while there is still potential for gas production. Depth to the Bullhead aquifer varies from less than 400 m in the north to more than 2800 m in the south and to the Falher aquifer varies from less than 200 m in the north to more than 2600 m in the south. Temperature at the top varies from less than 20 °C in the north to approximately 110 °C in the south for the Bullhead aquifer and from less than 20 °C in the north to more than 90 °C in the south for the Falher aquifer. Pressures in these aquifers vary from less than 4 MPa in the northeast to approximately 20 MPa in the south. Thus, CO_2 injected into these aquifers will be in supercritical, liquid, and gas phases, depending on location (Figures 9f and 9g).

The Paddy Formation is found everywhere in northeastern BC, at depths ranging from less than 200 m in the northwest to more than 2600 m at the southern tip, and with temperatures varying accordingly between less than 20 °C and approximately 90 °C. However, it is mostly shaly, and therefore an aquitard, over most of the region, except where it is deepest in the southern part (approximately south of latitude 56°N). Pressures in this area vary from less than 4 MPa to greater than 14 MPa. Consequently, CO_2 injected into the Paddy aquifer in northeastern BC will be in all

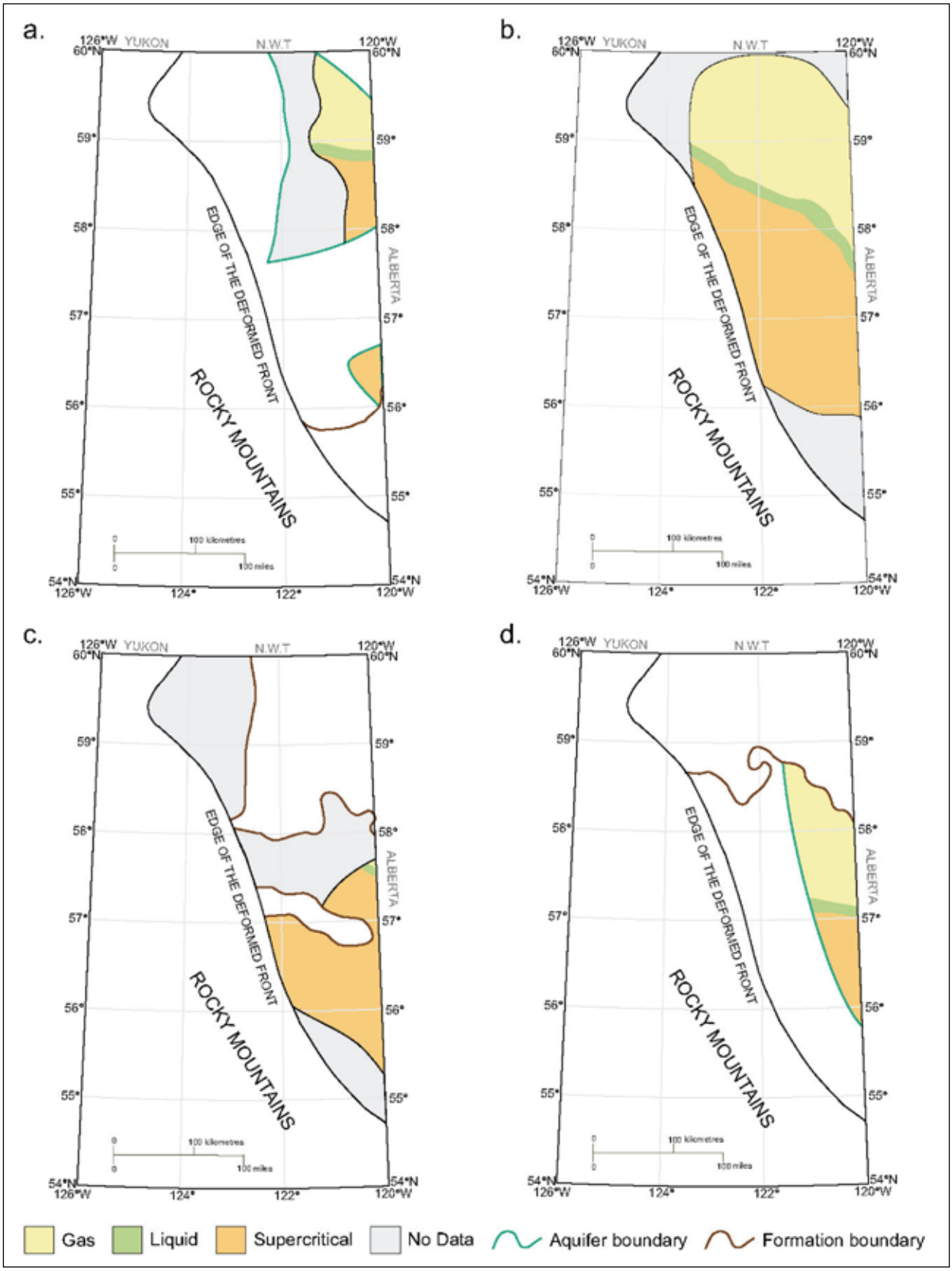

Figure 9. Phase distribution of CO_2 at the top of various aquifers in northeastern British Columbia: a) Jean Marie, b) Carboniferous, c) Permian, and d) Montney.

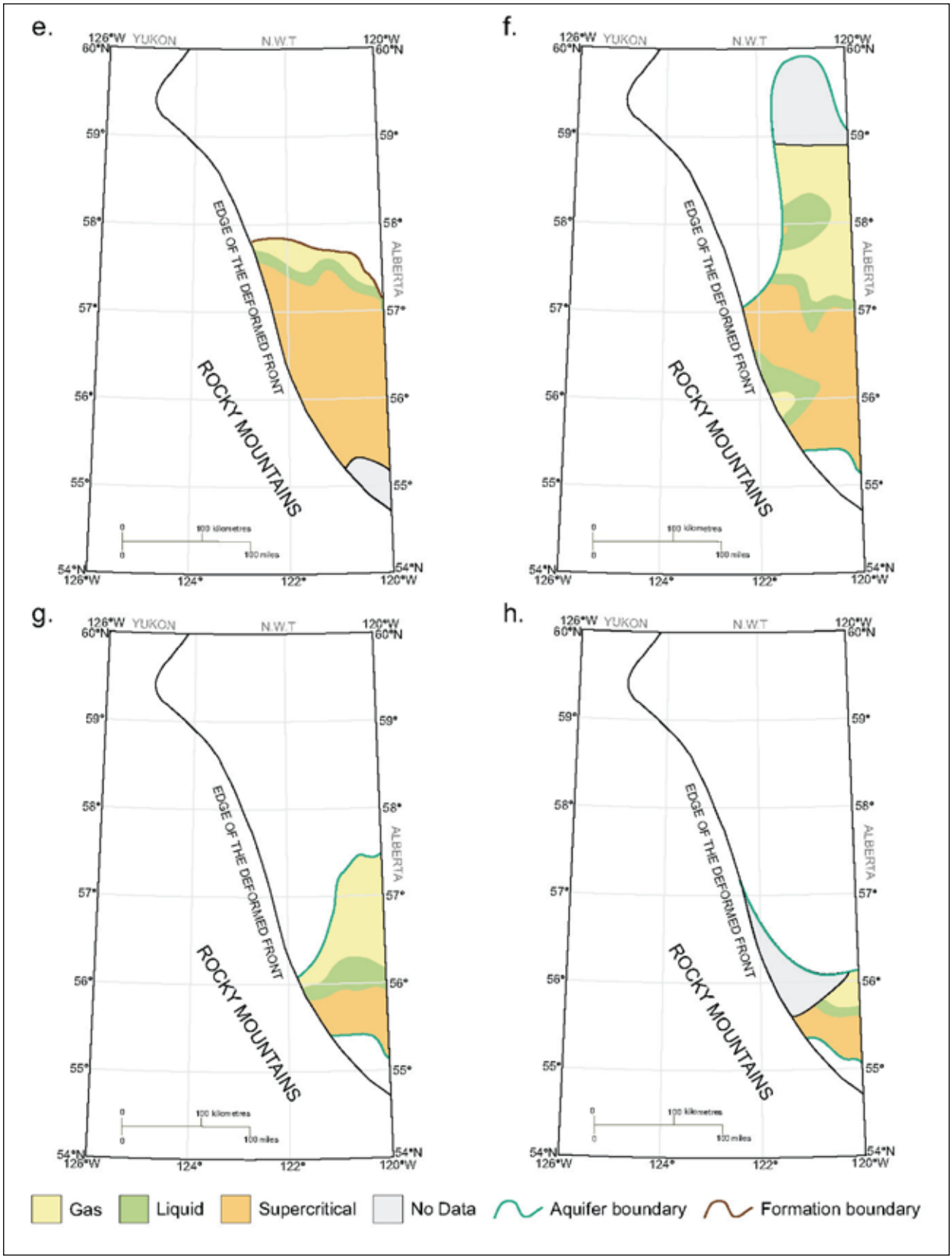

Figure 9 continued. Phase distribution of CO_2 at the top of various aquifers in northeastern British Columbia: e) Halfway, f) Lower Mannville (Bullhead), g) Upper Mannville, and h) Paddy.

three phases, depending on location (Figure 9h). Like the underlying Falher and Bullhead aquifers, the Paddy aquifer is saturated with gas at its southern tip (Figure 9h), hence this region should not be used for CO_2 storage.

Shallower aquifers such as Dunvegan and Cardium, which are present only in the southern part of northeastern BC as the result of Tertiary to Recent erosion, are not suitable for CO_2 injection for two reasons: first, pressures are less than 7.38 MPa (the CO_2 critical pressure), thus injected CO_2 will be in gaseous phase; second, these aquifers crop out along river valleys to the north, and CO_2 will migrate updip, driven by a very strong buoyancy, and will escape back into the atmosphere at outcrop.

Suitability of Coal Beds for CO_2 Storage

Coals are found in northeastern BC in the Lower Cretaceous Bullhead Group, having been deposited in a fluvial environment, and probably contain coalbed gas that could be produced. Consequently, CO_2 could be stored in these coal beds by adsorption, thereby producing methane concurrently. Because methane is a much cleaner fossil fuel than coal, substituting it for coal also contributes to lowering CO_2 emissions into the atmosphere. However, these coals are found at great depths that vary from approximately 600 m to more than 2800 m, with most of them being at depths greater than 1000 m (Figure 10a). As discussed previously in the section on "Challenges in Estimating CO_2 Storage Capacity in Deep Saline Aquifers and Uneconomic Coal Beds", serious challenges handicap the evaluation of the potential for CO_2 storage in coals in northeastern BC

One challenge is that coal permeability decreases with depth such that, generally, the coals have to be fractured at depths greater than approximately 1500 m in order to produce coalbed gas or inject CO_2, an operation that inherently would affect the integrity of the storage site; however, the precise depth of coal gas producibility without fracturing is not known. On the other hand, even if these coals are fractured, the thick Fort St. John and Shaftsbury shales above the coals will ensure CO_2 containment. Previous studies (e.g., Voormeij and Simandl, 2005) have considered 2000 m as the maximum coal depth for which CO_2 storage in northeastern BC would be possible; adopting this depth as the deep limit for CO_2 storage in coals of the Bullhead Group will also avoid targeting the deep, gas-saturated region at the southern tip of this unit (Figure 9f).

More serious challenges in estimating the potential for CO_2 storage in coal beds in northeastern BC are the lack of understanding of the storage mechanism for non-gaseous CO_2 (see discussion in Section 3.1.1) and the specific lack of data (adsorption isotherms in particular). It is worth noting that a micro pilot project for CO_2 injection and methane production from Lower Cretaceous Mannville Group coal beds at Fenn Big Valley in central Alberta reported permeabilities in the order of a few millidarcies at approximately 1250 m depth (Gunter *et al.*, 2005).

Based on the above considerations, three categories of potential areas for CO_2 storage in coals in northeastern BC are defined here (Figure 10b):

- high potential, in relatively shallow areas where injected CO_2 will be in gaseous phase;
- moderate potential at greater depths but shallower than 1400 m, where CO_2 will be in dense liquid or supercritical phase but where permeability is sufficient to allow CO_2 injection and coal gas production; and
- low potential at depths between 1400 and 2000 m, where CO_2 will be in dense liquid or supercritical phase and permeability will likely be very low such that the coals may have to be fractured for CO_2 injection and coal gas production.

Further studies of coal permeability, gas content, and CO_2 adsorption capacity are needed to improve this assessment of the potential for CO_2 storage in coal beds in northeastern BC.

STRATIGRAPHIC SUITABILITY FOR CO_2 STORAGE IN NORTHEASTERN BRITISH COLUMBIA

The stratigraphic and geographic assessment of the suitability for CO_2 storage of the sedimentary succession in northeastern BC is based on a unit-by-unit evaluation on the basis of geology, geothermal and pressure regimes, would-be phase of injected CO_2 in these units, and the presence and location of hydrocarbon reservoirs and coal beds.

Northeastern BC is rich in oil and gas (particularly the latter) as organic material was generally buried deeply and underwent maturation well beyond the oil window. The Cambrian strata contain no hydrocarbons, and the Devonian contain only gas. Oil reservoirs occur in Carboniferous and younger strata that have not been buried as deeply as the Devonian. Major gas pools are found in Middle Devonian reefal carbonate reservoirs in the north along the Presqu'ile Reef Barrier in the Elk Point Group (e.g., Yoyo, Sierra, and Klua) and along the Sulphur Point Reef Barrier in the Beaverhill Lake Group (e.g., Clarke Lake). Large gas reservoirs in the Upper Devonian are also found in the northern part of the region in the Jean Marie Formation of the Winterburn Group (e.g., Helmet North). Major gas pools in the Carboniferous are found in the southern part of the region, and oil reservoirs are present in the north. The Permian contains large oil pools at Eagle, Eagle West, and Stoddart West and gas pools at Stoddart, Stoddart West, Boundary Lake, and Fort St. John. Major oil pools are found in the Triassic (mainly in the Halfway Formation) at Boundary Lake,

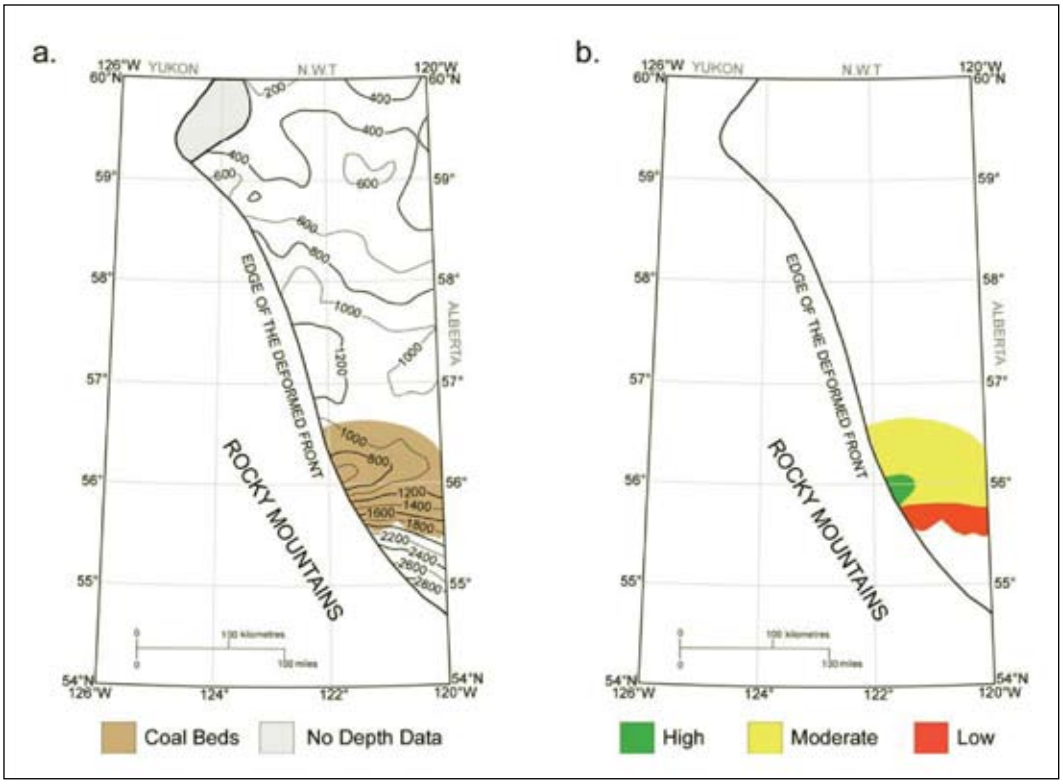

Figure 10. Area in northeastern British Columbia with potential for CO_2 storage in coal beds: a) coal distribution and depth to the top of the Bullhead Group that contains the coal beds; and b) regions of high, moderate and low storage potential based on CO_2 phase and likely coal permeability.

Peejay, Mulligan Creek, and Weasel, and major gas pools are found at Laprise, Monias, Jedney, Ring, Nig Creek, and Tommy Lakes. The Bullhead Group in the southern part of northeastern BC contains coal beds (particularly in the Gething Formation) and oil and gas pools, such as Rigel and Buick Creek. Major gas pools are found in the Paddy Formation in the deep basin toward the southern tip of the region.

Other than oil and gas reservoirs and, potentially, coal beds, CO_2 can be stored in aquifers mostly in the pre-Cretaceous sedimentary succession in northeastern BC. All of the Cambrian and Devonian aquifers (Basal Cambrian Sandstone, Keg River, Sulphur Point, Gilwood, Slave Point, Jean Marie, and Wabamun) are well confined by successive intervening aquitards (Cambrian, Elk Point, Muskeg, Waterways, Fort Simpson, Wabamun, Exshaw–Lower Banff). The solubility of CO_2 in the formation water of these aquifers is likely to be reduced as a result of high salinity and temperatures. Except for the northern part of the Jean Marie aquifer in the Winterburn Group, CO_2 will be in supercritical phase if injected into Devonian and Cambrian aquifers. Because of the high temperatures encountered in these strata, the CO_2 density will probably be relatively low, on the order of several hundred kg/m^3. Thus, buoyancy forces will be strong and CO_2 will migrate updip, although with very small velocities. In the south, depositional features around the Peace River Arch, such as Granite Wash detritus and reef buildup, create hydraulic communication between the Keg River, Gilwood, Slave Point, and Woodbend (Leduc Reefs) aquifers; however, this succession is confined by the thick shale units of the Winterburn and Wabamun Groups. In the northern part of the Jean Marie aquifer, CO_2 will be in gaseous phase, but this aquifer is well confined by the shale units of the overlying Wabamun and Exshaw–Banff aquitards.

The Carboniferous to Triassic aquifers (Carboniferous, Permian, Montney, Halfway, and Baldonnel) are partially confined by eroded intervening aquitards (Montney, Charlie Lake, Jurassic) and subcrop beneath Lower Cretaceous Bullhead Group strata in the north and northeast. However, since the entire Lower Cretaceous succession is shaly in the northern part of northeastern BC, practically all these aquifers are confined, either by intervening aquitards or by thick Cretaceous shale. Carbon dioxide injected into aquifers in this succession in the southern part of northeastern BC will be in dense liquid or supercritical phase. However, if injected into the Carboniferous in the northeast, or if it migrates there driven by buoyancy, it will change phase and become gaseous, with ever-increasing buoyancy as it moves updip. The time scale of this process is likely to be very large, unless the CO_2 finds paths of high permeability.

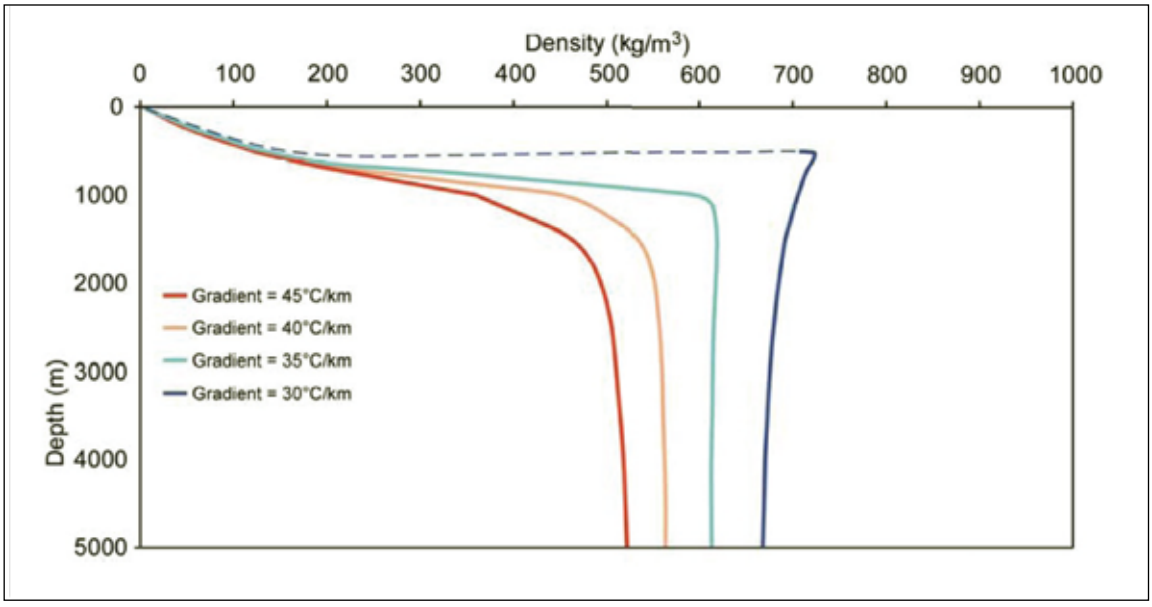

Figure 11. Variation of CO_2 density with depth assuming hydrostatic pressures and geothermal conditions characteristic of northeastern British Columbia.

The Lower Cretaceous aquifers (Bullhead, Falher, and Paddy) are only partially present in northeastern BC, and mostly in the south. The intervening and overlying aquitards (Wilrich, Harmon, Fort St. John), and their own lithofacies change into shale to the north, provide good confinement for CO_2 injected into these aquifers. Because of expected relatively low density of CO_2, the storage capacity of these aquifers is likely to be reduced. The Upper Cretaceous aquifers (Dunvegan and Cardium) are not suitable for CO_2 storage because of relatively shallow depth, low temperatures, and outcropping of these units along river valleys.

In terms of storage strategy, although northeastern BC has the potential for CO_2 storage in most of the sedimentary succession, attention should be paid to optimizing capacity. Because temperature and pressure have opposite effects on CO_2 density (Figure 6),

the effect of increasing pressure is cancelled by increasing temperature beyond certain depths (usually around 1000 to 1300 m), so that the CO_2 density increases very little with increasing depth (Figure 11). Thus, no gains in capacity are being realized by injecting CO_2 at greater depths, whereas the cost increases as a result of higher drilling and compression costs. From this point of view, CO_2 storage in Carboniferous to Lower Cretaceous strata in the south should be pursued before Devonian strata are considered. In the north, CO_2 storage should be considered only for Devonian strata.

In addition, care should be taken to avoid contamination of existing and potential energy resources, such as oil and gas reservoirs. Carbon dioxide injected close to and downdip from hydrocarbon reservoirs will migrate updip, drive buoyancy, and will accumulate in these reservoirs, thus contaminating the reservoirs' oil or gas. Thus, while most of the permeable strata in northeastern BC, whether hydrocarbon reservoirs or deep saline aquifers, are suitable for CO_2 storage, a strategy must be developed and implemented regarding the timing and location of CO_2 injection. This strategy should take into account the distribution of CO_2 sources and hydrocarbon reservoirs and the local characteristics of the sedimentary strata in the succession. In this respect, the experience of acid-gas injection in northeastern BC provides a good example of application of this strategy. Injection of acid gas (a combination of H_2S and CO_2 produced by gas plants during sour-gas desulphurization) currently occurs in the southern part of BC (Figure 12) and takes place in Carboniferous to Triassic strata, which are the best strata in terms of confinement, acid-gas phase and density, and cost of injection.

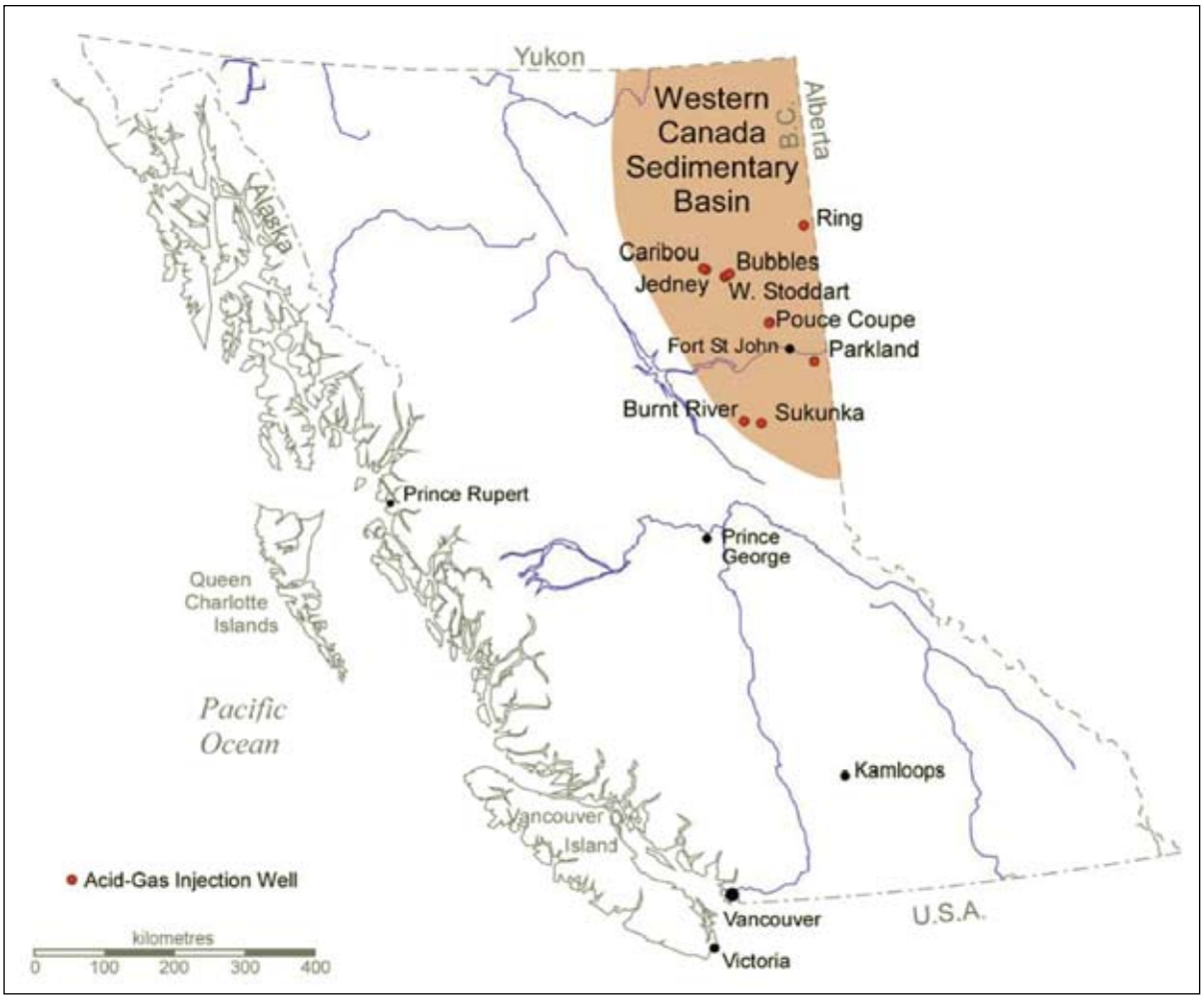

Figure 12. Location of acid-gas injection operations in northeastern British Columbia.

CONCLUSIONS

The sedimentary succession in northeastern British Columbia has significant potential for CO_2 storage in gas reservoirs and deep saline aquifers. This portion of the Western Canada Sedimentary Basin is the most suited and immediately accessible basin for geological CO_2 storage in British Columbia because this region is located in a tectonically stable area and has significant, large gas reservoirs and deep saline aquifers that are confined by thick, regional-scale shaly aquitards. In addition, there is significant infrastructure in place, there are several large CO_2 sources in the area, including high-purity sources (gas plants), and there is operational and regulatory experience with acid-gas disposal in both depleted hydrocarbon reservoirs and deep saline aquifers.

Northeastern BC has significant CO_2 storage capacity in gas reservoirs (more than 1900 Mt CO_2), of which approximately 1350 Mt CO_2 is in the largest 80 reservoirs. This capacity alone is likely sufficient to cover BC's needs for this century when considering that annual CO_2 emissions in BC are currently less than 70 Mt/year (Environment Canada, 2002), of which only about a third are from large stationary sources that are suitable for CO_2 capture and storage (CCS). If only local CO_2 sources (energy producers and paper mills) are considered, which currently are in the order of 4 to 5 Mt CO_2/year, then this storage capacity will still be available long after these sources have exhausted themselves. The CO_2 storage capacity in oil reservoirs is practically negligible at 5 Mt CO_2, and the only reason that this capacity would ever be realized is that additional oil may be produced in CO_2-EOR operations. Storage of CO_2 in coal beds does not have potential unless used in conjunction with coal gas recovery (technology that has yet to be proven), and even then it is questionable given the depth of the coal beds.

Besides gas reservoirs, northeastern BC has significant potential for CO_2 storage in deep saline aquifers. Although the storage capacity has not been quantified for a variety of reasons, a stratigraphic assessment of aquifers in the sedimentary succession, based on temperatures and pressures, indicates that the storage potential is very large. Carbon dioxide can be injected into almost all of the deep saline

aquifers in the sedimentary succession. All aquifers in the Cambrian to Lower Cretaceous succession are confined by intervening and overlying aquitards. The only aquifers that are not suitable for CO_2 storage are the shallower Upper Cretaceous Dunvegan and Cardium Formations, which crop out at river valleys as a result of Tertiary to Recent erosion. Carbon dioxide injected into Cambrian and Devonian strata will be mostly in supercritical phase, thus achieving conditions necessary for increased storage capacity. However, the high cost of injection into these very deep strata may delay their use for CO_2 storage. Carboniferous to Triassic aquifers, although they are eroded and subcrop beneath the Cretaceous strata, are well confined and are currently used for acid-gas injection in the south. Carbon dioxide injected into these strata will be in supercritical phase except for the northern part, where it will be gaseous and therefore have increased buoyancy with respect to formation water. Lower Cretaceous aquifers, present in the southern part of northeastern BC, are also suitable for CO_2 injection. Geographically, Carboniferous to Triassic aquifers are the best targets for CO_2 storage in the southern part of northeastern BC, while Devonian aquifers should be used for CO_2 storage in the northern part.

Carbon dioxide emissions in northeastern BC are likely to increase as more and deeper wells are drilled and more sour-gas reservoirs are discovered and brought into production. In the absence of economic, fiscal, or regulatory drivers, no CO_2 storage is likely to occur, but if such drivers are introduced by the provincial and/or federal governments, it is very likely that the industry will implement geological CO_2 storage in this region. Although there is great capacity and potential infrastructure for CO_2 storage in gas reservoirs, they will become available for CO_2 storage only after depletion, which, at current production rates, will occur in the next few decades. Until gas reservoirs become available, deep saline aquifers can be safely used for CO_2 storage in northeastern BC.

REFERENCES

Bachu, S., 1995: Synthesis and model of formation water flow in the Alberta basin, Canada; American Association of Petroleum Geologists Bulletin, v. 79, 1159–1178.

Bachu, S., 1997: Flow of formation waters, aquifer characteristics, and their relation to hydrocarbon accumulations, northern Alberta Basin. American Association of Petroleum Geologists Bulletin, v. 81, no. 5, 712-733.

Bachu, S., 2002: Sequestration of CO_2 in geological media in response to climate change: road map for site selection using the transform of the geological space into the CO_2 phase space. Energy Conservation and Management, v. 43, 87-102.

Bachu, S., 2003: Screening and ranking of sedimentary basins for sequestration of CO_2 in geological media. Environmental Geology, v. 44, no. 3, 277-289.

Bachu, S., 2005: British Columbia's Potential for Geological Sequestration of CO_2 and Acid Gas towards Reducing Atmospheric CO_2 Emissions, Report to the BC Ministry of Energy and Mines, 74 p.

Bachu, S. and R.A. Burwash, 1991, Regional-scale analysis of the geothermal regime in the Western Canada Sedimentary Basin; Geothermics, v. 20, 387–407.

Bachu, S. and J.C. Shaw, 2003: Evaluation of the CO_2 sequestration capacity in Alberta's oil and gas reservoirs at depletion and the effect of underlying aquifers. Journal of Canadian Petroleum Technology, v. 42, no. 9, 51-61.

Bachu, S. and J.C. Shaw, 2005: CO_2 storage in oil and gas reservoirs in western Canada: Effect of aquifers, potential for CO_2-flood enhanced oil recovery and practical capacity. Proceedings of the 7th International Conference on Greenhouse Gas Control Technologies (GHGT-7), Volume 1: Peer-Reviewed Papers and Overviews (E.S. Rubin, D.W. Keith and C.F. Gilboy, eds.), Elsevier, 361-369.

Bachu, S. and S. Stewart, 2002: Geological sequestration of anthropogenic carbon dioxide in the Western Canada Sedimentary basin: Suitability analysis. Journal of Canadian Petroleum Technology, v. 41, no. 2, 32-40.

Bachu, S., J.C. Shaw, and R.M. Pearson, 2004: Estimation of oil recovery and CO_2 storage capacity in CO_2-EOR incorporating the effect of underlying aquifers. SPE Paper 89340, presented at the Fourteenth SPE/DOE Improved Oil Recovery Symposium, Tulsa, OK, April 17-21, 2004, 13 p.

Bennion, B. and S. Bachu, 2005: Relative permeability characteristics for CO_2 displacing water in a variety of potential sequestration zones in the Western Canada Sedimentary Basin, Paper SPE 95547, presented at the 2005 SPE Technical Conference and Exhibition, Dallas, TX, October 9-12, 2005, 15 p.

Bondor, P.L., 1992: Applications of carbon dioxide in enhanced oil recovery, Energy Conversion and Management, v. 33, 579–586.

Bradshaw, J.B. and T. Dance, 2005: Mapping geological storage prospectivity of CO_2 for the world sedimentary basins and regional source to sink matching. Proceedings of the 7th International Conference on Greenhouse Gas Control Technologies (GHGT-7), Volume 1: Peer-Reviewed Papers and Overviews (E.S. Rubin, D.W. Keith and C.F. Gilboy, eds.), Elsevier, 583-591.

British Columbia Ministry of Water, Land and Air Protection, 2004: Weather, climate and the future: BC's plan. 42 p.

Clarkson, C.R. and R.M. Bustin, 1997: The effect of methane gas concentration, coal composition and pore structure upon gas transport in Canadian coals: Implications for reservoir characterization. Proceedings of International Coalbed Methane Symposium, University of Alabama, Tuscaloosa, Alabama, 12-17 May 1997, 1-11.

Doughty, C. and K. Pruess, 2004: Modeling supercritical carbon dioxide injection in heterogeneous porous media, Vadose Zone Journal, v. 3, no. 3, 837-847.

Environment Canada, 2002: Canada's Greenhouse Gas Inventory 1990-2000. Greenhouse Gas Division, EPS 5/AP/8, Environment Canada, ISBN 0-660-18894-5, 149 p.

Gunter, W.D., M.J. Mavor, and J.R. Robinson, 2005: CO_2 stor-

age and enhanced methane production: field testing at Fenn-Big Valley, Alberta, Canada, with application. Proceedings of the 7th International Conference on Greenhouse Gas Control Technologies (GHGT-7), Volume 1: Peer-Reviewed Papers and Overviews (E.S. Rubin, D.W. Keith and C.F. Gilboy, eds.), Elsevier, 413-421.

Hadlow, R.E., 1992: Update of industry experience with CO_2 injection, SPE Paper 24928, presented at the Sixty Seventh SPE Annual Technical Conference, October 4-7, 1992, Washington, D.C., 10 p.

Hitchon, B., S. Bachu and J.R. Underschultz, 1989: Regional subsurface hydrogeology, Peace River Arch area, Alberta and British Columbia; Bulletin of Canadian Petroleum Geology, v. 38A, 196–217.

Holloway, S., C.J. Vincent, M.S. Bentham and K.L. Kirk, 2006: Top-down and bottom-up estimates of CO_2 storage capacity in the UK sector of the Southern North Sea Basin, Environmental Geosciences, In press.

Holt, T., J.I. Jensen and E. Lindeberg, 1995: Underground storage of CO_2 in aquifers and oil reservoirs, Energy Conversion and Management, v. 36, 535–538.

IEA (International Energy Agency), 2004: Prospects for CO_2 Capture and Storage, IEA/OECD, Paris, France, 249 p.

IPCC (Intergovernmental Panel on Climate Change), 2005: IPCC Special Report on Carbon Dioxide Capture and Storage (B. Metz, O. Davidson, H.C. de Coninck, M. Loos and L.A. Mayer, eds.), Cambridge University Press, Cambridge, U.K., and New York, NY, U.S.A., 442 p.

Koide, H.G., Y. Tazaki, Y. Noguchi, M. Iijima, K. Ito and Y. Shindo, 1993: Underground storage of carbon dioxide in depleted natural gas reservoirs and useless aquifers. Engineering Geology, v. 34, 175-179.

Kovscek, A.R., 2002: Screening criteria for CO_2 storage in oil reservoirs, Petroleum Science and Technology, v. 20, no. 7-8, p. 841-866.

Kumar, A., M.H. Noh, K. Sepehrnoori, G.A. Pope, S.L. Bryant and L.W. Lake, 2005: Simulating CO_2 storage in deep saline aquifers. Carbon Dioxide Capture for Storage in Deep Geologic Formations—Results from the CO_2 Capture Project, Volume. 2: Geologic Storage of Carbon Dioxide with Monitoring and Verification, (Benson, S.M., ed.), Elsevier, London, UK, 977-898.

Larsen, J.W., 2003: The effects of dissolved CO_2 on coal structure and properties. International Journal of Coal Geology, v. 57, 63-70.

Lasater, J.A., 1958: Bubble point pressure correlation; Transactions AIME, v. 213, 379-381.

Masters, J. A., 1979: Deep basin gas trap, western Canada; American Association of Petroleum Geologists Bulletin, v. 63, 152–181.

Michael, K. and S. Bachu, 2001: Fluids and pressure distributions in the foreland-basin succession in the west-central part of the Alberta basin: evidence for permeability barriers and hydrocarbon generation and migration; American Association of Petroleum Geologists Bulletin, v. 85, 1231–1252.

Mossop, G.D. and I. Shetsen, 1994: Geological Atlas of the Western Canada Sedimentary Basin; Canadian Society of Petroleum Geologists and Alberta Research Council, Calgary, 514 p.

Mungan, N., 1981: Carbon dioxide flooding – fundamentals; Journal of Canadian Petroleum Technology, v. 20, no. 1, 87-92.

Perkins, E., I. Czernichowski-Lauriol, M. Azaroual, P. Durst, 2005: Long term predictions of CO_2 storage by mineral and solubility trapping in the Weyburn Midale Reservoir. Proceedings of the 7th International Conference on Greenhouse Gas Control Technologies (GHGT-7), Volume II, Part 2: Poster Papers (M. Wilson, T. Morris, J. Gale and K. Thambimuthu, eds.), 2093-2096.

Shaw, J. and S. Bachu, 2002: Screening, evaluation, and ranking of oil reservoirs suitable for CO_2-flood EOR and carbon dioxide sequestration, Journal of Canadian Petroleum Technology, v. 41, no. 9, 51–61.

Span, P. and W. Wagner, 1996: A new equation of state for carbon dioxide covering the fluid region from the triple-point temperature to 1100 K at pressures up to 800 MPa. Journal of Chemical Reference Data, v. 25, no. 6, 1509-1596.

Stephenson, D.J., A.G. Graham and R.W. Luhning, 1993: Mobility control experience in the Joffre Viking miscible CO_2 flood, SPE Reservoir Engineering, v. 8, no. 3, 183–188.

Stevens, S.H., V.A. Kuuskra and J. Gale, 2001: Sequestration of CO_2 in depleted oil & gas fields: global capacity, costs and barriers. Proceedings of the 5th International Conference on Greenhouse Gas Control Technologies (GHG- 5), (D.J. Williams, R.A. Durie, P. McMullan, C.A.J. Paulson and A.Y. Smith, eds.), CSIRO Publishing, Collingwood, VIC, Australia, 278-283.

Taber, J.J., F.D. Martin and R.S. Seright, 1997: EOR screening criteria revisited – part 1: introduction to screening criteria and enhanced recovery field projects, SPE Reservoir Engineering, v. 12, no. 3, 189–198.

Turkenburg, W.C., 1997: Sustainable development, climate change, and carbon dioxide removal (CDR). Energy Conversion and Management, v. 38S, S3-S12.

van der Meer, L.G.H., 1993: The conditions limiting CO_2 storage in aquifers. Energy Conversion and Management, v. 34, 959-966.

Voormeij, D.A. and G.J. Simandl, 2005: Options for sequestration of CO_2 from major stationary point sources, British Columbia, Canada. Proceedings of the 7th International Conference on Greenhouse Gas Control Technologies (GHGT-7), Volume 1: Peer-Reviewed Papers and Overviews (E.S. Rubin, D.W. Keith and C.F. Gilboy, eds.), Elsevier, 611-619.

Winter, E.M. and P.D. Bergman, 1993: Availability of depleted oil and gas reservoirs for disposal of carbon dioxide in the United States, Energy Conversion and Management, v. 34, no. 9-11, 1177–1187.

Xu, T., J.A. Apps and K. Pruess, 2003: Reactive geochemical transport simulation to study mineral trapping for CO_2 disposal in deep arenaceous formations. Journal of Geophysical Research, v. 108(B2), 2071–2084.

APPENDIX A

OIL RESERVOIRS IN NORTHEASTERN BC THAT LACK CRITICAL DATA NEEDED FOR CALCULATING CO_2 STORAGE CAPACITY.

Field Code	Pool Code	Field Name	Pool Name	Pool Sequence	Area (ha)	Net Pay (m)	Water Saturation	Porosity	Shrinkage
3560	4800	FLATROCK	HALFWAY	F			0.441000015	0.114	0.787401557
3580	4520	FLATROCK WEST	CECIL	C		0.800000012	0.324000001	0.134000003	0.843881845
3600	2700	FORT ST JOHN	GETHING	A					0.875656724
2020	4540	BOUNDARY LAKE NORTH	COPLIN	F	378	0.300000012	0.326999992	0.093999997	
380	4582	BEAR FLAT	BEAR FLAT	A			0.138999999	0.149000004	0.832639456
380	4582	BEAR FLAT	BEAR FLAT	D		1.600000024	0.368000001	0.064000003	0.832639456
1400	4500	BLUEBERRY	CHARLIE LAKE	A	71	2	0.224999994	0.119999997	
1400	4900	BLUEBERRY	DOIG	A	71	4	0.300000012	0.059999999	
2820	4800	BULRUSH	HALFWAY	B					0.807102501
2920	2600	CACHE CREEK	BLUESKY	C	66	4.699999809	0.479999989	0.090999998	
2985	4800	CHINCHAGA RIVER	HALFWAY	A	70	2.299999952	0.230000004	0.181999996	
3440	6250	EAGLE	BELLOY-KISKATINAW			4.949999809	0.218500003	0.120000005	0.77519381
3445	6200	EAGLE WEST	BELLOY	A		5	0.286500007	0.122499995	0.774593353
4925	4575	INGA SOUTH	INGA	A					0.74850297
5150	8200	JUNIOR	JEAN MARIE	A	68	4.400000095	0.017999999	0.057	
5600	4540	LAPRISE CREEK	COPLIN	A		0.699999988	0.192000002	0.105999999	
5600	4540	LAPRISE CREEK	COPLIN	B		0.600000024	0.123999998	0.108999997	
6490	2700	OSBORN	GETHING	C	74	2	0.305999994	0.209000006	
6500	4800	OSPREY	HALFWAY	G	71	1.200000048	0.514999986	0.174999997	
6530	4520	OWL	CECIL	A		1.400000095	0.289499998	0.142499998	0.802568197
7275	4520	PLUTO	CECIL	A	66	1.5	0.25	0.123000003	
7600	2900	RIGEL	DUNLEVY	A					0.870322049
7600	2900	RIGEL	DUNLEVY	B			0.180000007	0.109999999	0.870322049
7860	4100	SIPHON EAST	BALDONNEL	B	66	4.900000095	0.317999989	0.144999996	
8060	7250	STODDART SOUTH	KISKATINAW	A	65	6.800000191	0.349999994	0.050999999	
8100	4100	STODDART WEST	BALDONNEL	C	66	9.100000381	0.398999989	0.090999998	
8100	4582	STODDART WEST	BEAR FLAT	C	66	1	0.165999994	0.074000001	
8200	4800	TWO RIVERS	HALFWAY	D	65	4	0.361999989	0.177000001	
8240	2630	VELMA	BLUESKY-GETHING			1.5	0.432000011	0.135000005	0.89445436
8300	4520	WEASEL	CECIL	C	70	1	0.432999998	0.126000002	
8300	4805	WEASEL	LOWER HALFWAY	A					0.83822298
8360	4535	WILDER	BOUNDARY LAKE	B	65	0.899999976	0.349999994	0.119999997	
9000	4535	OTHER AREAS	BOUNDARY LAKE	09-22-083-14-W6M		3	0.310000002	0.090000004	0.802568197
9000	4535	OTHER AREAS	BOUNDARY LAKE	16-35-083-15-W6M		3	0.310000002	0.090000004	0.802568197

APPENDIX B

GAS RESERVOIRS IN NORTHEASTERN BC THAT LACK ORIGINAL GAS IN PLACE (OGIP), PRESSURE AND TEMPERATURE DATA NEEDED FOR CALCULATING CO_2 STORAGE CAPACITY.

Field Code	Pool Code	Field Name	Pool Name	Pool Seq.	Drive Mechanism
380	4582	BEAR FLAT	BEAR FLAT	B	ASSOCIATED
380	4582	BEAR FLAT	BEAR FLAT	D	ASSOCIATED
700	4805	BEAVERDAM	LOWER HALFWAY	A	ASSOCIATED
760	4800	BEAVERTAIL	HALFWAY	K	ASSOCIATED
1260	4100	BIRCH	BALDONNEL	C	ASSOCIATED
1280	4800	BIRLEY CREEK	HALFWAY	F	ASSOCIATED
1280	4800	BIRLEY CREEK	HALFWAY	H	ASSOCIATED
1400	4900	BLUEBERRY	DOIG	A	ASSOCIATED
1880	6200	BOUDREAU	BELLOY	B	ASSOCIATED
1880	6200	BOUDREAU	BELLOY	C	ASSOCIATED
2000	4535	BOUNDARY LAKE	BOUNDARY LAKE	A	ASSOCIATED
2000	4805	BOUNDARY LAKE	LOWER HALFWAY	A	ASSOCIATED
2000	4805	BOUNDARY LAKE	LOWER HALFWAY	B	ASSOCIATED
2000	6300	BOUNDARY LAKE	TAYLOR FLAT	A	ASSOCIATED
2020	4900	BOUNDARY LAKE NORTH	DOIG	A	ASSOCIATED
2020	4900	BOUNDARY LAKE NORTH	DOIG	D	ASSOCIATED
2020	4900	BOUNDARY LAKE NORTH	DOIG	E	ASSOCIATED
2240	4540	BUBBLES NORTH	COPLIN	A	ASSOCIATED
2400	2900	BUICK CREEK	DUNLEVY	L	ASSOCIATED
2400	2900	BUICK CREEK	DUNLEVY	P	ASSOCIATED
2400	4580	BUICK CREEK	NORTH PINE	D	ASSOCIATED
2400	4805	BUICK CREEK	LOWER HALFWAY	N	ASSOCIATED
2400	4805	BUICK CREEK	LOWER HALFWAY	O	ASSOCIATED
2400	4805	BUICK CREEK	LOWER HALFWAY	S	ASSOCIATED
2400	4805	BUICK CREEK	LOWER HALFWAY	T	ASSOCIATED
2400	4805	BUICK CREEK	LOWER HALFWAY	U	ASSOCIATED
2700	2900	BUICK CREEK NORTH	DUNLEVY	U	ASSOCIATED
2920	4900	CACHE CREEK	DOIG	C	ASSOCIATED
2920	4900	CACHE CREEK	DOIG	E	ASSOCIATED
2920	4900	CACHE CREEK	DOIG	F	ASSOCIATED
2920	4900	CACHE CREEK	DOIG	H	ASSOCIATED
2960	4510	CECIL LAKE	SIPHON	A	ASSOCIATED
2960	4520	CECIL LAKE	CECIL	A	ASSOCIATED
2960	4580	CECIL LAKE	NORTH PINE	B	ASSOCIATED
3300	4800	CURRANT	HALFWAY	D	ASSOCIATED
3440	2700	EAGLE	GETHING	A	ASSOCIATED
3445	6200	EAGLE WEST	BELLOY	C	ASSOCIATED
3520	2600	FIREBIRD	BLUESKY	F	ASSOCIATED
3540	4900	FIREWEED	DOIG	A	ASSOCIATED
3540	4900	FIREWEED	DOIG	B	ASSOCIATED
3560	6200	FLATROCK	BELLOY	A	ASSOCIATED
3580	4520	FLATROCK WEST	CECIL	B	ASSOCIATED
3600	6200	FORT ST JOHN	BELLOY	B	ASSOCIATED
4390	4520	GROUNDBIRCH	CECIL	A	ASSOCIATED
4600	4575	HALFWAY	INGA	A	ASSOCIATED
4600	4800	HALFWAY	HALFWAY	B	ASSOCIATED

APPENDIX B CONTINUED.

Field Code	Pool Code	Field Name	Pool Name	Pool Seq.	Drive Mechanism
4600	7400	HALFWAY	DEBOLT	A	ASSOCIATED
4650	2600	HAY RIVER	BLUESKY	B	ASSOCIATED
5600	4540	LAPRISE CREEK	COPLIN	A	ASSOCIATED
5600	4540	LAPRISE CREEK	COPLIN	B	ASSOCIATED
5860	4545	MICA	MICA	A	ASSOCIATED
6200	4520	MONTNEY	CECIL	B	ASSOCIATED
6230	4800	MUSKRAT	HALFWAY	E	ASSOCIATED
6230	4805	MUSKRAT	LOWER HALFWAY	A	ASSOCIATED
6460	4520	OAK	CECIL	B	ASSOCIATED
6460	4520	OAK	CECIL	I	ASSOCIATED
6460	4520	OAK	CECIL	K	ASSOCIATED
6530	4520	OWL	CECIL	A	ASSOCIATED
6800	4800	PEEJAY	HALFWAY	R	ASSOCIATED
7000	4800	PEEJAY WEST	HALFWAY	D	ASSOCIATED
7400	4900	RED CREEK	DOIG	C	ASSOCIATED
7600	2900	RIGEL	DUNLEVY	B	ASSOCIATED
7600	2900	RIGEL	DUNLEVY	D	ASSOCIATED
7600	4520	RIGEL	CECIL	B	ASSOCIATED
7600	4520	RIGEL	CECIL	G	ASSOCIATED
7600	4520	RIGEL	CECIL	I	ASSOCIATED
8000	4520	STODDART	CECIL	B	ASSOCIATED
8000	4520	STODDART	CECIL	J	ASSOCIATED
8000	4580	STODDART	NORTH PINE	E	ASSOCIATED
8000	4580	STODDART	NORTH PINE	G	ASSOCIATED
8000	6200	STODDART	BELLOY	C	ASSOCIATED
8060	6200	STODDART SOUTH	BELLOY	A	ASSOCIATED
8060	6200	STODDART SOUTH	BELLOY	C	ASSOCIATED
8100	4100	STODDART WEST	BALDONNEL	C	ASSOCIATED
8100	4520	STODDART WEST	CECIL	B	ASSOCIATED
8100	4582	STODDART WEST	BEAR FLAT	D	ASSOCIATED
8100	4900	STODDART WEST	DOIG	B	ASSOCIATED
8100	6200	STODDART WEST	BELLOY	L	ASSOCIATED
8130	4520	SUNSET PRAIRIE	CECIL	A	ASSOCIATED
8130	4520	SUNSET PRAIRIE	CECIL	C	ASSOCIATED
8240	2630	VELMA	BLUESKY-GETHING	N/A	ASSOCIATED
8300	2700	WEASEL	GETHING	B	ASSOCIATED
8300	4800	WEASEL	HALFWAY	K	ASSOCIATED
8400	4800	WILDMINT	HALFWAY	I	ASSOCIATED
8900	4610	ZAREMBA	A MARKER/BASE OF LIME	K	ASSOCIATED
8900	4610	ZAREMBA	A MARKER/BASE OF LIME	M	ASSOCIATED
8900	4610	ZAREMBA	A MARKER/BASE OF LIME	N	ASSOCIATED

APPENDIX C

LIST OF OIL RESERVOIRS IN NORTHEASTERN BC THAT ARE SUITABLE FOR CO_2-ENHANCED OIL RECOVERY, SHOWING ALSO THE ESTIMATED ADDITIONAL RECOVERABLE OIL AND CO_2 STORAGE CAPACITY.

Field Code	Pool Code	Field Name	Pool Name	Pool Sequence	OOIP ($1000\ m^3$)	Recovery Factor	OOIP * Oil Recovery @ 0.50 PV CO_2 Injection ($1000\ m^3$)	CO_2 Storage Mass (tonnes) at @ 0.50 PV CO_2 Injection
200	2700	AITKEN CREEK	GETHING	A	2233.5	0.600	356.708	277549.1
380	4582	BEAR FLAT	BEAR FLAT	B	159.8	0.150	16.406	27239.3
1260	4100	BIRCH	BALDONNEL	C	3666.9	0.200	397.716	461208.4
1260	4100	BIRCH	BALDONNEL	G	185.6	0.040	17.969	25758.6
1280	4800	BIRLEY CREEK	HALFWAY	F	193.0	0.100	19.040	18093.3
1400	7400	BLUEBERRY	DEBOLT	E	1334.0	0.246	175.490	293459.9
1800	7400	BLUEBERRY WEST	DEBOLT	B	195.4	0.200	27.929	44510.2
1800	7400	BLUEBERRY WEST	DEBOLT	C	643.6	0.200	91.018	158816.5
1880	6200	BOUDREAU	BELLOY	A	387.8	0.100	70.032	100260.5
1880	6200	BOUDREAU	BELLOY	B	206.2	0.100	38.606	51810.3
1880	6200	BOUDREAU	BELLOY	C	386.5	0.100	66.937	95334.8
2000	6200	BOUNDARY LAKE	BELLOY	L	764.1	0.063	127.049	176753.2
2000	4800	BOUNDARY LAKE	HALFWAY	H	220.5	0.100	33.519	43092.8
2000	4800	BOUNDARY LAKE	HALFWAY	K	237.0	0.200	32.226	27866.7
2000	4800	BOUNDARY LAKE	HALFWAY		2939.2	0.211	430.435	535488.4
2000	4805	BOUNDARY LAKE	LOWER HALFWAY	B	362.3	0.200	49.395	42532.6
2000	6300	BOUNDARY LAKE	TAYLOR FLAT	A	190.0	0.200	19.397	43227.4
2020	4900	BOUNDARY LAKE NORTH	DOIG	A	720.8	0.200	125.378	94396.8
2020	4900	BOUNDARY LAKE NORTH	DOIG	C	204.5	0.150	33.913	26518.4
2020	4900	BOUNDARY LAKE NORTH	DOIG	D	263.4	0.200	49.535	28686.0
2020	4900	BOUNDARY LAKE NORTH	DOIG	F	204.9	0.150	31.501	37470.5
2020	4800	BOUNDARY LAKE NORTH	HALFWAY	D	424.7	0.150	49.120	46244.3
2020	4800	BOUNDARY LAKE NORTH	HALFWAY	I	941.7	0.200	108.954	87167.8
2400	4100	BUICK CREEK	BALDONNEL	A	253.6	0.200	19.690	30862.3
2400	2900	BUICK CREEK	DUNLEVY	A	464.4	0.050	50.171	42468.3
2400	2900	BUICK CREEK	DUNLEVY	P	184.6	0.200	19.527	28152.2
2400	4805	BUICK CREEK	LOWER HALFWAY	A	542.0	0.150	84.378	135287.4

APPENDIX C CONTINUED.

Field Code	Pool Code	Field Name	Pool Name	Pool Sequence	OOIP ($1000\ m^3$)	Recovery Factor	OOIP * Oil Recovery @ 0.50 PV CO_2 Injection ($1000\ m^3$)	CO_2 Storage Mass (tonnes) at @ 0.50 PV CO_2 Injection
2400	4805	BUICK CREEK	LOWER HALFWAY	B	1080.1	0.150	168.319	270699.6
2400	4805	BUICK CREEK	LOWER HALFWAY	C	6821.5	0.150	1050.055	1516171.2
2400	4805	BUICK CREEK	LOWER HALFWAY	D	3393.5	0.150	514.750	802503.7
2400	4805	BUICK CREEK	LOWER HALFWAY	E	1844.0	0.100	294.778	425776.4
2400	4805	BUICK CREEK	LOWER HALFWAY	I	1636.8	0.125	245.591	355709.8
2400	4805	BUICK CREEK	LOWER HALFWAY	J	2701.3	0.150	414.232	632467.8
2400	4805	BUICK CREEK	LOWER HALFWAY	L	561.4	0.200	82.205	112928.4
2400	4805	BUICK CREEK	LOWER HALFWAY	N	508.7	0.050	74.852	107395.2
2400	4805	BUICK CREEK	LOWER HALFWAY	O	901.5	0.150	136.678	198179.0
2400	4805	BUICK CREEK	LOWER HALFWAY	S	273.9	0.200	42.501	63898.6
2400	4805	BUICK CREEK	LOWER HALFWAY	U	1038.1	0.150	153.895	222467.0
2920	4900	CACHE CREEK	DOIG	C	820.1	0.050	196.379	295316.2
2960	4520	CECIL LAKE	CECIL	B	266.3	0.087	26.758	52431.5
2960	4520	CECIL LAKE	CECIL	E	278.5	0.200	25.054	44465.9
2960	4580	CECIL LAKE	NORTH PINE	A	732.2	0.254	84.720	148344.4
2960	4580	CECIL LAKE	NORTH PINE	C	605.9	0.200	63.691	120625.0
2960	4510	CECIL LAKE	SIPHON	A	358.3	0.360	34.826	48721.5
3425	4100	DOE	BALDONNEL	B	411.6	0.200	41.680	82179.0
3426	4800	DOIG RAPIDS	HALFWAY	C	343.9	0.100	40.532	30180.2
3426	4040	DOIG RAPIDS	NORDEGG-BALDONNEL	F	194.3	0.100	15.761	13543.1
3440	6200	EAGLE	BELLOY	A	188.0	0.050	31.656	37700.6
3440	2700	EAGLE	GETHING	A	186.3	0.110	27.310	39829.0
3445	6200	EAGLE WEST	BELLOY	C	354.9	0.200	57.564	65638.1
3445	6200	EAGLE WEST	BELLOY	D	308.4	0.200	54.300	76274.8
3445	5000	EAGLE WEST	MONTNEY	A	333.8	0.200	85.038	98420.1
3540	4805	FIREWEED	LOWER HALFWAY	A	978.2	0.200	152.130	187071.1
3560	6200	FLATROCK	BELLOY	A	311.9	0.200	53.504	75272.9
3560	4535	FLATROCK	BOUNDARY LAKE	B	494.3	0.135	34.043	87584.4
3560	4800	FLATROCK	HALFWAY	E	1159.9	0.140	164.136	207393.9
3560	4800	FLATROCK	HALFWAY	J	412.1	0.200	50.303	47096.8

Field Code	Pool Code	Field Name	Pool Name	Pool Sequence	OOIP (1000 m^3)	Recovery Factor	OOIP * Oil Recovery @ 0.50 PV CO_2 Injection (1000 m^3)	CO_2 Storage Mass (tonnes) at @ 0.50 PV CO_2 Injection
3580	4533	FLATROCK WEST	FLATROCK	A	187.7	0.005	17.991	26228.5
3580	4800	FLATROCK WEST	HALFWAY	D	2007.2	0.175	270.196	280612.0
3580	4580	FLATROCK WEST	NORTH PINE	A	175.1	0.050	16.681	24781.1
3600	6200	FORT ST JOHN	BELLOY	B	229.3	0.023	39.321	57771.5
3600	6200	FORT ST JOHN	BELLOY	G	205.5	0.175	36.619	60683.2
3600	4580	FORT ST JOHN	NORTH PINE	A	663.1	0.501	84.166	141507.6
3600	4580	FORT ST JOHN	NORTH PINE	C	165.1	0.350	18.070	30175.7
4100	2600	GOOSE	BLUESKY	A	226.3	0.200	25.641	53279.0
4600	4800	HALFWAY	HALFWAY	B	800.4	0.200	130.277	202172.5
5860	4545	MICA	MICA	A	1026.0	0.300	107.051	238843.1
5880	2600	MIKE	BLUESKY	A	974.0	0.075	85.247	86737.6
6020	4800	MILLIGAN CREEK WEST	HALFWAY	I	579.0	0.100	62.329	36935.9
6200	4800	MONTNEY	HALFWAY	C	214.1	0.013	29.464	38408.0
6230	4800	MUSKRAT	HALFWAY	D	239.8	0.090	29.153	35550.4
6230	4800	MUSKRAT	HALFWAY	E	377.9	0.070	46.153	56164.0
6230	4800	MUSKRAT	HALFWAY		584.4	0.149	74.350	65701.1
6230	4805	MUSKRAT	LOWER HALFWAY	B	370.1	0.200	49.183	58088.6
6230	4805	MUSKRAT	LOWER HALFWAY	C	359.4	0.200	45.246	46576.8
6400	4100	NIG CREEK	BALDONNEL	A	220.7	0.100	19.092	22830.6
6400	4100	NIG CREEK	BALDONNEL	D	1056.6	0.100	86.213	108716.3
6460	4100	OAK	BALDONNEL	E	186.0	0.150	11.984	21488.3
6460	4100	OAK	BALDONNEL	H	309.2	0.200	24.540	33972.0
6460	4800	OAK	HALFWAY	B	1883.1	0.200	256.615	345879.9
6460	4800	OAK	HALFWAY	C	341.4	0.002	40.268	45502.1
6460	4805	OAK	LOWER HALFWAY	A	245.8	0.020	28.892	42289.2
6500	4800	OSPREY	HALFWAY	A	201.0	0.400	20.374	18988.5
6500	4800	OSPREY	HALFWAY	D	691.7	0.100	74.906	59873.1
6500	4800	OSPREY	HALFWAY	E	305.6	0.200	30.480	28184.0
6500	4800	OSPREY	HALFWAY	H	188.7	0.002	22.239	14994.8
6500	4800	OSPREY	HALFWAY	K	512.6	0.150	52.953	46602.6

APPENDIX C CONTINUED.

Field Code	Pool Code	Field Name	Pool Name	Pool Sequence	OOIP ($1000\ m^3$)	Recovery Factor	OOIP * Oil Recovery @ 0.50 PV CO_2 Injection ($1000\ m^3$)	CO_2 Storage Mass (tonnes) at @ 0.50 PV CO_2 Injection
9000	4100	OTHER AREAS	BALDONNEL	D-060-D/094-A-16	310.8	0.002	24.861	24088.0
6800	4800	PEEJAY	HALFWAY	L	201.7	0.060	20.965	24810.3
6800	4800	PEEJAY	HALFWAY	R	290.4	0.150	28.993	24747.6
7400	4900	RED CREEK	DOIG	B	300.9	0.150	63.565	86498.5
7410	4900	RED CREEK NORTH	DOIG	B	575.3	0.200	122.141	130011.8
7600	2900	RIGEL	DUNLEVY	E	290.6	0.200	34.030	26600.6
7600	4800	RIGEL	HALFWAY	DD	333.3	0.200	38.457	32341.2
7600	4800	RIGEL	HALFWAY	F	365.3	0.200	45.085	33508.5
7600	4800	RIGEL	HALFWAY	H	702.9	0.150	85.402	114079.6
7600	4800	RIGEL	HALFWAY	I	265.8	0.200	30.538	33872.7
7600	4800	RIGEL	HALFWAY	O	411.0	0.200	48.801	42484.5
7600	4800	RIGEL	HALFWAY	T	236.5	0.200	29.177	28945.7
7620	2700	RIGEL EAST	GETHING	A	173.4	0.115	20.834	14611.5
7750	4800	SEPTIMUS	HALFWAY	C	189.2	0.200	31.154	39014.9
7900	4580	SQUIRREL	NORTH PINE	A	174.5	0.250	17.930	26316.5
8000	6200	STODDART	BELLOY	C	1169.5	0.150	189.542	254101.8
8000	4520	STODDART	CECIL	A	187.2	0.065	12.022	33428.0
8000	4520	STODDART	CECIL	B	183.5	0.200	14.002	35631.0
8000	4580	STODDART	NORTH PINE	F	528.3	0.201	55.273	75062.5
8000	4580	STODDART	NORTH PINE	G	192.0	0.200	21.032	28478.5
8060	6200	STODDART SOUTH	BELLOY	A	980.1	0.154	162.517	211944.8
8060	6200	STODDART SOUTH	BELLOY	C	305.1	0.049	54.352	68602.6
8100	6200	STODDART WEST	BELLOY	C	8865.2	0.234	1345.867	1771182.2
8100	6200	STODDART WEST	BELLOY	E	190.5	0.100	31.865	38968.9
8100	6200	STODDART WEST	BELLOY	L	1272.0	0.100	186.571	252716.1
8100	4900	STODDART WEST	DOIG	A	663.3	0.200	148.595	165640.1
8100	4900	STODDART WEST	DOIG	B	548.7	0.200	119.759	155161.4
8100	4805	STODDART WEST	LOWER HALFWAY	A	172.2	0.180	26.492	41255.5
8100	4805	STODDART WEST	LOWER HALFWAY	B	1606.5	0.200	182.737	392423.6
8200	4800	TWO RIVERS	HALFWAY	B	406.1	0.025	60.037	84149.7
8700	4800	WOLF	HALFWAY	A	1241.0	0.300	144.498	120452.5

APPENDIX D

OIL AND GAS RESERVOIRS IN NORTHEASTERN BC THAT HAVE AN ESTIMATED CO_2- STORAGE CAPACITY GREATER THAN 1 MT CO_2. FOR OIL RESERVOIRS, THE STORAGE CAPACITY IN EOR AT DEPLETION AND IN TOTAL IS GIVEN. IF AN OIL POOL IS ASSOCIATED WITH A GAS POOL, THEN THE TOTAL CAPACITY IS THE SUM OF THE TWO, OTHERWISE THE TOTAL CAPACITY IS EQUAL TO THE CAPACITY OF THE RESPECTIVE OIL OR GAS POOL.

Field Code	Pool Code	Field Name	Pool Name	Pool Seq.	Longitude	Latitude	Depth (m)	Oil Reservoirs			Gas Reservoirs CO_2 Capacity (tonnes)	Combined Pool Capacity (tonnes)
								Mass CO_2 @ EOR (tonnes)	Effective Mass CO_2 (tonnes)	Total CO_2 capacity (tonnes)		
50	8400	ADSETT	SLAVE POINT	A	-122.690620	58.110417	2497.2				3,590,369	3,590,369
50	8400	ADSETT	SLAVE POINT	B	-122.630476	58.166799	2560.6				2,393,105	2,393,105
210	2600	AITKEN CREEK NORTH	BLUESKY	A	-122.008487	57.035382	1272.5				3,149,322	3,149,322
320	2600	ALTARES	BLUESKY	A	-122.029607	56.335368	899.8				1,370,348	1,370,348
320	2600	ALTARES	BLUESKY	B	-122.152527	56.384763	1009.2				1,151,589	1,151,589
350	7340	ATTACHIE	BASAL KISKATINAW	A	-121.442128	56.310703	2056.5				2,460,889	2,460,889
380	4800	BEAR FLAT	HALFWAY	B	-121.091729	56.318201	1618.9				1,850,753	1,850,753
740	8580	BEAVER RIVER	NAHANNI	A	-124.359374	59.926890	3830.4				8,251,410	8,251,410
700	4798	BEAVERDAM	UPPER HALFWAY	A	-120.453120	56.947917	1123.3				1,195,482	1,195,482
760	2600	BEAVERTAIL	BLUESKY	A	-120.863504	56.833882	1017.0				4,288,802	4,288,802
760	4800	BEAVERTAIL	HALFWAY	E	-120.725520	56.828757	1233.6				1,112,678	1,112,678
800	4100	BEG	BALDONNEL	A	-122.252229	57.100311	1342.5				5,903,633	5,903,633
800	4100	BEG	BALDONNEL	C	-122.419275	57.254051	1454.8				2,648,988	2,648,988
800	4800	BEG	HALFWAY	A	-122.240620	57.089583	1572.0				17,898,670	17,898,670
1280	2630	BIRLEY CREEK	BLUESKY-GETHING	A	-121.196880	57.135417	1021.8				1,258,911	1,258,911
1300	8200	BIVOUAC	JEAN MARIE	A	-120.080112	58.454249	1205.5				1,349,117	1,349,117
1400	4100	BLUEBERRY	BALDONNEL	B	-121.956469	56.623819	1422.3				1,308,276	1,308,276
1400	7400	BLUEBERRY	DEBOLT	A	-121.859760	56.690867	2031.5	0	561,924	561,924	497,372	1,059,296
1400	7400	BLUEBERRY	DEBOLT	B	-121.940675	56.789429	2184.0	0	253,970	253,970	1,932,224	2,186,194
1400	2900	BLUEBERRY	DUNLEVY	A	-121.865741	56.706063	1221.4				11,151,657	11,151,657
1400	2900	BLUEBERRY	DUNLEVY	B	-121.899272	56.781609	1257.5				7,307,111	7,307,111
1400	4800	BLUEBERRY	HALFWAY	B	-121.954747	56.829478	1685.2				6,326,076	6,326,076
1800	4100	BLUEBERRY WEST	BALDONNEL	A	-121.977555	56.680866	1239.3				1,159,023	1,159,023
1950	4060	BOULDER	PARDONET-BALDONNEL	A	-122.263984	55.467562	2497.2				9,776,675	9,776,675
1950	4060	BOULDER	PARDONET-BALDONNEL	B	-122.235220	55.448738	2517.4				5,592,541	5,592,541
2000	4100	BOUNDARY LAKE	BALDONNEL	B	-120.110000	56.369270	1211.0				2,975,872	2,975,872
2000	7340	BOUNDARY LAKE	BASAL KISKATINAW	N	-120.027324	56.370599	1944.5				1,415,922	1,415,922
2000	7340	BOUNDARY LAKE	BASAL KISKATINAW	N/A	-120.232478	56.266849	2133.4				2,287,010	2,287,010
2000	6200	BOUNDARY LAKE	BELLOY	B	-120.206890	56.314487	1782.7				3,561,080	3,561,080
2000	6200	BOUNDARY LAKE	BELLOY	G	-120.202038	56.314711	1786.7				2,766,893	2,766,893

Field Code	Pool Code	Field Name	Pool Name	Pool Seq.	Longitude	Latitude	Depth (m)	Oil Reservoirs			Gas Reservoirs CO_2 Capacity (tonnes)	Combined Pool Capacity (tonnes)
								Mass CO_2 @ EOR (tonnes)	Effective Mass CO_2 (tonnes)	Total CO_2 capacity (tonnes)		
2000	6200	BOUNDARY LAKE	BELLOY	J	-120.145788	56.295667	1746.2				11,671,670	11,671,670
2000	6200	BOUNDARY LAKE	BELLOY	K	-120.122926	56.308677	1733.5				3,637,718	3,637,718
2000	6200	BOUNDARY LAKE	BELLOY	O	-120.225073	56.309919	1058.5				1,019,100	1,019,100
2000	4540	BOUNDARY LAKE	COPLIN	A	-120.029720	56.518091	1380.0				1,176,649	1,176,649
2000	4800	BOUNDARY LAKE	HALFWAY	B	-120.012777	56.528281	1465.0				1,563,911	1,563,911
2000	4800	BOUNDARY LAKE	HALFWAY		-120.100005	56.382633	1324.5	87,778	22,545	110,323	957,984	1,068,308
2000	7300	BOUNDARY LAKE	LOWER KISKATINAW	B	-120.039223	56.294652	2023.2				1,728,838	1,728,838
2020	4800	BOUNDARY LAKE NORTH	HALFWAY	B	-120.198949	56.528646	1342.2				1,734,727	1,734,727
2020	4800	BOUNDARY LAKE NORTH	HALFWAY	L	-120.152605	56.601705	1342.6				1,355,140	1,355,140
2100	4700	BRASSEY	ARTEX	B	-120.797422	55.613089	2921.8	0	1,259,767	1,259,767		1,259,767
2150	4060	BRAZION	PARDONET-BALDONNEL	A	-121.991368	55.383576	2511.7				3,361,046	3,361,046
2150	4060	BRAZION	PARDONET-BALDONNEL	B	-122.091810	55.402430	2353.6				7,525,996	7,525,996
2200	4100	BUBBLES	BALDONNEL	A	-122.035434	57.193315	1468.0				7,890,510	7,890,510
2200	8400	BUBBLES	SLAVE POINT	A	-122.080698	57.287989	1886.0				4,387,956	4,387,956
2200	8400	BUBBLES	SLAVE POINT	B	-122.120502	57.281875	3274.0				1,881,975	1,881,975
2240	4150	BUBBLES NORTH	BALDONNEL/UPPER CHARLIE LAKE	A	-122.229458	57.331668	1443.1				7,575,460	7,575,460
2240	4800	BUBBLES NORTH	HALFWAY	A	-122.179012	57.331863	1648.0				1,927,244	1,927,244
2240	4800	BUBBLES NORTH	HALFWAY	C	-122.109301	57.314035	1516.8				1,363,995	1,363,995
2400	2600	BUICK CREEK	BLUESKY	C	-120.453120	56.756250	981.4				10,130,019	10,130,019
2400	2900	BUICK CREEK	DUNLEVY	A	-121.122618	56.756520	1093.8	4,122	2,015	6,137	8,464,521	8,470,658
2400	2900	BUICK CREEK	DUNLEVY	B	-121.001563	56.775114	1112.2	0	786	786	7,666,412	7,667,198
2400	2900	BUICK CREEK	DUNLEVY	C	-121.172983	56.751831	1137.6	0	2,134	2,134	11,072,132	11,074,265
2400	2900	BUICK CREEK	DUNLEVY	H	-120.898390	56.781162	1086.5				1,098,562	1,098,562
2400	2900	BUICK CREEK	DUNLEVY	K	-121.097536	56.835103	1056.0				1,494,852	1,494,852
2400	4805	BUICK CREEK	LOWER HALFWAY	C	-121.066992	56.738850	1213.2	270,836	468,807	739,643	1,321,126	2,060,769
2400	4805	BUICK CREEK	LOWER HALFWAY	D	-121.055626	56.782090	1356.9	139,864	210,193	350,057	923,626	1,273,683
2400	4580	BUICK CREEK	NORTH PINE	A	-121.046880	56.702083	1285.3				1,816,984	1,816,984
2400	8400	BUICK CREEK	SLAVE POINT	B	-121.096456	56.848341	3150.7				1,416,634	1,416,634
2400	8400	BUICK CREEK	SLAVE POINT	C	-121.006822	56.896075	3132.0				1,678,628	1,678,628
2700	2600	BUICK CREEK NORTH	BLUESKY	A	-121.271870	56.856250	1113.5				1,716,761	1,716,761
2700	2900	BUICK CREEK NORTH	DUNLEVY	A	-121.254642	56.818649	1098.9				2,116,786	2,116,786
2800	2600	BUICK CREEK WEST	BLUESKY	A	-121.479585	56.902062	1097.5				2,121,038	2,121,038
2800	2900	BUICK CREEK WEST	DUNLEVY	A	-121.285970	56.739950	1170.2	0	50	50	5,351,543	5,351,593

Field Code	Pool Code	Field Name	Pool Name	Pool Seq.	Longitude	Latitude	Depth (m)	Oil Reservoirs			Gas Reservoirs CO_2 Capacity (tonnes)	Combined Pool Capacity (tonnes)
								Mass CO_2 @ EOR (tonnes)	Effective Mass CO_2 (tonnes)	Total CO_2 capacity (tonnes)		
2800	2900	BUICK CREEK WEST	DUNLEVY	B	-121.322531	56.811738	1193.9	0	60	60	4,385,226	4,385,286
2800	2900	BUICK CREEK WEST	DUNLEVY	G	-121.499840	56.884054	1205.7				1,743,429	1,743,429
2800	2900	BUICK CREEK WEST	DUNLEVY	J	-121.440620	56.947917	1198.3				1,253,916	1,253,916
2860	4100	BULLMOOSE	BALDONNEL	A	-121.451909	55.148902	2440.2				7,921,425	7,921,425
2860	4100	BULLMOOSE	BALDONNEL	B	-121.498270	55.179456	2939.9				6,807,464	6,807,464
2860	4100	BULLMOOSE	BALDONNEL	C	-121.358544	55.114138	2958.1				6,758,089	6,758,089
2860	4100	BULLMOOSE	BALDONNEL	D	-121.158720	55.084610	3013.0				1,087,215	1,087,215
2860	4060	BULLMOOSE	PARDONET-BALDONNEL	A	-121.473286	55.142595	2720.4				2,079,822	2,079,822
2865	4060	BULLMOOSE WEST	PARDONET-BALDONNEL	B	-121.527845	55.113943	2795.7				1,480,735	1,480,735
2865	4060	BULLMOOSE WEST	PARDONET-BALDONNEL	C	-121.626035	55.150648	2425.9				6,593,968	6,593,968
2865	4060	BULLMOOSE WEST	PARDONET-BALDONNEL	D	-121.651747	55.154730	2714.4				6,593,251	6,593,251
2865	4060	BULLMOOSE WEST	PARDONET-BALDONNEL	E	-121.454361	55.089936	2943.4				1,504,200	1,504,200
2850	4060	BURNT RIVER	PARDONET-BALDONNEL	A	-122.012452	55.306289	2537.4				6,946,824	6,946,824
2900	8400	CABIN	SLAVE POINT	B	-121.727687	59.341880	2171.1				1,968,273	1,968,273
2920	4100	CACHE CREEK	BALDONNEL	A	-121.418757	56.645270	1227.7				2,218,899	2,218,899
2920	2600	CACHE CREEK	BLUESKY	A	-121.425321	56.641657	1082.4				1,146,608	1,146,608
2920	4540	CACHE CREEK	COPLIN	A	-121.445343	56.659903	1380.2				2,717,433	2,717,433
2920	4540	CACHE CREEK	COPLIN	B	-121.603961	56.732683	1453.5				1,193,615	1,193,615
2920	4800	CACHE CREEK	HALFWAY	A	-121.447535	56.681091	1584.9				6,238,586	6,238,586
2960	2700	CECIL LAKE	GETHING	A	-120.645584	56.288865	1000.5				1,153,584	1,153,584
2960	4580	CECIL LAKE	NORTH PINE	A	-120.712487	56.291824	1346.8	16,140	18,496	34,636	3,778,971	3,813,607
2985	2640	CHINCHAGA RIVER	BLUESKY-GETHING-DETRITAL	A	-120.009206	57.339109	940.9				1,510,601	1,510,601
2985	4995	CHINCHAGA RIVER	LOWER CHARLIE LAKE/MONTNEY	A	-120.090630	57.310417	962.6				6,020,139	6,020,139
2985	8400	CHINCHAGA RIVER	SLAVE POINT	A	-120.046048	57.338037	2630.7				1,438,412	1,438,412
2985	8400	CHINCHAGA RIVER	SLAVE POINT	B	-120.012928	57.255970	2667.9				2,104,443	2,104,443
2990	4100	CHOWADE	BALDONNEL	A	-122.484380	56.702083	1684.4				2,342,274	2,342,274
3200	8600	CLARKE LAKE	PINE POINT	C	-122.754093	58.698601	2191.0				2,276,916	2,276,916
3200	8600	CLARKE LAKE	PINE POINT	D	-122.741561	58.713921	2219.6				1,119,964	1,119,964
3200	8400	CLARKE LAKE	SLAVE POINT	A	-122.600366	58.730490	1918.7				88,553,247	88,553,247
3230	4060	COMMOTION	PARDONET-BALDONNEL	A	-121.901468	55.517044	3728.6				1,412,147	1,412,147
3230	4060	COMMOTION	PARDONET-BALDONNEL	B	-121.852228	55.531163	3622.1				1,550,248	1,550,248
3300	4800	CURRANT	HALFWAY	A	-120.317124	56.764510	1199.5	0	0	0	1,168,095	1,168,095
3340	2000	CUTBANK	PADDY	B	-120.211391	55.325324	1768.0				1,163,647	1,163,647

Field Code	Pool Code	Field Name	Pool Name	Pool Seq.	Longitude	Latitude	Depth (m)	Oil Reservoirs			Gas Reservoirs CO_2 Capacity (tonnes)	Combined Pool Capacity (tonnes)
								Mass CO_2 @ EOR (tonnes)	Effective Mass CO_2 (tonnes)	Total CO_2 capacity (tonnes)		
3340	2000	CUTBANK	PADDY	H	-120.227228	55.287732	1765.4				1,238,324	1,238,324
3360	4100	CYPRESS	BALDONNEL	A	-122.840514	56.852097	1358.2				1,943,388	1,943,388
3380	2630	DAHL	BLUESKY-GETHING	A	-120.655420	57.448034	1148.1				16,995,537	16,995,537
3380	8400	DAHL	SLAVE POINT	A	-120.510931	57.390262	2854.0				1,355,106	1,355,106
3390	4100	DAIBER	BALDONNEL	A	-122.448342	56.814224	1358.7				1,536,177	1,536,177
3400	5000	DAWSON CREEK	MONTNEY	A	-120.223563	55.862205	2047.3				8,513,387	8,513,387
3425	4100	DOE	BALDONNEL	A	-120.014836	55.966308	1420.9				1,641,172	1,641,172
3425	2700	DOE	GETHING	A	-120.008736	55.939912	1239.5				1,355,816	1,355,816
3425	2700	DOE	GETHING	B	-120.014836	55.966308	1239.9				1,506,335	1,506,335
3425	2330	DOE	PEACE RIVER	A	-120.255774	55.920847	778.3				3,247,746	3,247,746
3425	8100	DOE	WABAMUN	A	-120.208657	55.994451	3283.8				3,301,561	3,301,561
3428	4040	DOIG RAPIDS	NORDEGG-BALDONNEL	A	-120.340630	56.960417	1018.4				1,213,630	1,213,630
3430	2400	DRAKE	NOTIKEWIN	A	-120.088364	57.021502	1167.5				7,232,952	7,232,952
3445	6200	EAGLE WEST	BELLOY	A	-120.809565	56.312715	1634.7				1,807,042	1,807,042
3450	8200	EKWAN	JEAN MARIE	A	-120.834827	58.630816	1237.6				5,281,233	5,281,233
3453	7400	ELBOW CREEK	DEBOLT	C	-122.905043	57.097706	2580.0				1,236,041	1,236,041
3455	8200	ELLEH	JEAN MARIE	B	-121.972323	58.442121	1544.0				6,802,218	6,802,218
3540	2600	FIREWEED	BLUESKY	B	-121.471870	56.802083	1172.1				2,075,748	2,075,748
3540	2900	FIREWEED	DUNLEVY	A	-121.579469	56.834470	1251.2	0	552	552	4,445,250	4,445,802
3540	2900	FIREWEED	DUNLEVY	B	-121.553120	56.881250	1109.1				1,430,412	1,430,412
3540	2900	FIREWEED	DUNLEVY	D	-121.505809	56.818669	1232.1	0	354	354	2,180,093	2,180,447
3540	2900	FIREWEED	DUNLEVY	H	-121.672011	56.836784	1279.5				2,801,192	2,801,192
3560	4800	FLATROCK	HALFWAY	E	-120.547903	56.280890	1429.6	32,086	26,790	58,876	1,747,949	1,806,824
3560	4800	FLATROCK	HALFWAY	G	-120.494184	56.284614	1442.9				1,481,041	1,481,041
3580	4800	FLATROCK WEST	HALFWAY	C	-120.548803	56.353091	1459.7				2,098,525	2,098,525
3580	4800	FLATROCK WEST	HALFWAY	D	-120.602557	56.324149	1288.2	39,867	51,827	91,693	1,170,992	1,262,686
3600	4100	FORT ST JOHN	BALDONNEL	A	-120.819483	56.232754	1185.4				11,773,356	11,773,356
3600	6200	FORT ST JOHN	BELLOY	A	-120.811060	56.218398	1928.8				1,459,860	1,459,860
3600	4800	FORT ST JOHN	HALFWAY	A	-120.811737	56.217846	1486.6				6,133,278	6,133,278
3600	6222	FORT ST JOHN	LOWER BELLOY	A	-120.814899	56.220378	1987.2				1,483,907	1,483,907
4000	4100	FORT ST JOHN SOUTHEAST	BALDONNEL	A	-120.581208	56.173010	1186.8				3,081,931	3,081,931
4000	6200	FORT ST JOHN SOUTHEAST	BELLOY	A	-120.634325	56.174530	1924.2				7,179,477	7,179,477
4000	4800	FORT ST JOHN SOUTHEAST	HALFWAY	A	-120.594730	56.164457	1489.2				4,550,536	4,550,536

Field Code	Pool Code	Field Name	Pool Name	Pool Seq.	Longitude	Latitude	Depth (m)	Oil Reservoirs			Gas Reservoirs CO_2 Capacity (tonnes)	Combined Pool Capacity (tonnes)
								Mass CO_2 @ EOR (tonnes)	Effective Mass CO_2 (tonnes)	Total CO_2 capacity (tonnes)		
4200	8500	GOTE	SULPHUR POINT	A	-121.953852	59.533149	2321.7				3,682,954	3,682,954
4300	4100	GRAHAM	BALDONNEL	A	-122.327038	56.517851	1437.4				2,581,155	2,581,155
4300	4100	GRAHAM	BALDONNEL	C	-122.400139	56.480430	1588.6				1,914,608	1,914,608
4300	4100	GRAHAM	BALDONNEL	D	-122.299348	56.419567	1451.0				4,330,528	4,330,528
4300	4100	GRAHAM	BALDONNEL	E	-122.409370	56.547917	1489.0				1,289,344	1,289,344
4300	4100	GRAHAM	BALDONNEL	F	-122.388205	56.508707	1512.2				1,737,349	1,737,349
4350	7400	GRASSY	DEBOLT	A	-122.929922	57.310333	1878.5				4,369,251	4,369,251
4370	4800	GREEN CREEK	HALFWAY	A	-122.554603	57.435605	1371.0				4,776,225	4,776,225
4380	4100	GRIZZLY NORTH	BALDONNEL	A	-120.659370	54.889583	3500.0				2,669,737	2,669,737
4380	2900	GRIZZLY NORTH	DUNLEVY	A	-120.648288	54.885355	2590.4				3,779,561	3,779,561
4385	4100	GRIZZLY SOUTH	BALDONNEL	B	-120.708967	54.745795	1559.8				24,894,212	24,894,212
4385	2900	GRIZZLY SOUTH	DUNLEVY	A	-120.581535	54.774623	2544.9				2,366,653	2,366,653
4385	6300	GRIZZLY SOUTH	TAYLOR FLAT	A	-120.530656	54.750976	4219.0				1,902,113	1,902,113
4400	4800	GUNDY CREEK	HALFWAY	A	-122.055747	56.799175	1602.4				1,094,419	1,094,419
4460	4100	GUNDY CREEK WEST	BALDONNEL	A	-122.153478	56.751663	1281.1				1,166,164	1,166,164
4460	2900	GUNDY CREEK WEST	DUNLEVY	A	-122.159370	56.760417	1123.1				1,828,263	1,828,263
4470	8200	GUNNELL CREEK	JEAN MARIE	A	-121.794153	58.874530	1451.4				25,631,699	25,631,699
4500	4100	GWILLIM	BALDONNEL	A	-121.458789	55.357192	3575.3				1,781,054	1,781,054
4500	4060	GWILLIM	PARDONET-BALDONNEL	A	-121.360138	55.309390	3377.7				2,038,070	2,038,070
4500	4060	GWILLIM	PARDONET-BALDONNEL	B	-121.503120	55.381250	3663.9				2,488,064	2,488,064
4600	4100	HALFWAY	BALDONNEL	A	-121.851772	56.515652	1139.5				1,030,900	1,030,900
4700	8200	HELMET	JEAN MARIE	A	-120.817424	59.417185	1294.9				118,066,403	118,066,403
4700	8200	HELMET	JEAN MARIE	N/A	-121.180002	59.640120	1098.3				1,538,798	1,538,798
4700	8400	HELMET	SLAVE POINT	A	-120.702616	59.366786	1873.3				7,501,140	7,501,140
4780	2515	HIDING CREEK	FALHER C	B	-120.034033	54.794431	2893.0				1,691,630	1,691,630
4780	2520	HIDING CREEK	FALHER D	A	-120.026339	54.903739	2757.8				1,323,911	1,323,911
4800	4060	HIGHHAT MOUNTAIN	PARDONET-BALDONNEL	B	-121.883868	55.426838	3474.4				1,450,861	1,450,861
4800	4060	HIGHHAT MOUNTAIN	PARDONET-BALDONNEL	C	-121.846431	55.424713	3460.2				2,456,406	2,456,406
4800	4060	HIGHHAT MOUNTAIN	PARDONET-BALDONNEL	D	-121.959059	55.456009	3676.3				1,224,563	1,224,563
4800	4060	HIGHHAT MOUNTAIN	PARDONET-BALDONNEL	E	-121.776217	55.454964	3301.4				1,802,840	1,802,840
4850	8400	HOFFARD	SLAVE POINT	D	-122.181301	58.720273	1961.6				1,062,830	1,062,830
4900	4575	INGA	INGA	A	-121.693418	56.662279	1413.1	0	0	0	12,691,635	12,691,635
5000	4150	JEDNEY	BALDONNEL/UPPER CHARLIE LAKE	A	-122.248211	57.267997	1316.6				36,962,850	36,962,850

Field Code	Pool Code	Field Name	Pool Name	Pool Seq.	Longitude	Latitude	Depth (m)	Oil Reservoirs			Gas Reservoirs CO_2 Capacity (tonnes)	Combined Pool Capacity (tonnes)
								Mass CO_2 @ EOR (tonnes)	Effective Mass CO_2 (tonnes)	Total CO_2 capacity (tonnes)		
5000	4800	JEDNEY	HALFWAY	A	-122.228830	57.247937	1593.1				16,323,309	16,323,309
5160	4990	KAHNTAH RIVER	BLUESKY-GETHING-MONTNEY	A	-120.678953	57.843860	803.1				2,275,201	2,275,201
5160	5000	KAHNTAH RIVER	MONTNEY	A	-121.027109	58.087235	867.0				1,328,679	1,328,679
5170	2800	KELLY	CADOMIN	D	-120.028310	55.168824	2475.0				3,797,884	3,797,884
5170	2505	KELLY	FALHER A	A	-120.030022	55.197306	1457.0				1,485,945	1,485,945
5170	2505	KELLY	FALHER A	B	-120.098357	55.081165	2407.6				2,595,692	2,595,692
5170	2510	KELLY	FALHER B	A	-120.371880	55.114583	2256.8				2,568,733	2,568,733
5170	2510	KELLY	FALHER B	C	-120.271824	55.146075	2251.1				1,188,793	1,188,793
5180	8600	KLUA	PINE POINT	D	-122.234362	58.486469	2331.9				1,268,651	1,268,651
5180	8600	KLUA	PINE POINT	F	-122.212789	58.495280	2330.7				1,133,024	1,133,024
5180	8600	KLUA	PINE POINT	H	-122.276294	58.486732	2378.0				1,009,870	1,009,870
5180	8600	KLUA	PINE POINT	L	-122.202589	58.441202	2190.7				1,627,073	1,627,073
5180	8600	KLUA	PINE POINT	M	-122.231588	58.452782	2302.2				1,197,744	1,197,744
5180	8600	KLUA	PINE POINT	Q	-122.203565	58.595364	2285.1				3,547,224	3,547,224
5180	8600	KLUA	PINE POINT	R	-122.079042	58.562285	2302.9				1,740,216	1,740,216
5180	8400	KLUA	SLAVE POINT	B	-122.306235	58.645910	1956.3				2,627,291	2,627,291
5180	8400	KLUA	SLAVE POINT	D	-122.293081	58.565081	2046.8				1,725,422	1,725,422
5200	4100	KOBES	BALDONNEL	A	-122.209370	56.664583	1397.0				2,233,000	2,233,000
5200	4500	KOBES	CHARLIE LAKE	B	-122.061176	56.526284	1560.4				1,943,112	1,943,112
5200	7400	KOBES	DEBOLT	C	-122.103130	56.577083	2262.7				2,315,718	2,315,718
5200	2900	KOBES	DUNLEVY	A	-122.029243	56.500003	848.3				3,094,003	3,094,003
5200	4800	KOBES	HALFWAY	A	-122.040630	56.497917	1777.4				11,410,652	11,410,652
5400	8400	KOTCHO LAKE	SLAVE POINT	A	-121.299627	59.034468	2054.3				3,677,501	3,677,501
5420	8400	KOTCHO LAKE EAST	SLAVE POINT	C	-121.202882	58.924207	1994.2				1,624,805	1,624,805
5500	8400	LADYFERN	SLAVE POINT	A	-120.081270	57.161167	2764.6				30,540,369	30,540,369
5500	8400	LADYFERN	SLAVE POINT	B	-120.004499	57.135120	2802.5				2,673,264	2,673,264
5560	4800	LAPP	HALFWAY	A	-120.872901	57.518831	1029.8				1,238,292	1,238,292
5600	4150	LAPRISE CREEK	BALDONNEL/UPPER CHARLIE LAKE	A	-122.053387	57.360889	1362.2				59,792,495	59,792,495
5600	4150	LAPRISE CREEK	BALDONNEL/UPPER CHARLIE LAKE	B	-121.900548	57.397226	1162.1				12,019,956	12,019,956
5600	4150	LAPRISE CREEK	BALDONNEL/UPPER CHARLIE LAKE	D	-122.046880	57.314583	1349.7				2,548,993	2,548,993
5600	4150	LAPRISE CREEK	BALDONNEL/UPPER CHARLIE LAKE	F	-122.027604	57.493081	1285.5				1,004,208	1,004,208
5800	4100	LAPRISE CREEK WEST	BALDONNEL	B	-122.171880	57.431250	1316.8				1,302,454	1,302,454
5810	6200	LILY LAKE	BELLOY	A	-122.848389	57.167021	2111.4				1,583,735	1,583,735

Field Code	Pool Code	Field Name	Pool Name	Pool Seq.	Longitude	Latitude	Depth (m)	Oil Reservoirs			Gas Reservoirs CO_2 Capacity (tonnes)	Combined Pool Capacity (tonnes)
								Mass CO_2 @ EOR (tonnes)	Effective Mass CO_2 (tonnes)	Total CO_2 capacity (tonnes)		
5850	4100	MARTIN	BALDONNEL	A	-121.469337	57.348098	1168.0				1,968,862	1,968,862
5850	4100	MARTIN	BALDONNEL	E	-121.378120	57.414583	1167.2				1,292,963	1,292,963
5852	2805	MAXHAMISH LAKE	CHINKEH	A	-123.157247	59.710795	1427.7				22,981,632	22,981,632
5854	4060	MEIKLE CREEK	PARDONET-BALDONNEL	A	-121.412749	55.244141	3200.9				1,389,622	1,389,622
5855	8600	MEL	PINE POINT	B	-121.725575	59.214888	2265.7				1,218,844	1,218,844
5855	8400	MEL	SLAVE POINT	A	-121.592569	59.173861	2237.0				4,522,061	4,522,061
6000	8400	MILLIGAN CREEK	SLAVE POINT	A	-120.725461	57.114241	2904.5				3,221,953	3,221,953
6030	8600	MILO	PINE POINT	A	-123.094557	58.643784	2418.9				1,336,210	1,336,210
6030	8600	MILO	PINE POINT	B	-123.032894	58.695449	2343.9				1,949,173	1,949,173
6030	8600	MILO	PINE POINT	D	-123.243156	58.513985	3070.9				1,727,034	1,727,034
6140	4800	MONIAS	HALFWAY	N/A	-121.226168	56.107041	1449.1				42,853,185	42,853,185
6140	4800	MONIAS	HALFWAY	T	-121.293704	56.060579	1519.2				4,921,878	4,921,878
6140	4800	MONIAS	HALFWAY	U	-121.396315	56.027085	1697.3				1,925,017	1,925,017
6140	4800	MONIAS	HALFWAY	V	-121.447566	56.100863	1519.1				4,627,935	4,627,935
6210	2200	MOOSE	CADOTTE	A	-121.133656	55.331392	1854.2				1,430,094	1,430,094
6220	4100	MURRAY	BALDONNEL	A	-121.084370	54.960417	1773.3				5,143,467	5,143,467
6220	4100	MURRAY	BALDONNEL	B	-121.149821	55.005494	2727.3				5,813,993	5,813,993
6220	4100	MURRAY	BALDONNEL	E	-121.034141	54.957162	2291.7				7,766,167	7,766,167
6220	4150	MURRAY	BALDONNEL/UPPER CHARLIE LAKE	A	-121.060963	54.963652	1561.6				21,503,667	21,503,667
6220	4060	MURRAY	PARDONET-BALDONNEL	A	-121.204222	54.963557	1725.0				2,614,899	2,614,899
6400	4100	NIG CREEK	BALDONNEL	A	-121.629583	57.085325	1213.0	1,496	2,199	3,694	27,490,337	27,494,031
6410	2600	NIG CREEK NORTH	BLUESKY	A	-121.628120	57.206250	1203.4				6,963,813	6,963,813
6430	2200	NOEL	CADOTTE	A	-120.430131	55.264522	2043.0				3,236,669	3,236,669
6430	2200	NOEL	CADOTTE	M	-120.640620	55.222917	2151.7				1,998,044	1,998,044
6430	2510	NOEL	FALHER B	C	-120.448349	55.219956	2257.9				5,725,212	5,725,212
6440	4580	NORTH PINE	NORTH PINE	B	-120.707051	56.381901	1319.2	0	6,831	6,831	1,147,220	1,154,051
6460	4100	OAK	BALDONNEL	C	-120.804559	56.488229	1179.4				1,441,860	1,441,860
6460	4800	OAK	HALFWAY	A	-120.705973	56.473678	1246.2	0	3,193	3,193	6,374,381	6,377,574
6480	4100	OJAY	BALDONNEL	A	-120.397282	54.681303	3579.9				22,516,110	22,516,110
6480	4100	OJAY	BALDONNEL	B	-120.507808	54.677651	2813.9				1,681,101	1,681,101
6480	4100	OJAY	BALDONNEL	C	-120.590794	54.658425	1605.9				1,166,131	1,166,131
6480	7400	OJAY	DEBOLT	A	-120.155149	54.596371	4445.9				1,638,400	1,638,400
6480	2850	OJAY	NIKANASSIN	A	-120.390183	54.813529	3371.0				1,216,518	1,216,518

APPENDIX D CONTINUED.

Field Code	Pool Code	Field Name	Pool Name	Pool Seq.	Longitude	Latitude	Depth (m)	Oil Reservoirs			Gas Reservoirs CO_2 Capacity (tonnes)	Combined Pool Capacity (tonnes)
								Mass CO_2 @ EOR (tonnes)	Effective Mass CO_2 (tonnes)	Total CO_2 capacity (tonnes)		
6480	2850	OJAY	NIKANASSIN	B	-120.207900	54.629125	2894.2				1,180,335	1,180,335
6480	2850	OJAY	NIKANASSIN	C	-120.332426	54.795965	3398.9				1,240,612	1,240,612
6480	6300	OJAY	TAYLOR FLAT	A	-120.208051	54.629095	4249.1				1,998,863	1,998,863
6480	6300	OJAY	TAYLOR FLAT	C	-120.216732	54.566024	3698.1				3,091,653	3,091,653
6490	2700	OSBORN	GETHING	A	-120.157463	56.694305	1084.7				1,852,567	1,852,567
9000	4100	OTHER AREAS	BALDONNEL	06-35-087-15-W6M	-120.492138	56.797829	1122.3				1,848,170	1,848,170
9000	4100	OTHER AREAS	BALDONNEL	A-067-F/094-G-07	-120.492138	56.797829	989.3				2,109,349	2,109,349
9000	4100	OTHER AREAS	BALDONNEL	B-043-B/094-G-07	-120.492138	56.797829	1025.3				2,218,710	2,218,710
9000	4100	OTHER AREAS	BALDONNEL	C-018-G/093-O-09	-120.492138	56.797829	2706.3				1,300,101	1,300,101
9000	4100	OTHER AREAS	BALDONNEL	C-032-F/093-O-09	-120.492138	56.797829	3044.3				1,204,652	1,204,652
9000	4100	OTHER AREAS	BALDONNEL	C-055-J/094-B-10	-120.492138	56.797829	1634.3				2,152,595	2,152,595
9000	4100	OTHER AREAS	BALDONNEL	D-030-C/093-O-09	-120.492138	56.797829	2200.3				1,785,794	1,785,794
9000	4100	OTHER AREAS	BALDONNEL	D-033-K/094-A-11	-120.492138	56.797829	1176.3				1,937,004	1,937,004
9000	4100	OTHER AREAS	BALDONNEL	D-051-C/094-A-16	-120.492138	56.797829	1038.3				1,618,243	1,618,243
9000	2600	OTHER AREAS	BLUESKY	C-027-A/094-H-01	-120.848388	57.002001	899.3				1,430,960	1,430,960
9000	2600	OTHER AREAS	BLUESKY	C-055-J/094-B-10	-120.848388	57.002001	1586.3				1,479,503	1,479,503
9000	2600	OTHER AREAS	BLUESKY	D-049-B/094-A-16	-120.848388	57.002001	963.3				2,333,890	2,333,890
9000	2800	OTHER AREAS	CADOMIN	07-28-083-15-W6M	-121.894221	56.574076	1089.7				1,111,916	1,111,916
9000	7400	OTHER AREAS	DEBOLT	07-26-084-22-W6M	-121.529590	58.183388	1869.0				3,699,934	3,699,934
9000	7400	OTHER AREAS	DEBOLT	A-023-I/094-I-04	-121.529590	58.183388	783.0				3,629,816	3,629,816
9000	7400	OTHER AREAS	DEBOLT	A-051-H/094-B-10	-121.529590	58.183388	2657.0				2,993,815	2,993,815
9000	7400	OTHER AREAS	DEBOLT	A-063-G/094-I-01	-121.529590	58.183388	524.0				2,628,114	2,628,114
9000	7400	OTHER AREAS	DEBOLT	B-024-B/094-P-11	-121.529590	58.183388	471.0				2,433,289	2,433,289
9000	7400	OTHER AREAS	DEBOLT	B-030-E/094-B-08	-121.529590	58.183388	471.7				3,276,642	3,276,642
9000	7400	OTHER AREAS	DEBOLT	B-041-K/094-I-01	-121.529590	58.183388	525.0				2,719,559	2,719,559
9000	7400	OTHER AREAS	DEBOLT	B-064-E/094-G-15	-121.529590	58.183388	471.7				3,495,726	3,495,726
9000	7400	OTHER AREAS	DEBOLT	B-085-E/094-G-02	-121.529590	58.183388	471.7				4,988,907	4,988,907
9000	7400	OTHER AREAS	DEBOLT	C-053-D/094-P-06	-121.529590	58.183388	470.0				2,449,652	2,449,652
9000	7400	OTHER AREAS	DEBOLT	C-053-J/094-G-03	-121.529590	58.183388	471.7				5,790,890	5,790,890
9000	7400	OTHER AREAS	DEBOLT	C-074-L/094-A-14	-121.529590	58.183388	1390.0				3,914,604	3,914,604
9000	7400	OTHER AREAS	DEBOLT	C-097-D/094-G-15	-121.529590	58.183388	1190.0				4,182,374	4,182,374
9000	7400	OTHER AREAS	DEBOLT	D-019-E/094-G-15	-121.529590	58.183388	1299.0				3,718,180	3,718,180
9000	7400	OTHER AREAS	DEBOLT	D-027-H/094-G-10	-121.529590	58.183388	1326.0				3,449,588	3,449,588

Field Code	Pool Code	Field Name	Pool Name	Pool Seq.	Longitude	Latitude	Depth (m)	Oil Reservoirs			Gas Reservoirs CO_2 Capacity (tonnes)	Combined Pool Capacity (tonnes)
								Mass CO_2 @ EOR (tonnes)	Effective Mass CO_2 (tonnes)	Total CO_2 capacity (tonnes)		
9000	7400	OTHER AREAS	DEBOLT	D-055-L/094-P-11	-121.529590	58.183388	472.0				2,427,075	2,427,075
9000	7400	OTHER AREAS	DEBOLT	D-057-H/094-B-09	-121.529590	58.183388	2000.0				3,472,751	3,472,751
9000	7400	OTHER AREAS	DEBOLT	D-059-I/094-B-09	-121.529590	58.183388	1896.0				3,665,107	3,665,107
9000	7400	OTHER AREAS	DEBOLT	D-095-K/094-B-07	-121.529590	58.183388	2675.0				3,049,374	3,049,374
9000	7400	OTHER AREAS	DEBOLT	D-097-A/094-B-07	-121.529590	58.183388	2033.0				3,590,968	3,590,968
9000	4060	OTHER AREAS	PARDONET-BALDONNEL	A-050-H/093-I-14	-121.121941	54.866188	1801.6				2,080,951	2,080,951
9000	4060	OTHER AREAS	PARDONET-BALDONNEL	D-023-E/093-I-15	-121.121941	54.866188	1810.6				1,726,426	1,726,426
9000	7500	OTHER AREAS	SHUNDA	D-075-E/094-B-16	-122.604339	57.950708	2734.2				1,215,518	1,215,518
6600	4800	PARKLAND	HALFWAY	A	-120.333479	56.048706	1727.8				1,345,327	1,345,327
6600	8100	PARKLAND	WABAMUN	A	-120.313557	56.048992	3317.0				14,298,530	14,298,530
6800	4800	PEEJAY	HALFWAY		-120.479166	56.864488	1107.3	0	0	0	1,713,760	1,713,760
7000	4800	PEEJAY WEST	HALFWAY	A	-120.667121	56.872833	1191.7	0	35,884	35,884	1,106,082	1,141,965
7250	2400	PICKELL	NOTIKEWIN	A	-121.077284	57.216415	885.8				6,757,579	6,757,579
7300	7400	POCKETKNIFE	DEBOLT	A	-123.045186	57.473323	1727.9				1,450,143	1,450,143
7300	7400	POCKETKNIFE	DEBOLT	C	-123.004961	57.402439	1741.8				4,273,936	4,273,936
7340	4100	PRESPATOU	BALDONNEL	A	-121.218915	57.027596	1203.9				1,213,325	1,213,325
7400	4582	RED CREEK	BEAR FLAT	A	-121.235920	56.398357	1515.9				1,124,601	1,124,601
7410	4800	RED CREEK NORTH	HALFWAY	A	-121.282102	56.445510	1667.2				1,273,738	1,273,738
7600	4520	RIGEL	CECIL	A	-120.734380	56.756250	1162.0				1,473,356	1,473,356
7600	2900	RIGEL	DUNLEVY	F	-120.631095	56.655379	884.8				41,132,615	41,132,615
7600	4800	RIGEL	HALFWAY	I	-120.562574	56.614271	1310.7	3,650	6,375	10,025	1,428,753	1,438,778
7620	2700	RIGEL EAST	GETHING	A	-120.438310	56.644498	1062.2	1,708	1,574	3,281	2,817,457	2,820,739
7660	4990	RING	BLUESKY-GETHING-MONTNEY	A	-120.252960	57.769322	838.5				45,359,322	45,359,322
7660	4990	RING	BLUESKY-GETHING-MONTNEY	E	-120.103539	57.918535	804.9				4,586,292	4,586,292
7720	8600	ROGER	PINE POINT	A	-122.616142	58.769011	2100.5				3,497,291	3,497,291
7740	8200	SAHTANEH	JEAN MARIE	A	-121.711948	58.745381	1428.8				1,055,990	1,055,990
7740	8400	SAHTANEH	SLAVE POINT	B	-121.690201	58.738135	1977.2				1,549,807	1,549,807
7745	5000	SATURN	MONTNEY	A	-120.912304	55.907625	2408.9				1,121,167	1,121,167
7750	4800	SEPTIMUS	HALFWAY	A	-120.809042	56.063346	1707.0				1,791,022	1,791,022
7755	8400	SEXTET	SLAVE POINT	D	-121.625619	58.660597	1897.8				2,957,713	2,957,713
7770	8200	SIERRA	JEAN MARIE	A	-121.367734	58.828738	1458.7				6,162,646	6,162,646
7770	8600	SIERRA	PINE POINT	A	-121.347619	58.814306	2164.8				58,041,890	58,041,890
7770	8600	SIERRA	PINE POINT	B	-121.344058	58.742344	2142.3				23,953,640	23,953,640

Field Code	Pool Code	Field Name	Pool Name	Pool Seq.	Longitude	Latitude	Depth (m)	Oil Reservoirs			Gas Reservoirs CO_2 Capacity (tonnes)	Combined Pool Capacity (tonnes)
								Mass CO_2 @ EOR (tonnes)	Effective Mass CO_2 (tonnes)	Total CO_2 capacity (tonnes)		
7770	8600	SIERRA	PINE POINT	D	-121.381888	58.712224	2120.6				8,205,767	8,205,767
7770	8600	SIERRA	PINE POINT	E	-121.282709	58.827038	2209.9				3,253,073	3,253,073
7770	8600	SIERRA	PINE POINT	F	-121.231697	58.729359	2050.5				2,989,701	2,989,701
7770	8600	SIERRA	PINE POINT	G	-121.223327	58.831176	2205.3				2,036,297	2,036,297
7770	8600	SIERRA	PINE POINT	J	-121.460577	58.748161	2245.2				3,313,980	3,313,980
7775	7400	SIKANNI	DEBOLT	C	-123.030034	57.232110	1922.6				9,553,961	9,553,961
7775	7400	SIKANNI	DEBOLT	G	-122.948705	57.202528	1800.9				5,723,021	5,723,021
7775	7400	SIKANNI	DEBOLT	H	-123.030681	57.136235	2247.6				10,917,178	10,917,178
7775	7400	SIKANNI	DEBOLT	I	-122.953685	57.253209	2022.8				1,994,944	1,994,944
7775	7400	SIKANNI	DEBOLT	K	-123.162285	57.278452	1420.9				4,423,356	4,423,356
7780	2600	SILVER	BLUESKY	A	-121.378575	57.488151	1095.0				7,091,702	7,091,702
7820	4580	SILVERBERRY	NORTH PINE	A	-121.129630	56.630642	1408.1				1,078,745	1,078,745
7840	2900	SIPHON	DUNLEVY	A	-120.435988	56.499964	1131.3				3,152,973	3,152,973
7840	4800	SIPHON	HALFWAY	A	-120.439125	56.489230	1405.1				1,712,827	1,712,827
7860	2600	SIPHON EAST	BLUESKY	A	-120.329454	56.502418	1098.0	0	252	252	1,948,298	1,948,549
8000	6200	STODDART	BELLOY	A	-121.014613	56.452081	1936.4				29,214,894	29,214,894
8100	6200	STODDART WEST	BELLOY	A	-121.153960	56.488088	1976.7				2,820,277	2,820,277
8100	6200	STODDART WEST	BELLOY	C	-121.075252	56.425788	1447.1	310,999	668,660	979,659	740,431	1,720,089
8100	6200	STODDART WEST	BELLOY	H	-121.149530	56.513421	1962.2				1,758,458	1,758,458
8100	6200	STODDART WEST	BELLOY	I	-121.182748	56.513446	1935.2				1,143,500	1,143,500
8100	4900	STODDART WEST	DOIG	E	-121.325870	56.583487	1639.6	0	803,677	803,677	1,507,968	2,311,645
8100	4800	STODDART WEST	HALFWAY	B	-121.198158	56.489087	1626.2				1,201,234	1,201,234
8105	4060	STONE CREEK	PARDONET-BALDONNEL	A	-121.861886	55.640423	3585.7				1,191,979	1,191,979
8110	4060	SUKUNKA	PARDONET-BALDONNEL	A	-121.686544	55.302940	2657.6				1,651,100	1,651,100
8110	4060	SUKUNKA	PARDONET-BALDONNEL	B	-121.579240	55.282730	3386.8				1,411,111	1,411,111
8110	4060	SUKUNKA	PARDONET-BALDONNEL	C	-121.612779	55.260637	2969.7				1,987,211	1,987,211
8110	4060	SUKUNKA	PARDONET-BALDONNEL	E	-121.678120	55.210417	2018.0				22,431,634	22,431,634
8110	4060	SUKUNKA	PARDONET-BALDONNEL	G	-121.899031	55.305654	2884.0				2,325,446	2,325,446
8110	4060	SUKUNKA	PARDONET-BALDONNEL	H	-121.618660	55.223326	3235.7				2,294,302	2,294,302
8110	4060	SUKUNKA	PARDONET-BALDONNEL	I	-121.576201	55.234190	3258.2				1,374,237	1,374,237
8110	4060	SUKUNKA	PARDONET-BALDONNEL	J	-121.653526	55.283754	2642.0				3,635,286	3,635,286
8110	4060	SUKUNKA	PARDONET-BALDONNEL	L	-121.818749	55.333958	2942.5				6,049,712	6,049,712
8110	4060	SUKUNKA	PARDONET-BALDONNEL	M	-121.716196	55.247327	2535.5				7,171,136	7,171,136

Field Code	Pool Code	Field Name	Pool Name	Pool Seq.	Longitude	Latitude	Depth (m)	Oil Reservoirs			Gas Reservoirs CO_2 Capacity (tonnes)	Combined Pool Capacity (tonnes)
								Mass CO_2 @ EOR (tonnes)	Effective Mass CO_2 (tonnes)	Total CO_2 capacity (tonnes)		
8110	4060	SUKUNKA	PARDONET-BALDONNEL	P	-121.594674	55.189800	2807.3				5,739,363	5,739,363
8110	4060	SUKUNKA	PARDONET-BALDONNEL	Q	-121.803301	55.377945	3418.7				1,144,877	1,144,877
8110	4060	SUKUNKA	PARDONET-BALDONNEL	U	-121.712104	55.272462	2692.1				1,258,436	1,258,436
8110	4060	SUKUNKA	PARDONET-BALDONNEL	X	-121.786149	55.241410	3008.3				1,218,518	1,218,518
8110	6300	SUKUNKA	TAYLOR FLAT	A	-121.737014	55.225242	4226.2				1,616,555	1,616,555
8115	2800	SUNDOWN	CADOMIN	B	-120.609234	55.457533	2374.6				12,097,244	12,097,244
8115	2200	SUNDOWN	CADOTTE	A	-120.627890	55.434920	1819.5				5,797,026	5,797,026
8115	2200	SUNDOWN	CADOTTE	C	-120.632981	55.406880	1883.9				1,394,640	1,394,640
8140	7400	THETLAANDOA	DEBOLT	A	-121.359474	59.443973	635.7				4,719,797	4,719,797
8150	4800	TOMMY LAKES	HALFWAY	A	-122.127888	57.695193	1066.5				46,167,148	46,167,148
8160	4800	TOWN	HALFWAY	A	-122.234380	56.972917	1694.4				2,119,205	2,119,205
8180	8400	TSEA	SLAVE POINT	C	-121.861476	59.553057	2102.0				1,985,548	1,985,548
8200	4800	TWO RIVERS	HALFWAY	A	-120.469952	56.179704	1492.9				1,816,737	1,816,737
8220	2600	UMBACH	BLUESKY	A	-121.371957	57.136953	1059.4				1,139,415	1,139,415
8240	2630	VELMA	BLUESKY-GETHING	A	-120.579579	57.306140	1108.2				4,343,934	4,343,934
8260	4100	WARGEN	BALDONNEL	B	-121.228130	57.264583	1154.5				6,883,746	6,883,746
8260	2700	WARGEN	GETHING	A	-121.342102	57.289492	1112.7	0	714	714	1,377,572	1,378,286
8300	4800	WEASEL	HALFWAY		-120.679628	57.031158	1271.9	0	0	0	3,055,234	3,055,234
8360	4800	WILDER	HALFWAY	A	-120.988972	56.222423	1333.3				5,231,577	5,231,577
8360	4800	WILDER	HALFWAY	D	-120.936015	56.254260	1544.3				1,888,992	1,888,992
8400	4800	WILDMINT	HALFWAY	A	-120.567136	57.039489	1125.5	0	0	0	3,260,905	3,260,905
8600	4800	WILLOW	HALFWAY	A	-120.623350	57.085297	1114.5				1,634,633	1,634,633
8600	4800	WILLOW	HALFWAY	B	-120.579635	57.122832	1095.2				1,160,492	1,160,492
8800	8600	YOYO	PINE POINT	A	-121.453126	58.923699	2218.8				72,748,677	72,748,677

COAL UTILIZATION POTENTIAL OF GETHING FORMATION COALS, NORTHEAST BRITISH COLUMBIA

Barry Ryan[1] and Bob Lane[2]

ABSTRACT

Existing and some new coal quality data from Gething Formation coals are organized to help document changes in rank and coal quality. The formation outcrops in a number of fold trends extending along the length of the Peace River Coalfield. Trends are separated by thrusts or reverse faults. Within the formation the maceral composition of seams is very variable; also along strike within each trend, rank ranges from high-volatile bituminous to semi-anthracite. The coal quality, oxide, and trace metal data are interpreted in ways not often applied to data to help differentiate thermal coking and coal used for injection into blast furnaces (PCI coal).

KEYWORDS: Gething Formation, coal, rank, ash chemistry, ultimate analyses, Van Krevelen diagrams, synclinal trends

INTRODUCTION

There are two major coal-bearing formations in northeast British Columbia, both of which outcrop extensively along the length of the Peace River Coalfield (Figure 1). Coal seams of economic interest are generally contained in the younger Gates Formation (Table 1) in the southern part of the coalfield and in the older Gething Formation in the northern part of the coalfield. The area where exploration interest tends to switch formations is in the vicinity of Mount Spieker (Figure 2).

The Early Cretaceous Gething Formation overlies the Cadomin Formation (Table 1) and is therefore younger than the Mist Mountain Formation, which outcrops in southeast British Columbia and underlies the Cadomin Formation. The type section for the Gething Formation is in the Peace River Canyon, where it is 550 m thick (Gibson, 1992). It generally thins to the south and, at the Saxon property (Figure 2) at the southern end of the coalfield, is only 7 m thick but still contains coal seams.

Recently, coal prices have risen substantially, sparking a renewed interest in the economic potential of coal in the Gething Formation. In fact at present there are two mines extracting coal from the formation and at least four advanced exploration programs. In the north, Pine Valley Mining Corporation is mining coal from its Willow Creek mine at an average rate of about 60 000 tonnes per month and intends to increase annual production to 2.2 million tonnes in the near future. To the south, Western Canadian Coal Corporation is extracting coal from the small Dillon pit on its Burnt River property and hopes to commence operations on the adjacent, and much larger, Brule pit shortly. The mine is presently operating at a maximum of 80 000 tonnes per month. Several companies are exploring along the Gething coal trend from Pine Pass to Five Cabin Creek (Figure 2), and coal tenures cover most of the land underlain by coal.

Coal seams in the Gething and Gates Formations have different coal-quality characteristics. The quality and rank of coal in the Gates Formation do not vary greatly along the coal trend. In contrast, the rank of coal in the Gething Formation ranges from high-volatile bituminous to semi-anthracite, and there are also significant changes in other coal quality characteristics. The quality of Gething coals was studied by a number of authors and is summarized most recently by Ryan (1997). The wide range of coal rank in the formation means that, depending on location, Gething coals may be thermal coals, coking coals, or low-volatile PCI coals (coal used for pulverized coal injection in blast furnaces). In addition, the variable organic inerts content of seams has a major influence on the quality of coke made from coals in the coking-coal–rank window (approximately 1.0% to 1.6% mean maximum vitrinite reflectance, Rm%) and can extend or contract the rank range over which the coal has coking potential.

As a warning to the occasional reader, rank indicated by measurements of vitrinite reflectance is reported as mean maximum reflectance of vitrinite in polarized light in oil (Rm) or mean random reflectance of vitrinite in oil in non-polarized light (Ro) and occasionally as true maximum reflectance of vitrinite in oil in polarized light (Rmax). Mean maximum reflectance is about 10% greater than mean random reflectance based on various empirical relationships. In this paper an attempt is made to report all data as Rm.

[1]Resource Development and Geoscience Branch, BC Ministry of Energy, Mines and Petroleum Resources, PO Box 9323, Stn Prov Govt, Victoria, BC, V8W 9N3

[2]Health and Safety, Central/Northeast Region, Regional Geologist, BC Ministry of Energy, Mines and Petroleum Resources, 350 – 1011 4th Avenue, Prince George, BC, V2L 3H9

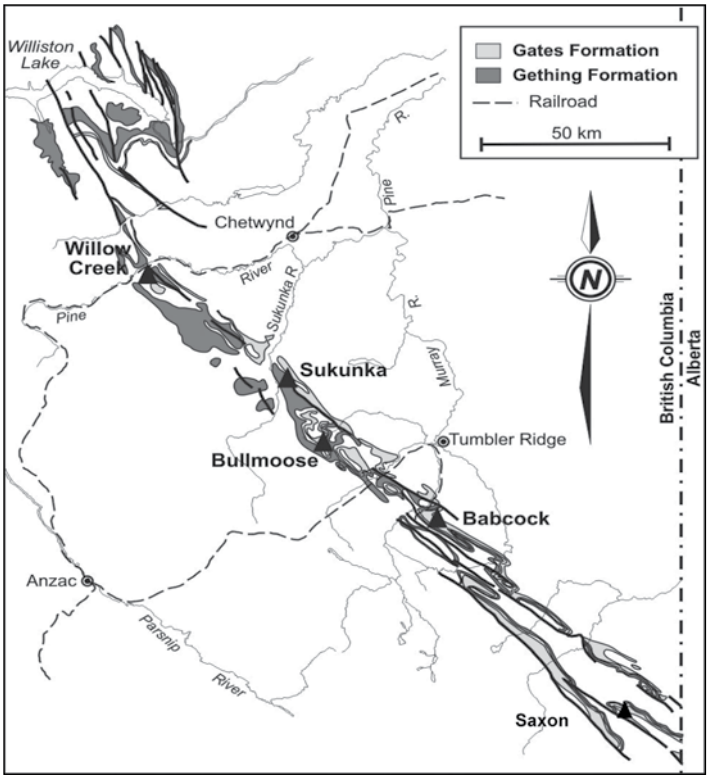

Figure 1. Regional geology of the Peace River Coalfield; outcrop of Gething and Gates Formations.

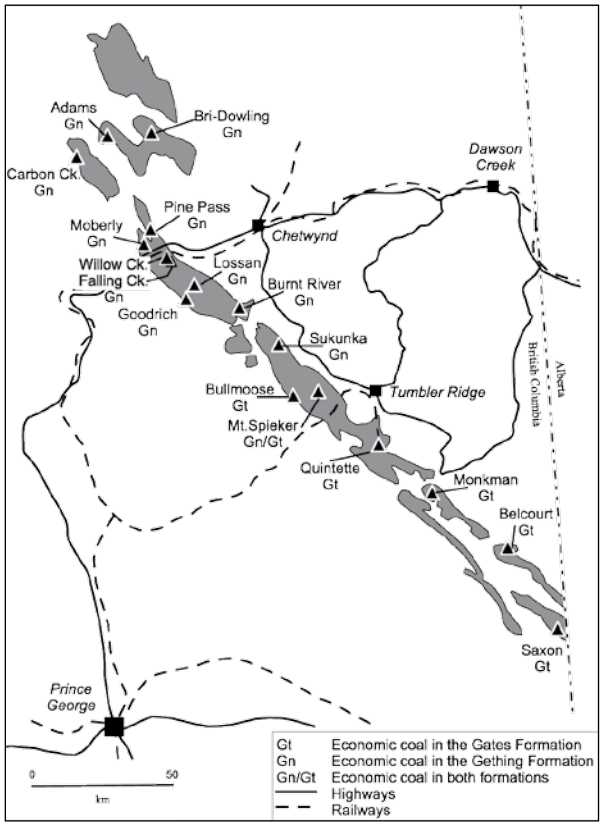

Figure 2. Property locations, Peace River Coalfield: Mount Spieker, Saxon, Sukunka, and Lossan.

TABLE 1. STRATIGRAPHIC TABLE, NORTHEAST BC.

NORTHEAST				SOUTHEAST	
Age	Group	Formation	Description	Formation	Group
Lower Cretaceous	Fort St. John	Hasler	Marine shale		
		Gates	Non marine sandstone, siltstone and **coal.**		
		Moosebar	Marine shale.		
	Bullhead	Gething	Siltstone, mudstone and **coal.**		Blairmore
		Cadomin	Conglomerate.	Cadomin	
Lower Cretaceous and Jurassic	Minnes		Non marine sandstone, siltstone and minor **coal.**	Elk	Kootenay
			Sltstone, mudstone and **coal.**	Mist Mountain	
	Fernie		Sandstone, siltstone and shale.	Morrisey	Fernie

There is a long history of coal exploration in the Peace River Coalfield, and numerous informal property names have resulted. With the upswing in exploration some of these names are retained, often applied to slightly different areas, and in other instances new names are used. Some of the long-standing names often connect to Coal Assessment Reports submitted to the government during the period of intensive exploration from 1975 to 1985; these reports are stored in the Ministry of Energy, Mines and Petroleum Resources building in Victoria or on the Ministry web page as pdf files. They often provide a treasure trove of coal quality information that is still useful today.

COAL QUALITY OUTLINE

Coals from the Gething Formation have the potential to be sold into three markets: thermal coals (low to moderate rank and low price); coking or metallurgical coals (medium rank and high price); and high-rank low-volatile PCI coals (moderate price). Each of these categories has somewhat different coal quality requirements. In simplistic terms, there are three important and fundamental coal quality parameters that interact to determine the quality of a coal, especially its coke-making potential; these are rank, coal petrography (inerts/vitrinite ratio), and ash chemistry. The Gething Formation, probably more than any other coal-bearing formation in British Columbia, exhibits a wide range in these three important quality parameters.

There are numerous quality parameters measured on coke that are predicted with more or less reliability using coal quality parameters. ASTM coke stability is predicted (sometimes not very well) using coal petrography and rank, whereas prediction of coke strength after reaction (CSR) requires the introduction of at least the third variable—ash chemistry—and often a fourth—coal rheology. Obviously these approaches ignore the effect of process variables and size-consist, both of which can substantially influence CSR and ASTM coke stability; in fact it is often forgotten that both stability and CSR decrease as the size of inert particles increases. It is important to consider the size of ash particles that remain in the wash coal but it is also important to consider the size of inert coal fragments (intertodetrinite fragments) in the coal, especially in coals with high proportions of inert macerals. Small inertinite fragments may actually enhance stability whereas large semifusinite particles may act to decrease stability (Lui and Price, 1991).

This report documents rank, which varies from high-volatile bituminous to semi-anthracite, using conventional reflectance analyses and rank calculated from volatile matter (dry, ash-free) values (VM daf). Variation in petrography is documented by microscope maceral analyses but is also indicated by variation in VM daf values *versus* depth and ultimate analyses plotted onto Van Krevelen diagrams. There is evidence in a lot of coal quality data from the formation that seams are characterized by large variations in inertinite content, and petrographic analyses indicate inert variations from 10% to over 70%. Many reports mention variable FSI values for apparently low-ash un-oxidized samples, and this probably indicates varying inertinite content. Plots of VM daf *versus* depth do not provide consistent trends of decreasing VM daf with depth, and the sawtooth pattern probably also reflects major changes in the inertinite content of seams.

Coal Assessment Reports provide a lot of coal quality information on Gething coals, though not always of a type that is relevant for the present study. As an example, there are many proximate analyses but very few rank or petrographic analyses, which are more useful for an overview study. Often rank is estimated from values of volatile matter corrected to a mineral-matter-free basis (VM dmmf) or dry, ash-free basis (VM daf). The relationship between VM daf and rank is illustrated by a number of authors (Figure 3, adapted from Taylor *et al.,* 1998). It should be noted that the diagram uses mean maximum reflectance (Rm) and presumably samples that are close to 100% vitrinite. As the amount of inertinite in a sample increases, a lower VM daf value corresponds to the same rank; consequently any estimation of rank from volatile-matter measurements must also take into account the petrography of the sample. Estimating VM daf from high-ash samples does not provide accurate values of VM daf. In this case it is better to plot a set of ash *versus* VM daf data and project back to derive the value VM daf value at zero ash.

An equation was derived to predict rank using VM daf and percent reactives in a previous paper (Ryan, 2002) and is adapted here based on data from the Lossan property (Figure 2), which includes proximate and petrographic analyses. The equation predicts rank based on VM daf and percent reactives or predicts variation in petrography if rank and VM daf values are known:

Rm=-0.7431*ln(VM daf)+0.004486*(reactives%)+2.967 Equation 1

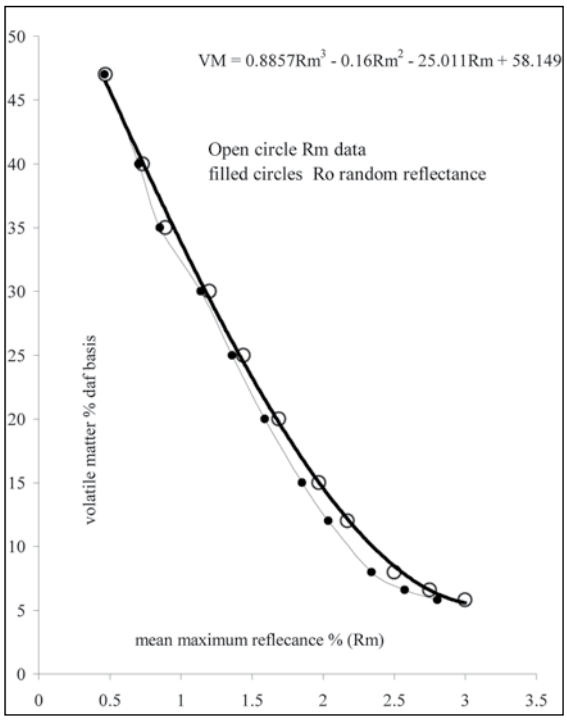

Figure 3. Relationship of VM daf to random reflectance; diagram simplified from Taylor *et al*., (1998).

Obviously the equation provides only an approximation of any one of the three variables if the other two are known. The estimation of the percent reactives in a sample depends on the assumption of the amount of semifusinite that is reactive. It is very important to document seam petrography through an area in order to blend a consistent coking-coal product.

Vitrinite reflectance is generally considered to be a measure of coal maturity, but it can also be influenced by environment. There are a number of papers that document vitrinite suppression related to hydrogen infusion into vitrinite. There is also the possibility of vitrinite enhancement. Diessel and Gammidge (1998) indicate that early coal-forming environments can influence vitrinite reflectance. Partial oxidation in an environment that gives rise to seams rich in inertinite will also produce vitrinite with a higher reflectance than vitrinite in seams that do not form in this type of environment and have higher concentrations of reactive macerals. The difference in reflectance is maintained as rank increases, so that vitrinite in seams that have the same maturity may have different reflectance values—vitrinite in

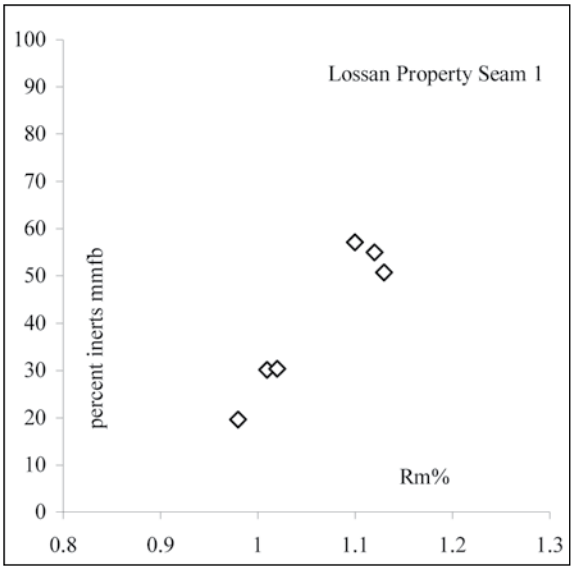

Figure 4. Percent reactives *versus* Rm for seam 1, Lossan property.

inertinite-rich seams having higher reflectance than seams rich in reactive macerals. There are indications that this might be the case for data from the Gething Formation. Rank and petrographic data from Seam 1 Lossan property correlate (Figure 4), and this may be a coincidence or indicate that vitrinite reflectance may be inversely correlated to the reactives content of a seam. The reactives range from 42% to 82%. A range of this magnitude will have major effects on rheology and coking properties and will make it difficult to estimate rank from VM daf data.

The Van Krevelen diagram illustrates the change in O/C and H/C as rank increases for various kerogen types. It tends to be used in more academic studies of coal, but is also useful for outlining coking potential of coals. Both atomic ratios (O/C and H/C) are sensitive to rank and to maceral composition of coal and consequently tend to bypass some of the confusion in determining the actual content of reactive macerals in coal samples. A previous study (Ryan *et al*. 1999) provides rheology and ultimate analyses for medium-volatile production coals (ash contents all close to 10%), and the data indicate the change in FSI within a Van Krevelen diagram (Figure 5).

Ash chemistry influences the quality of coal in terms of its use as thermal coals or for coke making. It has a major influence on CSR and is therefore important here because most Gething coals are planned for coke making or PCI use in blast furnaces. Ash chemistry is presented as base/acid ratios (oxides of Fe, Ca, Mg, Na, and K divided by oxides of Si, Al, and Ti). The mineral form of the base oxides also affects CSR (Price *et al,* 1992).

Generally, sulphur contents in Gething coals are less than 1% and not a concern, except for the seam underlying the marine Moosebar and Bluesky Conglomerate, which often has higher sulphur contents. This is important because

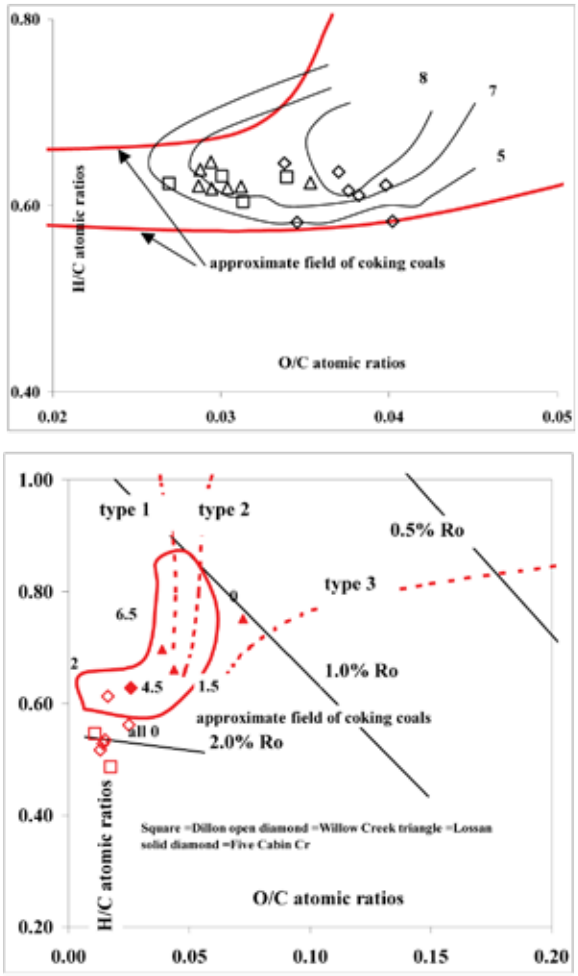

Figure 5. FSI contours for medium-volatile BC production coals in a Van Krevelen diagram; data from Ryan *et al*. (1999).

it means that most of the Fe in an ash oxide analysis is probably in iron carbonates. The relative concentrations of Ca, Mg, and Fe may be represented on triangular plots, which illustrate changing trends in relative carbonate concentrations with increasing rank. The oxides each have a different impact on CSR, and studies indicate that Ca from carbonates is probably more damaging to CSR than is Fe in carbonates (Ryan *et al*., 1999). The paper also documents the negative correlation of SO_3 to CSR. Probably breakdown of carbonates is forming sulphates in the ash, which results in the appearance of SO_3 in the ash analysis. Oxides of K and Na, which also negatively affect CSR, probably occur in clays dispersed in coal.

Variations in contents of Ca, Mg, and Fe tend to track changes in the composition and amount of carbonate in coal. The mix of carbonates present (siderite, ankerite, dolomite, and calcite) may be temperature-dependent and can therefore give an indication of when fluids infiltrated coal and caused precipitation of carbonates. Spears and Caswell (1986) outline a sequence of cleat mineralization that, from low to high temperature, is sulphide, silicate, and then carbonates. Carbonate mineralization starts with diagenetic deposition of siderite (becoming more Ca- and Mg-rich with increase in temperature). At higher temperatures, carbonates precipitate in the sequence ankerite, dolomite, Fe-rich calcite, and finally calcite (indicating a general decrease in Fe content). This sequence covers the temperature range from 50 °C to 150 °C and therefore coal ranks up to medium-volatile bituminous, which covers the temperature range when most of the thermogenic methane is generated.

The mix of carbonates in coal gives information on when fluids infiltrated the coal; they may also indicate the composition of the fluid associated with the coal. Van Voast (2003) reveals some interesting correlations of water chemistry with coal in productive coalbed gas (also referred to as coalbed methane, CBM) basins. He found that coal waters rich in bicarbonate and Na and impoverished in Ca, Mg, and SO_4 (mainly because of biogenic reduction of sulphate and precipitation of calcite and dolomite) are often associated with productive CBM basins. Obviously in coals with low sulphide content, the relative concentrations of Fe, Mg, and Ca may provide information about when carbonates were deposited and may also provide hints about the CBM potential. Coals with ash chemistries enriched in carbonates and impoverished in Na may have been in association with water with a CBM-favourable fingerprint.

Phosphorous is a significant contaminant in steel, and customers generally look to purchase coal with less than 0.1% P (sometimes down to 0.03%) concentration. Phosphorous concentrations are measured as P_2O_5 oxide concentrations in ash. A more useful value is the concentration of P in the total sample and it is these values that are presented here. Phosphorus has a complex association with coal, as discussed by Ryan and Grieve (1996) and Ryan and Khan (1997). It sometimes concentrates in the inert coal macerals and not ash and is therefore difficult to wash out.

COMMENTS ON THE REGIONAL STRUCTURE IN THE GETHING FORMATION

Within the Peace River Coalfield, the Gething Formation outcrops as synclinal cores in a number of fold or thrust blocks that follow the trend of the fold belt and in large part define the coalfield (Legun, 2003). East of the fold belt, a number of thrusts depress the Gething Formation below depths of interest for surface or underground coal mining, and interest switches to CBM, oil, or natural gas potential. However, in the north, east of the fold belt, the Gething is at shallower depths, and there are a number of open synclines and anticlines in the outer foothills where there is underground coal mining and CBM potential.

Rank and possibly other coal characteristics change as one traverses from southwest to northeast across the trend of the fold belt into different thrust blocks. Often rank is

lower on the west-southwestern edge of the fold belt and higher in the middle before decreasing again to the east-northeast along the eastern edge of the belt and into the Western Canadian Sedimentary Basin (Karst and White, 1980; Marchioni and Kalkreuth, 1982; Ryan *et al*. 2005).

In the north, coal is contained in the upper and middle part of a thick Gething section. To the southeast along the trend of the fold belt in the Sukunka area, (Figure 2) the Gething Formation contains a marine tongue (Bullmoose Member, Gibson, 1992; Duff and Gilchrist, 1983; Legun, 1987) with coal in the Upper Gething Chamberlain Member and in the underlying Gayland Member. The tongue does not extend to the south, and as the formation thins, coal is probably equivalent to the Lower Gething (Gayland Member) in the south. Broatch (1987) suggested that there may be other marine tongues in the Gething that wedge out to the south. This means that, on the regional scale, one can expect major coal quality variations across and along the trend of the fold belt within the formation.

Fold axes along the fold belt maintain a northwest-southeast trend, but plunge and direction both vary and in some cases there are major changes over short distances. There is no obvious pattern of cross-folding in the fold belt, however north of the Pine River, the synclines cored by the formation tend to be doubly plunging, forming basin structures. A line following the Peace River east of Hudson Hope and projected southwest into the fold belt outlines a possible structural high with structures plunging to the north on the north side and to the south on the south side. This line approximately follows the trend of the Peace River Arch and therefore may influence structures in the deformed belt. It also intersects the deformation front at a location where the trend deflects to a more northerly trend north of the line. This interaction may have implications for regional fracture patterns and local present-day extension important for CBM exploitation.

The orientation of the present-day horizontal maximum stress direction is northeast-southwest (Bell, 2002). Cross-folding may tend to open (anticline) or close (syncline) fold-axis–normal cleats and therefore have a fundamental influence on permeability, which is required for successful CBM production. Reversal of fold plunge even in individual thrust blocks may be key to understanding permeability. There is some evidence that in the northern part of the fold belt, cleats are axial planar, whereas in the south they tend to be fold-axis normal (Ryan, 2003). Based on the present orientation of the maximum horizontal stress direction, the axial planar cleats may indicate a local reorientation of the stress direction from a north-northeast trend to a south-southeast trend. This may signal areas of improved permeability.

Hughes (1967) discussed the structural style in the fold belt. Synclines are underlain by shallow dipping thrusts and appear to have ridden on the underlying thrusts somewhat passively. Where thrusts cut up-section, tight anticlines form in the thrust plate, and thrusts sometimes break through the hinges. In this geometry, the western limbs of anticlines above thrusts are more likely to be in extension than are the eastern limbs below thrusts. In areas of intense folding, coal seams often contain axial planar fractures that may or may not predominate over early-formed fold-axis–normal cleats.

Timing of coal maturation relative to the onset of deformation can influence coal quality parameters. If coal achieves moderate to high rank prior to onset of deformation, it will withstand deformation better, and shearing may be limited to areas of folds (hinges) that experience most strain. If coal has achieved only low or moderate rank when deformation starts, it is more likely to be pervasively sheared. The most obvious result of the latter situation will be fines generation and a high Hardgrove Index. This affects coal washability, fine circuit capacity in a wash plant, and plant yield, as well as causing handling problems for the producer and customer. In the southern part of the coalfield, deformation of Gates Formation coals post-dated coal maturation (Kalkreuth *et al*., 1989). Further north they considered results of reflectance studies across thrusts to be inconclusive. However, the form of the iso-rank contours mirror the folded outcrop pattern of the Gething, indicating imposition of rank prior to folding (Figure 6).

In the foothills, coal exploration companies have not traced the coal-bearing section of the Gething Formation much north of Williston Lake. However, coal exists in the formation at depth to the east in the Western Canadian Sedimentary Basin (Ryan *et al.* 2005) and to the north, for example Pink Mountain (Kalkreuth *et al*. 1989). To the southeast the fold belt trends into Alberta, and in this area the Gething Formation is thin.

MAJOR SYNCLINAL TRENDS AND RANK IN THE GETHING

It is possible to outline structural and coal quality trends in the Gething Formation using a combination of regional maps (for example, Legun, 2003) and Coal Assessment Reports. Major synclinal fold trends within the deformed belt are outlined in simplified figures (Figures 7 and 8) to help illustrate the following discussion. Exploration properties are located with reference to these approximate fold trends as this provides the easiest way to compare the major coal quality trends. Table 2 provides a summary of rank, ash chemistry, and phosphorous data for properties along each synclinal trend. Data are averaged and provide only a general idea of variations. The deformation front separating the foothills from the Western Canadian Sedimentary Basin is defined by a number of thrusts, some of which are responsible for considerable change in depth of the Gething Formation. In the Tumbler Ridge area, the Gething is down-

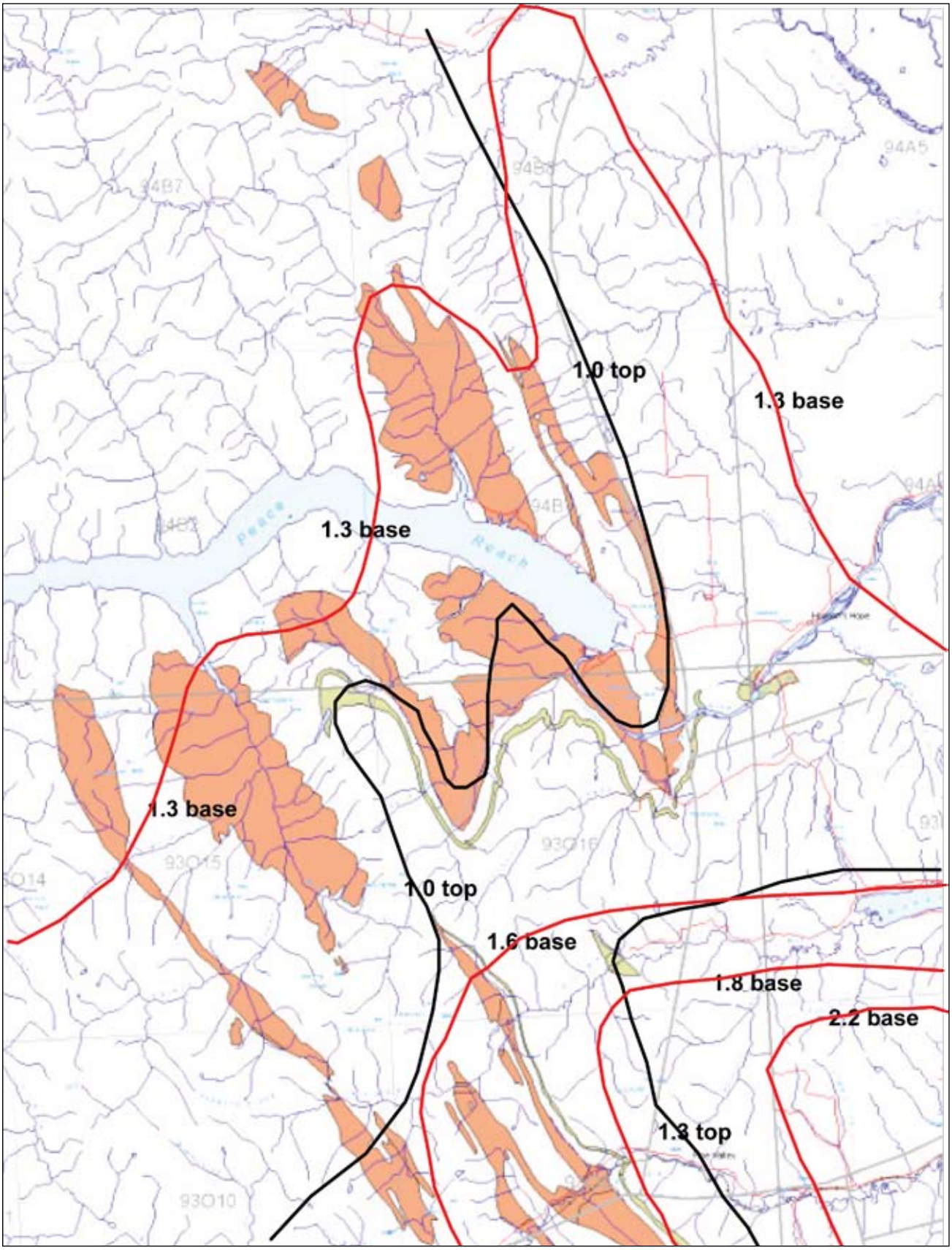

Figure 6. Reflectance values for top and bottom of the Gething (data from Kalkreuth *et al.*, 1989) with regional geology.

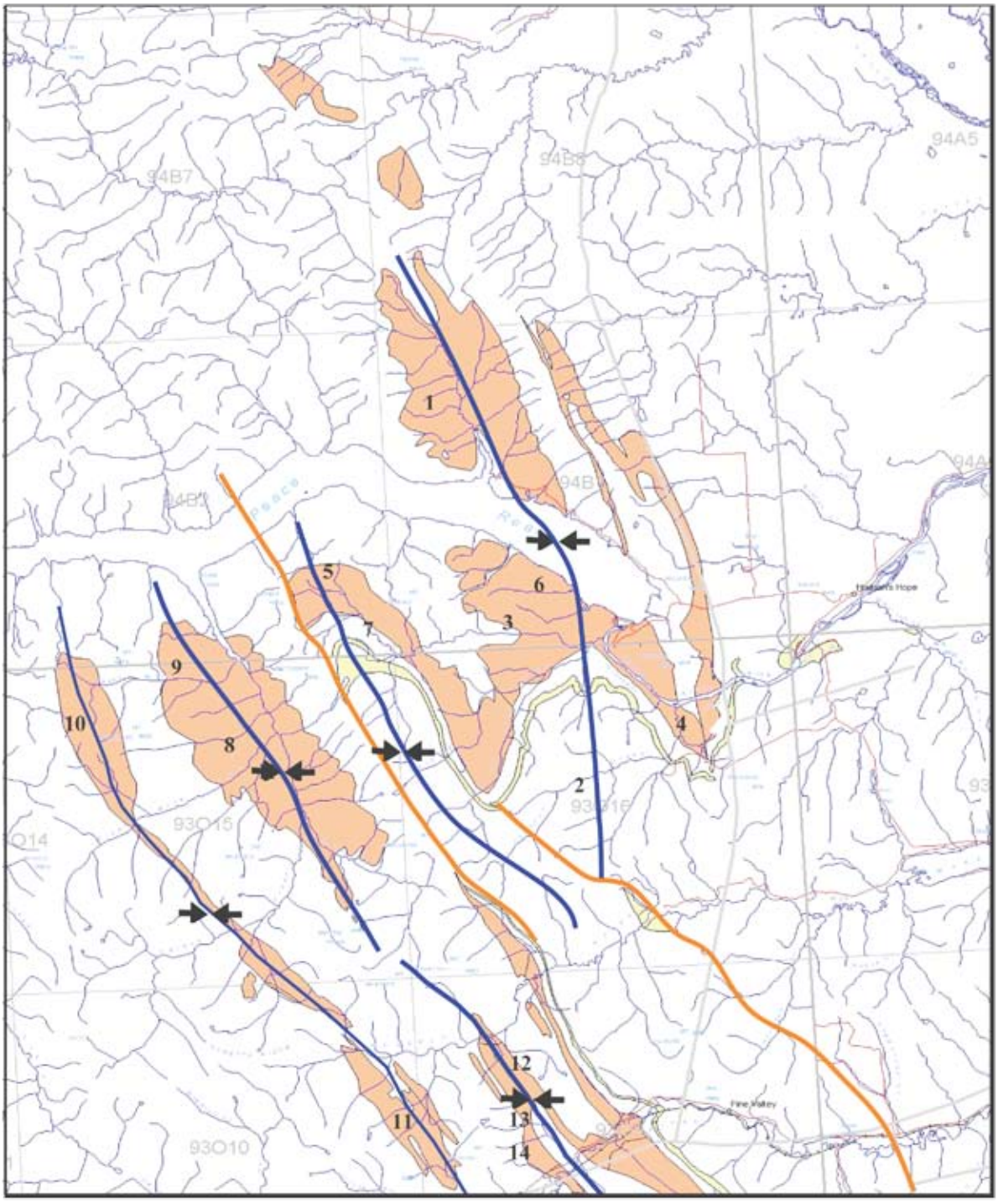

Dunlevey	1	South Mount Gething	7	Pine Pass	13
Bri Dowling	2	Carbon Creek	8	Norman Creek	14
Mount Gething	3	North Carbon Creek	9		
Cinnebar Peak	4	West Carbon Creek	10		
Adam Creek	5	Mount Bickford	11		
East Mount Gething	6	Fisher Creek	12		

Figure 7. Cartoon of regional structures in the Gething north of Pine River.

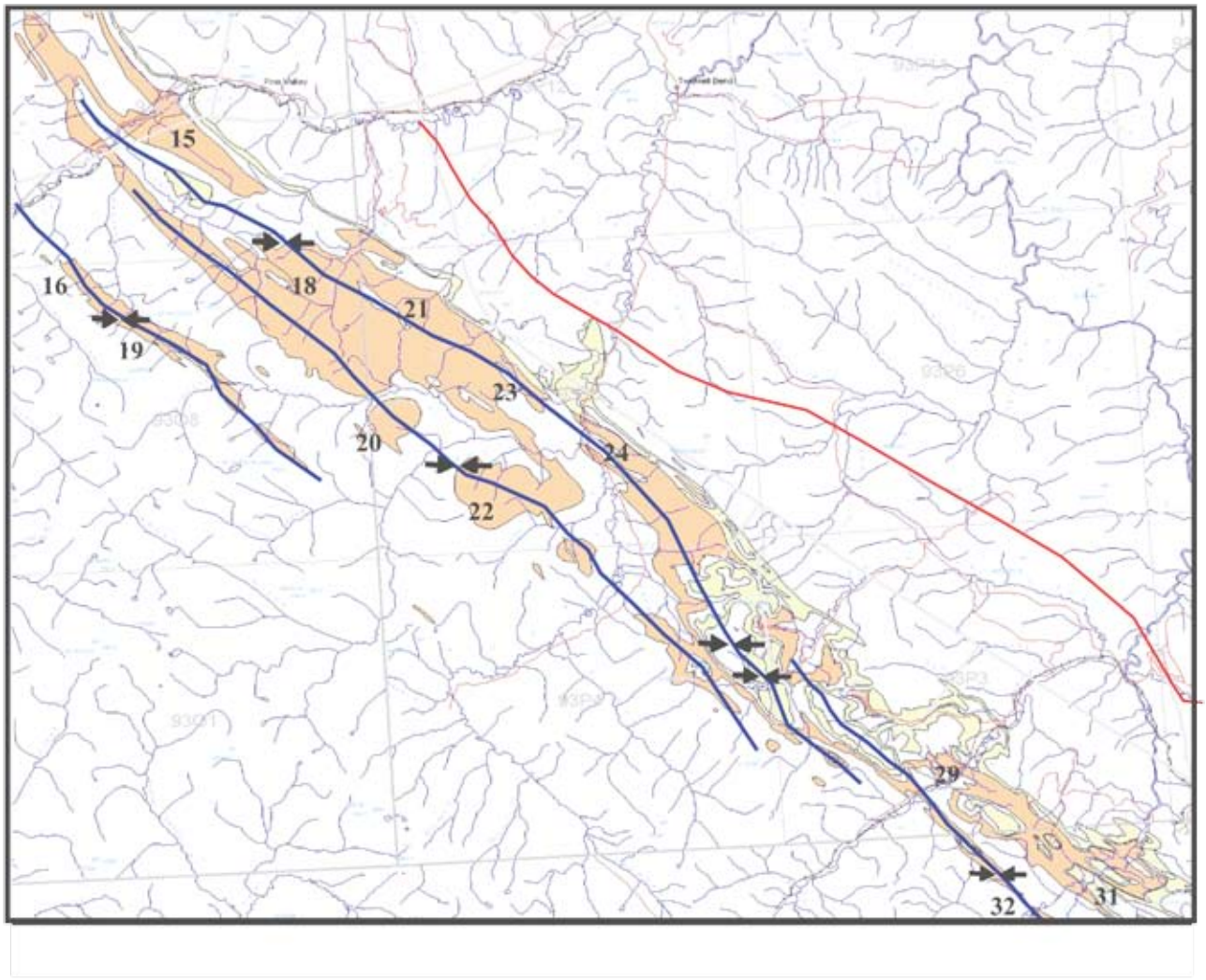

Willow Creek	15	Burnt River South	22
Goodridge central south	16	Dillon	23
Falling Creek	18	Sukunka	24
Lossan	19	Trend	31
West Brazion	20	Five Cabin	32
Hasler	21		

Figure 8. Cartoon of regional structures in the Gething south of Pine River.

dropped hundreds of metres by the Gwillam Lake Thrust. To the north and south in the foothills, there is less increase in depth of the Gething as the subcrop is traced into the Western Canadian Sedimentary Basin.

There are a number of regional studies of rank in the Gething Formation (Karst and White, 1980; Kalkreuth and McMechan, 1988; Kalkreuth *et al,* 1989; Marchioni and Kalkreuth, 1992). Most of these studies concentrate on rank of the formation east of the deformed belt and therefore do not provide a regional overview of rank in areas presently considered for surface or shallow underground mining. However, regional rank data of Kalkreuth *et al*. (1989), represented as contours for the top and bottom of the Gething (Figure 6), covers some of the area covered by Figure 7. When overlain on the regional geology (Figure 7), the data indicate that in the area south of Williston Lake, rank increases to the east. Rank in the East Mount Gething property (number 6, Figure 7) and Cinnabar Peaks (4) areas is higher than it is in Bri-Dowling (2) and South Mount Gething (7) properties to the west. In general, iso-rank lines trace the outcrop pattern of the Gething, and rank increases to the south as the depth of the Gething increases.

TABLE 2. RANK, BASICITY, AND PHOSPHOROUS DATA FOR PROPERTIES, GROUPED BY FOLD TRENDS.

West Carbon Creek				Carbon Creek				Fisher Creek				Dunlevey				Murray			
north	rank	basicity	P% total sample	north	rank	basicity	P% total sample	north	rank	basicity	P% total sample	north	rank	basicity	P% total sample	north	rank	basicity	P% total sample
				North Carbon Cr	0.9-1.03*	0.29	0.036					Dunlevey	0.9-1.35*	X	X				
West Carbon Cr	1.02-1.18	0.51	0.059	Carbon Cr	0.9-1.03*	0.29	0.036					Bri Dowling	1.01-1.45	0.43	0.07				
Bickford	1.0- 1.78			Fisher Cr	1.1							Mount Gething	0.95-1.45	0.55	0.11				
Goodridge Central South	1.24-1.54	0.26	0.072	Pine Pass	1.11-1.38	0.47	0.022	Willow Cr	1.61	0.43	0.02	Cinnebar Peak	X	X	X				
Lossan	0.98-1.33	0.11	0.19	Norman Cr	1.11-1.5*	X	X	Falling Cr		0.14	0.04	Adam Cr	1.11*	X	X				
				West Brazion	1.3-1.5*	X	X	Hasler	1.74			East Mount Gething	0.9-1.4	X	X				
				Burnt River South	X	X	X	Dillon	1.74	0.4	0.02	South Mount Gething	X	X	X				
								Sukunka	1.41	0.25	0.06								
																Five Cabin Cr	1.18-1.26	0.77	0.009
south				south				south				south				south			

Southeast and east of the Gwillam Lake Thrust, the Gething Formation is generally at considerable depth; however, to the northwest and east of the extension of the thrust, the formation is at shallower depths and defines a number of broad open folds. In the 1980s, the area north of Williston Lake (Figure 7) (Butler Ridge and Dunlevey Creek; area 1) was explored by Hudson Bay Oil and mapped by Legun (1984). The Gething Formation is about 500 m thick in the Dunlevey area and contains numerous thin seams. A hole in 1973 drilled 246 m of the formation and intersected 10 seams greater than 0.3 m thick with a cumulative thickness of 4.24 m. The hole was collared about 75 m below the Moosebar Formation. Seams intersected in the hole were considered to be too thin for mining, and no coal quality data were obtained. Rank in the area at the top of the Gething is less than 1% Rm and at the base greater than 1.3% (Kalkreuth *et al*. 1989). The Butler Ridge-Dunlevey area is underlain by a broad syncline in the outer foothills that, on the regional scale, plunges to the south-southeast, intersecting the northern extension of the Gwillam Lake Thrust system west of Moberly Lake.

The area south of Williston Lake and east of the projected trend of the Gwillam Lake Thrust, which is the southern extension of the Butler Ridge-Dunlevey Syncline, was explored by a number of companies. The area includes the properties Bri Dowling (2), Mount Gething (3), and East Mount Gething (6). An anticline to the east is represented by Cinnabar Peak (4) property, and an anticline to the west by the Adam Creek (5) and South Mount Gething (7) properties (Figure 7). This area, which is underlain by multiple thin seams of high- to medium-volatile rank at favourable depths, has potential for CBM exploration, and if individual seams are thick enough, also for underground coal mining.

The East Mount Gething property (6) explored by Utah Mines Limited (1978 to 1980) is the southern extension of the Dunlevey Creek Syncline and covers in general terms the western limb of the major syncline. A number of reflectance measurements were made on samples from the 1977 drill program (Figure 9, Creaney, ISPG, personal communication). The Rm data do not vary consistently with depth, which may indicate the influence of variable petrography on vitrinite reflectance values. Samples from thick seams have higher Rm values than samples from thin seams at the same depth. This may be a sampling problem that introduced oxidation or it may relate to different petrography in thin seams (reactive-rich) to thick seams (inertinite-rich). The rank at the top of the Gething is estimated to be about Rm = 1%, in agreement with Kalkreuth *et al*. (1989). The predicted rank at the base of the formation depends on using thin or thick seam data and varies from medium- to low-volatile bituminous, in general agreement with Kalkreuth *et al*. (1989).

West of the Gwillam Lake Thrust extension, there are a number of complex synclinal trends that extend southeast along the trend of the fold belt. Each trend is described using information collected from coal exploration reports covering properties along the trend. In the north the Carbon Creek (8) and West Carbon Creek (10) properties identify two trends (Figure 7). The most westerly synclinal trend is defined in the north by the West Carbon Creek property. Data from Kalkreuth *et al*. (1989) do not extend west of the northern projection of the Gwillam Lake Thrust except for some measurements in the vicinity of West Carbon Creek, where Rm values of 0.95% and 0.98% are given for the top of the formation. Exploration data provide Rm data that ranges from 1.02% to 1.08% measured on samples from

1980 holes. There are numerous thin seams in the West Carbon Creek area, and the formation is estimated to be the same thickness as on the Carbon Creek property. Tracing the trend to the southeast, on the north side of the Pine River it covers the area variously referred to as the North Moberly, North-Central Goodridge, or Mount Bickford property (11). Rank is medium- to low-volatile bituminous (Kalkreuth *et al*., 1989), and cumulative coal in the section is less than in the Gething to the east in the Carbon Creek trend, but details are sparse.

South of the Pine River (Figure 8**),** the West Carbon Creek trend continues as the South Central Goodridge (16), Lossan (19), and Cirque properties. Recent exploration has added to the data for the first two areas; however, there is little information on the Cirque property, which marks the end of this trend in terms of Gething outcrop. Rank on the Goodridge South Central property ranges from 1.29% to 1.54%, with no indication of the value at the top of the formation (Figure 10; data provided by First Coal). The data indicate a possible thrust in the section with upwards of 100 m of stratigraphic separation.

Most of the coal resource on the Lossan property is in the upper Seam 1, which is 40 m below the top of the Gething, and some is in Seam 5, which is 160 m below the top of the formation. Rank of Seam 1 ranges from 0.95% to 1.26%. An adit sample provided Rm values for the upper part of seam 1 of about 1.1% and for the lower part, 1.0% (Figure 4). The difference may relate to petrography, in that higher inerts contents sometimes correlate with higher Rm values, and high vitrinite contents with low Rm values. Alternatively, the upper part of the coal intersection may have been thrust on top of the lower part of the intersection and originate stratigraphically at least 50 m lower in the section. Rank of the lower Seam 5 is described as low-volatile bituminous; however, if the seam has a high inerts content and rank was estimated from VM daf data, then rank may be over-estimated. As an example, the inert- rich upper part of seam 1 has a rank of 1.1%. If rank is estimated from VM daf data using the plot from Taylor *et al.* (1998), then a Rm value of over 1.3% is derived. The coking potential of a high-volatile seam with high inerts content is very different from a medium-volatile seam with high reactives content.

North of Pine River, the Carbon Creek (8) property (Figure 7) defines a syncline trend that can be traced south. In the Carbon Creek area, the Gething Formation is estimated to be 1067 m thick (Legun, 1986), though Karst (1978) suggests that the formation may be thinner. It is possible that if the Cadomin is non-conglomeritic, some of the underlying Minnes Group may have been included in the Gething Formation. To the south, the formation is estimated to be about 500 m thick. Karst (1978) also provides reflectance data for 2 holes, and values range from 0.85% to 1.26% (Figure 11) and, based on where they were collared in the section, rank at the top of the formation is less than 0.8%. There are over 100 thin seams with a cumulative thickness of 18.8 m, though only 10 are of economic thickness.

The southern extension of the Carbon Creek Synclinal trend, north of the Pine River, is referred to as the Fisher Creek Syncline. The northeastern part was mapped as the East Moberly or Moberly property, which covers the eastern edge of the Gething trend. The Norman Creek property covers the west limb and center of the structure, the Pine Pass (13) property the centre and eastern part of the structure, and the Fisher Creek (12) property covers the eastern part of the structure (Figure 7). Along trend, folds get tighter and rank increases. On the Pine Pass (13) property, rank appears to be exclusively medium-volatile (Figure 12), and the cumulative coal thickness in the section is about 20 m. Rank values do not increase systematically with depth and correlate with VM daf values (Figure 12); this may indicate multiple stratigraphic repeats or indicate that inerts content is influencing (increasing) Rm values of seams, as discussed by Diessel and Gammidge (1998).

South of the Pine River, the Fisher Creek synclinal trend, in very generalized terms, broadens and is defined by the two limbs of the syncline. The eastern limb is covered by the Willow Creek (Pine Valley Mine), Hasler, and Dillon properties (locations 15, 21, and 23, Figure 8). Rank at Willow Creek is medium- to low-volatile bituminous (Table 3). To the south, rank increases and at Hasler Creek is low-volatile bituminous with Rm values averaging 1.74% and ranging from 1.6% to 1.87% (Table 3). Rank at the Dillon property further to the south is low-volatile bituminous, averaging 1.76% for the lower seam (Table 3). East of the Dillon Mine, Burlington drilled a coalbed methane (CBM) hole that intersected the Gething Formation at a depth of 972 m where it is 344 m thick. Rank at the top of the Gething is 1.81% Rm, and some seams are inertinite-rich with total inerts contents (mmfb) varying from 43% to 60% (Petro-Logic Services, 2003 report).

The Fisher Creek Synclinal trend projects approximately through the Sukunka property (location 24, Figure 8) and the Bullmoose Mine. Rank of Gething Formation coals at Sukunka is 1.32% Rm close to the top of the formation. The trend does not continue south. Rank in the trend is consistently higher than in the West Carbon Creek trend to the west and increases to the south, reaching a maximum at the Dillon property before decreasing somewhat at Sukunka.

The trend, which is the extension of the western limb of the Fisher Syncline south of Pine River, is defined by the West Brazion and Burnt River South properties (locations 20 and 22, Figure 8). Samples collected from the West Brazion property (Gilchrist, 1979) were analysed by Kilby (unpublished data) and have ranks of 1.38% and 1.35% Rm**.** Samples are from Lower Gething or from coal below the Cadomin. To the south, samples collected from Burnt River South property provide ranks ranging from 0.97% to

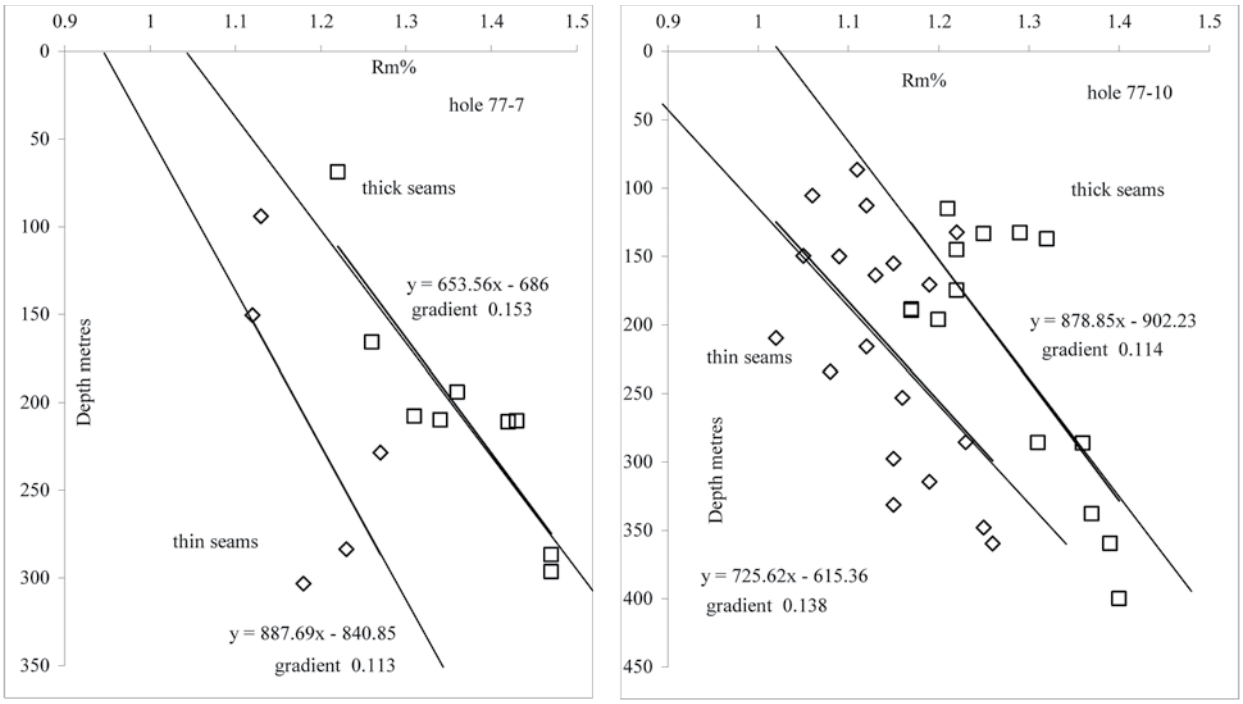

Figure 9. Reflectance values, East Mount Gething property (Creaney ISPG personal communication).

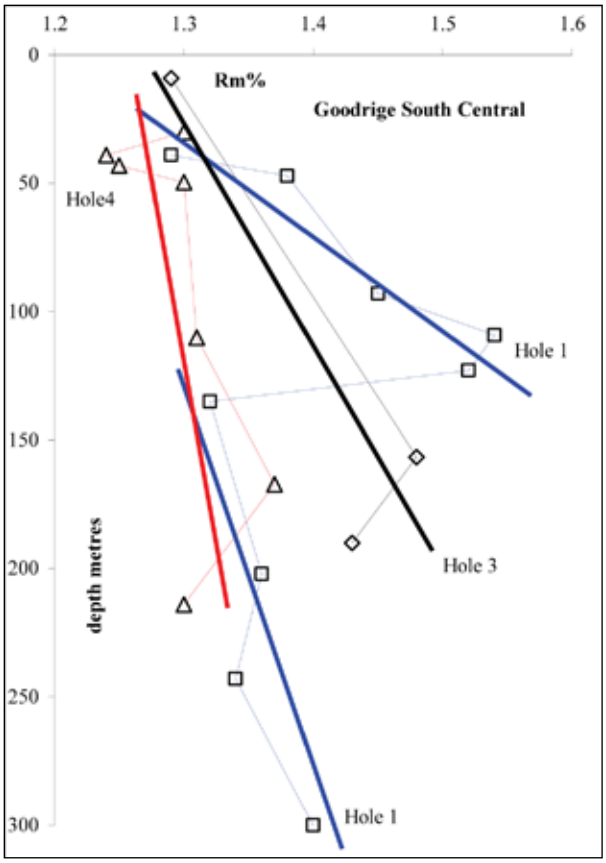

Figure 10. Rm% values from the South Central Goodrich property; data provided by Michael Hunter, First Coal.

1.16% Rm. The trend continues south to Mount Chamberlain before outcrop of the Gething Formation ends. Ranks in this trend increase to maximum in the vicinity of the Pine River and then decrease to the southeast. They are generally less than ranks in the trend to the east but similar to or higher than ranks in the West Carbon Creek trend to the west.

Further to the south (Figure 8), the Murray River Syncline has Gething coal potential between the Murray and Red Willow rivers (Five Cabin Creek property, location 32, Figure 8) and extends north as the Wolverine Mine in the Wolverine Valley. In this location, Koch drilled a hole for CBM into the Lower from approximately 30 to 305 m. Rank for the Lower Gething samples ranged from 1.59% to 1.7% Rm (Table 3). At Five Cabin Creek, rank of Gething coal is medium-volatile (Table 3) with indications that the rank is lower on the west limb than on the east limb. Southeast of the Five Cabin Creek property, the Gething Formation is thin but still contains coal. Based on rank in the overlying Gates Formation, rank is lower along the Murray River Syncline trend and increases to the east-northeast in the Monkman-Belcourt trend before decreasing at depth to the east-northeast. The Monkman property was explored mainly for the coal potential in the Gates Formation. The Gething Formation is 136 m thick in the area and contains 3 seams thicker than 1.5 m (Leckie *at al.,* 1988). The Rm value of the seams ranges from 1.3% to 1.32% with a fairly high rank gradient of 0.16 to 0.27%/100 m. In the extreme south Mount Gorman property, the Gething is 46 m thick and contains a single 3 metre-thick seam, which appears to be high-volatile bituminous in rank.

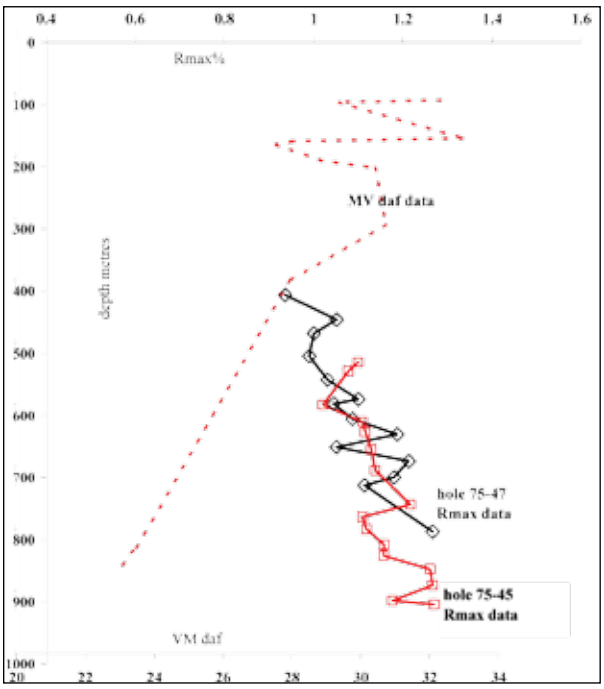

Figure 11. Reflectance values (Karst, 1978) and VM daf data for the Carbon Creek area.

TABLE 3. RANK AND PETROGRAPHY, WILLOW CREEK AND DILLON PROPERTIES.

		Mean maximum reflectance (Rm)
Willow Creek (This study)		
6 seam	full seam	1.61
7 seam	top	1.66
	bottom	1.61
	dull	1.65
	bright	1.5
Dillon Mine (This study)		
Lower Seam	full seam	1.75
	top	1.79
	bottom	1.75
	Vitrain grab	
	Durain grab	1.67
Lossan property (This study)		
Seam 1	Bottom	1.09
	Mid	1.10
	Top	1.02
	Grab	1.09
	Grab	1.08
	Grab	0.95
Five Cabin Creek (This study)		
seam B2	top	1.200
	grab	1.180
	core	1.260
Hasler Creek (Kilby)		
average Rm		1.74
range		1.60 to 1.87
High Hat (Burlington)	Depth, metres	
	1018	1.84
	1112	1.94
	1270	2.06
Wolverine (Koch)		
	Depth, metres	
Lower Gething	221.95	1.67
	222.98	1.67
	242.25	1.70
	242.95	1.68
	251.25	1.59
	255.5	1.64
	282.65	1.67

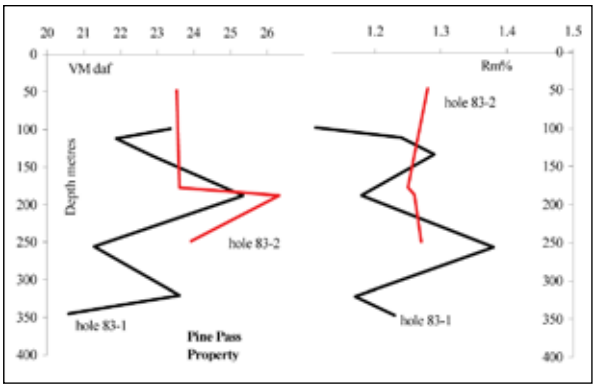

Figure 12. Vitrinite reflectance (Rm) values, Pine Pass property.

QUALITY TRENDS ALONG THE MAJOR SYNCLINAL TRACES

The Gething Formation is characterized by considerable variation in inerts content. Some of the early coal assessment reports confused oxidation with high inerts content when trying to explain low FSI values. In terms of coke-making potential, higher inerts content is favourable for medium-rank coals but is detrimental in low- and high-rank coals. The optimum inert line for ASTM stability (Pearson, 1980) indicates that the maximum optimum inerts for stability occurs at a rank of 0.9% (other studies indicate a higher rank). The maximum optimum inerts for CSR occurs at ranks in the range 1.3% to 1.5 % Rm (Price *et al*. 2001) (Figure 13). Variation in inerts content (mainly fusinite and semifusinite macerals) is easy to document using petrography, but the exact relationship of inerts content to coke quality is much more confused. There are many papers that discuss ways of partitioning semifusinite between reactive and non-reactive components. It is possible in part to bypass this confusion by using ultimate analyses plotted

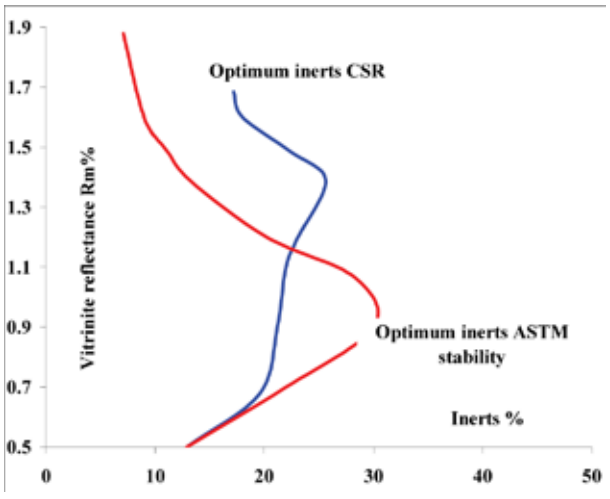

Figure 13. Optimum inerts line *versus* rank for ASTM stability or CSR; data from Pearson (1980) and Price et al. (2001).

onto a Van Krevelen diagram, which allows separation of samples based on degree of reactivity and rank.

South of Williston Lake (Figure 7), Van Krevelen diagrams of data from Butler Ridge-Dunlevey syncline East and South Gething properties (Figure 14) indicate that coal from the East Gething property is more reactive and of slightly higher rank than that from South Gething. Based on the scatter of data in the Van Krevelen diagrams, there appears to be a wide range of inerts content in the samples. This is corroborated by Vm daf data from the properties, which do not have a consistent relationship to depth (Figure 15).

Ash chemistry in this area is indicted by data from Bri-Dowling and South Mount Gething properties as base/acid ratios and phosphorus content data (Figure 16). Both base/acid ratios and phosphorous contents are higher for the Bri-Dowling than for the Mount Gething property. In addition, triangular plots of Ca, Mg, and Fe (Figure 17) indicate that there may be more Ca, relative to Fe and Mg, in samples from the Bri-Dowling property.

Moving west into the northern part of the deformed belt, ultimate analytical data for the West Carbon and Carbon Creek trends (Figure 14) indicate, in agreement with reflectance data (Figure 11), that rank is higher to the west and the coal is somewhat more reactive. Plots of VM daf *versus* depth data indicate wide variation in petrographic composition for seams from both the West Carbon Creek and Carbon Creek trends (Figure 15).

The southern extension of the Carbon Creek trend, north of the Pine River, is covered by the Pine River, East Moberly, and Fisher Creek properties. Rank increases in this direction, but there is limited ash chemistry and ultimate analytical data to add to the discussion (Figures 14, 16, and 18). A triangular plot of Ca, Mg, and Fe oxides for these properties and Willow Creek (Figure 19) indicate an increase in Ca content to the south. Though CSR correlates with base/acid ratio, it is disproportionally sensitive to particular cations, such as Ca (Ryan *et al*., 1999).

Three synclinal trends are traced south of the Pine River. The West Carbon Creek trend is represented by the South Central Goodridge and Lossan properties. Ash chemistry indicates that the Goodridge coal has more phosphorous and higher base/acid ratios than does coal to the north (Figure 20). In addition, ash is richer in Ca than are ashes to the north (Figure 19). This may be because fluids were emplaced at higher temperatures. The Lossan property is characterized by low base/acid ratios and phosphorous contents.

The trend roughly representing the east limb of the Fisher Creek Syncline is represented by the Hasler, Dillon, and Sukunka properties. No data were located for the Hasler property. Base/acid ratios for the Dillon property are high, but phosphorous contents low. The Sukunka property was explored in the 1970s as a potential underground cok-

ing-coal mine, and there is a lot of coal quality information available. Unfortunately, the exploration predated general introduction of some of the coke tests that are considered to be important today, such as CSR. Ash chemistry for the Sukunka property clearly indicates an increase in Ca carbonate (Figures 19, 20) and phosphorous contents are moderate with some higher values.

The Fisher Creek west trend is represented by the Brazion and Burnt River South properties, but no quality data were located.

The northern end of the Murray Creek syncline trend is represented by data from the Koch Petroleum Wolverine CBM hole that intersected Gething coal. In this location, base/acid ratios are low and the ash relatively richer in Mg (Figures 19, 20), but this is probably not a carbonate association. The Fiver Cabin Creek property to the south is characterized by high base/acid ratios and low phosphorous contents (Figure 21).

COAL PETROGRAPHY

Petrography data for Gething coals exist in a number of papers—for example, Ryan and Lane (2002) —but there is no systematic study, mainly because of the difficulty of getting representative samples from a full suite of Gething exploration properties. In this study, a few samples collected from Pine Valley Coal at Dillon, Lossan, and Five Cabin Creek were analysed for petrography (Table 4). Standard preparation techniques were employed with 300-point counts per sample. No attempt was made to differentiate between vitrinite and pseudo-vitrinite or to differentiate between reactive and non-reactive semifusinite. Generally samples contain variable amounts of semifusinite + marcinite + inertodetrinite that range from 25% to 53%. Most samples contain some pseudo-vitrinite, and the inert macerals tend to contain less structured semifusinite than in other Cretaceous coals. In some areas of intense shearing, the coal contains multiple curved surfaces that look a little like cone-in-cone structure (Bustin, 1982). A sample of this material was examined and found to be composed almost entirely of vitrinite. A lot of the vitrinite is pseudo-vitrinite but, other than that, there was no evidence of excessive micro-fracturing or intra-grain strain. The high inertinite content in some samples will decrease rheology and probably tend to contract the rank window over which Gething coals will make good coke.

COAL QUALITY DATA 2005 SAMPLES

A number of samples were analysed for proximate and ultimate parameters, ash oxides, and trace metals (Table 5). Trace metals data from the ICP-MS analyses are averaged by property and plotted into a correlation matrix (Table 6). Ash oxide analyses were made using XRF techniques on fused ash samples. Coal samples are ashed to provide the starting material, and consequently the analysis provides an ash concentration as well as an analysis of major oxide concentrations in the ash. A comparison of the ash concentration

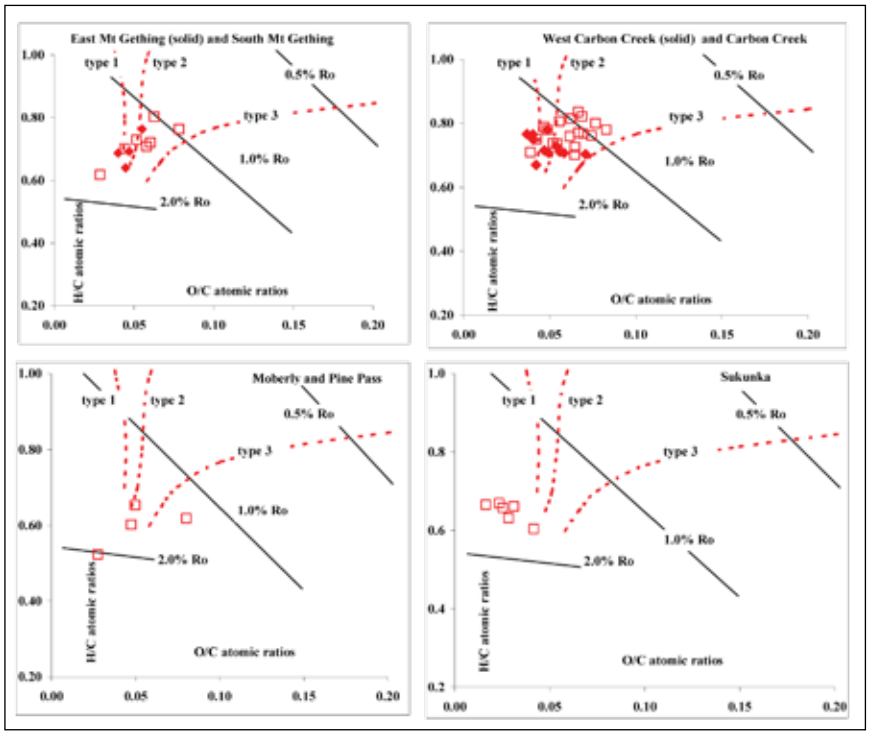

Figure 14. Kan Krevelen diagrams for data from properties East and South Gething, Carbon Creek, West Carbon Creek, Moberly, Pine Pass, and Sukunka.

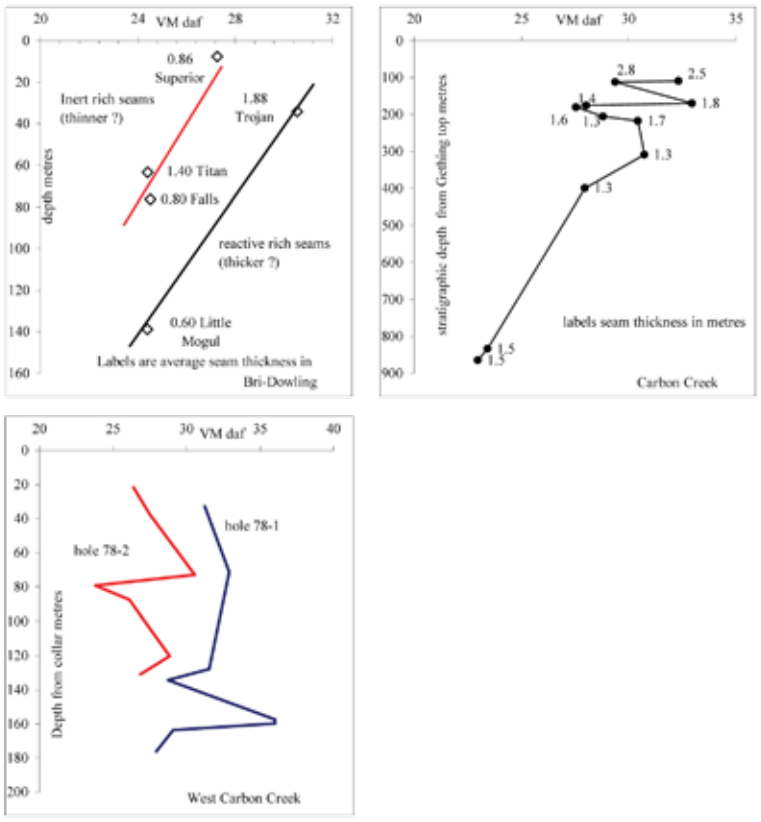

Figure 15. VM daf *versus* depth plots for Bri-Dowling, Carbon Creek, and West Carbon Creek properties.

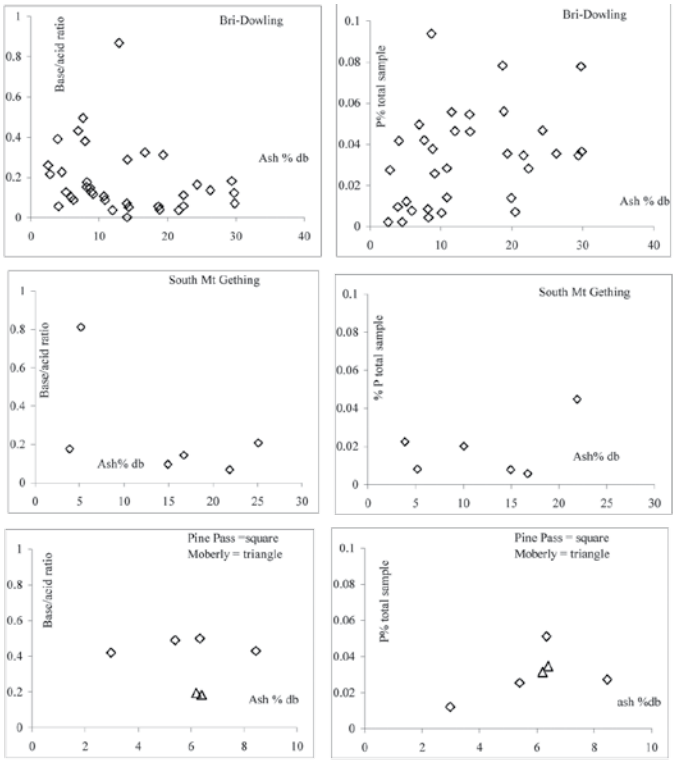

Figure 16. Base/acid and P% versus ash plots, Bri-Dowling and South Gething properties.

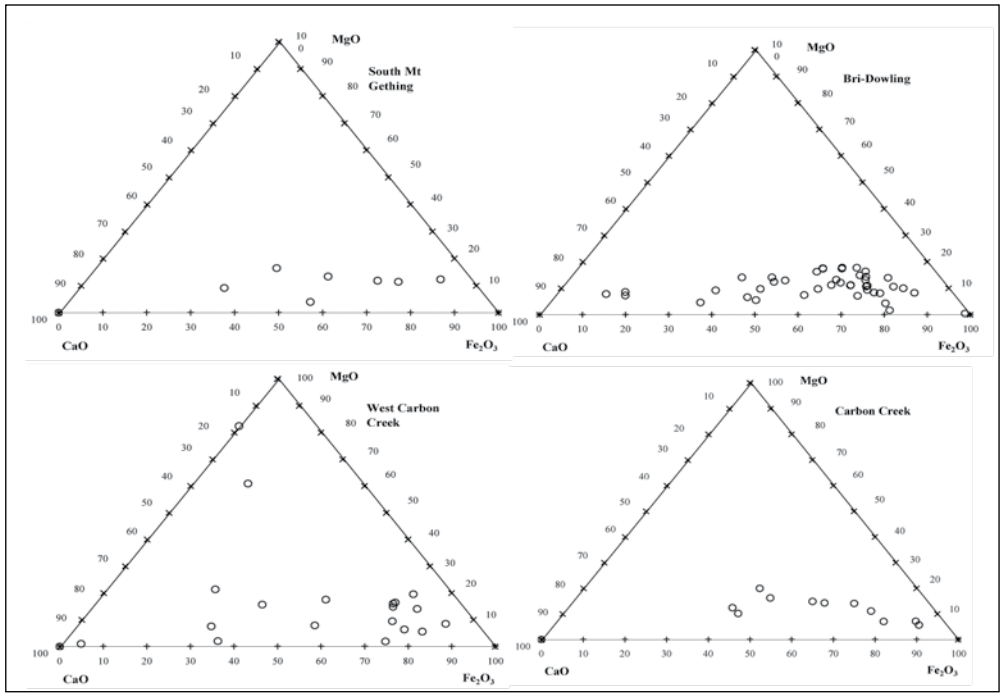

Figure 17. Triangular plots for Fe, Ca, and Mg for Bri-Dowling, South Mount Gething, Carbon Creek, and West Carbon Creek properties.

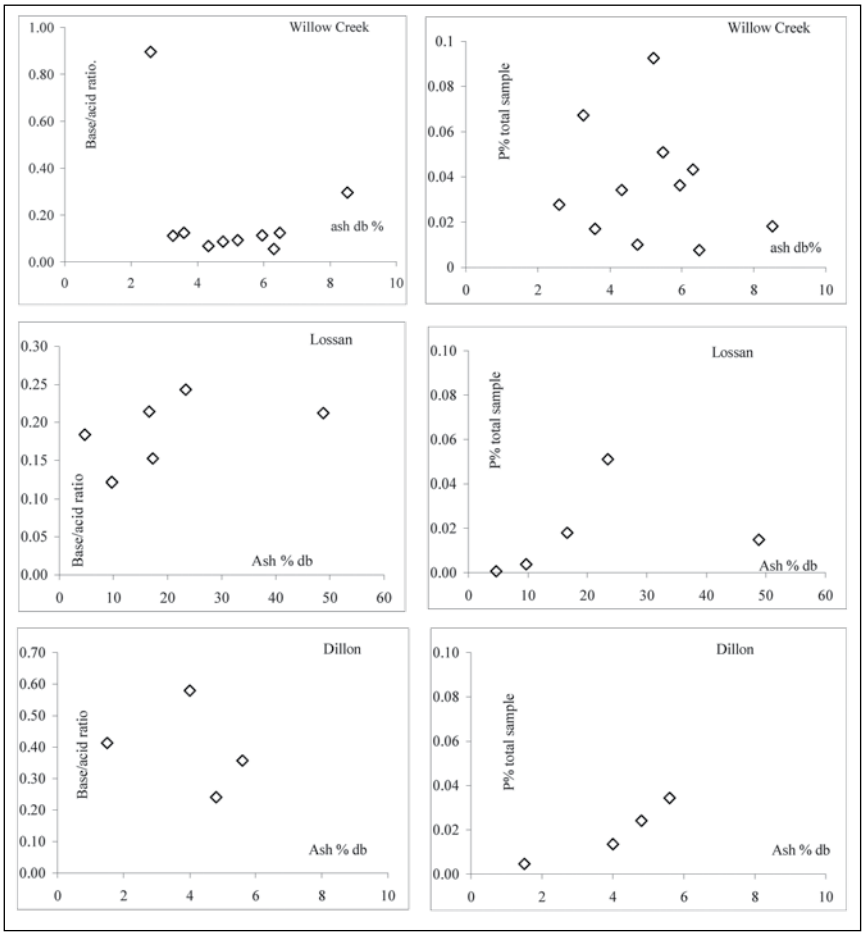

Figure 18. Base acid and P% *versus* ash plots, East Moberly, Pine Pass, and Willow Creek properties.

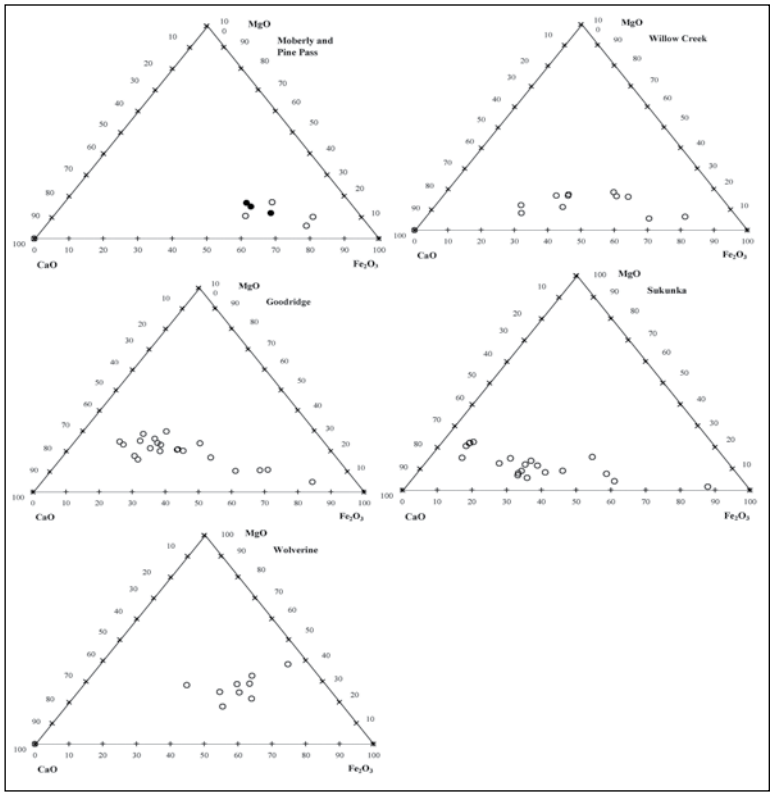

Figure 19. Triangular plots for Fe, Ca, and Mg for Pine Pass, East Moberly, Willow Creek, Goodrich, Sukunka, and Wolverine properties.

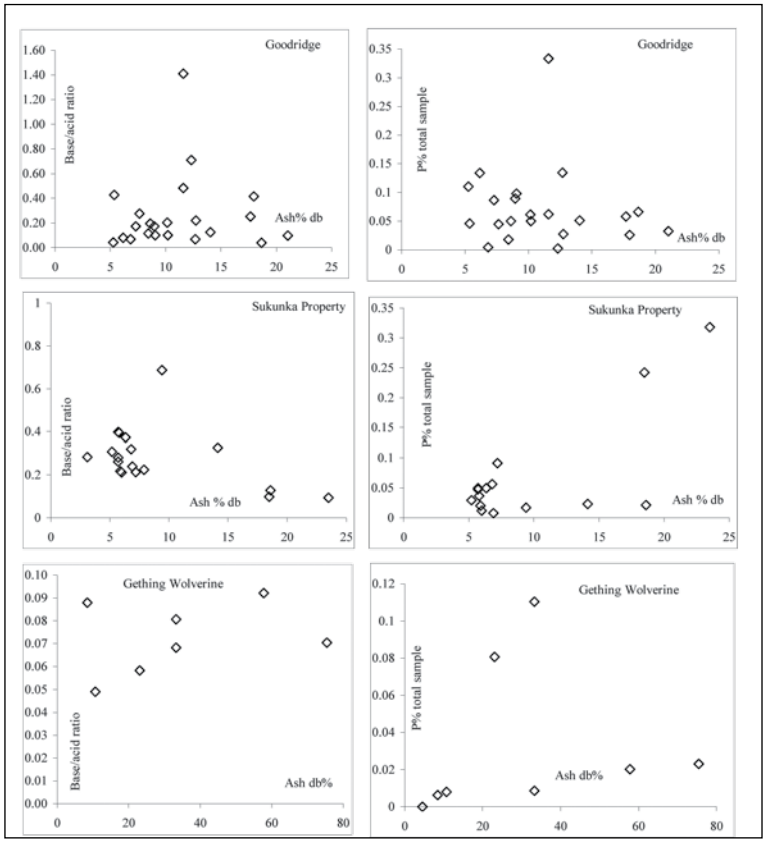

Figure 20. Base/acid and P% *versus* ash plots, Goodrich, Sukunka, and Wolverine properties.

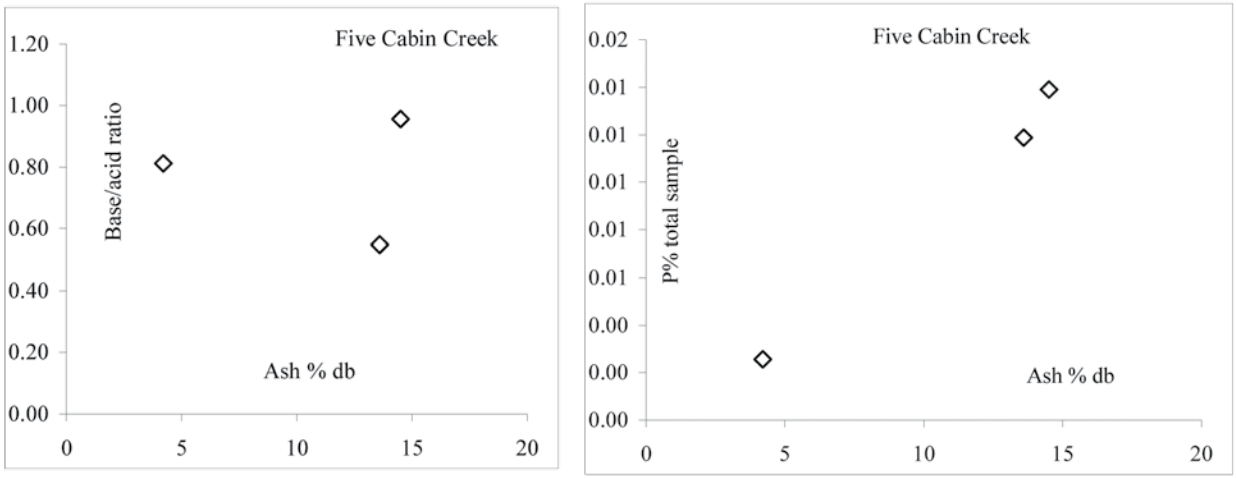

Figure 21. Base/acid and P% *versus* ash plots, Five Cabin Creek property.

TABLE 4. PETROGRAPHY FOR SAMPLES FROM LOSSAN, DILLON, PINE VALLEY COAL, AND FIVE CABIN CREEK.

Coal petrography 300 point count																
	telinite	collo telinite	collo detrinite	vitro detrinite	gelo vitrinite	liptinite	**total reactives**	micrinite	macrinite	semi fusinite	fusinite	inerto detrinite	**total inerts**	Volume mineral matter	wt mineral matter%	wt ash % (1.15)
	Lossan Seam 1															
bottom 1/3	2	20	23	1	0	2	**48.3**	0	3	24	1	5	**33.6**	18	30.5	26.6
mid seam	0	9	29	1	0	7	**45.3**	0	2	21	0	7	**29.3**	25	40.5	35.2
top of seam	7	28	33	0	0	5	**72.4**	0	3	17	0	5	**25.3**	2	4.5	3.9
Grab	3	16	41	0	1	4	**65.4**	0	3	19	2	7	**30.3**	4	8.3	7.2
Grab	3	13	29	0	1	2	**48.0**	0	3	29	0	5	**37.3**	15	25.6	22.2
Grab	11	41	30	0	0	5	**87.5**	0	0	4	0	1	**4.9**	8	14.2	12.3
	Dillon Lower Seam															
full seam	1	27	29	1	0	0	**58.4**	0	3	25	0	7	**36.0**	6	10.6	9.2
top 3 metres	0	7	35	0	0	0	**41.7**	0	5	39	0	9	**53.3**	5	9.5	8.3
bottom 1.7m	0	25	27	0	0	0	**51.7**	1	5	32	0	6	**43.0**	5	10.1	8.8
vitrain grab	1	41	53	0	0	0	**94.9**	1	0	2	0	1	**3.5**	2	3.2	2.7
cone in cone str	0	62	30	0	0	0	**92.3**	1	0	4	0	1	**5.7**	2	3.9	3.4
	Willow Creek															
top of seam 7 1.55m	0	8	38	0	0	0	**46.3**	0	11	28	1	8	**48.0**	6	10.6	9.2
bottom of seam 7 1.0m	0	22	21	0	0	0	**43.0**	1	3	25	0	11	**39.7**	17	29.5	25.7
full seam 6	0	15	34	0	0	0	**48.7**	1	4	31	0	11	**46.7**	5	8.9	7.8
	Five Cabin Creek															
seam B2 drill core	0	20	35	0	0	1	**56.0**	1	4	22	0	9	**35.7**	8	15.4	13.4

TABLE 5. SAMPLES ANALYSED BY ASHING ACID LEACH AND ICP-MS IN THIS STUDY; SOME VALUES COMPARED TO DATA FROM GRIEVE AND GOODARZI (1994). NA=NEUTRON ACTIVATION; AA=ATOMIC ADSORPTION. DATA CALCULATED TO CONCENTRATIONS IN TOTAL COAL SAMPLES.

element		Lossan	Five Cabin	Goodridge Central	Pine Pass	Willow Creek	Dillon	Grieve and Goodarzi 1994	analysis
Analyses by ICP-MS on ash		Properties arranged in order of increasing rank							
		1	2	3	4	5	6		
Mo	ppm	1.14	0.81	2.83	1.29	1.65	1.55		
Cu	ppm	3.93	4.73	8.04	4.36	2.62	2.56	14	AA
Pb	ppm	6.54	2.29	3.92	4.31	0.89	0.77		
Zn	ppm	21.28	8.11	20.67	20.78	8.47	6.92		
Ag	ppb	36.71	23.15	65.78	50.08	18.48	11.69		
Au	ppb	0.66	5.04	1.18	0.17	0.12	0.12		
Ni	ppm	8.08	5.08	8.18	17.54	4.52	2.92		
Co	ppm	2.46	1.10	1.00	1.54	0.53	0.38	2.59	NA
Mn	ppm	10.31	49.97	1.79	24.74	2.29	0.92		
As	ppm	3.24	4.49	4.75	8.29	9.15	9.12	2.2	NA
U	ppm	1.48	0.61	1.39	0.99	0.55	0.53	2.28	NA
Th	ppm	3.38	1.10	2.66	2.20	0.98	0.71	4.21	NA
Cd	ppm	0.08	0.10	0.16	0.05	0.14	0.14		
Sb	ppm	0.15	0.10	0.32	0.24	0.12	0.09	0.77	NA
Bi	ppm	0.13	0.04	0.05	0.02	0.03	0.02		
Cr	ppm	9.94	6.87	15.08	14.96	4.54	3.89	20.7	NA
B	ppm	8.31	11.57	5.46	10.72	2.32	1.87		
S	%	0.04	0.23	0.33	0.41	0.03	0.03		
Hg	ppb	1.01	0.63	0.74	0.38	0.74	0.52	51	AA
Se	ppm	0.12	0.14	0.35	0.68	0.36	0.01		

TABLE 6. TRACE METAL DATA BY ICP-MS, AVERAGED FOR THE PROPERTIES.

x	Mo	Cu	Pb	Zn	Ag	Au	Ni	Co	Mn	As	U	Th	Cd	Sb	Bi	Cr	B	S	Hg	Se
Mo	1.00																			
Cu	.63	1.00																		
Pb	-.04	.42	1.00																	
Zn	.30	.58	.90	1.00																
Ag	.58	**.86**	.65	**.87**	1.00															
Au	-.37	.28	-.06	-.29	-.10	1.00														
Ni	-.03	.28	.58	.74	.66	-.24	1.00													
Co	-.33	.17	**.95**	.75	.41	.03	.51	1.00												
Mn	-.66	.07	.08	-.13	-.07	**.84**	.20	.23	1.00											
As	.04	-.57	-.71	-.47	-.42	-.53	.00	-.69	-.33	1.00										
U	.36	.63	**.91**	**.93**	**.80**	-.18	.45	.76	-.21	-.69	1.00									
Th	.21	.52	**.96**	.94	.75	-.18	.52	.85	-.13	-.68	**.98**	1.00								
Cd	.71	.19	-.56	-.40	-.11	-.11	-.70	-.71	-.58	.18	-.19	-.35	1.00							
Sb	.71	**.83**	.48	.79	**.97**	-.23	.63	.21	-.21	-.21	.68	.61	.04	1.00						
Bi	-.16	.13	**.80**	.53	.20	.03	.00	**.84**	-.05	-.79	.73	.78	-.28	.01	1.00					
Cr	.40	.76	.70	**.90**	**.97**	-.10	**.82**	.50	.06	-.37	.76	.74	-.33	**.92**	.18	1.00				
B	-.51	.31	.57	.41	.36	.59	.59	.64	**.85**	-.55	.29	**.38**	-.79	.17	.27	.50	1.00			
S	.24	.69	.30	.53	.77	.20	.76	.14	.40	-.13	.30	.29	-.32	.76	-.28	**.84**	.60	1.00		
Hg	.08	.11	.45	.24	.05	.03	-.38	.48	-.26	-.66	.53	.53	.17	-.07	**.84**	-.09	-.11	-.51	1.00	
Se	.20	.26	.21	.51	.59	-.29	**.84**	.11	.06	.28	.19	.23	-.38	.66	-.33	.67	.30	.73	-.44	1.00

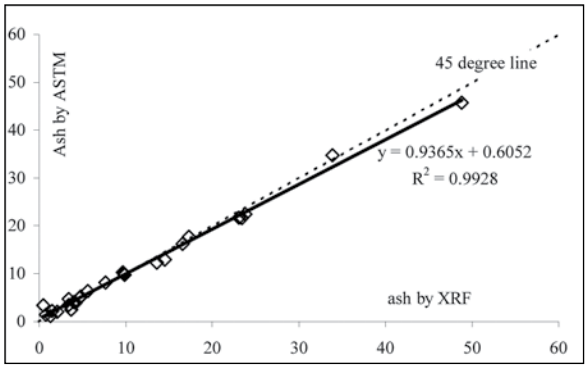

Figure 22. Comparison of phosphorous analyses by ICP-MS and XRF.

analyses done by the conventional ASTM method with the XRF procedure (Figure 22) indicates that there is very little difference between the two methods, and consequently an XRF analysis alone provides all the information necessary to calculate oxide concentrations on a total sample basis. The ashing of samples may volatilize some elements (for example, mercury), but most elements will not be affected.

Trace metals in ashed samples were analysed using ICP-MS with a hot $HCl+HNO_3$ acid leach. This leach will dissolve adsorbed metals, sulphides, and carbonates and may also partially remove some elements from silicates. A comparison of the results of XRF and ICP-MS analyses for the major oxides Fe, S, Mg, Ca, Na, K, and P provides information on amount of carbonate and sulphide in samples and amount of easily removed Na, K, and P.

The comparison of phosphorous XRF and ICP-MS data indicate that about one third of the phosphorous is removed by the acid leach (Figure 23). Phosphorous is usually contained in coal as apatite or alumino-phosphates (Gorceixite [Ba, Al, P] and Goyazite [Sr, Al, P]). There is a strong correlation of Sr with P in the ICP-MS data, so it appears that the acid leach is removing goyazite. Based on the strength of the leach and the fact that only about one third of the P is removed, it is unlikely that acid-washing of coal will be an economic way to reduce phosphorous contents.

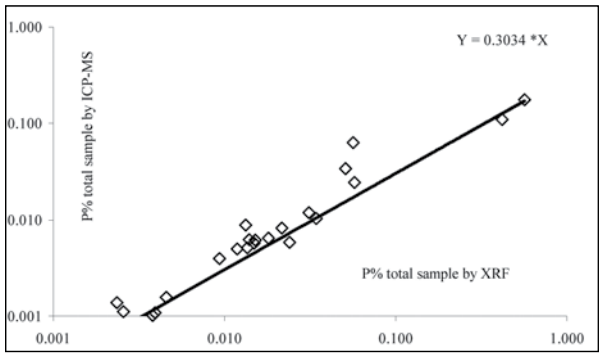

Figure 23. ICP-MS sulphur in ash acid leach *versus* total iron in ash by XRF.

A comparison of some average trace-metal concentrations derived by ICP-MS on leach samples from this study (Table 5) and the study by Grieve and Goodarzi (1994) (analysis methods indicated in the table) indicates that concentration of Hg by ICP-MS is definitely low and concentrations of other metals appear to be somewhat lower. This may indicate that trace amounts of metals are probably held in silicates and not leached. It is unlikely that the metals are volatilized by the ashing process. ICP-MS data may not provide reliable total concentrations of some trace metals but, more importantly, it may give a much better idea of the amount of trace metals that might be mobilized during mining and have environmental impact.

The data (Table 5) are arranged in order of increasing rank to the right. Most of the metal concentrations appear to decrease slightly as rank increases, except for arsenic concentrations, which appear to increase as rank increases. All concentrations are within normal limits for coal.

Comparison of concentrations derived from XRF analyses and from ICP-MS analyses on acid leach samples provides information on the amount of the element not held in insoluble silicates. Iron in samples may be bound in sulphides, carbonates, or silicates. A plot of total Fe (XRF) *versus* leach Fe (ICP-MS) indicates a constant amount of 0.25% Fe, probably in silicates (Figure 24). The leach Fe appears to be distributed between carbonates and sulphides based on how much the data plots right of the pyrite line in Figure 24. Some data plots to the left, probably because of

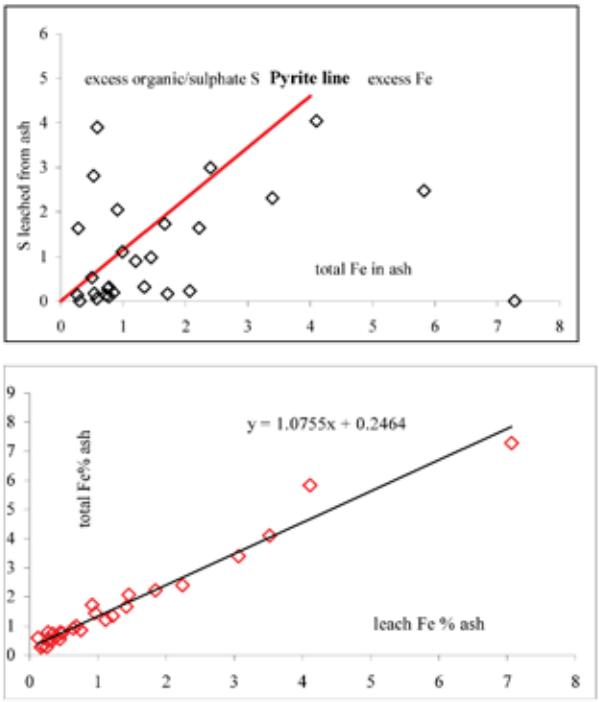

Figure 24. Triangular plot of Gething data ICP-MS leached Ca, Mg, and Fe identified by rank.

the presence of S leached from sulphate, which originates from weathered samples. It is apparent that a lot of the Fe in the samples is contained in carbonates.

Distribution of Fe, Ca, and Mg in carbonates may provide information about the origin and temperature of cleat and micro-fracture infilling. Plots of leach Ca *versus* total Ca and leach Mg *versus* total Mg indicate that nearly all Ca and Mg are removed by leaching. For Ca, an amount of 0.06% is contained in silicates, and for Mg, the amount is about 0.1%. It appears that the leach amounts of Fe, Ca, and Mg may provide a better picture of carbonate composition than the total concentrations derived from XRF. Concentrations plotted into a triangular plot (Figure 25) indicate a predominance of Fe, Ca carbonates (ankerite and siderite). There does not appear to be a change of carbonate composition as rank increases, possibly indicating either an early or late emplacement of carbonates rather than numerous emplacement events at different temperatures. The influence on CSR of Ca, Fe, and Mg in carbonates has been mentioned, and the ICP-MS data may provide an improved way of predicting the effect of ash chemistry on CSR.

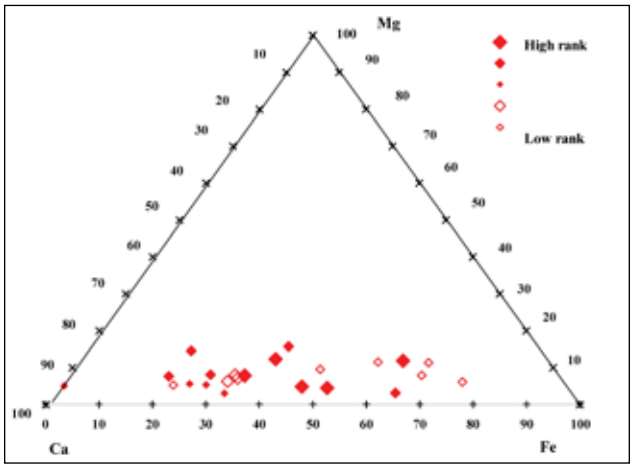

Figure 25. Total and leachable contents of Na and K in ash; solid symbols represent higher rank coals.

Increased concentrations of the alkalies K and Na decrease CSR values of coals. Volatile K or Na can cause problems in a blast furnace but may be less damaging to CSR than non-volatile K (Price and Gransden, 1987). A comparison of leachable K *versus* total K and Na (Figure 26) indicates that about 40% of K and Na is leachable, with amounts decreasing as total concentrations increase. Sodium concentrations appear to be higher in high rank coals, and K concentrations a bit lower.

The use of total major-element analysis and leachable concentrations can provide a fingerprint of ash chemistry that may help predict CSR values of cokes. Data may be cheap to obtain because both XRF and ICP-MS techniques are highly automated. Data (Figure 27) from the Dillon property (low-volatile bituminous rank) and the Lossan

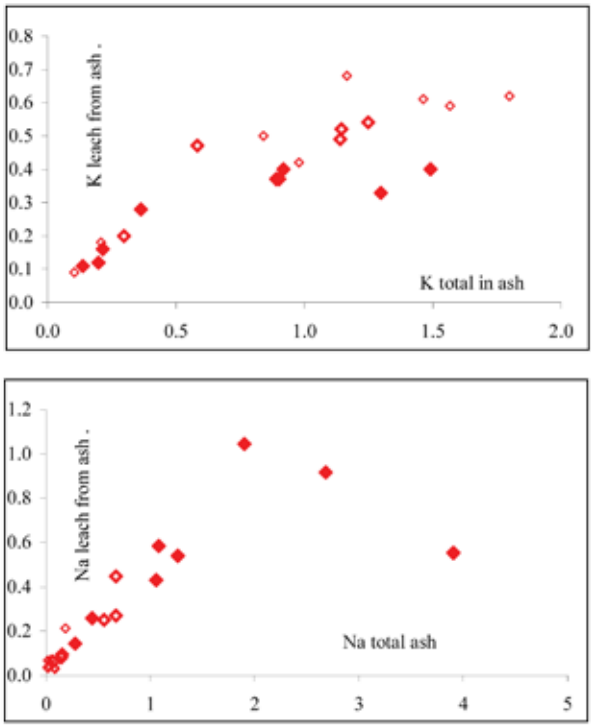

Figure 26. Fingerprints of leacheable and total major oxides in total samples for Dillon and Lossan properties.

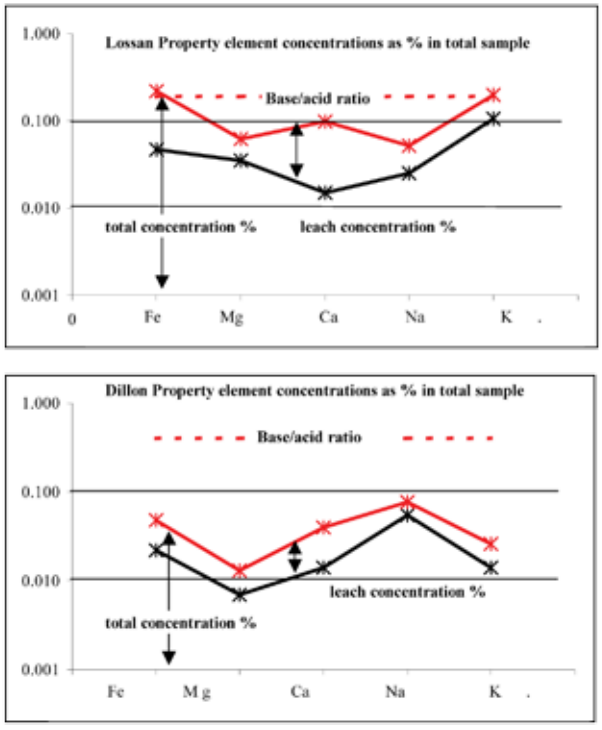

Figure 27. Fingerprints of leacheable and total major oxides in total samples for Dillon and Lossan properties.

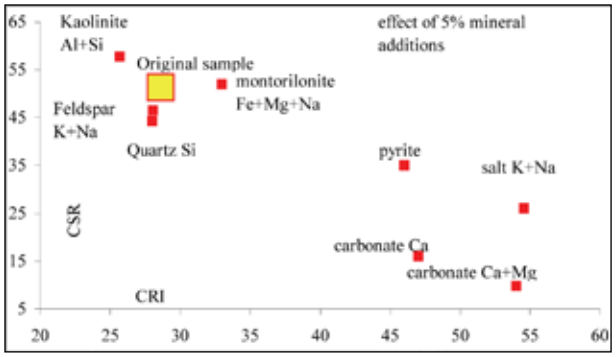

Figure 28. Plot from Mattila and Heiniemi (1996) illustrating the effect on CSR and CRI of 5% mineral additions to a coal.

property (high-volatile bituminous rank) illustrate the different fingerprints possible; ignoring rank, ash chemistry for Lossan coals is worse than that for Dillon coals in terms of CSR. It has more leachable Fe, Ca, and K than does Dillon coal. This approach is in addition to using base/acid ratios or modified basicity indices (MBI Price *et al.*1988). Mattila and Heiniemi (1996) and Price *et al.* (1992) discussed the effect of minerals on CSR, and Mattila and Heiniemi provide a figure (Figure 28) that illustrates the relative damaging effect of free Fe, Ca, Na, and K on CSR. Calcium and magnesium carbonates are worse than Fe, and also Na and K affect coke reactivity index (CRI) more than CSR.

CONCLUSIONS

Coal quality in the Gething Formation is highly variable and is best described using a number of synclinal trends that can be traced along the fold belt. It is possible to summarize the coal utilization potential of the Gething using properties along these trends and concentrating on the three major coal quality variables of rank, petrography, and ash chemistry.

Petrography data is not always available, but ultimate analyses plotted into a Van Krevelen diagram may provide a better summary of the influence of rank and petrography on coal utilization. The inerts content of Gething coals varies more than it does for Gates coals. Often it is difficult to estimate the percentage of reactive macerals in a petrographic analysis, and the Van Krevelen diagram may provide a more consistent way of separating samples based on the relative maceral reactivity.

The variable inerts content in Gething coals sometimes makes it difficult to use FSI to identify oxidation and can provide misleading estimates of rank if it is estimated from VM daf data..

Plots of VM daf data by depth provide a saw tooth pattern (even when calculated using low-ash samples). This may indicate faulting in the section or wide variation in the inerts content of seams. If the inerts content of seams is widely variable, this may make for difficulty blending to maintain a consistent coking-coal product, especially if rank is on the edge of the rank window for optimum coking coals.

There are many empirical equations that attempt to predict CSR using properties of coal samples. Using a combination of XRF oxide analysis of ash and ICP-MS analysis of leachate from ash samples, it is possible to fingerprint the ash chemistry in a way that might provide a better understanding of how ash chemistry affects CSR. The process is simple and may be cheap.

It is important, especially for the Gething Formation, to understand the implications of coal quality during the early stages of exploration. The coal market remains volatile and there is a wide separation in price and market opportunities between thermal coals, PCI coals, and coking coals of various qualities.

REFERENCES

Bell, S. (2002): In situ stress regime in the coal-bearing strata of the northeastern plains area of British Columbia; Sigma H. Consultants Ltd. Invermere BC. Report for the British Columbia Ministry of Energy, Mines and Petroleum Resources.

Broatch, T. (1987): Palynological zonation and correlation of the Peace River Coalfield, Northeastern British Columbia, an update; British Columbia Ministry of Energy, Mines and Petroleum resources, Paper 1987-1.

Bustin, R.M. (1982): Striated conical structures and related fractures in bituminous coal of the southern Canadian Rocky Mountains; International Journal of Coal Geology, Volume 2, pages 1-16.

Diessel, C.F.K. and Gammidge, L. (1998): Isometamorphic variations in the reflectance and fluorescence of vitrinite- a key to depositional environment; International Journal of Coal Geology, Volume 36, pages 167-222.

Duff, P.McL.D. and Gilchrist, R.D. (1981): Correlation of Lower Cretaceous coal measures, Peace River Coalfield, British Columbia; British Columbia Ministry of Energy, Mines and Petroleum resources, Paper 1981-3.

Gibson, D.W. (1992): Stratigraphy, Sedimentology, coal geology and depositional environments of the Lower Cretaceous Gething Formation, Northeastern British Columbia and West-central Alberta; Geological Survey of Canada Bulletin 431.

Gilchrist, R.D. (1979): Burnt River area; British Columbia Ministry of Energy, Mines and Petroleum Resources, Geological Fieldwork 1978, Paper 1979-1, pages 79-83.

Grieve, D.A. and Goodarzi, F. (1994): Trace elements in coals of the East Kootenay and Peace River coalfields, British Columbia; British Columbia Ministry of Energy, Mines and Petroleum Resources, Open File 1994-15.

Hughes, J.E. (1967): Geology of the Pine Valley Mount Wabi to Solitude Mountain Northeastern British Columbia; British Columbia Department of Mines, Bulletin 52.

Kalkreuth, W. and McMechan, M. (1988): Burial history and thermal maturity, Rocky Mountain Front Ranges, Foothills and foreland, East Central British Columbia and adjacent Alberta, Canada; American Association of Petroleum Geologists, Bulletin, Volume 72, pages 1395-1410.

Kalkreuth, W., Langenberg, W. and McMechan, M. (1989): Regional coalification pattern of Lower Cretaceous coal-bearing strata, Rocky Mountain Foothills and foreland, Canada - implications for future exploration; *International Journal of Coal Geology*, Volume 13, pages 261-302.

Karst, R.H. and White, G.V. (1980): Coal rank distribution within the Bluesky-Gething stratigraphic horizon of northeastern British Columbia (93L,O,P); *British Columbia Ministry of Energy, Mines and Petroleum Resources*, Geological Fieldwork 1978, Paper 1979-1, pages 103-107.

Karst, R.H. (1978): Vitrinite Reflectance As A Correlation Tool in the Carbon Creek Coal Measures; in Geological Fieldwork 1978, *British Columbia Ministry of Energy, Mines and Petroleum Resources*, Paper 1979-1, pages 73-78.

Leckie, D.A., Kalkreuth, W.D. and Snowdon, L.R. (1988): Source rock potential and thermal maturity of Lower Cretaceous strata: Monkman Pass area, British Columbia; *American Association of Petroleum Geologists*, Bulletin, Volume 72, pages 820-838.

Legun, A. (1984): Geology of the Butler Ridge Area; Geological Survey Branch, *British Columbia Ministry of Energy, Mines and Petroleum Resources*, Preliminary Map 57.

Legun A. (1986): Geology of the Carbon Creek area 93O/15; *British Columbia Ministry of Energy, Mines and Petroleum Resources*, Paper 1986-1, pages 155-160.

Legun, A. (1987): Coal trends in the Gething Formation-an update*; British Columbia Ministry of Energy, Mines and Petroleum Resources,* Paper 1988-1, pages 459-262.

Legun, A (2003): Coalbed methane geology of the Peace River District Northeastern British Columbia; Geological Survey Branch*, British Columbia Ministry of Energy, Mines and Petroleum Resources,* Geoscience Map 2003-2.

Lui, G and Price, J.T. (1991): Preliminary studies on stability prediction with western Canadian coals; CANMET internal publication.

Marchioni, D. and Kalkeuth, W. (1982): Vitrinite reflectance and thermal maturity in Cretaceous strata of the Peace River Arch region west-central Alberta and adjacent British Columbia; *Geological Survey of Canada,* Open File 2576.

Mattila, O.K.E. and Heiniemi, R. (1996): Correlation between reactivity and ash mineralogy of coke; 79th Steelmaking and 55th Iron making Conferences, March 24-27, 1996, Pittsburgh, USA.

Pearson, D.E. (1980): The quality of western Canadian coking coal; *Canadian Institute of Mining and Metallurgy,* Bulletin, 1980.

Price, J.T. and Gransden, J.F. (1987): Resistance of coke to alkali attack; *Canadian Carbonization Research Association*, technical paper.

Price, J.T., Gransden, J.F. and Khan, M. (1988): Effect of the properties of Western Canadian coals on their coking behavior; Proceedings of the 47th Iron making Conference AIME 47, pages 39-56.

Price, J.T., Gransden, J.F., Khan, M A. and Ryan, B.D. (1992): Effect of Selected Minerals on High Temperature Properties of Coke. Abstract, Proceedings 52nd Iron making Conference, AIME.

Price, J., Gransden, J. and Hampel, K. (2001): Microscopy, chemistry and rheology tools to determine coal and coke characteristics; McMaster University Coke Making Course, 2001.

Ryan, B.D. and Grieve, D.A. (1996): Source and Distribution of Phosphorus in British Columbia Coal Seams; in Geological fieldwork 1995, Grant, B. and Newell, J.M., Editors*, British Columbia Ministry of Energy, Mines and Petroleum Resources,* Paper 1996-1, pages 277-294.

Ryan, B.D. and Khan, M. (1997): Maceral Affinity of Phosphorus in Coals from the Elk Valley Coalfield, British Columbia*; British Columbia Ministry of Employment and Investment*, Paper 1998-1, pages 28-1 to 28-19.

Ryan, B. (1997): Coal Quality Variations in the Gething Formation Northeast British Columbia, (93O,J, I); Geological Survey Branch*, British Columbia Ministry of Energy and Mines*, Paper 1998-1, pages 373-397.

Ryan, B.D., Leeder, R. Price, J.T. and Gransden, G,J.F. (1999): The effect of coal preparation on the quality of clean coal and coke; Geological Survey Branch*, British Columbia Ministry of Energy and Mines*, Paper 1999-1, pages 247-276.

Ryan, B.D. (2002): Overview of the coalbed methane potential of Tertiary coal basins in the interior of British Columbia; Geological Survey Branch*, British Columbia Ministry of Energy, Mines and Petroleum Resources,* Paper 2003-1.

Ryan, B.D. and Lane, R. (2002): Adsorption characteristics of coals from the Gething Formation northeast British Columbia; *British Columbia Ministry of Energy and Mines*, Geological Fieldwork, Paper 2002-1.

Ryan, B.D. (2003): Cleat development in some British Columbia coals; *British Columbia Ministry of Energy and Mines*, Geological Fieldwork, Paper 2003-1.

Ryan, B.D., Karst, R., Owsiacki, G. and Payie, G (2005): Potential coalbed gas resource in the Hudson Hope area of Northeast British Columbia; Resource Development and Geoscience Branch, *British Columbia Ministry of Energy, Mines and Petroleum Resources*, Summary of Activities 2004.

Spears, D.A. and Caswell, S.A. (1986): Mineral matter in coals: cleat minerals and their origin in some coals from English Midlands; *International Journal of Coal Geology*, Volume 6, pages 107-125.

Taylor, G.H., Teichmuller, M., Davis, A., Diessel, C.F.K., Littke, R. and Robert, P. (1998): Organic Petrology*;* Gebruder Borntraeger, Berlin.

Van Voast, W.A. (2003): Geochemical signature of formation waters associated with formation water; *American Association of Petroleum Geologists*, Bulletin 87, pages 667 – 676.

GAS POTENTIAL OF THE FERNIE SHALE, CROWSNEST COALFIELD, SOUTHEAST BRITISH COLUMBIA

Barry Ryan[1] and Bob Morris[2]

ABSTRACT

Samples from the Fernie Formation were collected from the Crowsnest Coalfield and analysed for total organic carbon (TOC). It was possible to locate most samples in terms of their stratigraphic position within the formation, however, there were no major variations in TOC with stratigraphic position. TOC values were generally low and Tmax values indicate that the formation is over-mature. The formation rides on top of the Lewis Thrust and has experienced considerable deformation that may increase its potential as a shale gas resource.

KEYWORDS: Shale gas, total organic carbon, Fernie Formation, Crowsnest Coalfield

INTRODUCTION

Samples discussed in this report were collected from outcrops of the Jurassic Fernie Formation in the Crowsnest Coalfield (Figure 1). The Crowsnest Coalfield is located between the Elk River and Michel Creek drainages and covers a total area of about 600 km^2. The Alberta Natural Gas Company 36-inch pipeline, which connects the Alberta gas fields with the US market, trends north-south through the coalfield (Figure 2).

The most recent geology maps and sections for the area are by Johnson and Smith (1991). Other more recent studies—for example, Monahan (2002)—have used these maps and accompanying sections. One of the earliest regional papers on the Crowsnest Coalfield (Newmarch, 1953) provides a preliminary map of the coalfield and detailed geology of the Coal Creek area. The map was compiled at a time when the mines in the creek were still operating. Other mapping data includes Pearson and Grieve (1978). These maps provide strike/dip and seam location data not present on the maps in Johnson and Smith (1991). The regional map of Price (1961) covers the Crowsnest Coalfield and also provides strike/dip information.

The coalfield forms part of the Jurassic and lowest Cretaceous strata of the Rocky Mountains and Foothills (Table 1). This area has been the subject of several in-depth studies, including Poulton (1984, 1989, 1990) and Frebold (1957, 1969). The coalfield is defined by outcrops of the Jura-Cretaceous Kootenay Group and underlying Fernie Formation and in general terms is a structural basin rimmed by outcrops of the Fernie Formation (Figure 2). The coalfield forms part of the upper plate of the Lewis Thrust, and therefore formations in the coalfield have structural characteristics different from the same formations below the Lewis Thrust and penetrated by numerous oil and gas holes in the Western Canadian Sedimentary Basin to the east.

The coal-bearing Mist Mountain Formation, which overlies the Fernie Formation, varies in thickness from 490 to 660 m (Ryan, 2004). Rank of seams in the Mist Mountain Formation range from 0.82% to 1.64%, with ranks increasing with depth and generally being higher in the southwestern part of the coalfield (Pearson and Grieve, 1985). The formation is the target for conventional coal exploration and, since 1990, coalbed gas (CBG; also referred to as coalbed methane, CBM) exploration. The most recent CBM exploration program is by Shell in the northern part of the basin where the company has drilled 3 holes.

The marine Fernie Formation, which does not contain coal seams, was designated as the "Fernie Shales" on a map of the Crowsnest Coalfields by McEvoy (1902). Leach (1914) was the first to use the term "Fernie Formation" while the term "Fernie Group" was first used by Henderson and Douglas (1954).

Coalbed methane exploration in the overlying Mist Mountain Formation has resulted in interest in the shale gas potential of the underlying Fernie Formation, and this report provides some preliminary data on the subject. The study is composed of two parts. The mapping portion of the study aimed to define the distribution of the various subdivisions of the Fernie Formation and to examine the formation as a potential fractured-shale reservoir; fieldwork included mapping, structural analysis, and collection of outcrop, core, and cuttings samples within the Fernie Formation (Morris, 2004). The second part of the study, which forms this report, includes a discussion of total organic carbon (TOC) analysis of samples.

[1]Resource Development and Geoscience Branch, BC Ministry of Energy, Mines and Petroleum Resources, PO Box 9323, Stn Prov Govt, Victoria, BC, V8W 9N3

[2]Morris Geological, Fernie, British Columbia

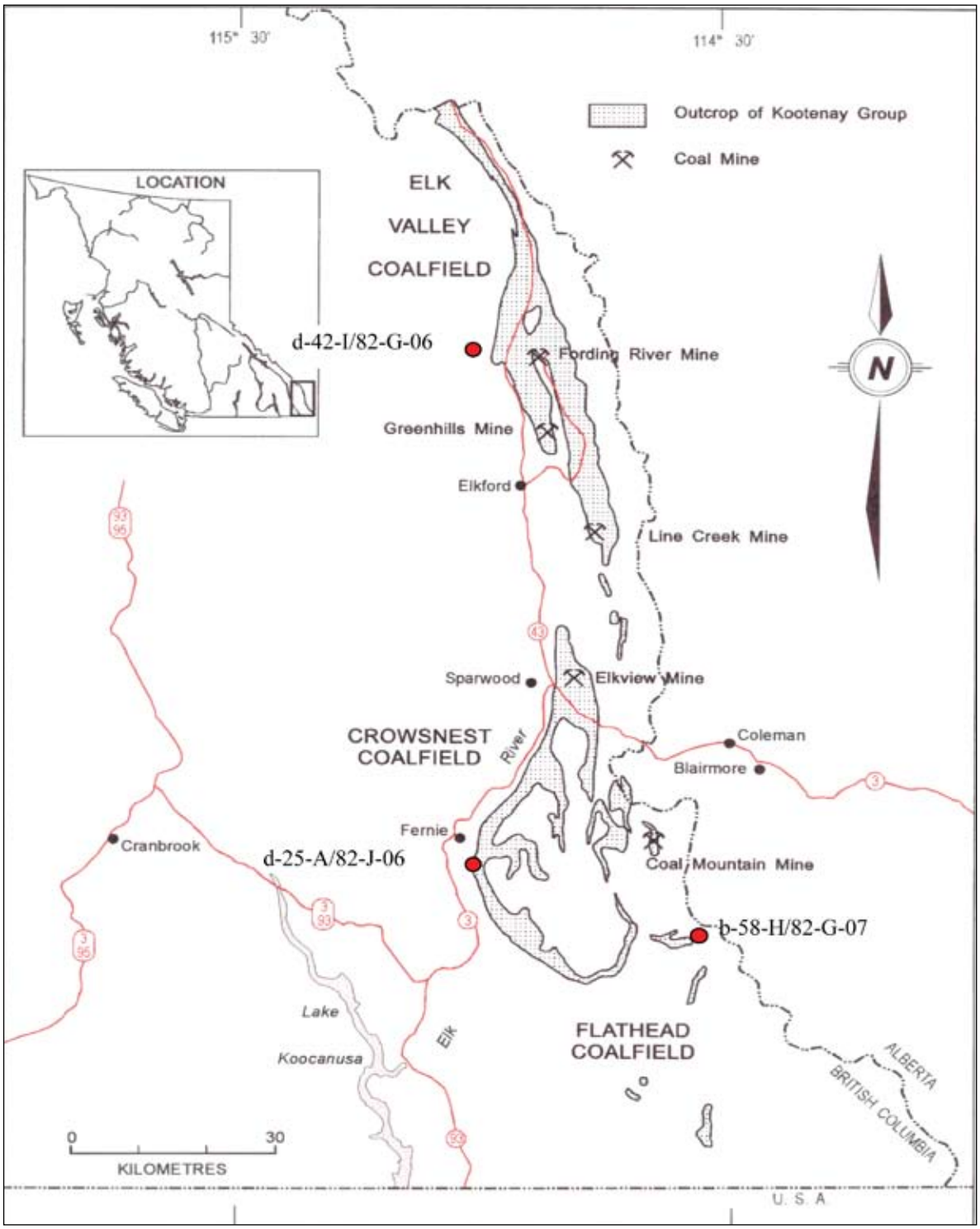

Figure 1. Regional map, southeast British Columbia.

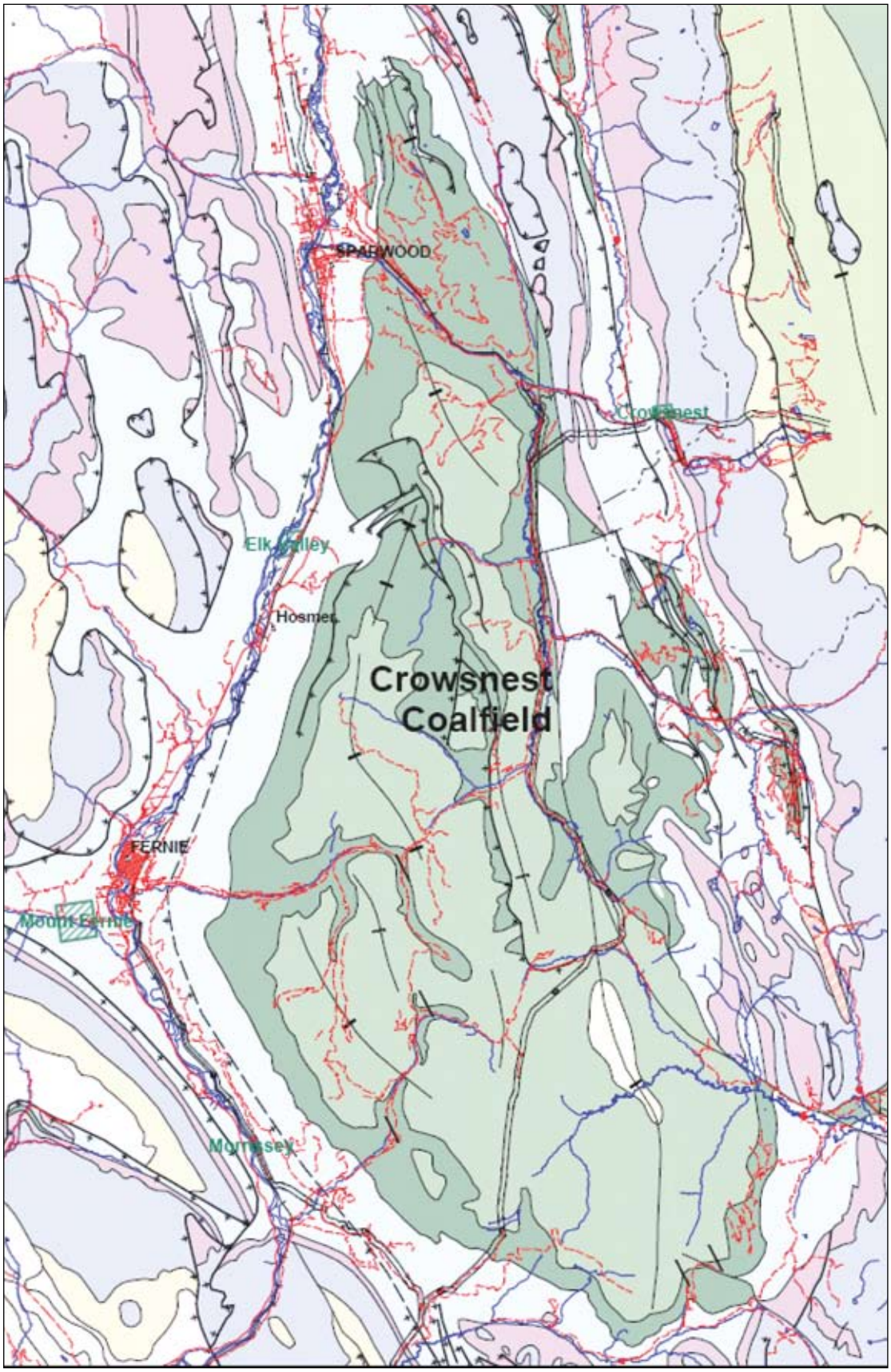

Figure 2. Regional geology of the Crowsnest Coalfield extracted from Ministry of Energy, Mines and Petroleum Resources MapPlace geology map, East Kootenay.

TABLE 1. STRATIGRAPHY OF SOUTHEAST BRITISH COLUMBIA AND FERNIE FORMATION

LOWER CRETACEOUS	CADOMIN FORMATION		
JURASSIC AND CRETACEOUS	KOOTENAY GROUP	ELK FORMATION **minor coal**	
		MIST MOUNTAIN FORMATION **coal seams**	
		MORRISSEY FORMATION	MOOSE MOUNTAIN MEMBER
			WEARY RIDGE MEMBER
JURASSIC	FERNIE FORMATION	PASSAGE BEDS	

STRATIGRAPHY

The Fernie Formation was first described by McEvoy and Leach (1902), who designated the "Fernie Shales" on their map of the Crowsnest Coalfield. There is no type locality designated for the formation, and no known mappable complete section. Price (1961) mapped the area and divided the Fernie Formation into units that, from bottom to top, are the Dark Grey Shales, Rock Creek, Grey Beds, Green Beds, and Passage Beds. The cumulative thickness of these units ranges from 120 to 240 m. More recently Poulton *et al.* (1994) provide a section through southeast British Columbia that indicates a thickness of about 200 m. They also provide a stratigraphic column for southeast British Columbia, a part of which gives a breakdown of the Fernie Formation (Figure 3), listing all of the subdivisions that are referred to as Lower, Middle, and Upper Members of the formation as well as units and beds.

The Lower Fernie Member contains four units. The lowest unit is the Phosphorite unit, which is overlain by the Basal unit, the Lower Shale unit, and the Poker Chip Shale unit. All these units are described by Frebold (1957)

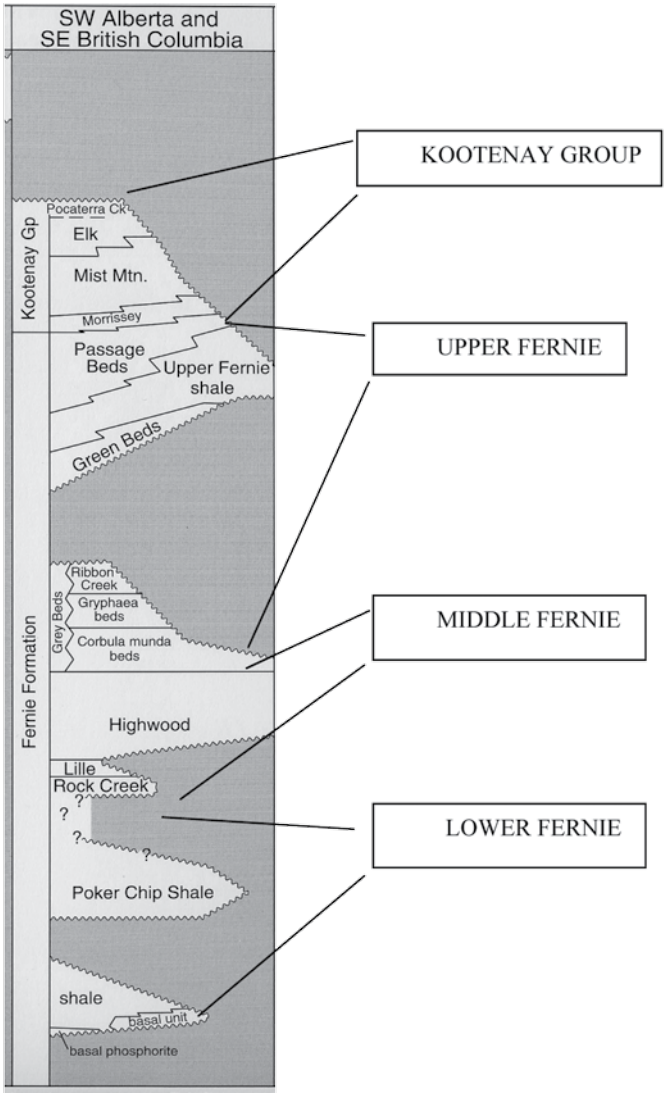

Figure 3. Stratigraphic section of the Fernie Formation, adapted from Poulton *et al.* (1994).

and Poulton *et al*. (1994). The Poker Chip Shale unit, also known as the "Paper Shale" unit, is described as organic rich (Monahan 2002) and, in conjunction with the Phosphatic unit, as potential hydrocarbon source rocks. Fossils in this unit are generally restricted to ammonites, which are preserved as imprints or films. Locally, vertebrate remains have been found, as well as belemnites.

The Middle Fernie Member is represented by four units. The lowest is the Rock Creek unit, overlain successively by the Lille, Highwood, and Grey Beds unit. Only the Grey Beds unit was observed during this study; three main facies are recognized in the unit: the *Corbula munda* beds, the *Gryphaea* beds (a predominantly shaly facies), and a facies characterized by grey shales with sandstone intercalations. The Corbula munda and *Gryphaea* beds consist of grey shales with brown or green tinges intercalated with bands and lenses of hard grayish calcareous sandstone.

Most of these strata are fossiliferous, containing abundant pelecypods and, less commonly, ammonites. The shale facies is characterized by indurated grey, limy, somewhat sandy shales that in places form steep cliffs. Most have a greenish tinge and are easily recognizable from a distance. Belemnites are numerous in the upper part.

The top of the Fernie Formation is marked by the Passage Beds.

STRUCTURE

It is important to recognize that rocks in the Crowsnest Coalfield ride on top of the Lewis Thrust and therefore have structural imprints and present-day stress regimes that differ from those in the same formations below the thrust to the east. Coal seams, and often the intervening rock in the overlying Mist Mountain Formation, are highly fractured, and this tends to decrease permeability in seams. However, fracturing in the underlying shale may be advantageous for shale gas extraction because shale formations often have extremely low permeability, as measured in microdarcies. Gas extraction depends on natural fracture intensity. The ultimate amount of gas recovered may be proportional to the ratio of the surface area of fracture blocks to their volume. Small blocks or blocks with non-spherical shapes provide a high ratio of surface area to volume, which aids diffusion out of shale fragments. The Fernie Shale is a major zone of detachment within the Lewis Thrust sheet and the formation is often structurally thickened (Monahan 2002).

As a part of sample collection, a total of 129 outcrops were examined, and structural data (including orientation of bedding and joints) were collected. Poles to bedding outline a north to north-northwest fold trend with shallow plunge to the north (Figure 5), in agreement with regional fold trends outlined by Price (1961), Johnson and Smith (1991), and Monahan (2002). Poles to joints indicate the presence of axial planar joints and a maximum pole concentration at 330°/6° (Figure 6). This set is fold-axis normal based on the fold trend outlined by bedding (Figure 5) and is the most likely to be open. Other joints are axial planar. It is important to identify areas where there may be more complex patterns of joints in the Fernie Formation or areas where joints intersect bedding at oblique angles, generating higher surface-area-to-volume ratios for fragments.

SAMPLING

A total of 106 samples were collected from various exposures of the Fernie Formation around the Crowsnest Coalfield (Figure 4). In general the outcrop samples represent grab samples across as much as 6 m of exposure, though some of the samples represent individual rocks from an outcrop. The UTM grid coordinates and general location were recorded (Table 2). Samples were also designated in terms of stratigraphic position in the Fernie Formation (Table 3) using the stratigraphy described by Poulon *et al*. (1994) (Figure 3). In addition to outcrop samples, a further 7 samples of core were obtained from a single well and 12 samples of cuttings from 3 wells drilled in the area (Table 4).

In the Lower Fernie Member, at least 20 outcrops of the Lower Shale unit were sampled (Table 4). In addition, samples were collected from the Poker Chip Shale unit. The Middle Fernie Member is represented by at least 56 samples of the Grey Beds unit. The Upper Fernie Member is represented by samples from the Green Beds unit, which was observed and sampled in at least 12 localities, and the Upper Fernie Shale unit, which was sampled at 14 localities. The top of the Fernie Formation is marked by the Passage Beds, which were sampled at one locality.

Fifty outcrop samples and all 19 drillhole samples were analysed using a RockEval 6 (Re6) instrument to provide information on total organic carbon (TOC), organic maturity (Tmax, °C), and kerogen type. Outcrop samples were picked for analysis based on lithology, with preference given to shale or black shale samples as these are more likely to have higher TOC contents.

RESULTS

Rock-Eval analyses provide information on the amount and maturity of the organic matter. A number of parameters are provided and listed in Tables 5 and 6. The S1 value is an indication of the amount of free hydrocarbons in the sample, and the S2 value an indication of the amount of hydrocarbon material that could be generated if the remaining organic matter is cracked during increased burial and heating. The S3 value indicates the amount of CO_2 generated by destruction of kerogen in the sample during analysis. The production index (PI= S1/[S1+S2]) is a measure of the evolution level of the organic matter. The Tmax (°C) value is the temperature at which there is a maximum release of hydrocarbon from cracking kerogen in the sample during pyrolysis. The Tmax temperature correlates to vitrinite reflectance and is therefore an important indicator of organic maturity.

Values calculated from measured data include the total organic carbon (TOC), which is calculated by adding the residual organic carbon content to the amount of pyrolyzed organic carbon. The amount of inorganic carbon is calculated using the S3 and S5 peaks. The hydrogen index (HI = 100*S2/TOC) and the oxygen index (OI = 100*S3/TOC) are used to represent the sample in a modified Van Krevelen diagram, which indicates the maturity and type of kerogen present.

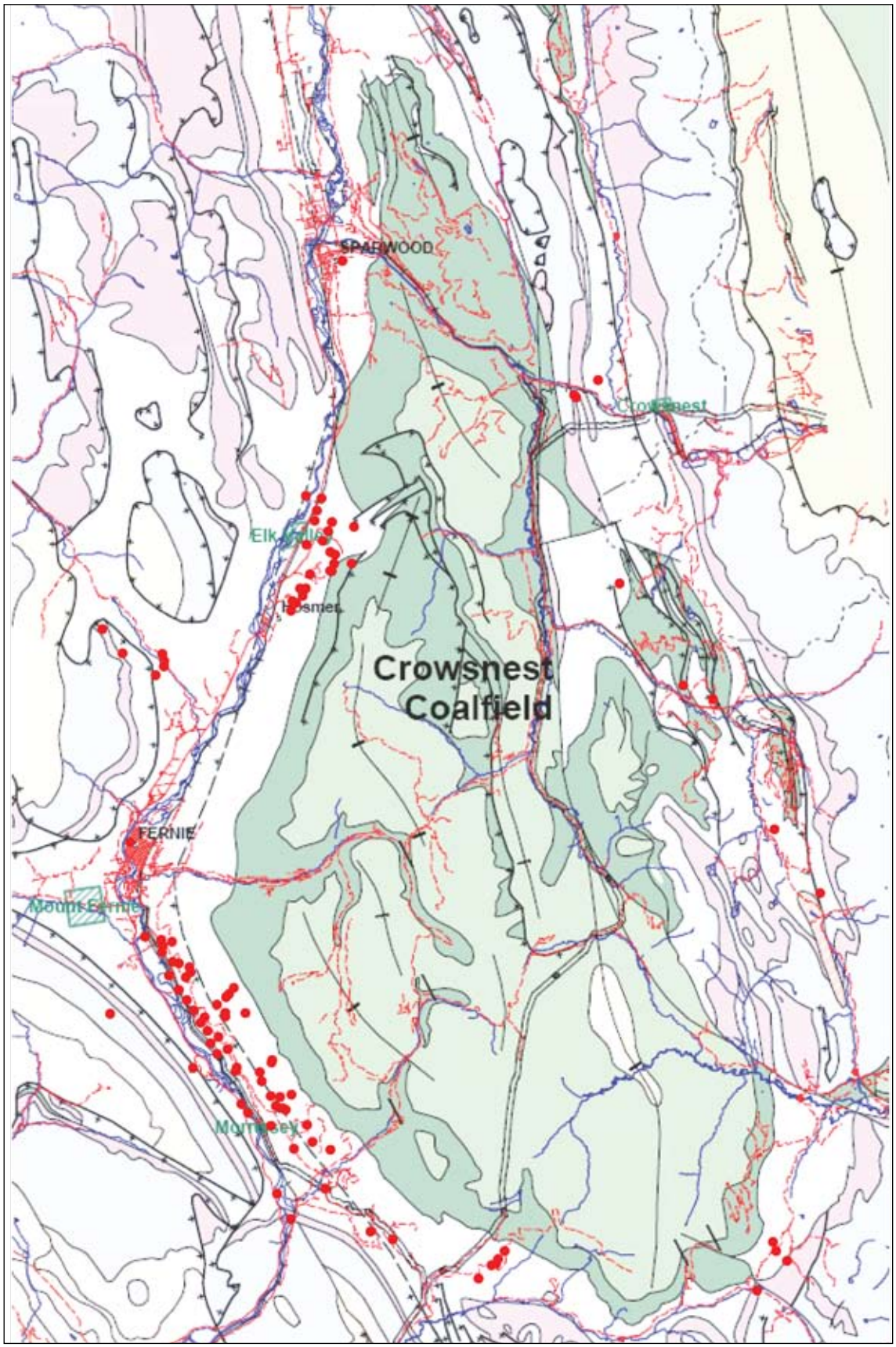

Figure 4. Map of the Crowsnest Coalfield with sample locations.

Calculated Tmax values are related to vitrinite reflectance, and a number of papers provide data sets of Tmax *versus* vitrinite reflectance (usually random reflectance). The Rock-Eval instrument has evolved over time, and this has produced a number of relationships of Tmax measured by the equipment and Ro measured on the organic matter. The Re2 instrument was not capable of differentiating rank above a reflectance of about 2% whereas the Re6 instrument can identify ranks over a reflectance of 4% (Lafargue *et al.* 2000). As a further complication, the Tmax *versus* Ro relationship depends on the type of kerogen present in the sample. Type 3 kerogen tends to have a lower Tmax for the same rank than does type 2 kerogen (Taylor *et al.* 1998, page 131).

Relationships of Tmax *versus* vitrinite reflectance vary (Figure 7). Lafargue *et al*. (1998) provide a relationship for Tmax *versus* Ro for coal using Re6. Krivak (2005) provides a relationship that seems to provided high estimates of Ro. Leachie *et al.* (1988) measured Tmax and Ro values in marine and non-marine rocks in northeast BC; their relationship of Tmax *versus* Ro values for marine rocks seems to provide the best relationship for the Fernie data based on knowledge of the rank of coals in the overlying Mist Mountain Formation. The relationship provided by Ibrahimbas and Riediger (2005) for Cretaceous samples seems to provide Ro values that are too low.

Tmax temperatures for the outcrop samples range from 449 °C to 541 °C (Table 5) and place the formation in the dry gas field (Figure 8). Based on these values, Ro values range from 0.9% to 3.1% and average 1.62% using the relationship for marine rocks (Leachie *et al.* 1998). The data are sorted by unit within the Fernie Formation (Table 6) and plotted into a modified Van Krevelen diagram (Figure 9). The data indicate low hydrogen indices, plotting in the type 3 kerogen field with a high degree of maturity.

Chip samples collected from 3 holes were analysed; most of the samples came from 2 of the holes (Table 4). Holes ware located a) to the west of the Elk Valley Coalfield, b) below the Bourgeau Thrust, west of the Crowsnest Coalfield in subcrop of Fernie, and c) east of the Crowsnest Coalfield intersecting the Fernie below the Lewis Thrust (Figure 1). Hole d-25 intersects the Fernie above and below the Bourgeau Thrust. The Tmax temperatures are low and do not predict realistic ranks, indicating the possible presence of contamination (Figure 10). Hole d-42 drilled into Fernie below the Bourgeau Thrust where the formation is steeply dipping. Tmax temperatures increase consistently with depth and do not indicate any major thrusts. The single sample from below the Lewis Thrust (hole b-58; Figure 1) indicates a low rank equivalent to high-volatile A bituminous.

DISCUSSION

Organic material that collects in low-energy environments, where fine sediments accumulate, is preserved if the environment is anoxic. Shales with moderate contents of preserved organic material have the potential to be source rocks for oil or gas, depending on the kerogen type and its maturity. Shale also has the potential to act as a reservoir for gas, based on the adsorption ability of the organic matter and the ability of the shale to retain gas in the microporosity.

At depth to the east, the Jurassic Fernie Formation is divided from base upwards in part into the Nordegg, Gordondale, Poker Chip, Rock Creek, and Grey Beds. The Nordegg Member underlies part of southeast British Columbia and a large area of southern Alberta. The Gordondale Member underlies southeast and northeast BC and a large area of Alberta. Both members have good source rock potential for oil.

In northeast British Columbia, the Fernie Formation is overlain by the Nikanassin, Cadomin, Gething, and Bluesky Formations, and on top the Lower Cretaceous Moosebar or Wilrich Formation, which is a marine shale with shale gas potential. Ibrahimbas and Riediger (2005) provide an average TOC for the Wilrich of 2.1%. Leckie *et al*. (1988) analysed samples for TOC from the Monkman Pass area. TOC values range from 0.75% to 2.36%, and rank ranges from 1.2% to 1.24% Rmax. They derived approximate Tmax versus Ro relationships, which are depicted in Figure 7, for marine and non-marine rocks.

Total organic carbon values of samples from the Crowsnest Coalfield and adjoining area, sorted by units (Table 6), provide averages of 1.67% for the Upper Fernie, 1.41% for the Lower Fernie, and 1.75% for the Grey Beds. These reflectances are in the range of what would be expected based on measured reflectance values in the overlying Mist Mountain (Pearson and Grieve 1985). The Tmax values indicate that the formation is in the dry gas field (Figure 8) and values indicate a poor to fair source rock potential, especially as the kerogen appears to be type 3 (Figure 9).

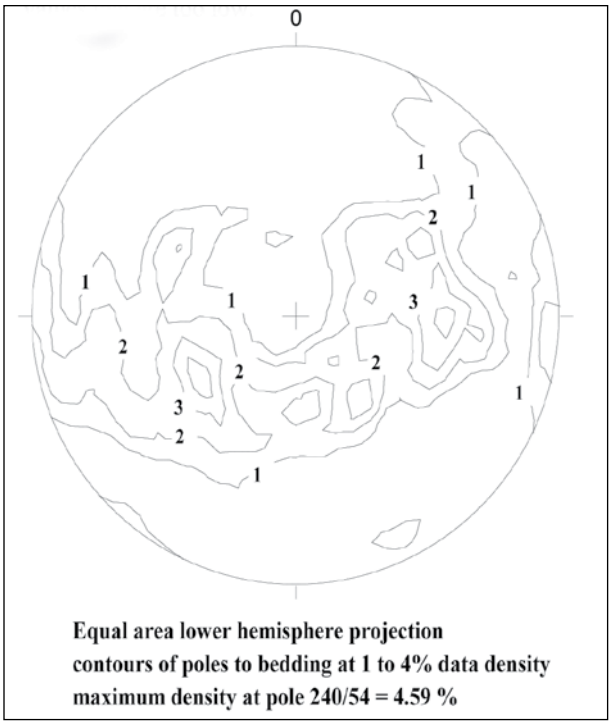

Figure 5. Lower hemisphere equal-area projection of poles to bedding.

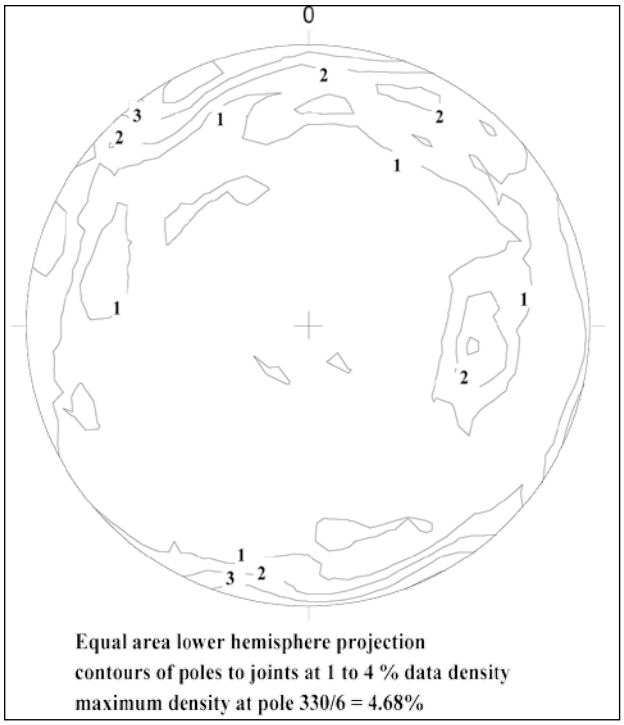

Figure 6. Lower hemisphere equal-area projection of poles to joints.

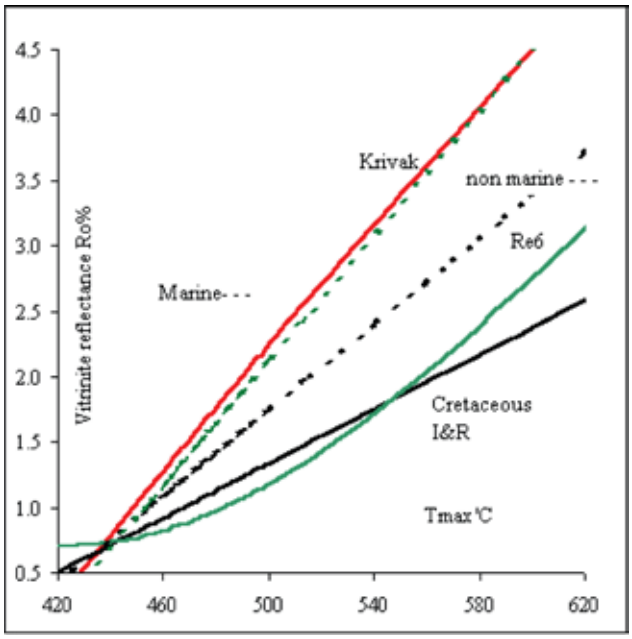

Figure 7. Tmax versus Ro relationships derived from Lafargue *et al.* (1998) (Re6), Krivak (2005), Lechie, *et al.* (1988) (marine and non-marine), and Ibrahimbas and Riediger (2005).

TABLE 2. LOCATION OF ALL OUTCROP SAMPLES COLLECTED WITH COORDINATES AND BRIEF DESCRIPTION.

	Easting	Northing	Location	analysed		Easting	Northing	Location	analysed
26	645897	5472614	Morrissey Ridge, Branch B		160	641951	5480994	Morrissey Ridge, Branch H	
29	645799	5473399	Morrissey Ridge, Branch B		161	641935	5481219	Morrissey Ridge, Branch H	
33	645036	5472461	Morrissey Ridge, Branch B		164	641239	5481584	Morrissey Ridge, Branch H	164
39	644990	5474228	Morrissey Ridge, Branch C1		165	641503	5481471	Morrissey Ridge, Branch H	
39a	644990	5474228	Morrissey Ridge, Branch C1		166	640974	5481014	Morrissey Ridge, Branch H	166
44	644593	5474478	Morrissey Ridge, Branch C	44	167	640855	5482094	Morrissey Ridge, Branch I	
47	644875	5474317	Morrissey Ridge, Branch C	47	169	640924	5482636	Morrissey Ridge, Branch I	
49	644848	5474834	Morrissey Ridge, Branch C		170	640946	5482365	Morrissey Ridge, Branch I	170
52	645358	5474844	Morrissey Ridge, Branch C	52	171	641377	5482468	Morrissey Ridge, Branch I	
54	644446	5474947	Morrissey Ridge, Branch C	54	172	664072	5462577	Upper Lodgepole	
58a	644170	5475666	Morrissey Ridge, Branch C		174	665621	5463632	McLatchie Pass	174
59	644159	5476076	Morrissey Ridge, Branch C		175	665224	5464147	McLatchie Pass	
64	644750	5476400	Morrissey Ridge, Branch C		176	665157	5464567	McLatchie Pass	176
64a	644750	5476400	Morrissey Ridge, Branch C		180	643328	5474398	Elk River	180
66	644796	5476506	Morrissey Ridge, Branch C		181	643100	5474839	CPR	181
67	644333	5469425	River, tunnel	67	183	641532	5495447	Hartley Lake road	183
68a	643938	5470537	Hwy, road cut	68a	184	640841	5496659	Hartley Lake road	
68b	643938	5470537	Hwy, road cut		191	642797	5494227	Hosmer Mt.	191
69a	641285	5476803	Hwy road cut	69a	193	643232	5494547	Hosmer Mt.	193
69b	641285	5476803	Hwy road cut	69b	195	643291	5494778	Hosmer Mt.	
71	640345	5487143	Fernie bridge, north	71	197	643260	5495103	Hosmer Mt.	197
72	640236	5482907	Cokato road	72	200	650418	5498713	Main road	200
73	642453	5477207	Cokato road		205	651584	5498052	Main road	
74	643117	5476315	Cokato road	74	207	651467	5497661	Main road	207
79	647708	5468237	Lodgepole Pass		212	652239	5497531	Main road, Kootenay shale	
80a	648616	5467722	Lodgepole Pass	80a	215	651311	5497358	Main road, south	215
80b	648616	5467722	Lodgepole Pass	80b	216	651240	5497381	Fernie Ridge, Branch E	216
86	644220	5473651	River Road Ext	86	220	651396	5498206	Fernie Ridge, Branch D	220
90	643193	5476463	River Road Ext		221	651157	5498747	Fernie Ridge, Branch D	
92	642935	5477336	River Road Ext	92	223	651469	5499127	Fernie Ridge, Branch D	
94	643098	5478780	Morrissey Ridge, Branch E		225	651710	5499495	Fernie Ridge, Branch D	
96	643130	5478944	Morrissey Ridge, Branch E	96	230	650785	5500850	Fernie Ridge, Branch A	
102	644006	5478772	Morrissey Ridge, Branch E		252	650969	5499693	Fernie Ridge, Branch B	252
106	641977	5478710	Morrissey Ridge, Branch G		253	651146	5500118	Fernie Ridge, Branch B	
107	642195	5478910	Morrissey Ridge, Branch G		255	651444	5500618	Fernie Ridge, Branch B	
112	642833	5479363	Morrissey Ridge, Branch G		260	650337	5497394	Fernie Ridge, Branch C	260
117	643292	5479624	Morrissey Ridge, Branch G	117	262	649789	5496853	Fernie Ridge, Branch C1	
120	642641	5477943	Morrissey Ridge, Branch E	120	263	649842	5496510	Fernie Ridge, Branch C	
122	646068	5470478	Morrissey road	122	264	649497	5496255	Fernie Ridge, Branch C	
130	646617	5472127	Morrissey ridge, Pine Grove rd		265a	649351	5496370	Fernie Ridge, Branch C	
138	642246	5477731	River Road Ext	138	265b	649351	5496370	Fernie Ridge, Branch C	
139	642213	5478297	River Road Ext	139	266	649213	5495958	Fernie Ridge, Branch C	266
145	652032	5465328	Flathead Ridge, Pipeline		267	650042	5496809	Fernie Ridge, Branch C1	
146	652702	5465804	Flathead Ridge, Pipeline		274	652633	5499115	Fernie Ridge, Branch E	
148	653040	5466019	Flathead Ridge, Pipeline		277	654256	5510803	Michel Creek bridge	277
149	653390	5466319	Flathead Ridge, Pipeline	149	279	665698	5489562	Tent Mtn.	279
151	652917	5465837	Flathead Ridge, Pipeline	151	280	666885	5488725	Tent Mtn.	280
154	643445	5479734	Morrissey Ridge, Branch G		283	668528	5482557	Michel Creek	
155	643703	5479963	Morrissey Ridge, Branch G	155	287	670007	5479409	Flathead Pass	287
156	641778	5479300	River Road Ext		288	663341	5502978	Hwy. road cut	288
157	641558	5479804	River Road Ext	157	290	663270	5503110	Alexander Creek	290
158	641293	5480312	Morrissey Ridge, Branch G	158	296	664433	5503562	Alexander Creek	296
159	641698	5480807	Morrissey Ridge, Branch H	160	308	638104	5479822	Ski hill	308

TABLE 3. ALL SAMPLES COLLECTED DESIGNATED BY UNIT WITHIN THE FERNIE FORMATION.

Outcrop Samples by Member	
with analyzed samples high-lighted	
Member	Sample number
	Kootenay Group
Kootenay	212
	Upper Fernie
Passage beds	277
Upper Fernie	49, **52**, **54**, **149, 155**, **176**, **207**, **215, 216**, 263, 264, **266**, 274, **280**
Green beds	29, 39, 39a, **47**, 64, 64a, **117**, 154, 161, 165, 265, 265a
	Middle Fernie
Grey beds	26, 33, **44**, 58a, 59, 66, **71**, **72**, **74**, 79, **80a**, **80b**, **86**, 90, **92**, 94, **96**, 102, 106, 107, 112, **120, 122**, 130, **138, 139**, 145, 146, 148, **151**, 156, **157, 158, 159, 160, 164, 166,** 167, 169, **170**, 171, 172, 175, **200**, 205, **220**, 221, 223, 225, 230, **252**, 253, 255, **260**, 262, 267
Ribbon Creek	No sample
Gryphaea beds	No sample
Corbula Munda beds	No sample
Highwood	No sample
Lille	No sample
Rock Creek	No sample
	Lower Fernie
Poker Chip Shale	73
Lower Shale	**67**, **68a**, 68b, **69b**, **174, 180, 181, 183**, 184, **191, 193**, 195, **197**, **279**, 283, **287, 288, 290, 296, 308**
Basal Unit	No sample
Basal Phosphorite	No sample

TABLE 4. LOCATION, DEPTH, AND ROCK-EVAL DATA FOR DRILLHOLE SAMPLES.

			from	to
d-42-I/82-G-06	core	Core 1, #1	1548.38	1549.91
d-42-I/82-G-06	core	Core 1, #2	1553.57	1553.57
d-42-I/82-G-06	core	Core 1, #3	1557.53	1557.53
d-42-I/82-G-06	core	Core 2, #1	1921.46	1921.46
d-42-I/82-G-06	core	Core 3, #1	2592.32	2592.32
d-42-I/82-G-06	core	Core 3, #2	2595.52	2595.52
d-42-I/82-G-06	core	Core 3, #3	2600.25	2600.25
d-42-I/82-G-06	chips	WA 1113	350.52	432.82
d-42-I/82-G-06	chips	WA 1113	853.44	935.74
d-25-A/82-J-06	chips	WA 6095	605	610
d-25-A/82-J-06	chips	WA 6095	630	640
d-25-A/82-J-06	chips	WA 6095	2680	2720
d-25-A/82-J-06	chips	WA 6095	2880	2935
d-25-A/82-J-06	chips	WA 6095	2940	2995
d-25-A/82-J-06	chips	WA 6095	3125	3200
d-25-A/82-J-06	chips	WA 6095	3970	4010
d-25-A/82-J-06	chips	WA 6095	4015	4060
d-25-A/82-J-06	chips	WA 6095	4065	4116
b-58-H/82-G-07	chips	WA 6241	3440	3520

TABLE 5. ROCK-EVAL DATA FOR TOTAL ORGANIC CARBON ANALYSES FOR SAMPLES AND RO CALCULATED USING MARINE RELATIONSHIP FROM LEACHIE ET AL. (1988).

Sample No.	Colour	Texture	Rock Type	Notes	MINC%	TOC	HI	OI	Tmax	Ro-1	Ro-2	Av Ro
52	dark grey	fissile	shale	small conc	0.1	1.42	29	66	484	1.01	1.16	1.08
54	dark grey	mod. platy	shale	sericite, concretions	0.1	1.34	25	59	488	1.04	1.21	1.13
68a	dark grey	thin bedded	shale	sericite, belemnite	1.4	0.91	58	51	461	0.82	0.93	0.87
69a	dark grey	thin bedded	shale		1.2	1.23	42	41	474	0.92	1.06	0.99
71	dark grey	fissile	shale		4.3	0.47	23	55	475	0.93	1.07	1.00
72	dark grey	fissile	sh/slst	ca veins	1.7	0.26	12	138	490	1.06	1.23	1.15
74	dark grey	platy	shale	ca veins, clay	2.0	0.33	36	139	472	0.90	1.04	0.97
80a	dark grey	massive	sh/slst		10.7	0.12	0	333	516	1.37	1.50	1.43
80b	dark grey	platy	shale	clay	0.6	0.61	7	118	541	1.73	1.76	1.74
86	dark grey	mod. platy	sh/slst		0.8	0.23	17	178	490	1.06	1.23	1.15
96	dark grey	massive	siltstone	ca veins	1.2	0.21	19	176	490	1.06	1.23	1.15
122	dark grey	massive	siltstone	ca veins	1.1	0.11	18	182	489	1.05	1.22	1.14
138	dark grey	fissile	siltstone	green tint	0.8	0.17	24	212	479	0.96	1.11	1.04
151	dark grey	massive	siltstone		0.3	0.41	20	195	499	1.16	1.32	1.24
155	dark grey	massive	siltstone		0.1	1.51	25	72	478	0.95	1.10	1.03
157	dark grey	mod. platy	shale	clay	0.1	1.40	21	103	477	0.94	1.09	1.02
158	dark grey	massive	shale	mini concretions	1.8	0.25	20	100	466	0.86	0.98	0.92
159	dark grey	platy	shale	ca veins	3.3	0.25	12	216	494	1.11	1.27	1.19
160	dark grey	platy	shale	bivalve	2.7	0.42	14	164	490	1.06	1.23	1.15
164	dark grey	massive	siltstone	mini conc., bivalve?	1.6	0.19	11	168	485	1.01	1.17	1.09
170	dark grey	fissile	siltstone		1.6	0.28	11	139	501	1.18	1.34	1.26
174	dark grey	platy	shale	muddy, dirty, coaly?	0.2	1.18	6	136	513	1.33	1.47	1.40
176	dark grey	mod. platy	siltstone	sericite	0.1	1.43	12	110	493	1.10	1.26	1.18
183	dark grey	platy	siltstone	concretions, sericite	1.3	0.77	34	56	484	1.01	1.16	1.08
191	dark grey	platy	siltstone	rusty	0.2	2.45	17	67	500	1.17	1.33	1.25
197	dark grey	massive	siltstone	ca veins, green tint	0.8	0.27	41	63	472	0.90	1.04	0.97
200	dark grey	massive	shale	belemnite? Rusty	3.8	0.09	11	333	480	0.97	1.12	1.05
260	dark grey	massive	siltstone		0.2	1.19	42	76	474	0.92	1.06	0.99
266	dark grey	fissile	siltstone	very fine sericite	0.1	1.22	34	75	472	0.90	1.04	0.97
277	dark grey	massive	siltstone	slicks	1.3	1.49	34	55	498	1.15	1.31	1.23
280	dark grey	platy	siltstone	sericite, concretions	0.9	0.62	56	71	462	0.83	0.94	0.88
287	gray/brown	fissile	shale	clay, concretions	0.1	0.39	10	259	474	0.92	1.06	0.99
296	dark grey	fissile	shale	sericite	0.2	2.56	36	59	468	0.87	1.00	0.93
308	dark grey	mod. platy	siltstone	sericite	0.1	0.50	42	134	453	0.78	0.84	0.81
47	dark grey	massive	slst/lmst	bivalves, black	1.1	0.33	18	73	453	0.78	0.84	0.81
44	black	massive	siltstone	concretions, dense	2.9	0.14	14	179	463	0.84	0.95	0.89
67	gray/brown	thin bedded	ss/slst	ammonite	4.4	0.37	14	349	483	1.00	1.15	1.07
69b	black	thin bedded	shale	ca veins, plant debris	0.9	0.64	22	45	449	0.76	0.80	0.78
92	dark grey	mod. platy	siltstone		0.1	1.57	31	55	473	0.91	1.05	0.98
117	dark grey	massive	sandstone		3.0	0.16	25	256	493	1.10	1.26	1.18

TABLE 5. CONTINUED.

Sample No.	Colour	Texture	Rock Type	Notes	MINC%	TOC	HI	OI	Tmax	Ro-1	Ro-2	Av Ro
139	dark grey	platy	siltstone		0.9	0.18	39	111	480	0.97	1.12	1.05
149	dark grey	platy	siltstone	sericite, carb	0.1	0.92	7	139	500	1.17	1.33	1.25
166	dark grey	mod. platy	siltstone		1.1	0.22	18	195	489	1.05	1.22	1.14
180	black	mod. platy	siltstone	fossils, carb., slicks	0.4	1.35	43	15	452	0.77	0.83	0.80
181	dark grey	mod. platy	siltstone	green tint	1.6	0.25	20	120	459	0.81	0.90	0.86
193	black	mod. platy	shale	carb., slicks	0.7	2.93	20	7	463	0.84	0.95	0.89
207	dark grey	massive	siltstone	rusty, sericite	0.2	1.45	19	110	485	1.01	1.17	1.09
215	very dark grey	massive	siltstone	sericite, ca veins	0.9	1.82	31	70	465	0.85	0.97	0.91
216	very dark grey	massive	siltstone	ca veins	1.1	2.28	58	21	461	0.82	0.93	0.87
220	very dark grey	fissile	siltstone	concretions	0.9	1.64	60	21	463	0.84	0.95	0.89
252	very dark grey	massive	siltstone	very fine sericite	0.6	1.46	60	18	467	0.86	0.99	0.93
279	dark grey	massive	siltstone	concretions	1.1	1.54	42	80	456	0.79	0.87	0.83
288	black	platy	siltstone	carb.	5.0	5.94	58	11	475	0.93	1.07	1.00
290	dark grey	platy	siltstone		2.2	0.88	30	31	455	0.79	0.86	0.83

Ro-1 uses relationship from Lafargue et al (1998)

Ro-2 uses Cretaceous relationship from Ibrahimas and Riediger (2005)

TABLE 6. OUTCROP SAMPLES SORTED BY UNITS WITH TOC, HI, AND OI DATA.

Unit /No	TOC	Hi	OI	Tmax	Ro
Passage beds					
277	1.49	34.0	55.0	498.0	1.78
Upper Fernie					1.36
52	1.42	29.0	66.0	484.0	1.53
155	1.51	20.0	195.0	499.0	1.42
280	0.62	56.0	71.0	462.0	1.13
54	1.34	25.0	59.0	488.0	1.60
149	0.92	7.0	139.0	500.0	1.81
176	1.43	12.0	110.0	493.0	1.69
207	1.45	19.0	110.0	485.0	1.55
215	1.82	31.0	70.0	465.0	1.19
216	2.28	58.0	21.0	461.0	1.12
266	1.22	34.0	75.0	472.0	1.31
average	1.40	29.1	91.6	480.9	1.43
Green beds Upper Fernie					
47	0.47	18.0	73.0	453.0	1.37
117	0.16	25.0	256.0	493.0	1.69
average	0.32	21.5	164.5	473.0	1.53

Unit /No	TOC	Hi	OI	Tmax	Ro
Grey beds Upper Fernie					
122	0.11	18.0	182.0	489.0	1.62
200	0.09	11.0	333.0	480.0	1.46
80a	0.12	0.0	333.0	516.0	2.10
80b	0.61	7.0	118.0	541.0	2.55
44	0.14	14.0	179.0	463.0	1.15
71	0.47	23.0	55.0	475.0	1.37
72	0.26	12.0	138.0	490.0	1.64
74	0.33	36.0	139.0	472.0	1.31
86	0.23	17.0	178.0	490.0	1.64
92	1.57	31.0	55.0	473.0	1.33
96	0.21	19.0	176.0	490.0	1.64
120	0.23	26.0	235.0	471.0	1.29
122	0.11	18.0	182.0	489.0	1.62
138	0.17	24.0	212.0	479.0	1.44
139	0.18	39.0	111.0	480.0	1.46
151	0.41	20.0	195.0	499.0	1.80
157	1.40	21.0	103.0	477.0	1.40
158	0.25	20.0	100.0	466.0	1.21
159	0.25	12.0	216.0	494.0	1.71
160	0.42	14.0	164.0	490.0	1.64
164	0.19	11.0	168.0	485.0	1.55
166	0.22	18.0	195.0	489.0	1.62
170	0.28	11.0	139.0	501.0	1.83
200	0.09	11.0	333.0	480.0	1.46
220	1.64	60.0	21.0	463.0	1.15
252	1.46	60.0	18.0	467.0	1.22
260	1.19	42.0	76.0	474.0	1.35
average	0.47	22.0	161.3	484.6	1.54

Unit /No	TOC	Hi	OI	Tmax	Ro
Lower Fernie					
67	0.37	14.0	349.0	483.0	1.51
181	0.25	20.0	120.0	459.0	1.08
183	0.77	34.0	56.0	484.0	1.53
197	0.27	41.0	63.0	472.0	1.31
287	0.39	10.0	259.0	474.0	1.35
68a	0.91	58.0	51.0	461.0	1.12
69a	1.23	42.0	41.0	474.0	1.35
69b	0.64	22.0	45.0	449.0	0.90
174	1.18	6.0	136.0	513.0	2.05
180	1.35	43.0	15.0	452.0	0.95
191	2.45	17.0	67.0	500.0	1.81
193	2.93	20.0	7.0	463.0	1.15
279	1.54	42.0	80.0	456.0	1.03
288	5.94	58.0	11.0	475.0	1.37
290	0.88	30.0	31.0	455.0	1.01
296	2.56	36.0	59.0	468.0	1.24
308	0.50	42.0	134.0	453.0	0.97
average	1.42	31.5	89.6	470.1	1.28

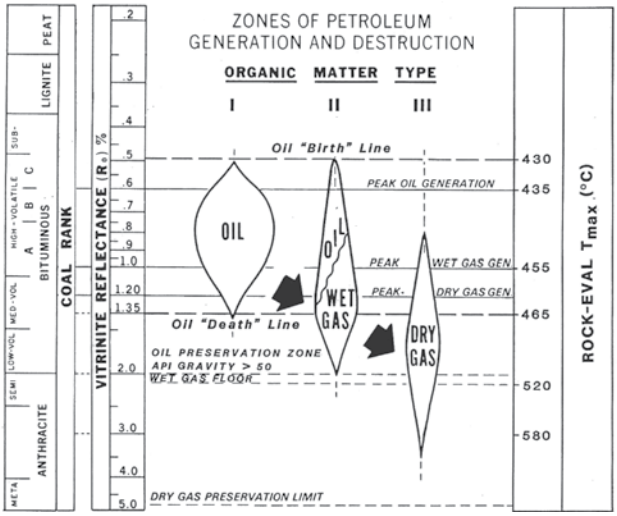

Figure 8. Generation of oil and gas from kerogen; figure from Dow (1974).

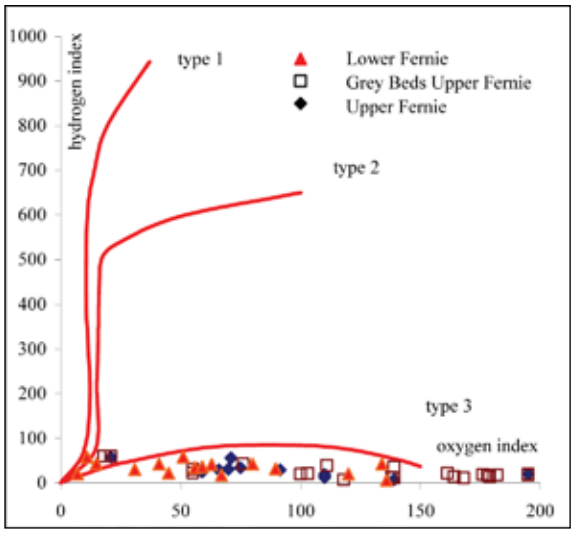

Figure 9. Van Krevelen diagram for outcrop samples.

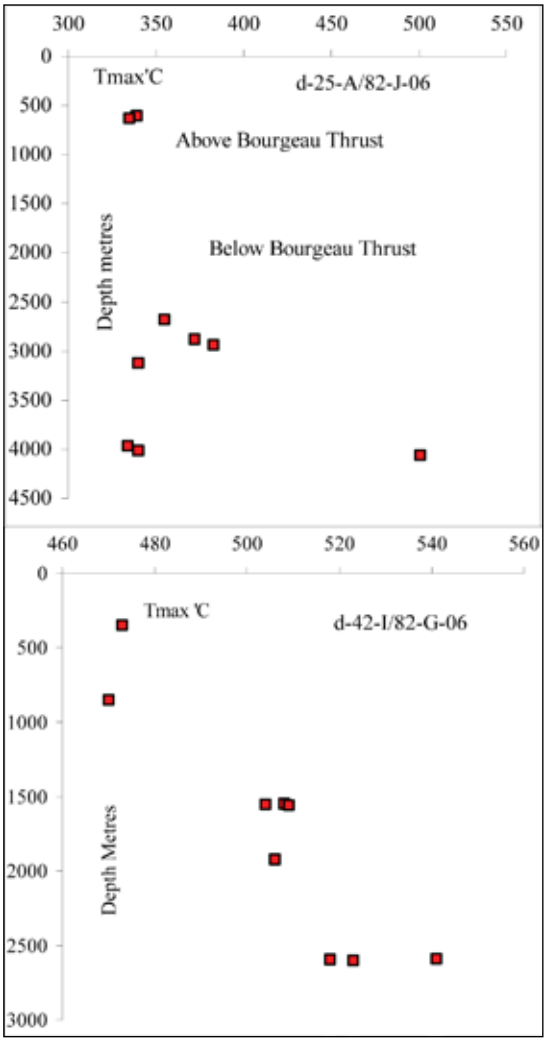

Figure 10. Depth *versus* Tmax plots for holes d-42-I/82-G06 and d-25-A/82-G-07.

Contours of Tmax values indicate higher values to the southwest (Figure 11), which agrees with the general rank trends for the overlying Mist Mountain Formation. Plots of Grey Beds and Lower Fernie data sets separately (Table 6) indicate, with the limited amount of data available, that it is not possible to distinguish any maturity difference between units within the Fernie Formation.

The TOC contents of producing shale units range from 0.5% to over 20% (Table 7), and in terms of TOC content and rank, the Fernie Formation is similar to the Lewis Shale. The Lewis Shale is 300 to 450 m thick and occurs at a depth of 1000 to 2000 m in the San Juan Basin. Well productivity correlates with natural fracture spacing (Dart, 1992). Permeability is improved by dissolution of carbonate cement on some fractures. The presence of inorganic carbon is identified by Rock-Eval analyses, and contents are generally low in the Fernie shale samples. The shale is considerably under-pressured, which decreases gas contents (which range from 0.3 to 0.6 cc/g) but probably aids permeability and produceability. There are no data on pressure gradients in the Fernie Formation, though unpublished data probably exist for the overlying Mist Mountain Formation.

Shale gas contents are composed of gas adsorbed on organic material, gas in the non-organic rock that is tightly held free gas, and possibly some gas adsorbed onto clay surfaces. Adsorption on non-organic material is suspected when any isotherm on a sample with low organic content predicts unrealistically high adsorption ability when calculated to the equivalent 100% TOC sample. The effect of clay adsorption or tight free gas is greater for lower TOC samples, and it can cause a double accounting of gas because it is not part of the gas adsorbed on the organic material. Many isotherms on shale, for which the TOC content is also provided, permit estimation of the adsorption characteristics of the equivalent sample with 100% TOC. As

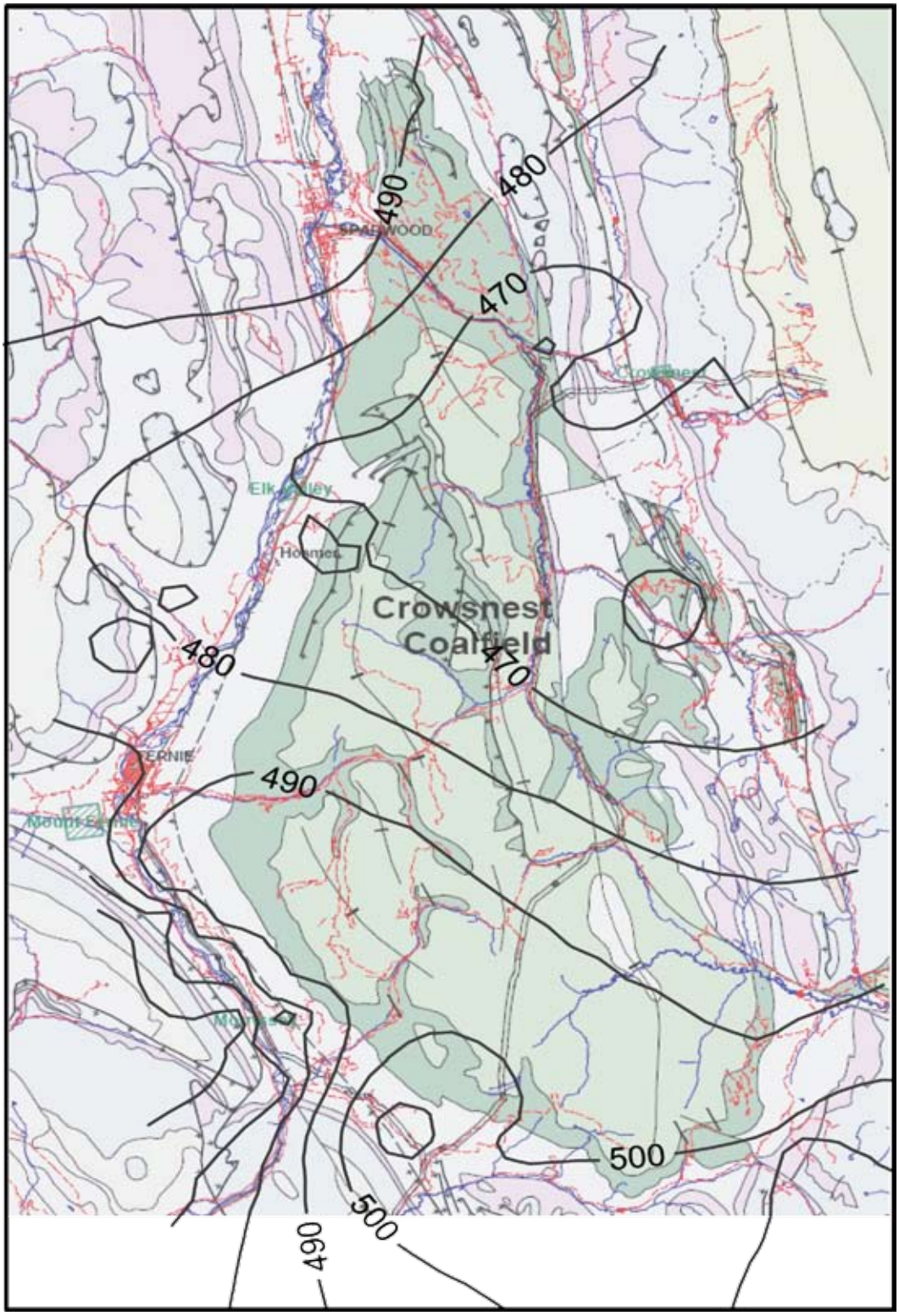

Figure 11. Contours of Tmax for all samples, Crowsnest Coalfield.

noted previously, (Bustin, PC 2005) calculated Langmuir volumes (Vl) at 100% TOC often appear to be unrealistically high, indicating double accounting or the possibility that sample preparation may have artificially increased the adsorption ability of the shale component of the sample. The lower the TOC content, the more this will affect estimation of Vl at 100% TOC.

Data from the Nordegg Member (Bustin and Nassichuk, 2002) with a Tmax of 430 'C and variable TOC values are sufficient to calculate the Langmuir volume for 100% TOC samples (Figure 12). As the TOC content decreases, Langmuir volumes increase to unrealistic values, indicating that adsorption values measured on small contents of TOC should be treated with caution.

No isotherms for the TOC from the Fernie Formation are available; however, it is possible to estimate the adsorption capacity of the rock using isotherms on coal of similar rank and kerogen type. The Gething Formation in northeast British Columbia has similar rank, and some samples are inertinite-rich (kerogen type 3 to 4) (Ryan and Lane, 2002). Using Langmuir constants from these samples, a TOC content of 1.5% and a normal hydrostatic gradient predicts a gas content of about 0.3 cc/gm at 1500 m. There is no way of estimating the amount of free gas that might be held in the microporosity.

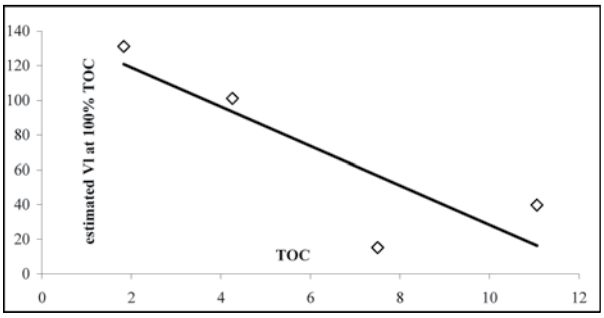

Figure 12. Langmuir volume calculated for 100% TOC sample *versus* actual TOC content Nordegg samples Tmax 430; data from Ramos (2002).

It is not proven that finely dispersed organic matter in shales has the same adsorption characteristics as various coal macerals in coal seams of the same maturity. Some indication is available from studies of adsorption on samples with different maceral composition. It appears that as kerogen type changes from type 2 to type 3 or 4, adsorption ability (Langmuir volume) decreases but Langmuir pressure remains constant (Ryan and Lane, 2002). Estimated Langmuir pressures for shales appear to be higher than for coals with similar rank and kerogen type. The reason for this is not clear but may in part be related to both increased solubility of methane in water as pressure increases and the fact that in shales the ratio water/organic matter is much higher than it is in coals.

In the literature, there are plots of adsorption ability for samples with different Tmax values at a single fixed pressure and with varying TOC contents (Bustin and Nassichuk, 2002, Figure 8-10). Best-fit lines through data sets (Figure 13a) with more than 4 points (data for Tmax>470 and Tmax=460 combined) provide relationships of TOC to adsorption for kerogen type 3? for different ranks. Slope of lines generally increase as Tmax increases, indicating that adsorption ability increases with rank of kerogen; also lines generally have positive Y intercepts that increase with rank and indicate that at TOC = 0 (i.e., 100% shale), samples still have the ability to adsorb gas and that the adsorption ability of clays may be rank-dependent. The equation of the lines indicates that at 5 Mpa and 100% TOC, adsorption varies from 6 cc/g to 10 cc/g. A study (Bustin, 2005) provides data similar to that from Bustin and Nassichuk (2002) (Figure 13b), except that adsorption is calculated at 11 Mpa and represents kerogen that has high Tmax values. Using the Exshaw data (Figure 13b) and data with Tmax values of 460 or greater (Figure 13a) provides 2 lines of adsorption versus TOC; one for a pressure of 5 Mpa and another for a pressure of 11Mpa. These two lines provide pairs of points on isotherms for increasing TOC contents. Calculation of Langmuir volumes and Langmuir pressures for increasing TOC indicates that at 100% TOC, Langmuir volume increases to about 30 cc/g and pressure remains fairly constant as TOC increases, as would be expected (Figure 14). The approach is interesting but is in danger of over-working the data. However, it appears that adsorption ability increases as kerogen maturity increases. Langmuir volume may be high or at least similar to macerals in coal seams, and Langmuir pressure is high and higher than it is for coals of similar rank. There is no indication that higher kerogen maturity is accompanied by low Langmuir pressures, which is the case for high-rank coal.

TABLE 7. SUMMARY OF DATA ON SHALE GAS SYSTEMS; DATA COLLECTED FROM BUSTIN (2004).

Formation	location	Age	Pressure gradient	rank Ro %	total porosity	TOC	gas content scf/t	Av gas in porosity	Av % gas adsorbed	GIP bcf/sect	gross thickness ft	total resource tcf
Lewis	San Juan Basin	Late Cretaceous	0.2-0.25	1.6-1.88	0.5--5	0.5-2.5	15-45	75-85	15-25	8--50	500-1900	100
Barnett	ft Worth Basin	Mississippian	0.43-0.44	1.1-1.4	1--6	1.0-4.5	60-250	35-75	25-65	30-40	200-300	26.2
Antrim	Michigan basin	Late Devonian	0.35	0.4-1.6	2--10	0.5-20	40-100	15-25	75-85	6--15	160	12--20
New Albany	Illinois Basin	Late Devonian	0.43	0.63-1.3	5--15	1.0-20	40-80	25-35	65-75	7--10	180	2--20
White Speckled	Alberta	Lower Cretaceous				3--5		55-75	25-45		20--90	
Ohio	Appalachian	Late Devonian	0.15-0.4	1.0-1.3	2--5	0.5-23	60-100	50	50	5--10	300-1000	225---250

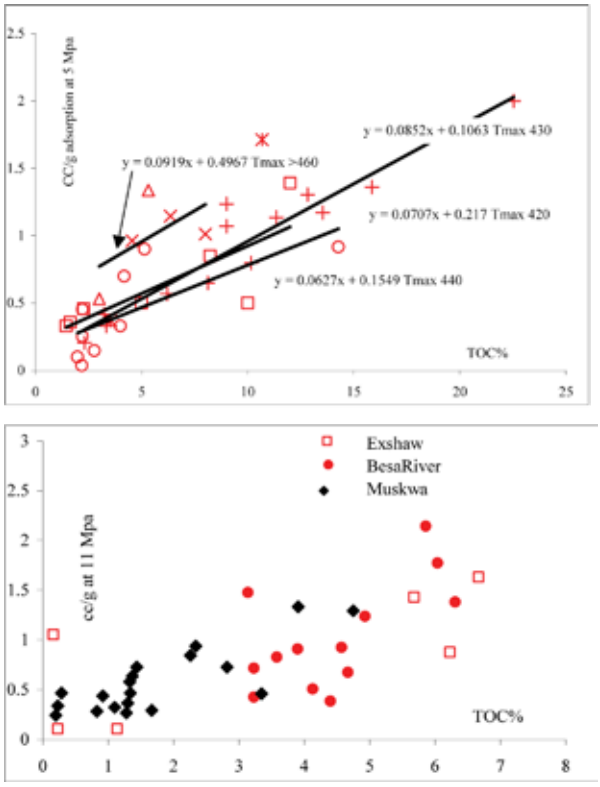

Figure 13. Plots of adsorption (a) from Bustin and Nassichuk (2002) at 5 Mpa for samples with varying TOC and Tmax values and (b) data from Bustin (2005) at 11 Mpa for samples with varying TOC and Tmax values.

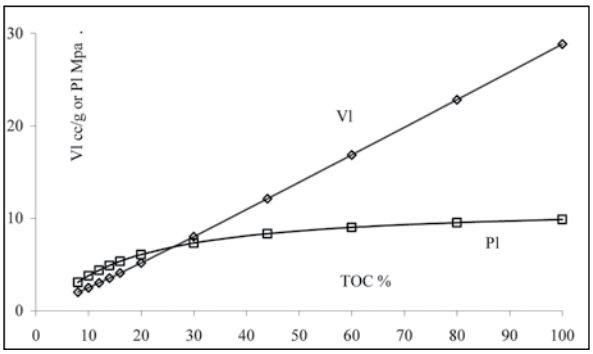

Figure 14. Estimated trend of Langmuir volume and pressures for high Tmax samples with increasing TOC contents.

CONCLUSIONS

The Fernie shale that underlies the Crowsnest Coalfield and is contained in the upper Lewis Thrust sheet generally contains moderate to low concentrations of TOC with high maturity. Rank is well-constrained by data on coal seams in the overlying Mist Mountain Formation, and Tmax values indicate similar trends of increasing rank to the south.

The regional structure of the coalfield is well-documented by a number of papers. Joint measurements indicate a normal relationship of joints to fold geometry. Field observations and CBM exploration experience in the overlying Mist Mountain Formation indicate that the Fernie Formation is moderately to highly fractured.

The lithology of the formation is variable on the regional scale as indicated by the number of members of varying lithology that form the formation. More local variations in lithology are documented by numerous descriptions, and these all help to enhance permeability.

In many aspects, the Fernie Formation in the Crowsnest Coalfield area is similar to the Lewis Shale in the San Juan Basin (Table 7). Based on a very rough estimate of the volume of the upper and lower members of the formation that underlie the Crowsnest Coalfield, the total resource in the area could be in the range of 1 to 5 trillion cubic feet (tcf). At this time there are no isotherm or adsorption data to permit a reasonable estimate of the resource.

REFERENCES

Bustin, R.M. and Nassichuk, B. (2002): Gas shale geology, engineering application to exploration and development; Short course notes Course Calgary October 10th and 11th 2002.

Bustin R.M. (2005): Gas shale potential of Devonian strata northeastern British Columbia; British Columbia Ministry of Energy, Mines and Petroleum Resources, Petroleum Geology Special Paper 2005-1.

Dart, Jr. S.W. (1992): Evaluation of San Juan Basin fractured reservoirs from surface data; Rocky Mountain Association of Geologists, page 95-114.

Dow, W. (1974): Kerogen studies and geological interpretations; Journal of Geochemical Exploration, Volume 7, pages 79-99.

Frebold, H. (1957): The Jurassic Fernie Group in the Canadian Rocky Mountains and foothills; Geological Survey of Canada, Memoir 287, 197 p.

Frebold, H. (1969): Subdivision and facies of Lower Jurassic rocks in the southern Canadian Rocky Mountains and foothills. Proceedings of the Geological Association of Canada, v. 20, pages 76-89.

Henderson, G.G.L. and Douglas R.J.W. (1954): Southern Rocky Mountains of Canada, tectonic compilation Map; Alberta Society Petroleum Geology Guide Book.

Ibrahimbas, A. and Riediger, C. (2005): Thermal maturity and implications for shale gas potential in northeastern British Columbia and northeastern Alberta; paper presented Canadian Society of Unconventional Gas, Conference, November 2005, Calgary.

Krivak, D. (2005): Progressive analysis in the development of tight gas shale plays; Canadian Institute Shale Gas Short curse Calgary, January 31.

Johnson, D.G.S. and Smith, L.A. (1991): Coalbed Methane in southeastern British Columbia; British Columbia Ministry of Energy and Mines, Petroleum Geology Branch, Special paper 1991-1.

Lechie, D.A., Kalkrueth, W.D. and Snowdon, L.R. (1988): Source rock potential and thermal maturity of Lower Cretaceous Strata: Monkman Pass area, British Columbia; American Association of Petroleum Geology, Bulletin, Volume 72, pages 820-838.

Leach, W.W. (1914): Blairmore map area, Alberta; Geological Survey of Canada, Summary Report 1912, page 234.

Lafargue, E., Espitalie, J., Marquis, F. and Pillot, D. (2000): Rock-Eval 6 applications in hydrocarbon exploration, production and soil contamination studies; Revuede I'institut Francais du Petrole, volume 53, number 4, pages 421-437.

McEvoy J. (1902): Geological and topographical map of Crowsnest Coal Fields; Geological Survey of Canada Map Number 767.

Monahan, P. (2002): The Geology and oil and gas potential of the Fernie-Elk Valley Area, southeastern British Columbia, British Columbia Ministry of Energy and Mines.

Morris, B. (2004): Geochemistry, Fracture Analysis, and Hydrocarbon Potential of the Jurassic Fernie Formation, Crowsnest Coalfield, Southeast British Columbia; Report submitted to Resources Development and Geosciences Branch, British Columbia Ministry of Energy, Mines and Petroleum Resources.

Newmarch, C.B. (1953): Geology of the Crowsnest Coal Basin; British Columbia Department of Mines, Bulletin Number 33.

Pearson, D.E. and Grieve, D.A. (1978): Preliminary geological map of the Crowsnest Coalfield, west part; British Columbia Ministry of Energy, Mines and Petroleum Resources, Preliminary map 27.

Pearson, D.E. and Grieve, D.A (1985): Rank variation, coalification pattern and coal quality in the Crowsnest Coalfield, British Columbia; Canadian Institute of Mining and Metallurgy Bulletin, Volume 78, pages 39-46.

Poulton, T.P., Christopher, J.E., Hayes, B.J.R., Losert, J., Tittemore, J. and Gilchrist, R.D. (1994): Jurassic and lowermost Cretaceous strata of the Western Canada Sedimentary Basin; Chapter 18 Geological Atlas of the Western Canada Sedimentary Basin.

Poulton, T.P. (1984): Jurassic of the Canadian Western Interior, from 49°N Latitude to Beaufort Sea, In: The Mesozoic of Middle North America, D. F. Stott and D. Glass (eds.); Calgary, Canadian Society of Petroleum Geologists, Memoir 9, pages 15-41.

Poulton, T.P. and Aitken, J.D. (1989): The Lower Jurassic phosphorites of southeastern British Columbia and terrane accretion to western North America; Canadian Journal of Earth Sciences, v. 26, pages 1612-1616.

Price, R.A. (1961): Fernie map area east half Alberta and British Columbia 82G E1/2; Geological Survey of Canada Paper 61-24.

Price, R.A. (1964): Flathead map area British Columbia and Alberta; Memoir 336.

Ramos, S.(2002): The effect of shale composition on the gas adsorption potential of organic rich mudrocks in the Western Sedimentary Basin; University of British Columbia, Department of Earth and Ocean Sciences; Masters of Science Thesis.

Ryan, B.D. and Lane, R. (2002): Adsorption characteristics of coals from the Gething Formation northeast British Columbia; British Columbia Ministry of Energy and Mines, Geological Fieldwork, Paper 2002-1.

Ryan, B.D. (2004): Coalbed gas Resource of prospective areas of the Crowsnest Coalfield; Report of activities 2003, Resources Development Branch, Oil and Gas Division, British Columbia Ministry of Energy, Mines and Petroleum Resources.

Taylor, G.H, Teichmuller, M., Davis, A., Diessel, C.F.K., Littke, R. and Robert, P. (1998): Organic Petrography; Geruder Borntraeger, Berlin-Stuttgard.

THE NECHAKO BASIN PROJECT: NEW INSIGHTS FROM THE SOUTHERN NECHAKO BASIN

Filippo Ferri[1] and Janet Riddell[1]

ABSTRACT

The Nechako Basin is the region of south-central BC that is underlain by poorly exposed Lower Jurassic to Upper Cretaceous sedimentary sequences overlain by extensive Tertiary volcanic rocks and thick Pleistocene to Holocene glacial deposits. Jura-Cretaceous strata have potential for oil and gas.

The Nechako Basin has seen intermittent exploration for oil and gas. The Nechako Basin Project is a multi-year research program designed to generate new geoscience data and interpretations to facilitate continued oil and gas exploration. The program includes geological field reconnaissance, biostratigraphy, radiometric dating, apatite fission track thermochronometry, and Rock-Eval and thermal maturity analyses.

Work completed in the first year of the project included reconnaissance and sampling of Jura-Cretaceous strata in the southern and central parts of the Nechako Basin, new sampling and analysis of drill core and cuttings from 7 old oil and gas exploration wells, and new interpretations of well stratigraphy and regional geophysical data.

KEYWORDS: Nechako Basin, oil and gas, petroleum, hydrocarbons, Taylor Creek Group, Jackass Mountain Group, Last Creek Formation, Relay Mountain Group, Silverquick conglomerate, Powell Creek volcanics, thermal maturity, vitrinite reflectance, source rocks, thermochronometry, biostratigraphy, Rock-Eval, gravity, Aptian, Albian

INTRODUCTION

The government of British Columbia, through the Ministry of Energy, Mines and Petroleum Resources, is committed to realizing BC's ultimate hydrocarbon potential within its relatively under-explored portion of the Western Canada Sedimentary Basin (WCSB) and seeing oil and gas exploration within its interior and offshore basins. The government has initiated projects designed to improve the province's petroleum geology information base and to identify new energy development opportunities.

The Resource Development and Geoscience Branch (RDGB) is mandated to identify, quantify, and promote the hydrocarbon potential of onshore regions of British Columbia; in onshore regions outside of the WCSB, oil and gas potential occurs primarily within Mesozoic and Cenozoic clastic sediments of the Interior Basins. The main areas include the Whitehorse Trough and the Bowser, Sustut and Nechako Basins (Figure 1). Although the Bowser and Nechako Basins have seen limited subsurface exploration, these regions remain 'frontier basins' because of deficiencies in both infrastructure and geological information.

In accordance with the goals of the Interior Basins Strategy (Hayes *et al.,* 2004), the RDGB has initiated or supported projects within these areas, leading to the capture of new energy-related geoscience information.

The Nechako Basin lies in the Interior Plateau physiographic region of British Columbia, as defined by Holland (1964). Prospective horizons for petroleum are poorly exposed Lower Jurassic to Upper Cretaceous sedimentary sequences, which are overlain by extensive Tertiary volcanic rocks and thick Pleistocene to Holocene glacial deposits. The boundaries of the Nechako Basin are variously defined (e.g., Koch [1970], Hannigan *et al.* [1994]), but they are generally considered to be the Skeena Arch in the north, Highway 97 to the east, the Tyaughton Basin in the Chilcotin and Camelsfoot Ranges to the south, and the Coast Mountains to the west. Surface exposures in this area are dominated by Paleogene to Neogene volcanics and Quaternary deposits that hide underlying geology. Although there are exposures of Jura-Cretaceous sedimentary sequences within the Nechako region, the dominance of older volcanic terranes in certain areas, together with geophysical and subsurface data, suggests that the area currently defined as the Nechako Basin is actually composed of smaller sub-basins. It is not known whether these represent separate depocentres or the remnants of one large basin.

[1]Resource Development and Geoscience Branch, BC Ministry of Energy, Mines and Petroleum Resources, PO Box 9323, Stn Prov Govt, Victoria, BC, V8W 9N3

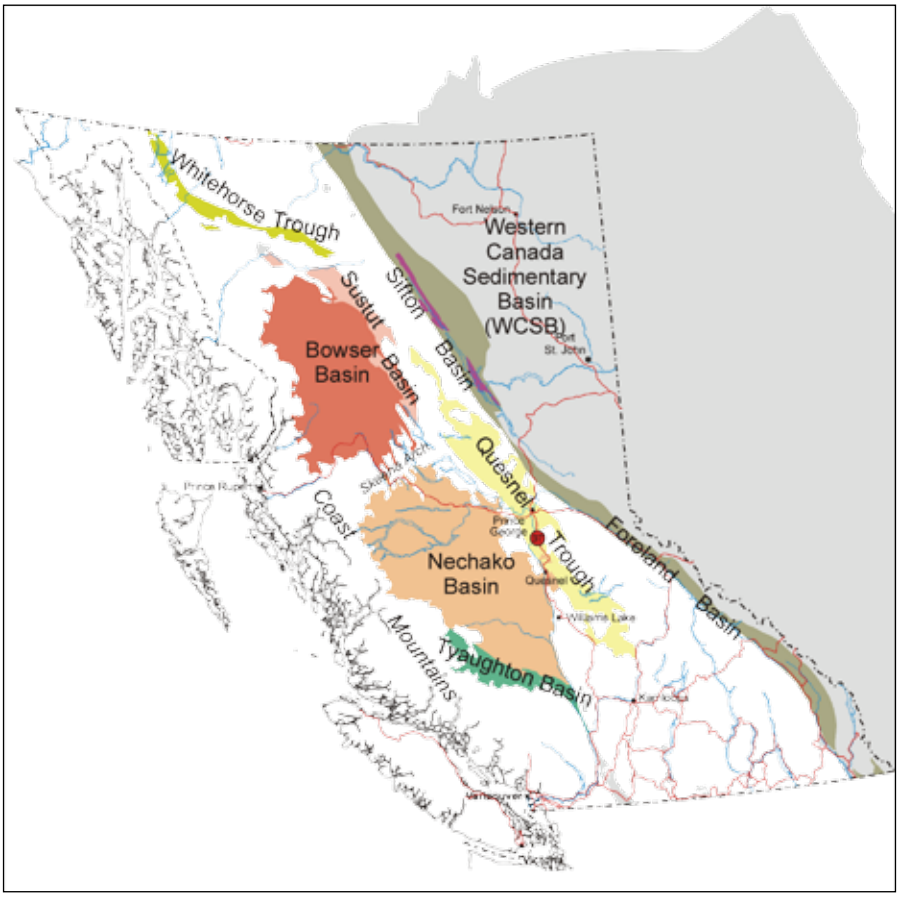

Figure 1. British Columbia's Interior basins (outlines adapted from P. Hannigan, P.J. Lee, K. Osadetz, unpublished 1993-1998).

OIL AND GAS EXPLORATION HISTORY OF THE NECHAKO BASIN (FIGURE 2)

Oil and gas exploration in south-central British Columbia began with investigation of reported oil and gas shows at surface in the Kersley area, about 55 km south of Quesnel (Hayes, 2002). One hole was drilled in 1931, and several others in the early 1950s. All penetrated 500 to 600 m of unconsolidated Quaternary deposits and Tertiary sedimentary rocks before reaching limestone bedrock (probably of the Cache Creek Group); no significant oil or gas shows were found. One hole was drilled by Northern Lights Resources in 1981 in the Kersley area, with no success (Hayes, 2002).

Honolulu Oil Corporation began exploring the Nechako Basin in 1959, concentrating in the Nazko River area (Taylor, 1960). They conducted air photo interpretation and reconnaissance surface mapping over the region, followed in 1960 with more detailed geologic investigation and the drilling of the Honolulu Nazko well a-4-L/93-B-11. The hole was dry but had spotty live oil shows and gas in one drill stem test. Limited seismic work was done: about 43.5 total line km in the Nazko area and small surveys (a few shot points each) in the Alexis Creek and Puntzi areas (Taylor, 1961). In the same year, the Hudson's Bay Oil and Gas Company drilled a 1300 m well (c-75-A/93-B-04) for stratigraphy (Williams, 1959) south of Redstone. All exploration permits were subsequently dropped (Halliday, 1969). Amoco Canada filed permits for 2.5 million acres in the Nechako Basin in 1969, conducted geological investigation, and collected magnetic susceptibility data (Halliday, 1969). An aeromagnetic survey, a seismic program, and drilling were recommended but were not conducted. Texalta Resources drilled a well (c-38-J/93-G-06) in the Punchaw area south of Prince George in 1972 (Hayes, 2002). The target Jura-Cretaceous section was not intersected; the hole penetrated 250 m of unconsolidated material over volcanic rocks of the Cache Creek Terrane. Oil staining was noted at fault contacts (well file WA 3149).

From 1979 to 1985, Canadian Hunter Exploration ran the largest and most comprehensive oil and gas exploration program that the Nechako Basin has seen, culminating in the drilling of 5 exploration wells. The company acquired 43 permit parcels late in 1979 (Province of BC News Release, January 15, 1980) and in the ensuing 2 years completed several integrated gravity and seismic surveys (3070 total line km and about 965 line km respectively). Two wells were drilled in 1980. A north-south anticline parallel to the Naz-

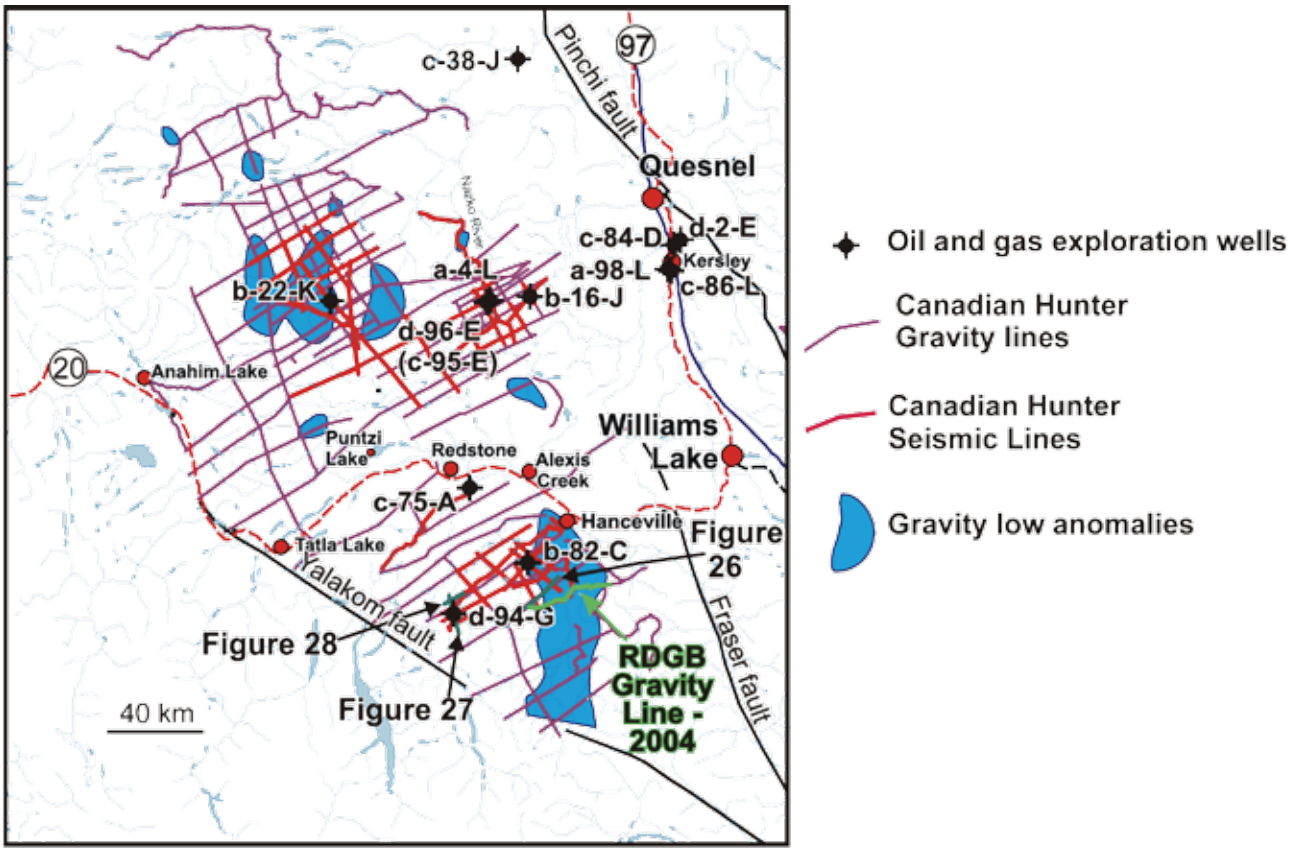

Figure 2. Oil and gas exploration to-date within the Nechako Basin.

ko River valley, identified by surface mapping and seismic testing, was tested by wells d-96-E/93-B-11 and b-16-J/93-B-11. The first hole intersected broadly similar stratigraphy to a-4-L, but the second hole did not intersect the target strata and reached economic basement at about 1100 m. Two more holes were drilled in 1981. Well b-22-K/93-C-9 is on a seismic high (Hayes, 2002) and is also positioned over the largest and deepest gravity low (Figure 2) identified by the gravity survey in the early 1980s. The drilling intersected volcanic and volcaniclastic rocks instead of the expected sedimentary package. Well site b-82-C/92-O-14 sits on the western margin of another significant gravity low, a large north-pointing arrow-shaped feature centred in the Big Creek area south of Hanceville. The drilling pierced Tertiary volcanic rocks over sedimentary rocks of probable Albian ages. Granitic rocks intersected at 1638 m explained the seismic high. The fifth and last well (d-94-G/92-O-12) was drilled in 1985. The well was sited on a seismically defined rollover associated with a thrust fault (Hayes, 2002) but did not intersect the expected Jura-Cretaceous sedimentary package. Fine-grained, feldspathic, volcaniclastic sedimentary rocks overlie volcanic rocks at this site.

No significant physical oil and gas exploration work has been done in the Nechako Basin since well d-94-G/92-O-12 was abandoned in 1986. Several workers have compiled and evaluated existing data and discussed their implications for oil and gas exploration (e.g., Hannigan *et al.* [1994]; Hayes [2002]; Hunt and Bustin [1997]). Julie Hunt (1992) collected and analysed new data on thermal maturity and biostratigraphy for the basin, which improved understanding of the stratigraphy of some well sections and of the oil and gas potential in the basin.

REGIONAL GEOLOGICAL FRAMEWORK (FIGURE 3)

Relatively little is known about the geological history of the Nechako Basin due to limited bedrock exposure. The assumption that Jura-Cretaceous sedimentary rocks exist beneath the Tertiary and Quaternary volcanic rocks is based on the occurrence of Mesozoic sedimentary rocks along the northern and southern fringes of the Nechako Basin. Oil and gas exploration drilling in the Nazko Valley in 1960 and 1980 confirmed that over 2000 m of Cretaceous sedimentary rocks underlie at least parts of the Nechako Basin. Rocks exposed at the northwest end of the basin in the Fawnie and Nechako Ranges are associated with Stikine Terrane and include the Hazelton, Bowser Lake, and Skeena Groups. Rocks of the Cadwallader Terrane and the overlying Jura-Cretaceous Tyaughton-Methow overlap assemblages border the southern end. The nature and loca-

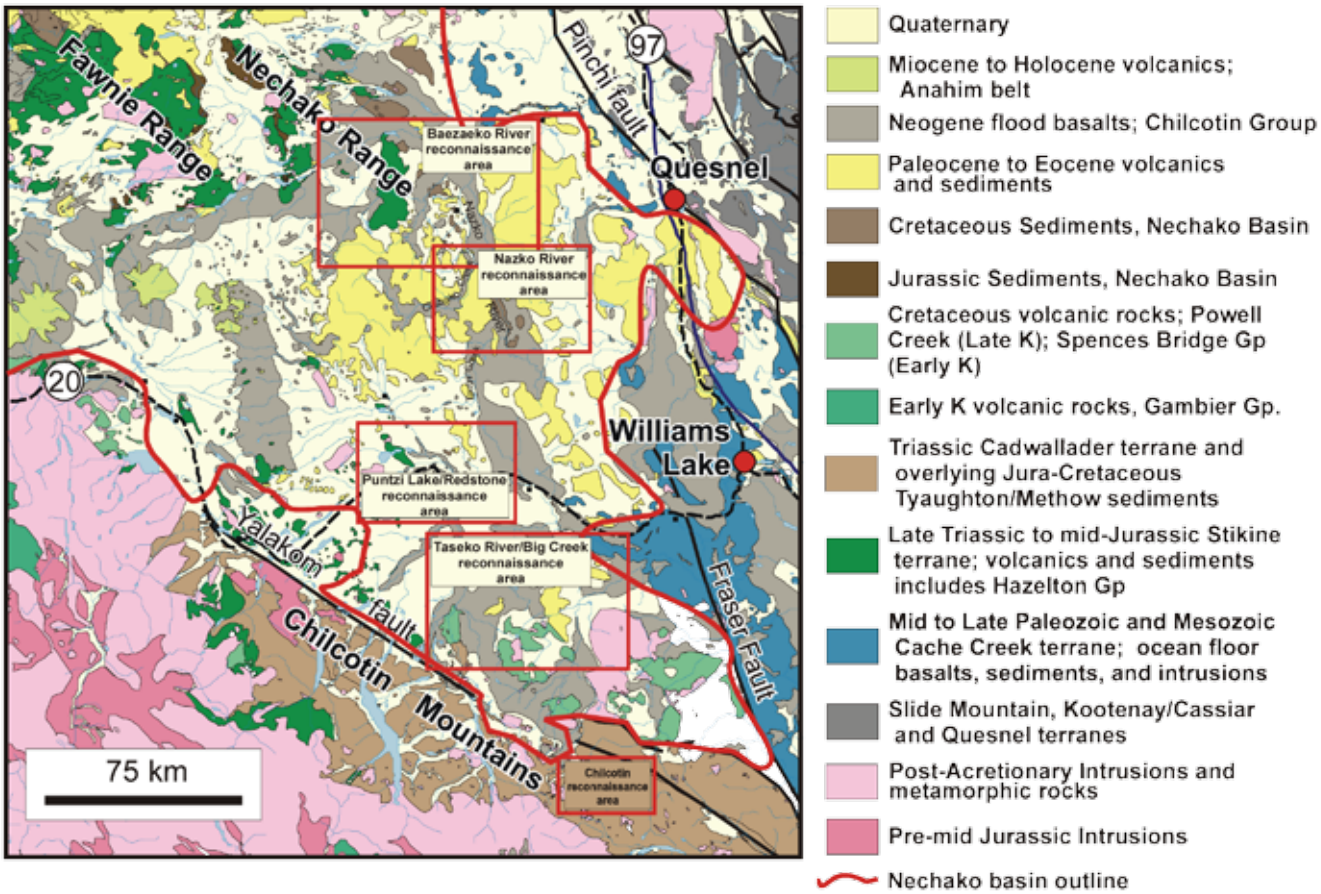

Figure 3. Regional geological framework of the southern Nechako Basin. Red rectangles outline 2005 field reconnaissance and sampling areas.

tion of the boundary between the Cadwallader/Tyaughton-Methow Terranes and Stikine Terrane is unknown because it is largely masked by the overlying Chilcotin basalts and Quaternary deposits, therefore interpretation of subsurface stratigraphy must include consideration of units of both Stikinia and Cadwallader affinities.

The best exposures within the Nechako region are found along the Nazko River between its confluence points with the Clisbako River and Tautri Creek. Outcrops occur in the river valley where it has incised below the 1065 to 1100 m elevation level of the Chilcotin basalts—an area about 25 km long from north to south and about 5 km wide. Exploration drilling in this area and elsewhere in the Nechako region intersected various thicknesses of sedimentary rocks, but lateral correlations are not readily apparent; this is a function of the large distances between the wells but probably also reflects structural complexity in the subsurface.

THE NECHAKO BASIN PROJECT

This paper reports on a comprehensive research program for the Nechako Basin that began in 2004 with acquisition of new gravity and magnetic data along a 30 km transect (the green line on Figure 2) along Highway 20 west of Williams Lake (Best, 2004a). In addition, in 2003 a 2-year joint program was initiated between the RDGB and the Geological Survey of Canada (GSC) towards a new resource estimate of the Nechako Basin (Hayes, 2004). This has produced several products, such as a new Rock-Eval database for subsurface samples (Osadetz *et al.*, 2003), detailed subsurface sample descriptions (Thorsteinsson, *in preparation*), and a current heat flow study of the Interior basins (Majorowicz *et al.,* 2004).

In 2005, we began integrated fieldwork and sampling, regional stratigraphic correlation, thermal history studies, and radiometric and fossil dating. The project also provides technical and financial support for ongoing geophysical studies conducted by the GSC, including the positioning of 7 passive seismic stations and the initiation of a magnetotelluric survey across the Nechako Basin. The passive seismic array will provide insight into large-scale basin architecture, and the magnetotelluric survey will help image through surface basalts to distinguish volcanic from sedimentary sequences.

The current project will continue to assess the oil and gas potential of the Nechako Basin, specifically by evaluating some of the critical factors of a petroleum system: the presence of petroleum source and reservoir rocks, an appropriate thermal history, and timing of petroleum migration. This paper reports on current activities, with emphasis on regional correlations within the basin, structural style, source bed analysis, and thermal maturation. The reader is referred to Hayes (2002) and Hannigan *et al.* (1994) for our current understanding of Nechako petroleum geology.

We have begun the project by studying the Cadwallader/Tyaughton-Methow Terrane stratigraphy and structure in the Chilcotin Mountains along the southern fringe of the Nechako Basin and by re-evaluating the limited subsurface data from existing exploration wells in the context of those southern correlations. In 2006, we plan to approach the Nechako Basin from its northern boundary to assess the applicability of the Stikine Terrane stratigraphic and structural history to interpretation of the subsurface.

STRATIGRAPHY AND STRUCTURE IN THE CHILCOTIN MOUNTAINS

The Chilcotin Mountains were uplifted and incised in Neogene (specifically 2 to 14 Ma) time, exposing late Paleozoic basement and Mesozoic sedimentary and volcanic rocks (Table 1) that are expected to underlie at least part of the Nechako Basin region. The exposed rocks include Mississippian to Jurassic oceanic rocks of the Bridge River Complex, arc-derived volcanic and sedimentary rocks of the Cadwallader Terrane, and Late Jurassic to mid-Cretaceous rocks of the Tyaughton-Methow Basin. Volcanic rocks of the Powell Creek Formation overlie these. The Tyaughton-Methow Basin can be considered a single entity during deposition of the Jurassic to Lower Cretaceous Relay Mountain Group. In the late Early Cretaceous, the basin was partitioned into the Tyaughton and Methow subbasins by landforms that emerged in response to contractional deformation (Garver, 1992). The Tyaughton Basin is represented by the Taylor Creek Group and the overlying Silverquick conglomerate, and the Methow Basin by coeval but lithologically distinct Jackass Mountain Group (Schiarizza, 1996).

The Chilcotin region has been divided by Schiarizza (1996) into 3 separate domains (Figure 4) based on distinct structural styles: the south Chilcotin domain, the Methow domain, and the Niut domain. The south Chilcotin domain (Figure 5) is characterized by middle to Late Cretaceous southwest-directed contractional faults and tight folds and Late Cretaceous to Early Tertiary strike-slip faults. The Methow structural domain occurs northeast of the south Chilcotin domain and is characterized by a less complex structural style—faults are more widely spaced, and folds are broad and open. The Niut domain affects rocks west of Chilko and Tatlayoko Lakes that are deformed by easterly-directed mid-Cretaceous thrust faults (Rusmore and Woodsworth, 1994). The faults that characterize the Niut domain are interpreted as the easternmost component of the mid-Cretaceous contraction event that deformed the Coast Plutonic Complex (Rusmore and Woodsworth, 1991). A detailed discussion of the structural history of the Chilcotin Mountains is provided by Schiarizza *et al.* (1997).

Current understanding of subsurface geology in most of the Nechako Basin is inadequate to reliably determine the structural style in the rocks hosting prospective horizons. An understanding of the structural styles exhibited in the Chilcotin Mountains could provide working models for interpretation of the limited existing data and for the design of effective research methods.

For oil and gas prospects, the less-complex structural style that characterizes the Methow domain is clearly preferable to that of the south Chilcotin domain or the Niut domain. An important question for oil and gas exploration is whether or not the closely spaced fault patterns of the south Chilcotin or Niut domains continue to the northeast beneath the area covered by Neogene basalt and Quaternary glacial deposits.

Within the south Chilcotin domain, late strike-slip faults represent closely spaced disruptions to the continuity of source and reservoir horizons as well as steep to vertical conduits to the surface that breach stratigraphic or structural traps. The southern Nechako Basin occupies the basalt and till-covered region between two major Eocene dextral strike-slip fault systems—the Yalakom and the Fraser. Post-accretionary plutons of the Coast Belt young to the northeast, reflecting their formation over the advancing east-dipping plate (Friedman *et al.*, 1995). Three large plutons within the south Chilcotin domain—the Beece Creek pluton, the Lorna Lake stock, and the Mission Ridge pluton (Figure 5)—yielded 44 Ma Ar-Ar dates (Archibald *et al.*, 1989), indicating the presence of an Eocene zone of thermal weakening (Friedman and Armstrong, 1988). This weakened thermal zone likely accommodated northerly-directed movement of outboard rocks with respect to North America that began sometime after 57 Ma and continued until at least 37 Ma (Engebretson, 1985). The resulting spatial intensity of faulting that characterized the south Chilcotin domain is therefore likely restricted to this northwest-striking corridor and may not continue to the northeast beneath the Chilcotin Group basalt cover.

The extent of the influence of the characteristic Niut domain structural style is not known. Similar northeast-directed thrust faults were documented by Mahoney *et al.* (1992) in the Churn Creek area (near its confluence with the Fraser River) in the southeastern corner of the Nechako Basin.

2005 FIELD SEASON

In 2005, we examined and sampled Jurassic and Cretaceous rocks of the Chilcotin and Camelsfoot Ranges (Figures 3 and 7); these Mesozoic prospective horizons may underlie the Chilcotin basalts in much of the Nechako Basin. We sampled potential source beds for type, content, and maturity of organic matter (Rock-Eval analysis) and potential reservoir units for characterization of porosity; we also collected vitrinite reflectance and apatite fission track samples for thermal history studies. We visited pre-Neogene outcrops in the southern Nechako Basin area (Figures 6, 7, and 8) to evaluate their place in the regional geological framework and to sample for biostratigraphy (palynology) and thermal history (vitrinite reflectance and fission track). At all field stations (except for those in the Chilcotin Mountains reconnaissance area), we measured the magnetic susceptibility of rock units for use in the modeling and interpretation of magnetic survey data (Figures 6, 7a, and 8; Table 5). Subsequently, we examined core and drill cuttings from old exploration wells and sampled them for vitrinite reflectance, palynology, and apatite fission track studies. The analyses of vitrinite reflectance and surface Rock-Eval samples are complete, and results are discussed below. Results of palynology and apatite fission track analyses are pending and will be reviewed in a future publication.

DESCRIPTION OF TYPE AREAS IN THE CHILCOTIN AND CAMELSFOOT RANGES

We visited and sampled type sections of Last Creek Formation, Relay Mountain Group, most formations of the Taylor Creek Group, the Silverquick Formation in the Chilcotin Mountains, and the Lillooet and Jackass Mountain Groups along the Fraser River canyon between Lillooet and Boston Bar.

Last Creek Formation

The Early to Middle Jurassic Last Creek Formation consists of a fining-upward sequence of Hettangian to Sinemurian volcanic pebble conglomerate, sandstone, and sandy siltstone, with rare tuff bands, overlain by a markedly finer unit of Sinemurian to Bajocian calcareous black shale, minor sandstone, and rare conglomerate (Umhoefer and Tipper, 1998), with a total thickness of at least 450 m. The formation is rich in ammonoid and bivalve fossils as well as woody debris. Umhoefer and Tipper (1998) interpret the lower coarse-grained part as a transgressive sequence of nearshore to inner-shelf deposits, and the higher fine-grained part as outer-shelf to slope deposits. Shaly intervals of the Last Creek Formation were sampled for total organic carbon (TOC) analysis to test their potential as a source rock.

Rocks that are time-equivalent and similar in lithology to the Last Creek Formation occur throughout the interior basins of British Columbia. They include the Nemaia Formation in the Potato Range and, elsewhere (Umhoefer and Tipper, 1998), the Junction Creek unit in the Bridge River area (Schiarizza *et al.*, 1997), parts of the Ashcroft Formation in southwestern BC (Travers, 1978), parts of the Spatsizi Formation of the Hazelton Group in north-central BC (Thomson *et al.*, 1986), the Ladner Group near Boston Bar, the Lillooet Group near Lillooet (Mahoney, 1993), and others. Regionally, these rocks may include viable hydrocarbon source horizons (Ferri and Boddy, 2005).

Relay Mountain Group

The Relay Mountain Group comprises several sequences of fossiliferous Middle Jurassic to Lower Cretaceous clastic sedimentary rocks, which are best exposed on the ridge that includes Teepee and Relay Mountains. Umhoefer *et al.* (2002) divide the Group into 3 formal formations. The Callovian and Early Oxfordian Tyoax Pass Formation comprises marine shale and sandstone turbidites. The Teepee Mountain Formation is Late Oxfordian to Valanginian in age and consists of shallow marine clastic rocks with common *Buchia* fossils. The Hauterivian to Barremian(?) Potato Range Formation consists of marine and non-marine sandstone and conglomerate. We walked the length of the sequence exposed along the Relay Mountain/Teepee ridge and sampled all fine-grained, dark-coloured units for Rock-Eval analysis. Sandstone with woody fragments was sampled for vitrinite reflectance.

The Relay Mountain Group is a widespread and regionally important sequence in southwestern BC as it underlies Aptian and younger Cretaceous rocks of both the Taylor Creek Group (Tyaughton Basin) and the Jackass Mountain Group (Methow Basin).

Taylor Creek Group

The Taylor Creek Group includes over 3000 m of sedimentary rocks inferred to have been deposited in response to uplift and erosion of older oceanic and arc-related rocks during the accretion of the Insular Superterrane to North America (Garver, 1992, and references therein). Strata that are correlative with the Taylor Creek Group are widespread in southwestern BC and were intersected by several of the Nechako oil and gas exploration wells. These rocks clearly represent a significant component of the subsurface geology of the Nechako Basin. The Taylor Creek Group includes several shaly and conglomeratic sequences, which have potential as source and reservoir rocks respectively. Taylor

TABLE 1. SIMPLIFIED TABLE OF FORMATIONS IN THE CHILCOTIN MOUNTAINS, BRITISH COLUMBIA. ADAPTED FROM TIPPER (1963), SCHIARIZZA *ET AL.* (1997), UMHOEFER AND TIPPER (1998), AND GRADSTEIN AND OGG (2004).

Era	Period Or Epoch	Age		Group / Formation and thickness	Lithology
Cenozoic	Quaternary	Recent			Alluvium, river gravel, colluvium
		Neogene	Pleistocene	Glacial deposits	Till, outwash sands and gravels
	Tertiary		Pliocene	Chilcotin Group	Vesicular basalt, andesite flows, related breccia and tuff
			Miocene		
		Paleogene	Oligocene	Ootsa Lake Group or Kamloops Group	Ootsa Lake: Felsic and intermediate volcanics and associated sediments Kamloops: Andesite, trachyandesite and latite flows.
			Eocene		
			Paleocene		
Mesozoic	Cretaceous	Late	Maastrichtian		Taseko River strata: Purplish feldspathic sandstone and conglomerate, cross-bedded Powell Creek: Hornblende and feldspar phyric andesitic volcanics and volcaniclastics Silverquick: Chert and volcanic lithic pebble conglomerate, non-marine, cross-bedded, with interbedded siltstone and sandstone, silty redbeds
			Campanian	Taseko River strata >400m ? ? ? ? ?	
			Santonian		
			Coniacian		
			Turonian	Powell Creek volcanics >3000 m Silverquick formation >800 m	
			Cenomanian		
		Early	Albian	Taylor Creek Group >3000 m: Lizard Fm; Elbow-Dash Fm; Paradise Fm	Taylor Creek: Chert pebble conglomerate, black shale, siltstone, feldspathic sandstone, muscovite-rich sandstone
			Aptian		Jackass Mountain Group: Polylithic conglomerate, siltstone, shale and sandstone
		Neocomian	Barremian	Jackass Mountain group >5000 m	
			Hauterivian	Relay Mountain Group ~2250 m	Fossiliferous brown sandstone, siltstone and shale, buchia coquina, minor conglomerate
			Valanginian		
			Berriasian		
	Jurassic	Late			
		Middle	Callovian		
			Bathonian		
			Bajocian	Last Creek Formation > 450 m; Nemaia Formation >3000m	Last Creek: Calcareous sandstone, siltstone, minor conglomerate and tuffs
			Aalenian		
		Early			
	Triassic	Late		Tyaughton Group ~2500 m; Cadwallader Group >3000 m	Tyaughton: conglomerate, limestone, sandstone Cadwallader: siltstone,shale, limestone, conglomerate, mafic volcanics
		Middle			
		Early			
				Bridge River Complex Thickness unknown, at least 400 metres	Bridge River Group: Ribbon chert, argillite, greenstone, serpentinite, blueschist
Paleozoic	Permian				
	Carboniferous	Pennsylvanian			
		Mississippian			
	Devonian				

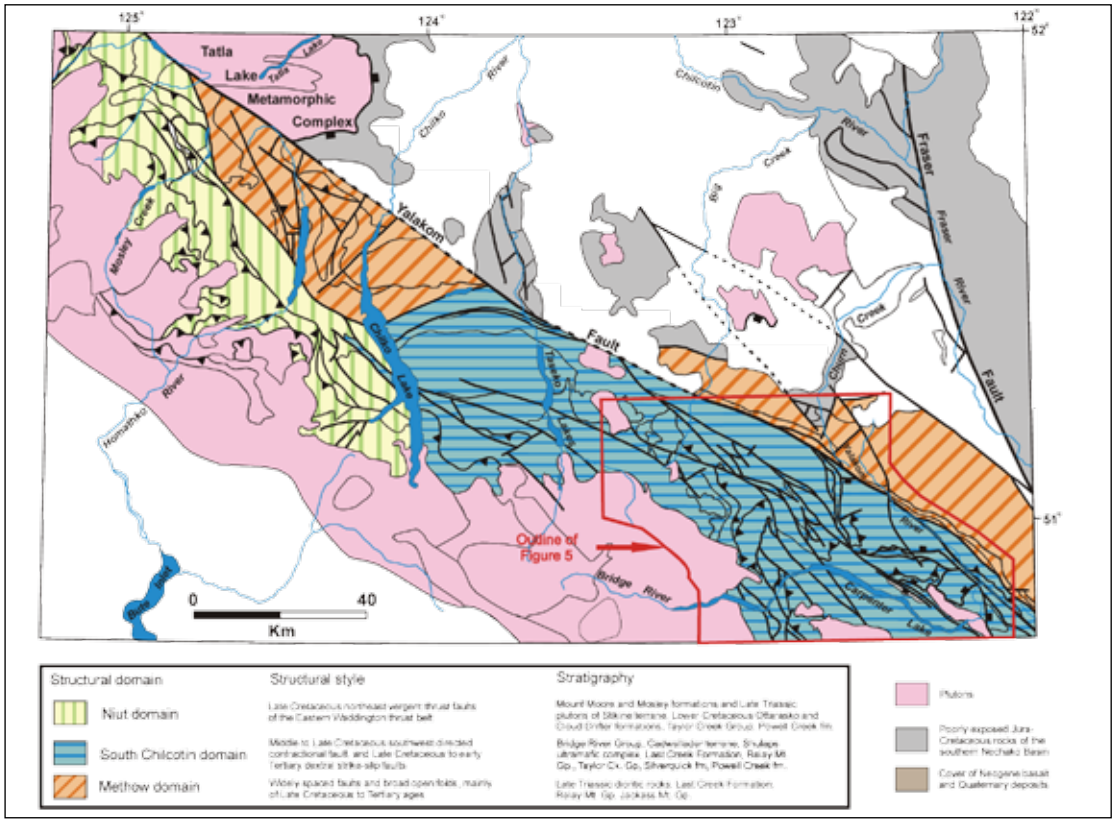

Figure 4. Structural domains of the Chilcotin Mountains (after Schiarizza, 1996).

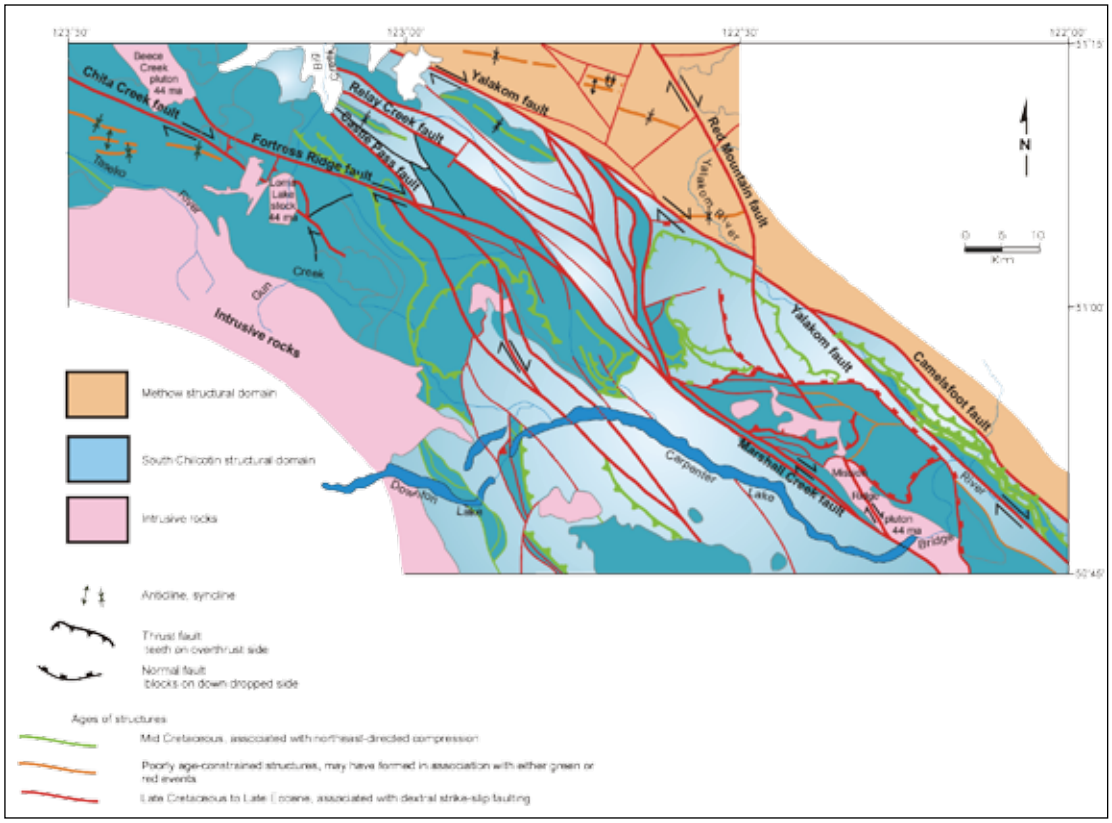

Figure 5. Structural styles in the Methow and South Chilcotin structural domains of the Chilcotin Mountains (after Schiarizza *et al*., 1997).

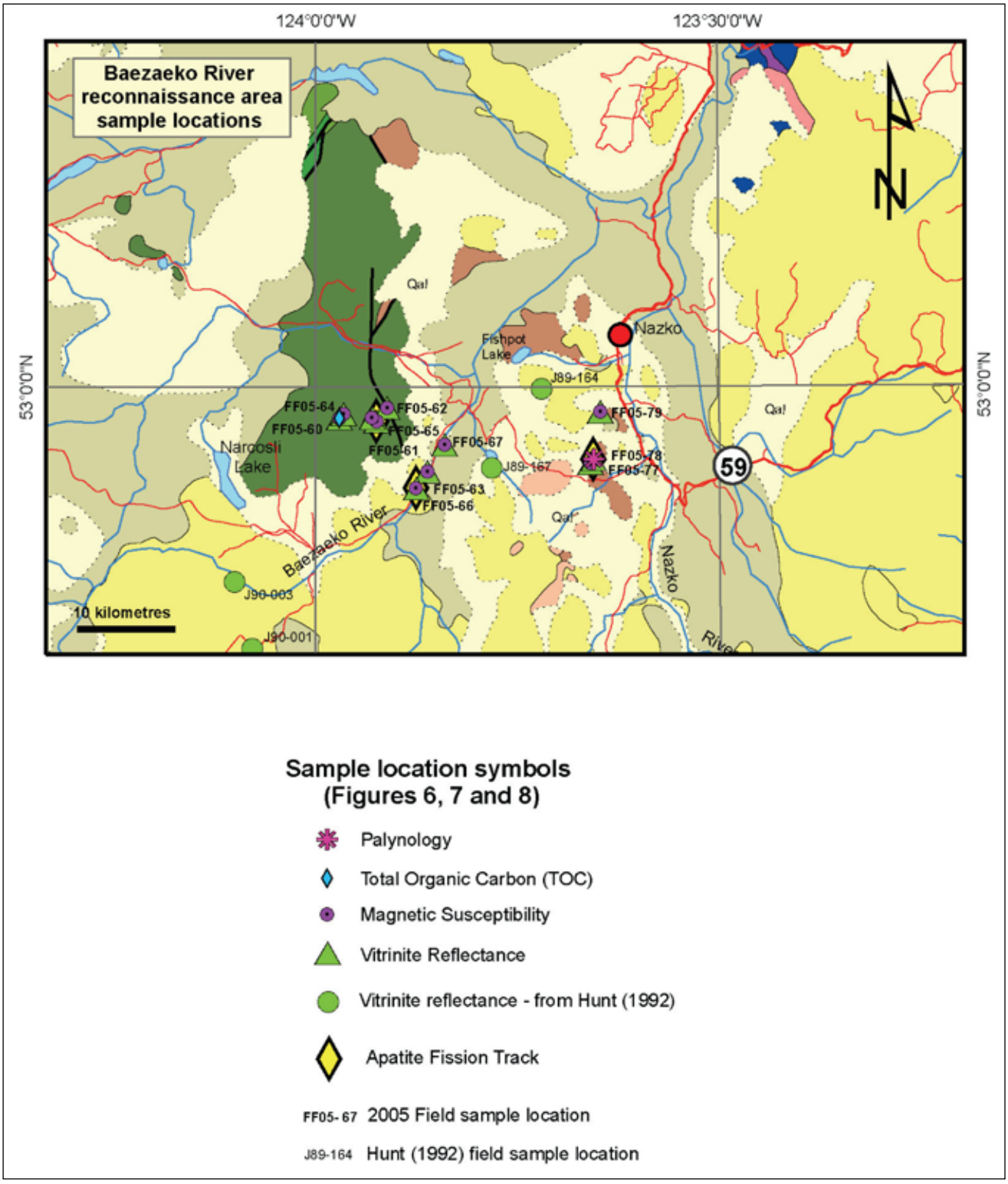

Figure 6. Reconnaissance area and sample locations for Baezaeko River. See Figure 3 for geological colour legend.

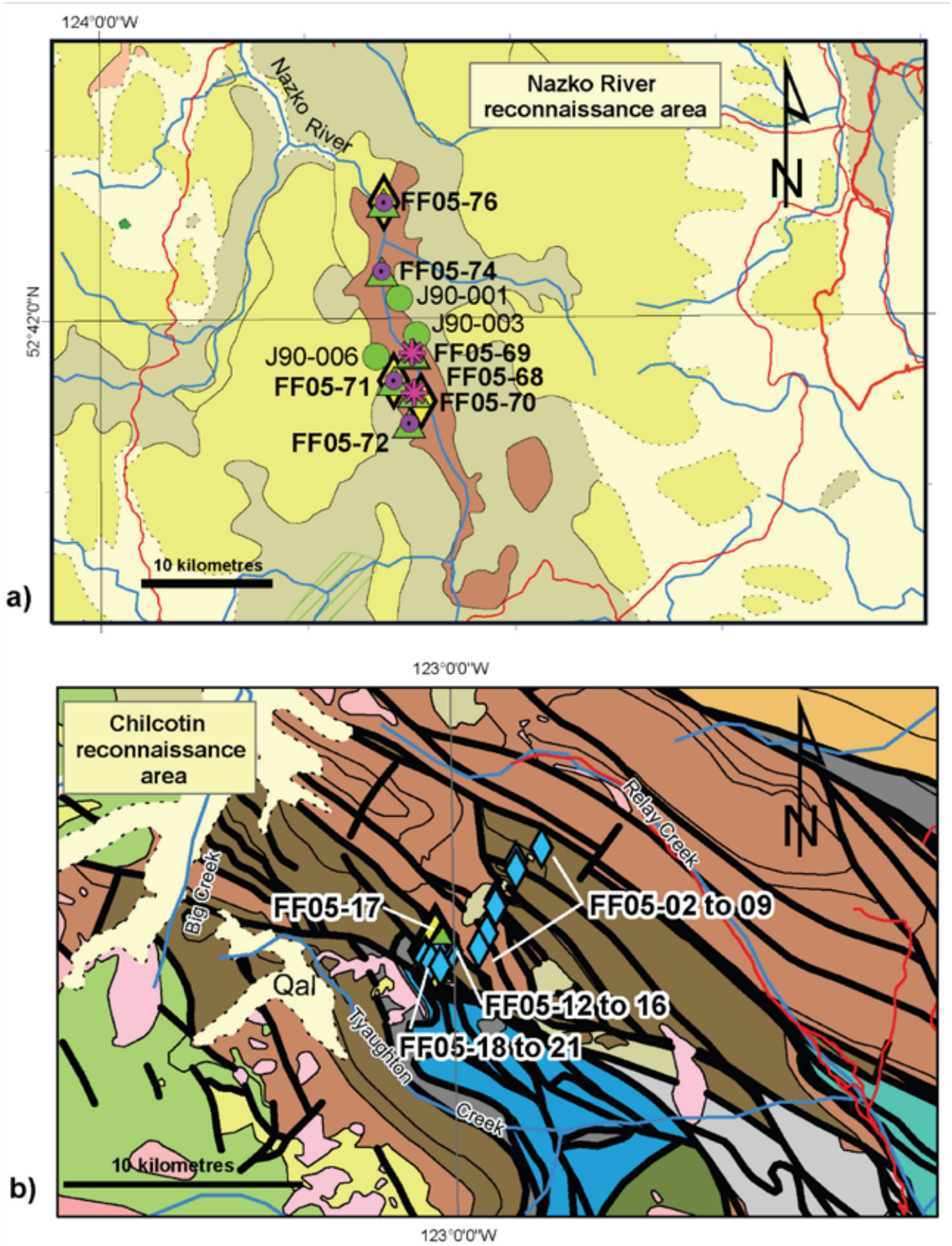

Figure 7. Reconnaissance areas and sample locations for a) Nazko and b) Chilcotin Mountains. Sample symbols are as for Figure 6. Geological colour legend for 7a) is as for Figure 3. Geological colour legend for sampled units for 7b): Light brown – Taylor Creek Group (samples were taken from the Paradise formation); Dark brown – Relay Mountain Group; Grey – Last Creek Formation.

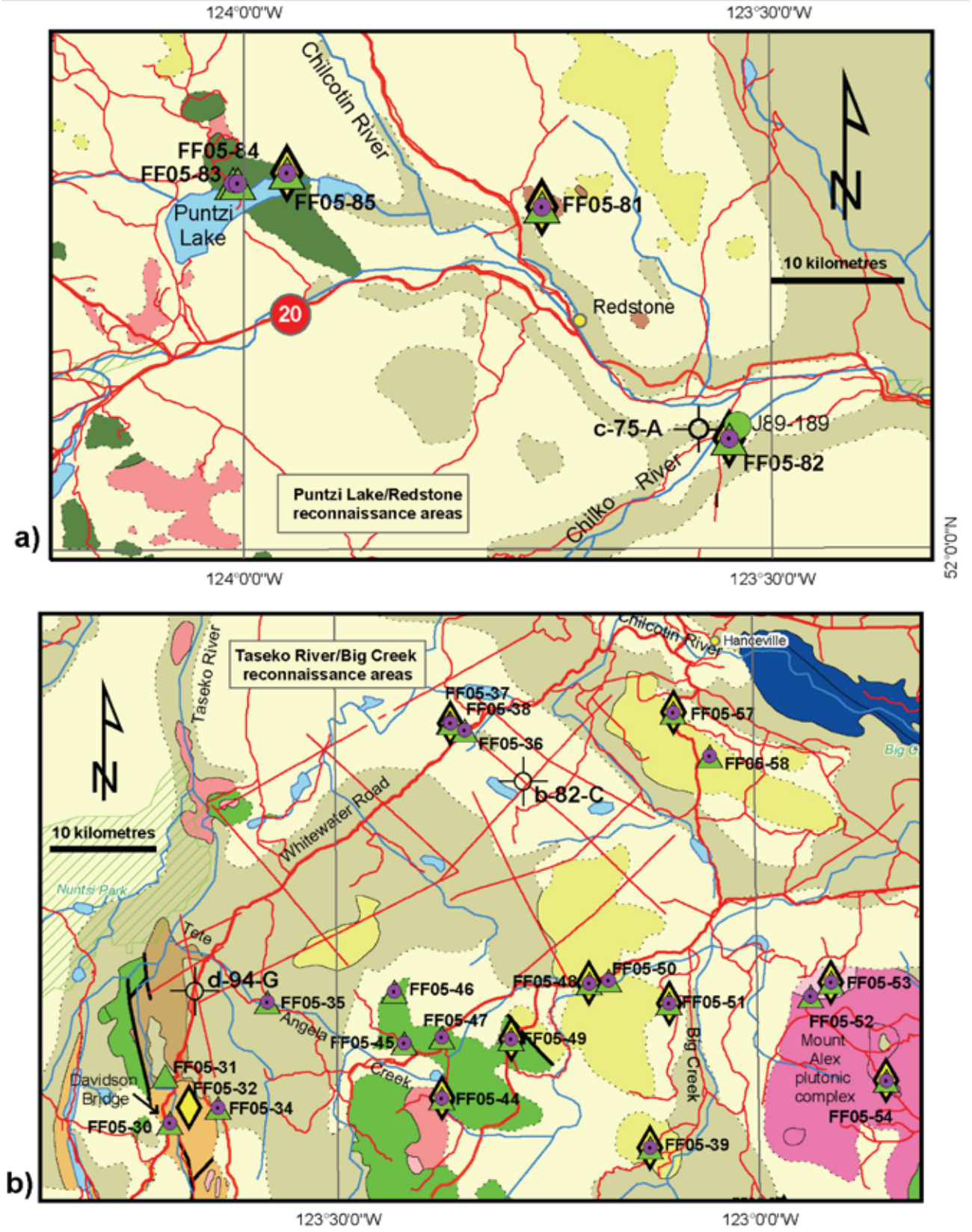

Figure 8. Reconnaissance areas and sample locations for a) Puntzi Lake/Redstone and b) Taseko River/Big Creek. Sample symbols are as for Figure 6.

Creek Group stratigraphy is more complex than is described here and is summarized in Table 1 (see Schiarizza, 1997, and Garver, 1992); lateral facies changes reflect different source terranes in various parts of the syn-tectonic basin and sub-basins.

The formations of the Taylor Creek Group sampled during the 2005 field season are the Aptian to early Albian Paradise Formation and the Albian Dash and Lizard formations. The Paradise formation is exposed on the southern flank of Relay Mountain and comprises about 80% black shale (Garver, 1992); the coarse component is mainly volcanic-rich conglomerate. Three samples of the shale were taken for Rock-Eval analysis to evaluate source rock potential.

The Dash and Lizard formations were examined along a ridge north of North Cinnabar Creek in the Taylor Creek type area. The mid-Albian Dash conglomerate is a chert-rich pebble conglomerate with lesser chert-lithic sandstone that marks the emergence and erosion of the oceanic Bridge River Terrane in Albian time (Garver, 1992). Samples of the Dash formation were collected for thin-section determination of porosity (for reservoir quality determination) and vitrinite reflectance. The middle to upper Albian Lizard Formation is a marine turbiditic sequence mainly composed of muscovite-rich lithic sandstones interbedded with shale. Shale from the North Cinnabar Creek area was sampled for Rock-Eval analysis.

Silverquick Formation

The Silverquick formation is an Albian to Cenomanian unit dominated by non-marine, cross-bedded, chert-rich pebble conglomerate with associated lesser sandstone, siltstone, and shales; redbeds are common in the silty and shaly intervals. Silverquick conglomerates are distinguished from the chert pebble conglomerates of the Taylor Creek Group by their more varied clast content; in addition to chert, they contain abundant sedimentary rock fragments and intermediate volcanics and lesser greenstone, quartz, and dioritic plutonic rocks. This formation is interpreted to have been deposited primarily in a braided fluvial system (Garver, 1989). In its type area, the Silverquick Formation is about 1500 m thick and is deposited on Taylor Creek Group strata on a sharp contact with an unconformity of 10° to 20° (Garver, 1992). Elsewhere, correlative rocks (the Beece Creek succession of Schiarizza 1997) may be gradational with underlying Taylor Creek Group units. The Silverquick conglomerate passes gradationally into overlying Late Cretaceous volcanic rocks of the Powell Creek Formation.

Lillooet Group

The Lillooet Group is age equivalent, at least in part, with the Early to Middle Jurassic Last Creek Formation and its equivalents (Schiarizza, 1997). They are correlated with the Dewdney Creek Formation (the upper part of the Ladner Group) (Mahoney, 1993). They underlie the Jackass Mountain Group near Lillooet and are exposed in the cliffs along Highway 12 between Lillooet and Lytton. There they consist of brown to rusty brown and grey-banded siltstones and shales with lesser sandstones and conglomerates. Finer-grained intervals were sampled for Rock-Eval analysis.

Jackass Mountain Group

The Jackass Mountain Group is a Barremian to early Albian sedimentary sequence that is dominated by sandstone but also contains sections of siltstone and shale, along with the thick and distinctive conglomerates that are its hallmark (Kleinspehn, 1985). The group varies laterally but shows mappable common characteristics over time (Schiarizza *et al.*, 1997). The Jackass Mountain Group is at least 5000 m thick locally. Barremian to Aptian strata are dominantly sandy, and clast types demonstrate a mainly volcanic source; distinctive massive, dark bluish-green volcanic sandstones with abundant plant fossils are common. An abrupt transition from volcanic to plutonic clasts marks the mappable transition into the overlying Albian strata (Schiarizza *et al.*, 1997); these upper units contain abundant cobble to pebble polylithic conglomerates rich in granitoid clasts. This change in clast character is inferred to reflect the late Early Cretaceous uplift of Intermontane Belt source terrain. We examined boulder conglomerates and blue-green sandstones in the rocks along Highway #1 north of Boston Bar.

Barremian to Aptian strata of the Jackass Mountain Group contain significant shaly intervals that may have potential as source rocks; these intervals will be sampled and analyzed in 2006.

RECONNAISSANCE WITHIN THE NECHAKO BASIN

TASEKO RIVER

We examined outcrops along Whitewater Road (adjacent to Taseko River) from Davidson Bridge to Tete Angela Creek (Figure 8b) to better interpret the stratigraphy encountered in the 1985 CanHunter Redstone well (d-94-G/92-O-12). Boulder conglomerate and sandstone of the Jackass Mountain Group are exposed on the east side of the road near Davidson Bridge. A prominent section of volcaniclastic, cross-bedded sandstones are exposed at a big bend in the Taseko River (about 2500 m north of the bridge, where Vick Creek empties into Taseko River); this sec-

tion of rocks has been identified as Silverquick Formation (Hickson, 1993, and subsequent workers) but they do not resemble Silverquick strata (except for the cross-bedding) and are not correlative with any of the formations described above. A hornblende Ar-Ar age of 79.93 +/- 7.41 Ma (or a range from Turonian to Campanian) was obtained from a volcanic clast at the site, implying a depositional age no earlier than Turonian (Maxson, 1996). This is consistent with U-Pb ages as young as ca. 86 Ma obtained from detrital zircons in the upper part of this section by Enkin *et al.* (in press). Clearly the Taseko River strata, as we informally call them, are too young to correlate with the Silverquick conglomerate—they are as young as upper Powell Creek volcanic rocks, whereas the Silverquick underlies the Powell Creek section. These rocks may be correlative with those mapped as Silverquick by Mustard and van der Heyden (1997) on the south side of Highway 20 about 25 kilometres northwest of Tatla Lake; otherwise, correlative rocks have not been recognized. It is unknown whether this unit is widespread in the subsurface to the north or if it is limited in extent.

BIG CREEK

The area around Big Creek, south of Hanceville, is characterized by low relief and scarce outcrop (Figure 8b); most outcrops are found on subdued topographic highs. Andesitic to dacitic flows and breccia occur on topographic highs throughout the area; these have been correlated with the Albian Spences Bridge Group (Hickson, 1993) based on their similarity to volcanic rocks east of the Mount Alex plutonic complex, which returned a U-Pb age of ca. 105 Ma (Albian) (Hickson, 1992). Volcanic and sedimentary rocks of Eocene(?) ages (Hickson, 1993; Tipper, 1978) include quartz-phyric rhyolite, olivine basalt, minor conglomerate, and sandstone and occur on subdued topographic highs. These are broadly similar to and correlated with the Ootsa Lake Group. Large boulders of Chilcotin Formation basalts are common in the Big Creek area; they are not in place but sit on surficial material. The Big Creek area is the locus of a significant gravity low (discussed further below) and most likely a thick sedimentary package, which is of interest to this project for its oil and gas potential. Outcrop exposure is non-existent in the area of the gravity low, so the identity of the sedimentary package (i.e., is it Jura-Cretaceous strata, Tertiary graben fill, or something else?) cannot be established by surface mapping.

REDSTONE AREA

The area around the community of Redstone (Figure 8a) is notable for the striking rim rock of Chilcotin Group plateau basalts on either side of the Chilcotin River valley from 960 to 1035 m elevation. Exposures are scarce below the rim rocks, but a few scattered outcrops of chert-rich pebble conglomerate and associated cherty sandstone resemble the Albian to Cenomanian strata of the Chilcotin Mountains. An outcrop at Gap Narrows bridge over the Chilko River is chert-rich polylithic conglomerate with large (> 1 m) crossbeds. We have tentatively correlated this with the Silverquick Formation, and it is probably the unit at the top of the nearby 1960 well c-75-A/93-B-4. Chert and muscovite sandstones with floating chert pebbles and lesser chert rich pebble to granule conglomerates underlie the westernmost part of the Sisters Hills northeast of the road to Chezacut.

PUNTZI LAKE

Rocks on the north shore of Puntzi Lake (Figure 8a) were mapped as lower Jurassic Hazelton Group by Tipper (1959 and 1969). Outcrops at the east end of the lake resemble Late Cretaceous Powell Creek volcanic rocks. A sample was taken for Ar-Ar radiometric dating to test this correlation. They may also correlate with the hundreds of metres of volcanic rock that were intersected by the exploration well b-22-K/93-C-09.

NAZKO RIVER

Gently dipping sedimentary rocks that resemble strata of the Lizard and Dash Formations of the Cretaceous Taylor Creek Group are exposed along the Nazko River valley and on the hills between Fishpot Lake and the community of Nazko. Tan- to brown-weathering chert- and quartz-rich sandstone with floating chert pebbles is the dominant lithology. Silty and conglomeratic horizons are common, as are carbonaceous coatings on partings. On the west side of the river, near the a-4-L/93-B-11 well site, we encountered muscovite-rich grey sandstone that resembles the Lizard Formation of the Taylor Creek Group. Neogene and Holocene volcanic rocks overlie the Cretaceous rocks in the Nazko River valley. West of Nazko, Taylor Creek correlative rocks sit at higher elevation than the younger volcanics. The Nazko valley likely represents the down-dropped centre of a north-striking graben active in post-Cretaceous, pre-Neogene times.

BAEZAEKO RIVER

Rocks mapped by Tipper (1959) as Hazelton Group underlie the highlands west of the Baezaeko River (Figure 6). Pale to dark grey, rusty-weathering siliceous argillite is the dominant rock type. Locally, argillite is dark grey with a dark bluish weathering colour. These sedimentary rocks are markedly more fractured and rubbly than the Cretaceous rocks. Some feldspar and pyroxene-phyric basalts are present.

GRAVITY DATA AND BASIN STRUCTURE

A Bouguer gravity map covering the southern part of the Nechako Basin is shown in Figure 9. The precursor to this map was produced by Canadian Hunter Exploration Ltd. during its exploration efforts in the Nechako Basin and submitted as part of a geological report (Salt, 1980a, b; 1981a, b; 1982a, b). The original hand-contoured line drawing was digitized by the RDGB. This allowed the production of the coloured and shaded Bouguer anomaly maps shown in Figure 9 and derivative shown in Figure 10. (The original data points from which this diagram was produced can be obtained from ARCIS Geophysical of Calgary, Alberta). The RDGB obtained gravity data along a transect across the north end of the large negative anomaly located in the southern part of Figure 9 (near line 1; Best, 2004a) and Figure 2 (green line marked RDGB Gravity Line 2004) . The new gravity profile obtained by the Branch essentially mimics the Canadian Hunter data, verifying its robustness.

The general coincidence of gravity and magnetic highs (Figure 10) suggests that the gravity highs are the reflection of underlying rocks rich in volcanics and higher-density intrusions and that the gravity lows correspond to less-magnetic sedimentary sequences. This does not preclude the possibility that the gravity lows represent low-density intrusions (i.e., granite) within a denser, dominantly volcanic host rock.

Simple modeling of the two prominent lows (Figures 11 and 12) in the vicinity of wells b-82-C and b-22-K suggests that they are produced by a thick package of sedimentary rocks of average density. The southern anomaly (Figure 11) may be a result of a section of sediments up to 3.5 km thick; the b-82-C well pierces the western margin of this anomaly and intersects up to 1600 m of sedimentary rocks above its termination in an intrusive body. The gross stratigraphy of this well is consistent with the gravity model over this low. The upper 1200 m of this well is probably Tertiary sedimentary material and represents a significant portion of the sedimentary section that is called for by the model.

The second prominent gravity feature (Figure 12) is a cluster of three smaller lows in the vicinity of the b-22-K well. Again, simple modeling of these anomalies suggests that they may represent one or more lenses of sedimentary rocks with a total thickness of up to 2.5 km. The top of this sedimentary sequence would be encountered at a depth of 3 to 4 km, which agrees roughly with the stratigraphy described in the well data from the b-22-K well. Age and lithology of volcanic rocks within the b-22-K well indicate that they belong to the Powell Creek volcanics, suggesting that rocks of the Silverquick conglomerate and Taylor Creek Group may underlie them at depth.

If one assumes that the Bouguer gravity lows represent sedimentary rocks, then the pattern presented in Figure 9 suggests that the configuration of the Nechako Basin is more complicated than a simple trough or depocentre and is probably composed of several smaller basins. The sharp northwest- and northeast-trending patterns southwest of the c-75-A well suggest structural control. The map patterns apparent on Figure 9 may be a reflection of motion on strike-slip faults and associated faults, syn-sedimentary deposition in down-thrown blocks, preservation of older sedimentary sequences, or a combination of these, produced in response to the Late Cretaceous to Paleogene right-lateral strike-slip deformation affecting this part of the Cordillera (and bounding the Nechako Basin).

Surface exposures in the Nazko River valley and results of seismic lines submitted as part of Canadian Hunter Exploration Ltd. work commitments (Focht, 1982a to 1982i) indicate that Jura-Cretaceous strata underlying these parts of the Nechako Basin are generally gently dipping. The Methow domain (described above) is probably the most applicable structural working model for the subsurface in at least the southern half of the Nechako Basin. This model predicts broad open north- to northwest-striking homoclinal folds, cut by steep northwest-striking strike-slip and associated faults at spacings in the order of tens of kilometres.

Data quality for submitted seismic lines is poor due to attenuation of returning seismic energy by surface and subsurface volcanics (Figures 26–28). In addition, most of the seismic lines within submitted reports generally follow the northwest trend of structures associated with Cretaceous shortening, so that the gentle warping seen in some of these sections (e.g., Figure 27) might represent along-strike variations in structural plunge. One line (Figure 28) trends northeasterly and contains a moderately northeastward-dipping series of reflectors. Offset of reflectors within the upper parts of sections in the vicinity of the b-22-K well suggest steep normal faults of Tertiary(?) age. Given the location of the Nechako Basin between the Yalakom and Fraser/Pinchi fault zones, this area was probably affected by extensional tectonics as documented in the central Nechako Basin by Lowe *et al*. (2001) (See also Struik [1993]).

A simple, first-order cross-section through the northern and southern parts of the basin is shown in Figure 25, which is modified from Hannigan *et al.* (1994). It is possible that middle Cretaceous sediments penetrated by the d-96-E and a-4-L wells dip westward and are found stratigraphically below the volcanics penetrated by the b-22-K well. The structural geometry does not require a fault between the two wells, but neither is there evidence to preclude the existence of such a structure.

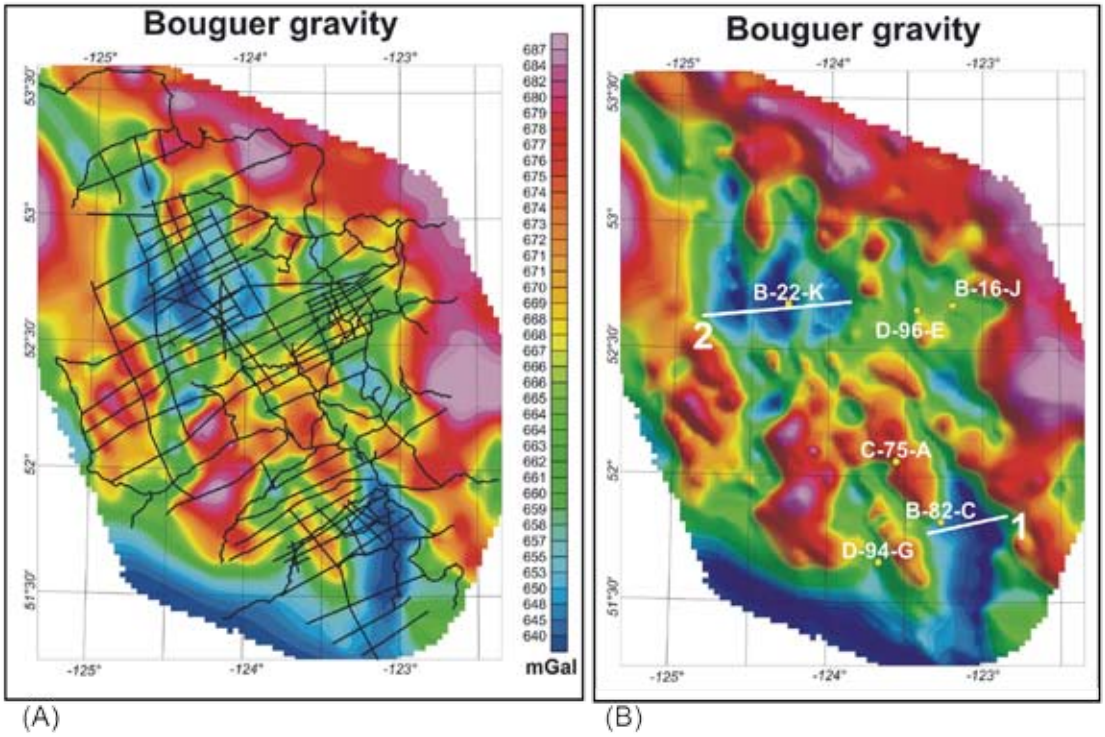

Figure 9. Bouguer gravity map of Canadian Hunter Exploration Ltd. data for the Nechako Basin produced by digitizing hand-contoured line drawing as found in Salt, 1980a,b; 1981a,b; 1982a,b. A) Coloured Bouguer gravity map showing location of data lines. B) Coloured and shaded Bouguer gravity map of the Nechako Basin (Modified from Ferri *et al.*, 2004).

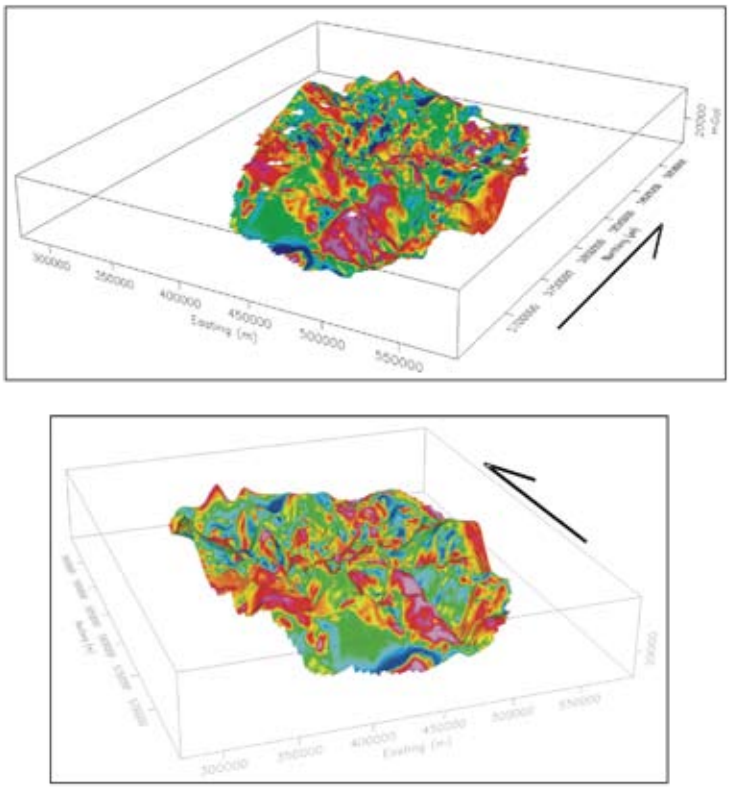

Figure 10. Magnetic field data draped over 3-dimensional rendering of Bouguer gravity map. Note that in general, zones with high magnetic values correspond to gravity highs. (Modified from Ferri *et al.*, 2004).

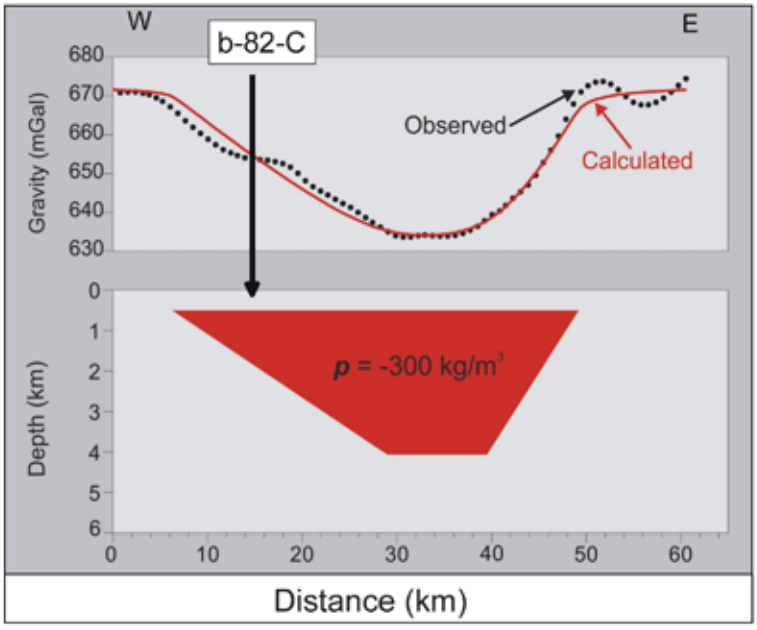

Line 1

Figure 11. A simple modeling exercise for the large southern anomaly through a section across line 1 in Figure A. A simple body with a density contrast of –300 kg/m³ readily satisfies the observed gravity across anomaly 1. As illustrated here, the eastern side of the model body is required to be substantially steeper than western side. Projection of the b-82-C well geology onto the model profile suggests that the negative anomaly is due to buried sedimentary rocks more than 3.5 km thick. The average bulk density of sedimentary rocks encountered in the well is 2580 kg/m3, substantially lower than published mean values for granodiorite (2730 kg/m3) or mafic volcanic rocks (2990 kg/m3) (Modified from Ferri *et al.*, 2004).

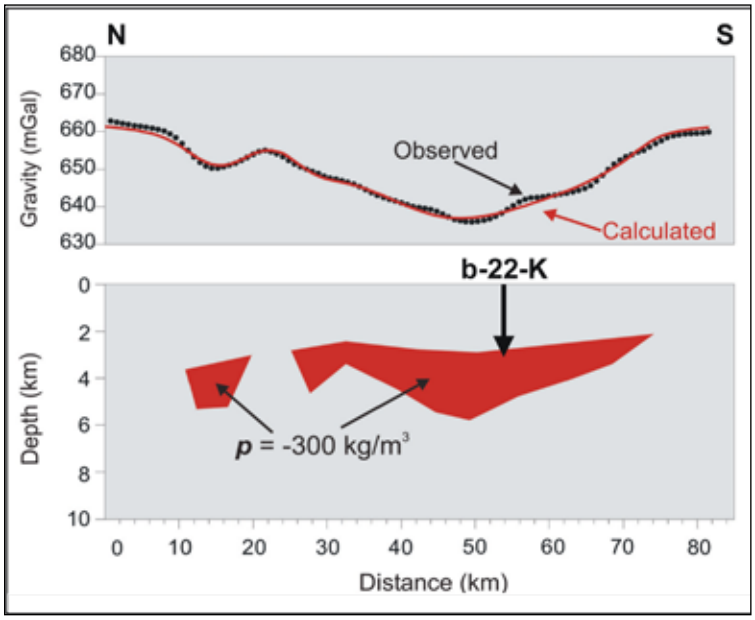

Figure 12. Modeling of the northern anomalies (line 2 in Figure 9) suggests that it can be produced by two simple bodies with a density contrast of –300 kg/m3. In this case, the model bodies can be more than 3 km deeper than that associated with large southern anomaly (Modified from Ferri *et al.*, 2004).

SUBSURFACE STRATIGRAPHY

The variability of the stratigraphic sections penetrated by 8 wells in the southern Nechako Basin suggests a complicated basin architecture and/or structural history for this part of the Nechako Basin. Our current understanding of the subsurface stratigraphy is hampered by a general lack of biostratigraphic control. Only the b-22-K and d-96-E wells have subsurface age constraints based on palynomorph collections (Hunt, 1992). As part of this study, samples from the a-4-L, b-16-J, b-82-C, c-75-A, and d-94-G wells have been collected and processed for palynology. Core samples were also taken from the d-96-E well to augment the current age database. Fifty subsurface samples were acquired, 17 of which were barren. Preliminary results are currently available and will be discussed in the following sections.

Canadian Hunter et al Nazko d-96-E

Palynological dates (Hunt, 1992) from the d-96-E well (Figure 13) provide an age range from Aptian to Cenomanian (late Early to early Late Cretaceous) for sedimentary rocks that occur above a dominantly volcanic sequence. This mafic volcanic sequence (from the 3324 m base to 2950 m) includes minor varicoloured chert, intrusive rocks, and shale and probably belongs to the Cache Creek Group. Above this, between 2950 m and 2490 m, the well logs describe greenish, tight sandstone, dark shale (some bituminous), and siltstone (Cosgrove, 1981a). This green sandstone is feldspathic and contains clasts of volcanic rocks and some chert. The lithology and the Aptian to middle Albian age suggest this section may be equivalent to the lower part of the Jackass Mountain Group. Several sections of cuttings between 2510 and 2520 m and between 2592 and 2615 m contain pieces of igneous rock and limestone intermixed with greenish sandstone and shale; these are suggestive of the polymict boulder and cobble Albian Jackass Mountain conglomerate, which is characterized by abundant intrusive clasts with lesser limestone and volcanic material (Plate A). An alternative correlation for this Aptian to middle Albian section is the Paradise Formation of the Taylor Creek Group, which is time equivalent with the Jackass Mountain Group.

Late Albian to Cenomanian conglomerate, sandstone, siltstone, and shale occur at depths between 2490 m and about 650 m. These rocks are time-equivalent to the Taylor Creek Group (Lizard and Elbow-Dash Formations) and Silverquick Formation. The 'salt and pepper' chert-rich, micaceous sandstones in this sequence contrast with sandstones in the Aptian section in that they are cleaner, lack the green colour, are less feldspathic, and have a higher proportion of chert clasts. They are more typical of sandstones of the Taylor Creek Group and Silverquick conglomerate. Shale and siltstone are most abundant in the sections below 2100 m and between 650 and 950 m depth. A section dominated by chert-pebble conglomerate and sandstone occurs between 1720 and 2060 m. Grey, chert-rich sandstone is the dominant lithology between 960 and 1300 m. The remaining parts of the section comprise dark grey to grey and mauve siltstone and shale punctuated by sections of chert-rich sandstone and conglomerate up to tens of metres thick.

Sedimentary features observed within core are consistent with a marine depositional environment; these include mud drapes and ripple-cross laminations (Plate B). Cored sections of conglomerate and sandstone show clast content to be dominated by well-rounded chert grains with lesser volcanic clasts. Evidence of marine environments occurs in core as shallow as about 700 m. Sandstone and/or conglomerate dominated sections within this interval might represent coarser clastics described within the Lizard and Elbow-Dash Formations of the Taylor Creek Group.

Late Albian to Cenomanian sandstone, conglomerate, and lesser siltstone and shale occur from 650 to 50 m depths; this interval may correlate with the non-marine Silverquick Formation.

Well logs describe Tertiary felsic volcanics in the top 50 m of this drill hole.

Honolulu Nazko a-4-L

The nearby a-4-L well (Figure 14) has gross overall similarities to the d-96-E well, although several coarse clastic sequences have 'shaled-out' to the east, suggesting abrupt lateral variation within these marine and fluvial systems. Direct correlation, particularly with the gamma ray log, is difficult and may reflect the varying amounts of mica and feldspar in the clastics, both of which would affect the response of this instrument by virtue of their high potassium content.

The lowest part of the well is equivalent to the Cache Creek Group and contains diorite in the lowest part (below 10,600 ft [3230 m]) overlain by basalt (?), tuff, chert and shale up to 7790 ft (2375 m). Greenish sandstone, shale and siltstone between 7790 and 6900 ft (2375 and 2100 m) probably correlate with the Jackass Mountain Group or Paradise formation. The succeeding sequence (from 6900 to 50 ft [2100 to 15 m]) is correlated with the Lizard and Elbow-Dash Formations of the Taylor Creek Group. The Albian to Cenomanian conglomerate and (Silverquick?) sandstone at the top of the d-96-E well are absent in the a-4-L well; instead, this stratigraphic interval consists predominantly of shale, some of which has high total organic carbon (TOC) content. Conglomerate and sandstone comprise over 50% of the sequence between 1000 and 750 ft. A thick conglomerate/sandstone section is present between 5300 and 4450 ft (1615 and 1355 m) (Thorsteinsson, *in preparation*; Landreth, 1961).

Canadian Hunter et al Chilcotin b-22-K

The stratigraphy of the b-22-K well (Figure 15), located some 50 km to the west of the d-96-E well, contrasts sharply with those of the a-4-L (Figure 14) and d-96-E (Figure 13) wells. Palynology data from Hunt (1992) together with overall lithologies indicate that this stratigraphy is entirely younger than the sequence within d-96-E (compare Figures 13 and 15). The lowest 1000 m of this well are composed of maroon to greenish hornblende-plagioclase porphyry volcanic rocks resembling the Powell Creek volcanics in lithology and age. Powell Creek volcanic rocks are Cenomanian to Santonian in age and regionally conformably overlie conglomerates of the Silverquick Formation. Succeeding these, between 2700 and 1550 m, are volcanics and reworked volcanics. These are in turn succeeded by approximately 1200 m of greenish claystone, shale, and minor volcanics of Santonian, Campanian, and Maastrichtian ages. The affinity of these immature sediments and volcanics is uncertain, although they are approximately age-equivalent to immature, volcanically derived sediments (herein informally named Taseko River strata) exposed along part of the Taseko River.

The upper part of b-22-K (from 1550 m to surface) contains shale and mafic volcanics of Eocene, Oligocene, and Miocene age. Eocene to Oligocene strata are correlated with the Kamloops Group and younger units (Australian Creek Formation), while uppermost Miocene basalt is correlated with the Chilcotin Group.

The sequence penetrated by b-22-K probably sits stratigraphically above the section in d-96-E, as first shown by Hunt (1992) and Hunt and Bustin (1997). Conceivably, and as suggested by simple modeling of gravity data, underlying sedimentary rocks belonging to the Silverquick Formation and Taylor Creek Group are producing the large gravity anomaly below b-22-K.

Canadian Hunter Esso Nazko b-16-J

Volcanic rocks dominate the stratigraphy in this well (Figure 16), located only 15 km east of d-96-E. A sedimentary sequence in its central part is probably Tertiary in age. No stratigraphic control is available for this well; palynology samples taken from the sedimentary sequence were barren.

The basal 300 m of the well (2700 to 2395 m) are composed of basalt, probably part of the Cache Creek Group; this is overlain by approximately 700 m of light- to dark-coloured tuff and minor mafic lava. The lower 80 m of this tuffaceous succession contain shale, claystone, and sandstone intervals (Thorsteinsson, *in preparation*; Cosgrove, 1986a). Sample descriptions suggest that this tuffaceous sequence is interbedded with overlying sandstone and conglomerate of Tertiary(?) age over an interval of some 70 m. The affinity of these overlying tuffs and minor sediments is uncertain; if they truly are interbedded with the overlying sedimentary sequence, then they conceivably are Tertiary in age. The tuffs are light in colour and lack cherty lithologies, which is typical of local Tertiary rocks, but not of the Cache Creek Group.

Maroon, grey, and green polymict conglomerate, sandstone, siltstone, and lesser shale form a monotonous sequence from 1682 to 517 m (Figure 16); subrounded clasts are composed of mafic to intermediate volcanics and varicoloured chert (Plate C). These sediments appear poorly consolidated based on the caliper log, core samples, and well site descriptions. The lack of consolidation suggests a relatively young age. This sedimentary sequence bears little resemblance to rocks of the Taylor Creek Group or Silverquick Formation, suggesting they are younger and probably stratigraphically above the Powell Creek volcanics. They are found below a thick section of mafic to intermediate volcanics in the upper part of the well, which likely are subsurface continuations of the Endako Group mapped at surface. This position between the top of the Powell Creek volcanics and base of the Ootsa Lake Group would bracket this sedimentary sequence within the late Campanian to Eocene.

Canadian Hunter et al Redstone b-82-C

This well (Figure 17) intersected granite to granodiorite at a depth of 1625 m and was abandoned at 1670 m in these intrusive rocks. The upper 20 m of the igneous section has been interpreted to consist of reworked igneous material, suggesting an unconformity between Cretaceous sediments and the intrusive body (Cosgrove, 1981b). The absence of anomalous maturation values (T_{max} and R_o) that would be expected at an intrusive contact is consistent with the interpretation of this boundary as a nonconformity.

Up to a depth of approximately 1275 m, the lithologies comprise dark grey shale (some of which is bituminous and produced higher gas readings on the mud log; Cosgrove, 1981b) and interbedded 'salt and pepper' chert sandstones and conglomerate (Figure 17). The latter are generally much cleaner than overlying coarse clastics above 1275 m and indicate marine depositional environments (Plate D). The general character of these rocks is very similar to those of the Taylor Creek Group. This is supported by preliminary identification of palynomorphs indicating a middle Cretaceous age (A. Sweet, personal communication, 2006).

The section between 1275 and 220 m is a fairly monotonous section of poorly consolidated maroon to green or grey sandstone, polymict conglomerate, siltstone, and shale. Clearly an unconformity exists at the bottom of this section (1275 m). Conglomerate and sandstone are poorly sorted and contain abundant finer matrix material. Conglomerate is composed of sub-angular to well-rounded varicoloured volcanic, chert, and siltstone clasts. The basal part of this section contains a tuffaceous bed some 10 or 15 m thick

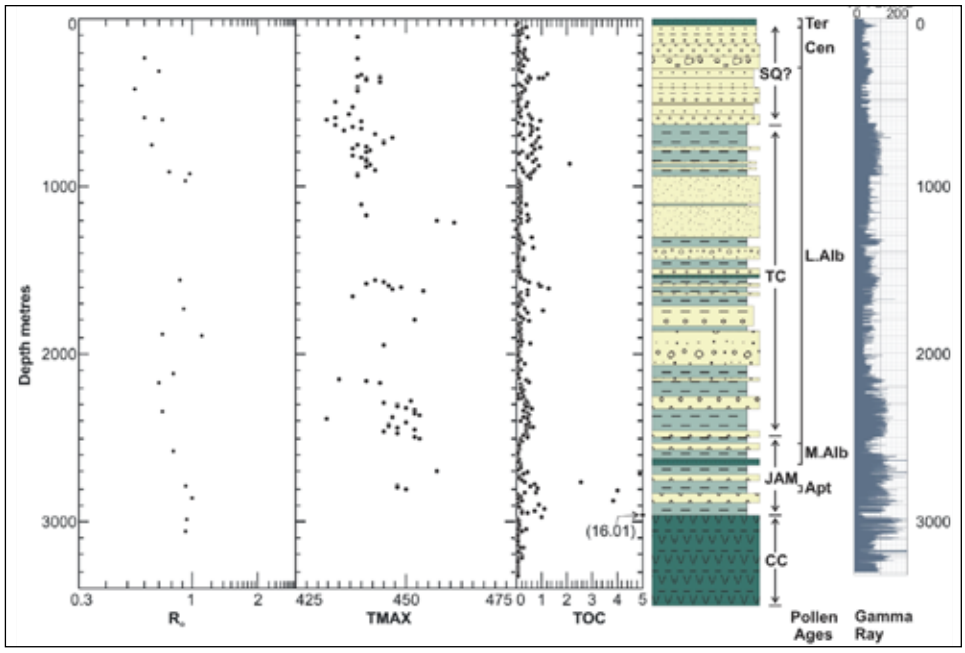

Figure 13. Simplified stratigraphic column of the Canadian Hunter et al Nazko d-96-E well plotted with the natural gamma ray log, total organic carbon (TOC), T_{max}, and vitrinite reflectance values. Only T_{max} values where TOC > 0.3% were plotted. Stratigraphic column is a simplification of descriptions by Thorsteinsson (*in preparation*) and Cosgrove (1981a). Organic geochemistry is taken from Osadetz *et al.* (2003). CC: Cache Creek Group; JAM: Jackass Mountain Group; TC: Taylor Creek Group; SQ: Silverquick Formation; M.Alb: Middle Albian; L.Alb: Late Albian; Cen: Cenomanian; Ter: Tertiary.

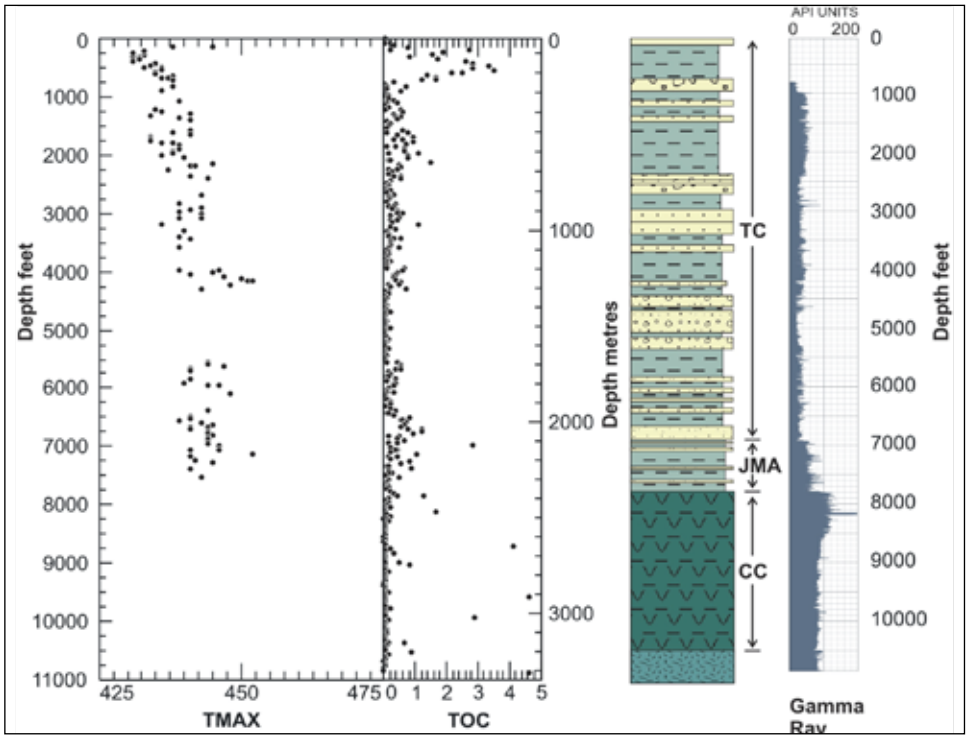

Figure 14. Simplified stratigraphic column of the Honolulu Nazko a-4-L well plotted with the natural gamma ray log, total organic carbon (TOC), T_{max}, and vitrinite reflectance values. Only T_{max} values where TOC > 0.3% were plotted. Stratigraphic column is a simplification of descriptions by Thorsteinsson (*in preparation*) and Landreth (1961). Organic geochemistry is taken from Osadetz *et al.* (2003). CC: Cache Creek Group; JAM: Jackass Mountain Group; TC: Taylor Creek Group.

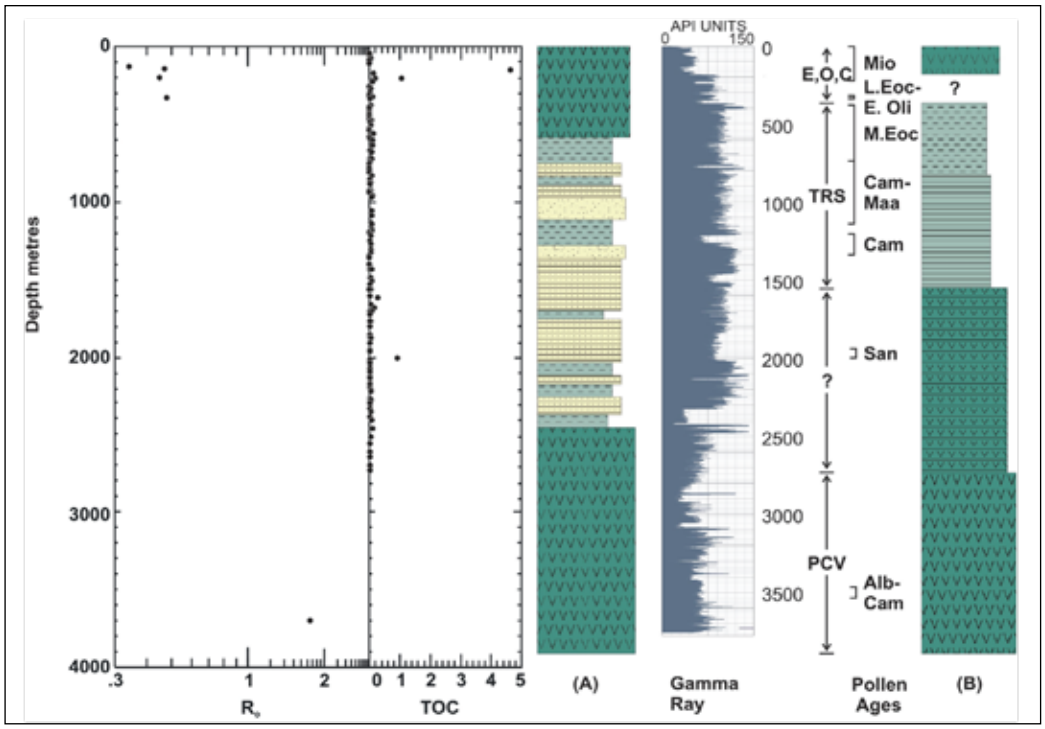

Figure 15. Simplified stratigraphic column of the Canadian Hunter et al Chilcotin b-22-K well plotted with the natural gamma ray log, total organic carbon (TOC), and vitrinite reflectance values. Stratigraphic columns are a simplification of descriptions by (A) Hunt (1992) and (B) Thorsteinsson (*in preparation*) and Cosgrove (1982). Organic geochemistry is taken from Hunt (1992). PCV: Powell Creek volcanics; TRS: Taseko River strata; E: Endako Group; O: Ootsa Lake Group; C: Chilcotin Group; Alb: Albian; Cam: Campanian; M. Eoc: Middle Eocene; L. Eoc: Late Eocene; Mio: Miocene; E.Oli: Early Oligocene; Maa: Maastrichtian.

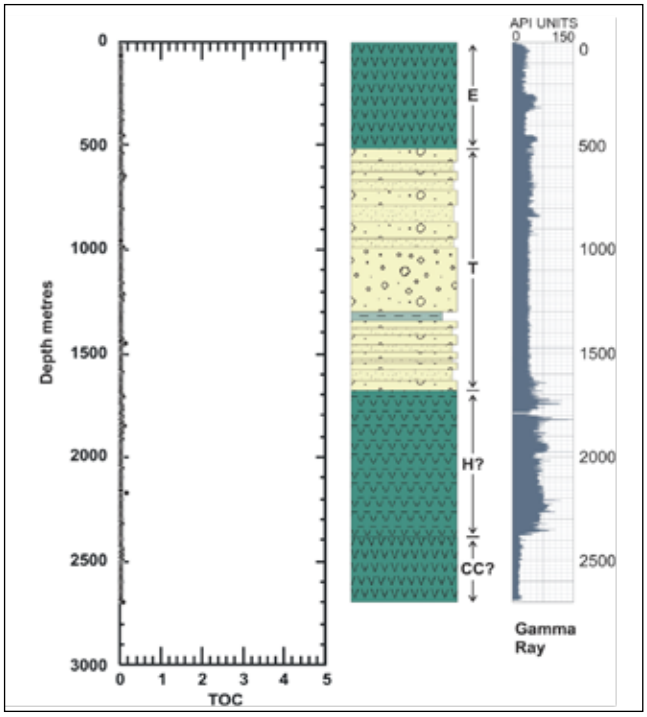

Figure 16. Simplified stratigraphic column of the Canadian Hunter Esso Nazko b-16-J well plotted with the natural gamma ray log and total organic carbon (TOC). Stratigraphic column is a simplification of descriptions by Thorsteinsson (*in preparation*) and Cosgrove (1986a). Organic geochemistry is taken from Osadetz *et al.* (2003). CC: Cache Creek Group; H: Hazelton Group; Ter: Tertiary; E: Endako Group.

Plate A. (A) Typical section of Jackass Mountain conglomerate near the Taseko River in 92-O-12/F showing the coarse nature of conglomerate. (B) Jackass Mountain conglomerate along the Trans Canada Highway, south of Lytton. Note the abundant intrusive clasts, some of which are up to boulder in size. Limestone clasts can constitute a significant proportion of clast types.

Plate B. (A) Mud drapes and ripple cross-laminations from the 959 m depth of the d-96-E well. These features suggest a tidal marine depositional environment. Similar cross-laminations are seen at the 595 m depth. (B) Ripple cross-laminations and fine mud laminations from the 1551 m depth of the d-96-E well, suggesting a marine depositional environment.

Plate C. Possible Tertiary-aged maroon conglomerate (A) and sandstone and siltstone (B) within the b-16-J well, from depths of approximately 1271 and 1273 m, respectively. Note the abundance of volcanic clasts in the conglomerate.

(Cosgrove, 1981b) as well as organic-rich horizons (Figure 17). This sequence is very similar to the sedimentary section of the b-16-J well to the north, suggesting that it also is Tertiary in age. Furthermore, the well was drilled on the edge of the large gravity low (Figure 9) suggesting that this anomaly may be a reflection of a thick section of Tertiary sedimentary rocks. Palynology samples were taken within this sequence, but all were barren.

The top 220 m of the b-82-C well penetrated mafic flows and tuff, all of which fit general descriptions of the nearby outcropping Endako Group.

Hudson's Bay Redstone c-75-A

This well was spudded just northwest of a small window of sedimentary rocks exposed at the Gap Narrows bridge across the Chilko River. The outcrops display varicoloured chert-pebble conglomerate, sandstone, and minor siltstone with large cross-sets, suggesting a fluvial environment and possible correlation with the Silverquick Formation.

The base of the section (Figure 18) is dominated by dark-grey to grey shale, dark red siltstone, and lesser sandstone. Dark red siltstone resembles red to maroon siltstone seen in the d-96-E and a-4-L wells. These lithologies are punctuated by sections of chert sandstone similar to those seen higher in the well. These occur at depths near the 4000 ft (1220 m) mark, from 3330 to 3050 ft (1015 to 930 m), and between 2880 and 2580 ft (880 and 785 m).

A tuffaceous section with interbedded chert (greenish to 'salt and pepper') sandstone and grey to dark shale comprises much of the section between 370 and 2070 ft (113 and 630 m); sandstone is feldspathic and grains are subrounded (Well Report 630). Several horizons of varicoloured chert pebble conglomerate occur in the section.

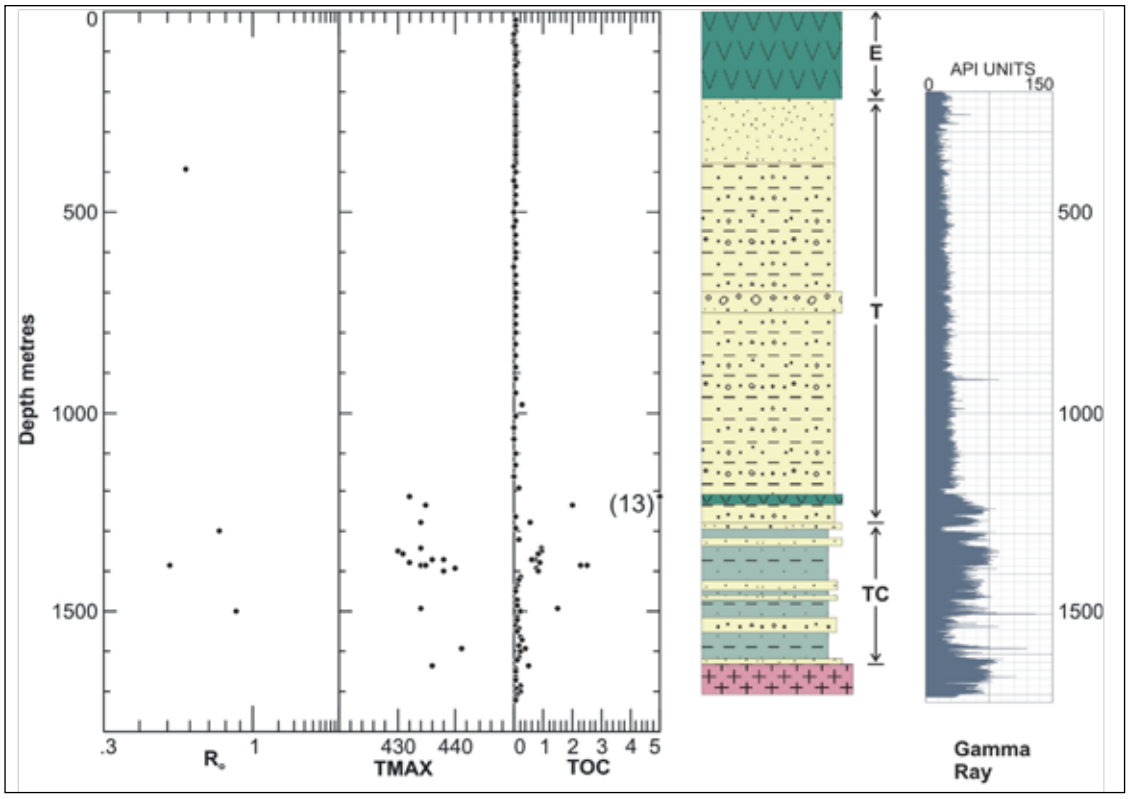

Figure 17. Simplified stratigraphic column of the Canadian Hunter et al. Redstone b-82-C well plotted with the natural gamma ray log, total organic carbon (TOC), T_{max}, and vitrinite reflectance values. Only T_{max} values where TOC > 0.3% were plotted. Stratigraphic column is a simplification of descriptions by Thorsteinsson (*in preparation*) and Cosgrove (1981b). Organic geochemistry is taken from Osadetz *et al.* (2003). TC: Taylor Creek Group; Ter: Tertiary; E: Endako Group.

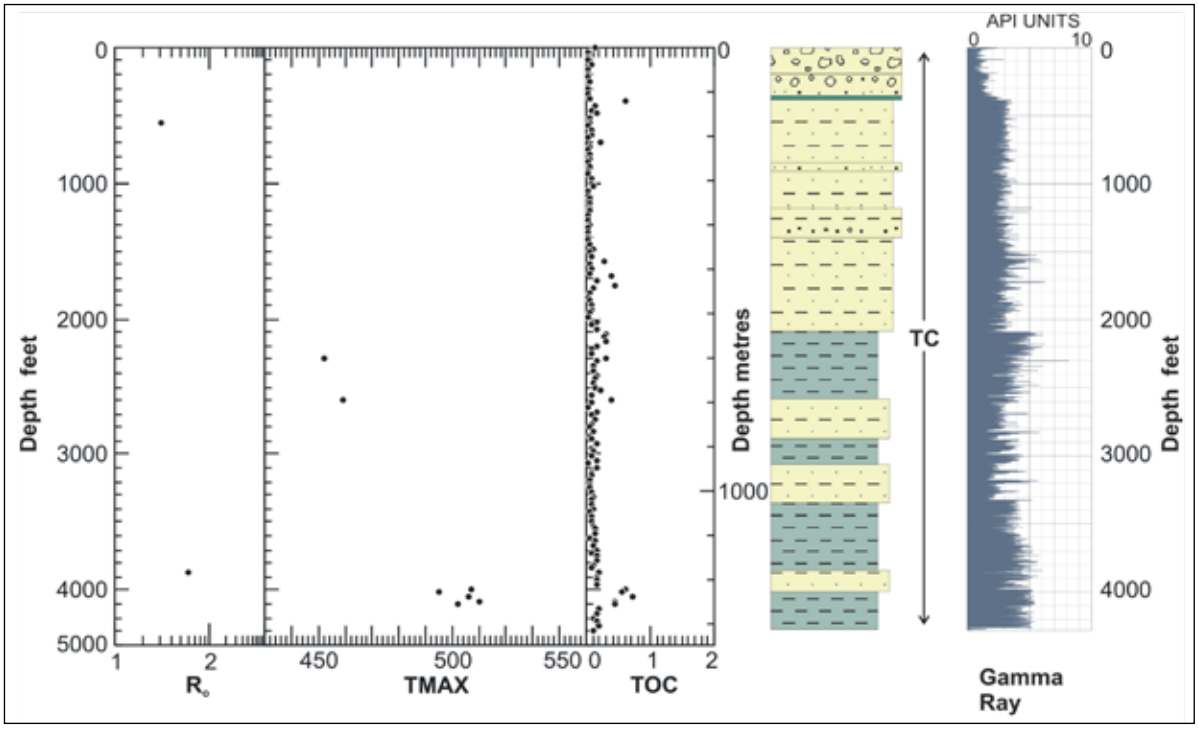

Figure 18. Simplified stratigraphic column of the Hudson's Bay Oil and Gas Company Redstone c-75-A well plotted with the natural gamma ray log, total organic carbon (TOC), T_{max}, and vitrinite reflectance values. Only T_{max} values where TOC > 0.3% were plotted. Stratigraphic column is a simplification of descriptions by Thorsteinsson (*in preparation*) and Well File 630. Organic geochemistry is taken from Osadetz *et al.* (2003). TC: Taylor Creek Group.

Plate D. Finely interbedded chert sandstone, dark grey shale, and siltstone from the 1295 m depth of the b-82-C well. Note the flaser bedding, flame structures, and associated dewatering features. Faint ripple cross-laminations are present locally. These features suggest marine depositional environments.

The lithologies in the top 300 ft (90 m) of the well resemble those in the surface exposures at Gap Narrows bridge. Although the surface exposures share some similarities with the Silverquick Formation, the abundance of dark grey to grey shale, maroon siltstone, together with chert sandstones, suggest that they are part of the Taylor Creek Group. This is supported by preliminary palynology results from core indicating a middle Cretaceous or younger age (A. Sweet, personal communication, 2006); additional palynology collections will be taken from cuttings. If rocks in this well are part of the Taylor Creek Group, the higher thermal maturity values suggest either deeper burial or the effects of a nearby intrusion.

Canhunter et al Redstone d-94-G

This sequence (Figure 19) of thinly to thickly interbedded immature sandstone, shale, and siltstone is unique among all the sections drilled in the southern Nechako Basin. Cutting descriptions indicate a fairly homogenous interbedded succession with local dominance of sandstone, siltstone, or shale. Sandstone is grey to greenish and tends to be immature with abundant sub-angular feldspar, mafic volcanic, mafic mineral, mica, and varicoloured chert clasts (Cosgrove, 1986b). The intra-clast, authigenic clay and chlorite reflect the abundant volcanic detritus. Shale and siltstone are grey-green to dark grey and commonly silty. Carbonaceous horizons are present from 1050 to 950 m and 550 to 450 m, corresponding to increased TOC and gas levels in the mud log (Figure 19; Cosgrove, 1986b).

Volcanic rocks occur from 1976 m to the bottom at 2165 m. These are varicoloured feldspar and hornblende(?)-bearing and of an intermediate to felsic(?) nature (Cosgrove, 1986b). Of locally exposed volcanic successions, these rocks most closely resemble the early Albian to Santonian (late Early to Late Cretaceous) Spences Bridge Group.

This well was spudded in surface rocks tentatively assigned to the informally named Taseko River strata. Although the bulk of the well section is much finer-grained than its surface exposure, the immature, arkosic to lithic nature of the sandstone within the well bears some similarities to sandstone of the Taseko River strata. Sandstone that most likely correlates with surface exposures of the Taseko River strata dominates the upper 80 m of the hole. Thermal maturation levels for this well are the highest observed for any of the wells in the Nechako Basin area (R_o from 0.9 to 1.5). Maturation data from nearby surface exposures of the Taseko River strata (R_o 1.2) fall within this range.

Preliminary age determinations based on palynomorphs extracted from well cuttings suggest a middle Cretaceous or younger age, although rocks below 684 m may be older (A. Sweet, personal communication, 2006). Taseko River strata are thought to be Coniacian (Late Cretaceous) and younger.

Vieco Texacal Punchaw c-38-J

The most northerly well, the Punchaw c-38-J, was spudded in Quaternary gravels and penetrated a thin section of poorly consolidated Tertiary or Quaternary polymict (volcanic, limestone, and sedimentary) conglomerate and sandstone. At about 200 m the drill intersected sedimentary, volcanic, and igneous rocks of the Cache Creek Group (Ramsay, 1972).

SOURCE ROCK POTENTIAL AND THERMAL MATURATION

The presence of a viable source rock is the foundation of any petroleum system, and its recognition is one of the keystones in building a new petroleum province such as the Nechako Basin. To this end, the RDGB sampled and closely examined prospective strata for source rock potential. Further sampling is planned for the 2006 field season.

HYDROCARBON SEEPS AND OIL STAINING

Early in the exploration history of the Nechako Basin, indications of source rock potential were afforded by local reports of surface oil and gas seeps, many of which could not be substantiated (Hannigan *et al.*, 1994; Taylor, 1961; Perry and Bullock, 1960). Tar or asphalt was reported in the vicinity of Batnuni Lake by Tipper (1963). This locality occurs at the north end of the belt of Cretaceous strata penetrated by the d-96-E and a-4-L wells, some 70 km north-northwest of the well sites. Koch (1973) questioned the authenticity of these occurrences, citing subsequent investigations by petroleum geologists that suggest they represent recent organic material or iron-oxide deposits.

Live and dead oil staining and gas shows in drill stem tests (DSTs) were encountered over several intervals in the a-4-L and d-96-E wells (Cosgrove, 1981a). In addition, a DST in well b-82-C contained possible gas (Cosgrove, 1981b). Dead oil staining, bitumen, and bituminous shale are present in well d-94-G (Cosgrove, 1986b).

As part of a more comprehensive and robust determination of thermal maturation in the subsurface, numerous cutting and core samples were obtained for vitrinite reflectance determination (Table 4). During standard petrographic work on samples of core from well d-96-E, oil was noted as inclusions within calcite crystals and carbonaceous material and as intragranular stains (L. Stasiuk, personal communication 2006). These were seen at depths of 418, 590.5, 913, 920, 1554, 1727, 1884, and 1894 m within well d-96-E. Oil has been extracted from samples at these intervals and preliminary gas chromatograph data were obtained, although no interpretation was available when this report was published.

In addition, recent Rock-Eval analysis of cuttings from several of the wells has indicated high S_1 values from samples with high organic carbon contents (see Osadetz *et al.*, 2003). The S_1 peak is a reflection of free hydrocarbons within the sample, suggesting either the presence of unmigrated oil produced in situ by this shale (Lafargue *et al.*, 1998) or contamination from drilling fluids (e.g., diesel). T_{max} values from these samples were much lower than expected, given the maturity levels determined by vitrinite reflectance and the higher T_{max} values in adjacent strata. This 'suppression' of T_{max} values may be a result of oil staining in the sample (L. Stasiuk, personal communication, 2006). Petrological studies are underway to determine the reasons for the high vitrinite reflectance and corresponding low T_{max} values. Any formation oil that is present will be extracted and analysed. Samples taken for further analysis are from wells (and subsurface depths) d-96-E (1740, 2710, and 2960 m); a-4-L (6980, 8700, 9930 ft); b-82-C (1208, 1380, 1383 m); and c-75-A (1690 m). Preliminary analysis of cuttings from the 27 010 and 2960 m level of the d-96-E suggests that some of the material analysed was organic material of recent origin (i.e., drilling additives). Further work is being performed to verify this. Oil inclusions were observed in samples from the 1740 m level of d-96-E and c-75-A and 1383 and 1380 m of b-82-C. An attempt will be made to extract these oils and characterize them.

SOURCE ROCK POTENTIAL

Julie Hunt performed Rock-Eval analysis of subsurface and surface samples from the southern Nechako Basin as part of her M.Sc. thesis at the University of British Columbia (Hunt, 1992; Hunt and Bustin, 1997). This preliminary work indicated that, in this region, subsurface samples produced T_{max} values bracketing the oil to upper gas windows. No thick, high quality source rock was recognized within the wells or at surface exposures. This work also indicated that the kerogen within the sedimentary sequences was dominantly of Type II to Type III affinities, suggesting that any potential hydrocarbon accumulations would be dominantly gas.

A more systematic Rock-Eval analysis of subsurface cuttings was undertaken by the Geological Survey of Canada as part of a cooperative program with the RDGB (Osadetz *et al.*, 2003). Some of these new data are shown in Figures 20 to 24. In general, the new data are very similar to those obtained by Hunt (1992); kerogen is of Type II to Type III. However there are indications of Type I to Type II material within several horizons of wells d-96-E, a-4-L, and b-82-C.

Another outcome of this recent Rock-Eval analysis was the recognition of several organic-rich horizons in the lower part of the d-96-E well, between 2700 and 3000 m, which were not sampled by Hunt (Figures 13 and 20). The original well-site geologist noted bituminous shales with source rock potential within this interval (Cosgrove, 1981a); in addition, the mud log showed increases in C1 and C2 hydrocarbons over this zone. Data points from these horizons are shown as black squares on Figure 20. Organic-rich shales within similar horizons from the nearby a-4-L well are also shown as black squares on Figure 21. Plots of TOC versus S_2 (Figures 20b and 21b) indicate HI (hydrogen index) values of approximately 350 and 700 mg HC/g TOC for samples from these horizons. Although this is encouraging, analysis of cuttings from some of these horizons (see above) suggests that the high TOC values may reflect analysis of recent organic material, which may have been added to the well to facilitate drilling. Further work will be performed to correctly characterize these bituminous shales.

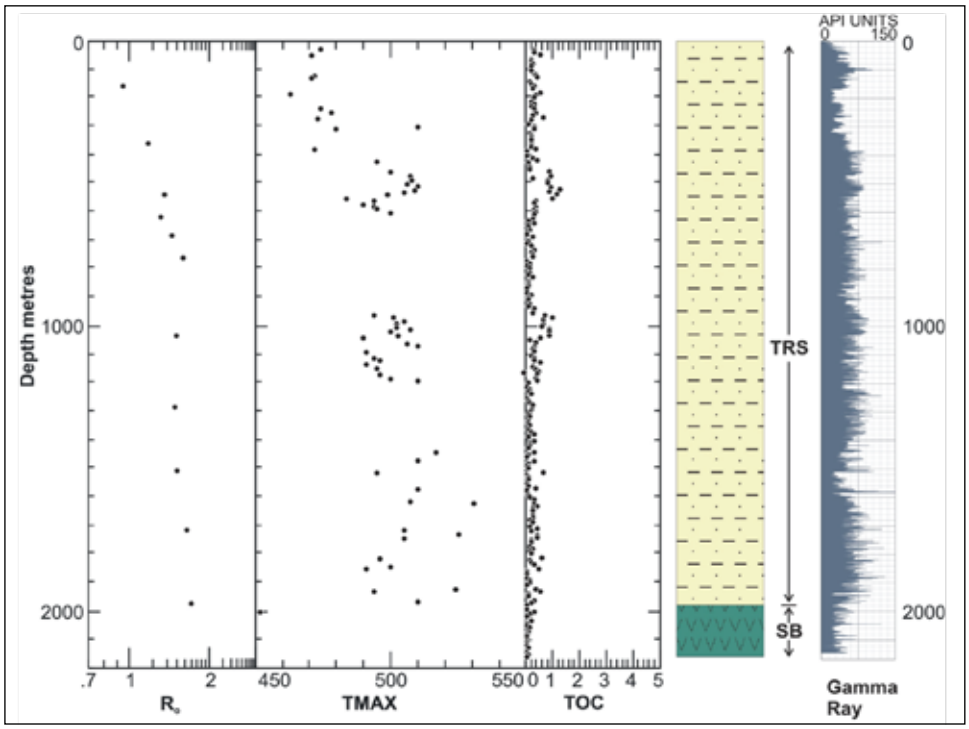

Figure 19. Simplified stratigraphic column of the Canadian Hunter et al Redstone d-94-G well plotted with the natural gamma ray log, total organic carbon (TOC), T_{max}, and vitrinite reflectance values. Only T_{max} values where TOC > 0.3% were plotted. Stratigraphic column is a simplification of descriptions by Thorsteinsson (*in preparation*) and Cosgrove (1986b). Organic geochemistry is taken from Osadetz *et al.* (2003). SB: Spences Bridge Group; TRS: Taseko River strata.

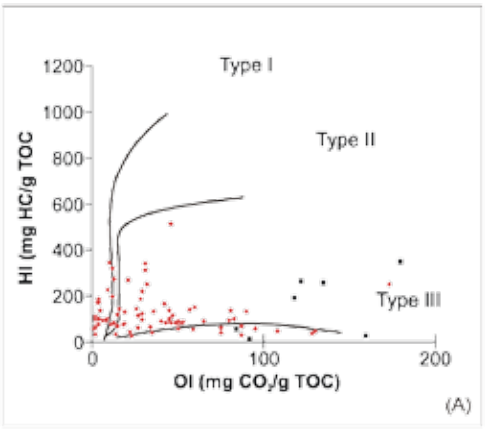

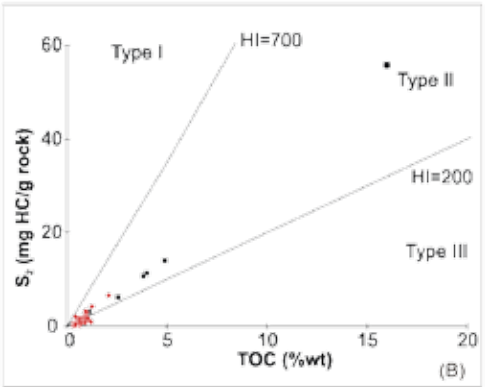

Figure 20. Graphs of Rock-Eval data of kerogen from the d-96-E well. (a) HI (hydrogen index) *versus* OI (oxygen index) diagram. (b) S_2 *versus* TOC (total organic carbon) diagram. Data points from Osadetz *et al.* (2003). Only data with TOC > 0.3% plotted. Black squares represent data from 2700 m to total depth.

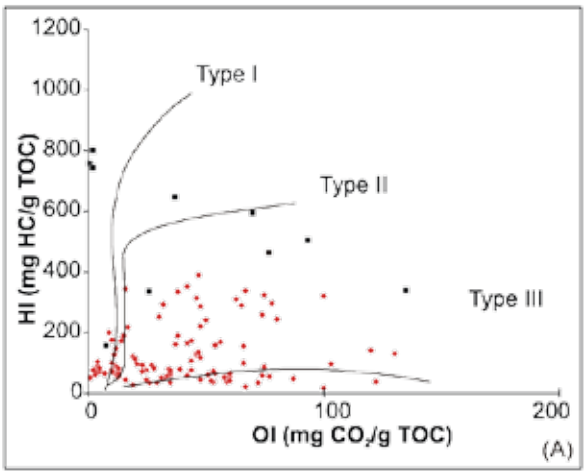

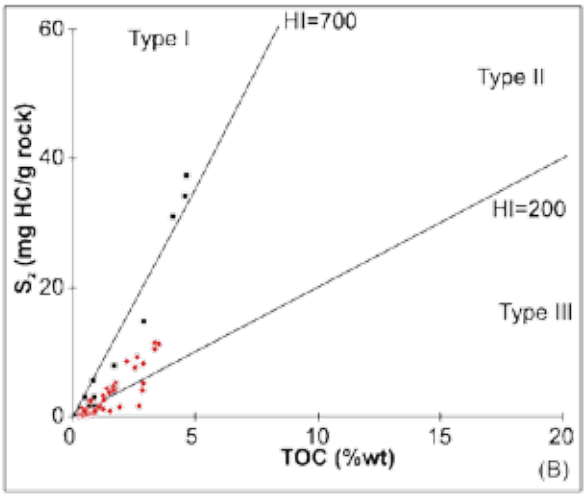

Figure 21. Graphs of Rock-Eval data of kerogen from the a-4-L well. (a) HI (hydrogen index) *versus* OI (oxygen index) diagram. (b) S_2 *versus* TOC (total organic carbon) diagram. Data points from Osadetz *et al.* (2003). Only data with TOC > 0.3% plotted. Black squares represent data from 8135 ft (2480 m) to total depth.

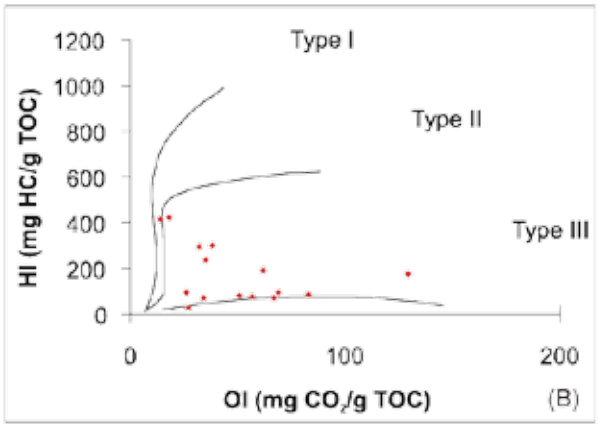

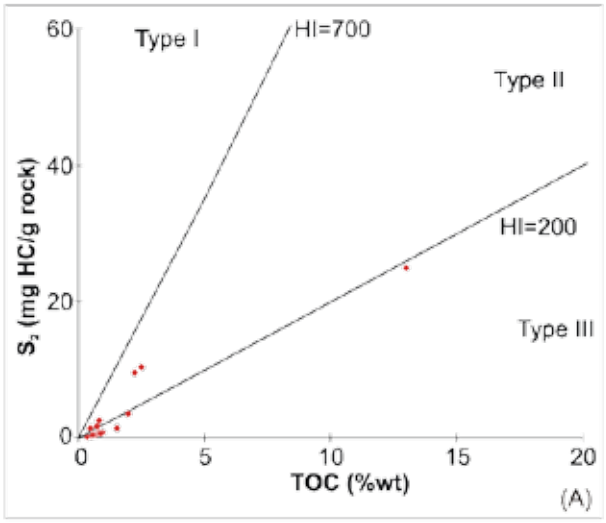

Figure 22. Graphs of Rock-Eval data of kerogen from the b-82-C well. (a) HI (hydrogen index) *versus* OI (oxygen index) diagram. (b) S_2 *versus* TOC (total organic carbon) diagram. Data points from Osadetz *et al.* (2003). Only data with TOC > 0.3% plotted.

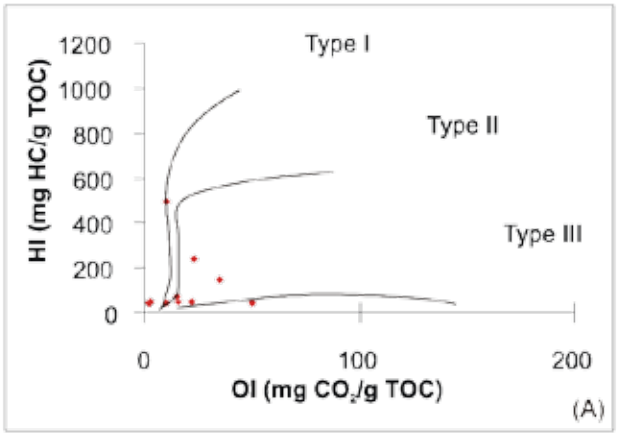

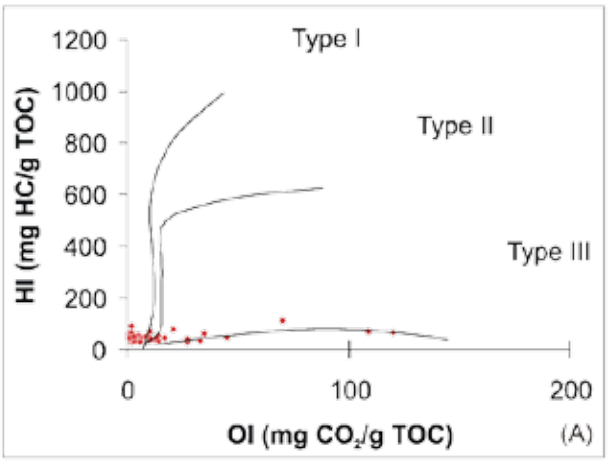

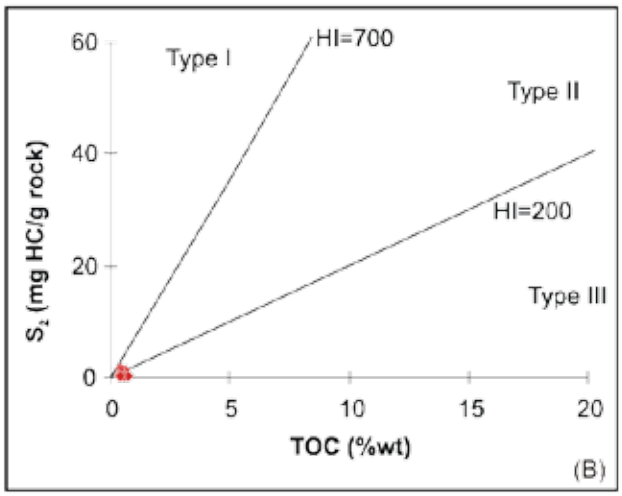

Figure 23. Graphs of Rock-Eval data of kerogen from the c-75-A well. (a) HI (hydrogen index) versus OI (oxygen index) diagram. (b) S_2 versus TOC (total organic carbon) diagram. Data points from Osadetz *et al.* (2003). Only data with TOC > 0.3% plotted.

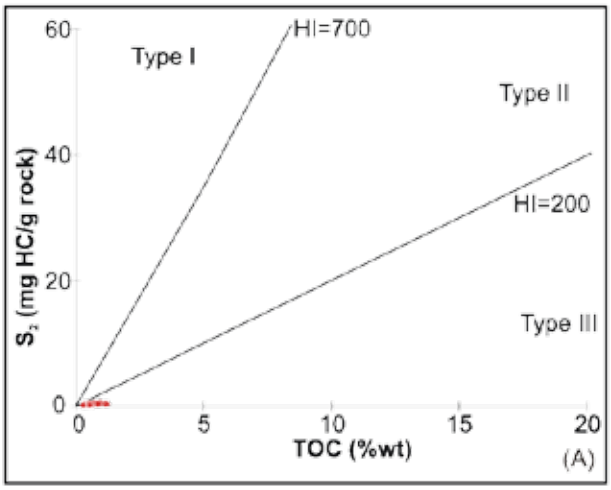

Figure 24. Graphs of Rock-Eval data of kerogen from the d-94-G well. (a) HI (hydrogen index) versus OI (oxygen index) diagram. (b) S_2 versus TOC (total organic carbon) diagram. Data points from Osadetz *et al.* (2003). Only data with TOC > 0.3% plotted.

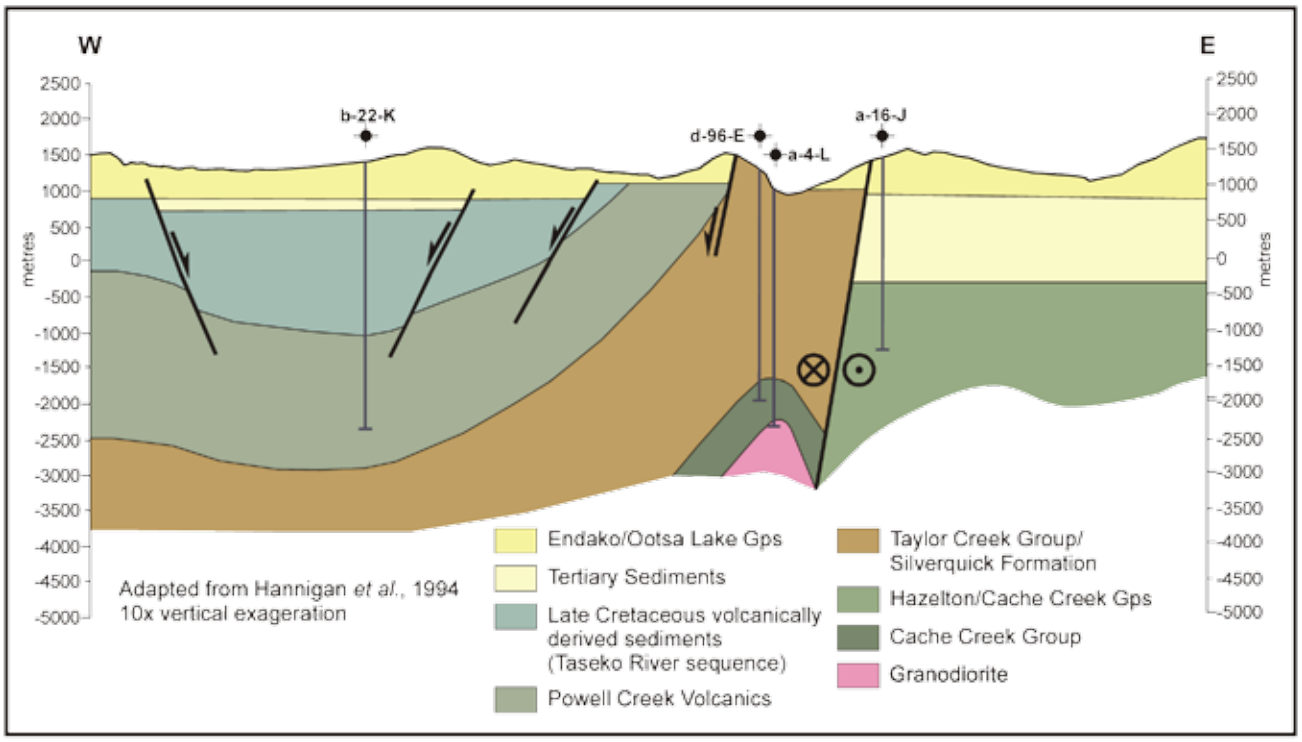

Figure 25. Simple cross-section across the southern Nechako area. Modification of a diagram by Hannigan *et al.* (1994) through the b-16-J, a-4-L, d-96-E, and b-22-K wells. In this interpretation, the general westward dip of Cretaceous strata projects under the volcanics penetrated by the b-22-K well satisfies both biostratigraphic control and gravity modeling.

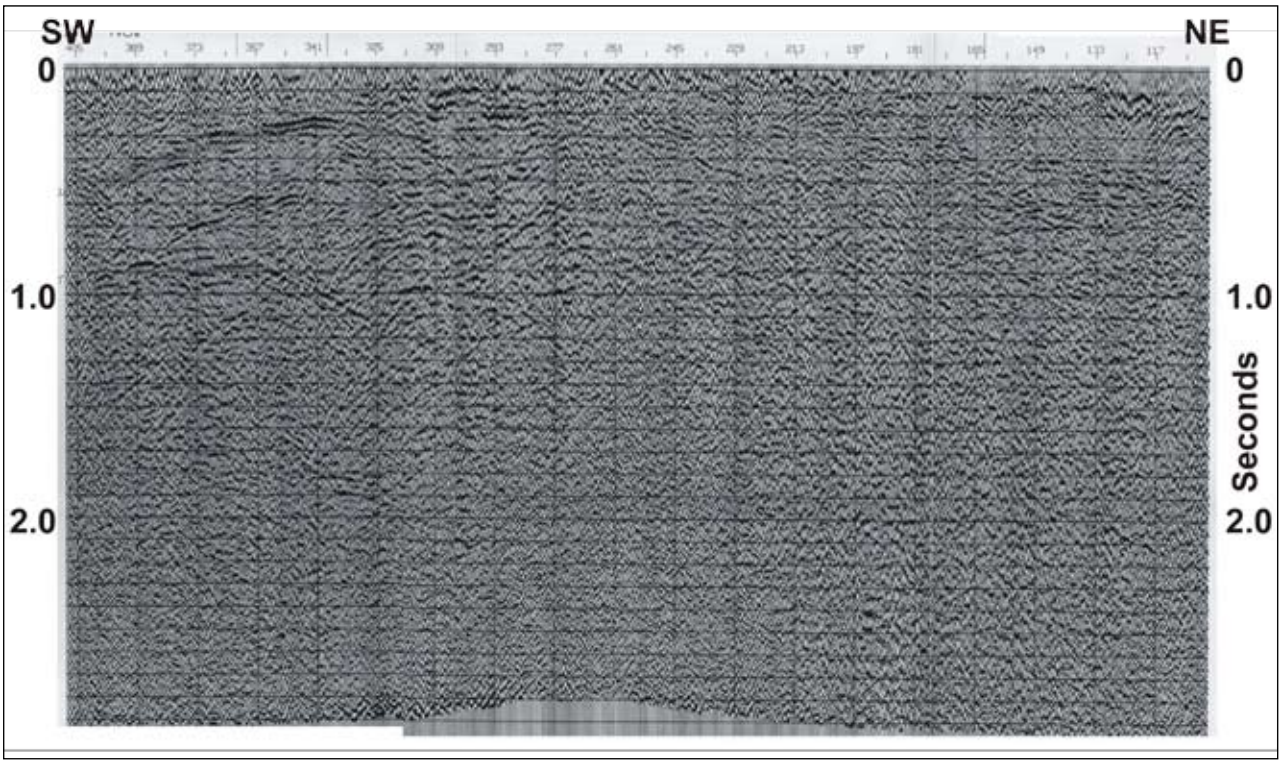

Figure 26. Seismic line across the western margin of the large negative anomaly in the southern part of the map area (Line 1, Figure 9). Seconds are two-way travel times. Line is from Focht (1982b).

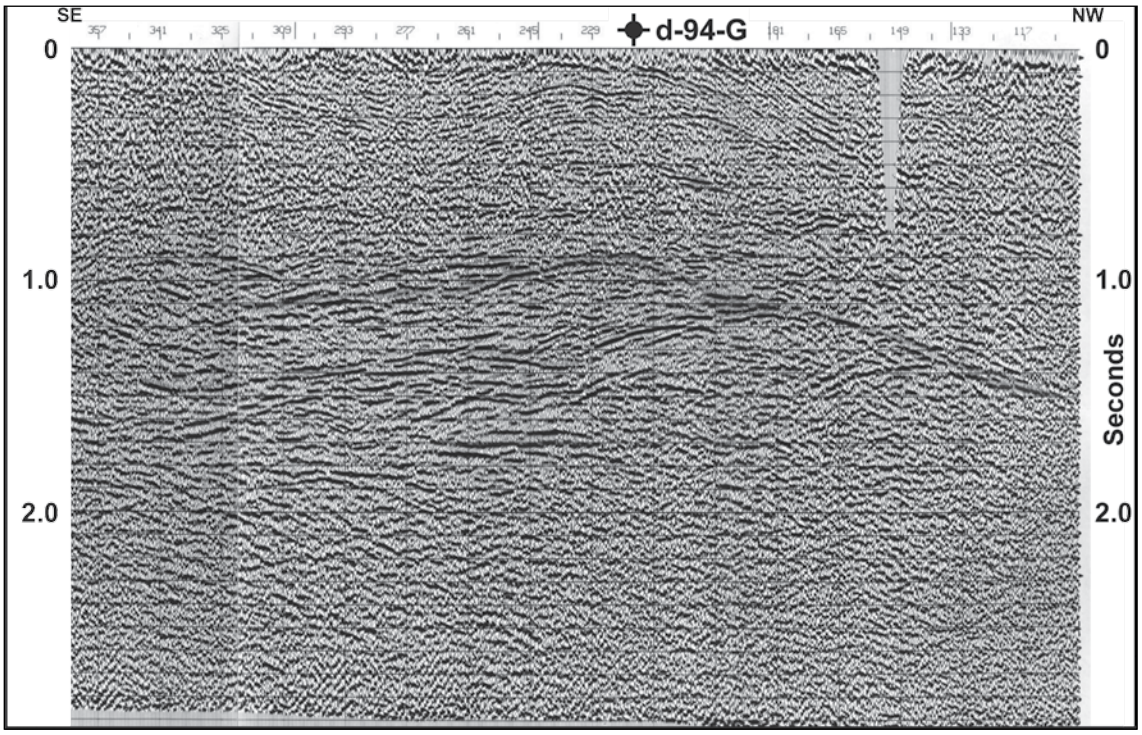

Figure 27. Northwest-trending seismic line cutting through the d-94-G well. The d-94-G well is shown; the drillhole pierces a large closure in the section. Seconds are two-way travel time. Line is from Focht (1982a). See Figure 2 for location.

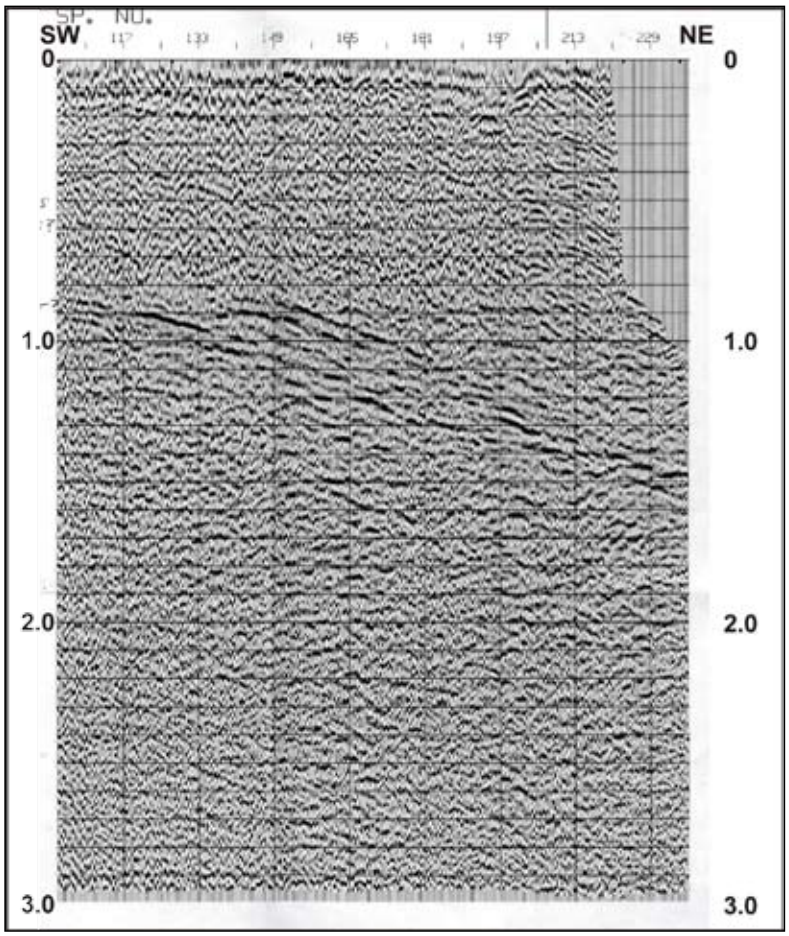

Figure 28. Northeast-trending seismic line in southern part of Nechako Basin, immediately north of the d-94-G well (see Figure 2 for location). Seconds are two-way travel time. Line is from Focht (1982a). Length of section is approximately 14 km.

TABLE 2. ROCK-EVAL RESULTS FROM SURFACE SAMPLES FROM SHALY UNITS IN THE CHILCOTIN AND CAMELSFOOT RANGES.

Station	Group/Formation	Rock type	Location	Easting	Northing	TOC %	T_{max} (degrees C)
				All stations UTM zone 10, NAD 83			
FF05-03	Relay Mt Gp-Teepee Mt Fm	siltstone	Relay Mt	503501	5666334	0.16	476
FF05-04	Relay Mt Gp-Potato Range Fm	siltstone	Relay Mt	502497	5665822	0.35	478
FF05-05	Relay Mt Gp-Potato Range Fm	siltstone	Relay Mt	502488	5665495	0.62	481
FF05-06	Relay Mt Gp-Unit 5 of Umhoefer et al	siltstone	Relay Mt	501698	5664338	0.82	490
FF05-07	Taylor Ck - Paradise	siltstone	Relay Mt	501689	5664115	0.31	504
FF05-08	Taylor Ck - Paradise	siltstone	Relay Mt	501655	5664066	0.40	499
FF05-09	Taylor Ck - Paradise	siltstone	Relay Mt	501309	5663026	0.42	506
FF05-11	Taylor Ck - Paradise	siltstone	Relay Mt	500966	5662427	0.47	516
FF05-12	Relay Mt Gp-Tyoax Pass Fm	siltstone	Relay Mt	499859	5662331	0.56	521
FF05-13	Relay Mt Gp-Teepee Mt Fm	wacke-siltstone	Relay Mt	499643	5662637	0.16	508
FF05-14	Relay Mt Gp-Tyoax Pass Fm	siltstone	Relay Mt	499493	5662675	0.76	511
FF05-15	Relay Mt Gp-Tyoax Pass Fm	siltstone	Relay Mt	499429	5662596	0.31	510
FF05-16	Relay Mt Gp-Tyoax Pass Fm	siltstone	Relay Mt	499321	5662403	0.43	514
FF05-18a	Last Creek Fm	siltstone	Relay Mt	498924	5662127	0.56	515
FF05-18b	Last Creek Fm	sandstone	Relay Mt	498924	5662127	0.60	517
FF05-19	Last Creek Fm	siltstone	Relay Mt	498842	5662086	0.72	513
FF05-20	Last Creek Fm	limestone	Relay Mt	499092	5661912	0.98	507
FF05-21	Last Creek Fm	siltstone	Relay Mt	499440	5661756	1.72	564
FF05-27	Taylor Ck-Lizard fm	siltstone	Taylor Basin	513203	5647338	0.33	338
FF05-64	Hazelton	siltstone	Baezaeko River	434844	5870204	0.39	336
FF05-86	Jackass Mountain	siltstone	Highway 99-Fountain	578068	5622707	0.26	608
FF05-87	Lillooet Group	siltstone	Highway 99-Lillooet	575706	5631828	1.00	310
FF05-88	Lillooet Group	siltstone	Highway 12	584825	5601877	0.36	363

TABLE 3. VITRINITE REFLECTANCE VALUES FROM SURFACE SAMPLES COLLECTED IN 2005.

Station	Group/Formation	Rock type	Location	Easting	Northing	RoR %
				All stations UTM zone 10, NAD 83		
FF05-02	Relay Mt Gp-Teepee Mt Fm	siltstone	Relay Mt	503603	5666419	1.20
FF05-15	Relay Mt Gp. -Tyoax Pass Fm	siltstone	Relay Mt	499429	5662596	n/a
FF05-26	Taylor Ck.Gp – Dash fm	conglomerate	Taylor Basin	512762	5647072	1.34
FF05-31	Taseko River strata	sandstone	Taseko River	451622	5716506	1.22
FF05-64	Hazelton Gp	siltstone	Baezaeko R	434844	5870204	n/a
FF05-68	Taylor Cr- Dash?SQ	sandstone	Nazko River	471631	5836686	0.60
FF05-73	Taylor Ck Gp	sandstone	Nazko River	471588	5834194	1.00

TABLE 4. VITRINITE REFLECTANCE VALUES FROM SUBSURFACE SAMPLES COLLECTED IN 2005 FROM DRILLHOLE CUTTINGS AND CORE.

Well #	Depth (m)	Sample type	%RoR
a-4-L	1356	core	0.68
b-16-J	310	drill cuttings	4.98
b-22-K	47.5	drill cuttings	n/a
b-22-K	72.5	drill cuttings	n/a
b-22-K	132	drill cuttings	0.34
b-22-K	145	drill cuttings	0.47
b-22-K	170	drill cuttings	n/a
b-22-K	205	drill cuttings	0.45
b-22-K	325	drill cuttings	0.48
b-22-K	637.5	drill cuttings	n/a
b-22-K	2500	drill cuttings	n/a
b-22-K	3696-3702.5	drill cuttings	1.76
b-82-C	830-840	drill cuttings	n/a
b-82-C	1295.1	core	0.58
b-82-C	1300	drill cuttings	0.76
b-82-C	1380-1385	drill cuttings	0.51
b-82-C	1450-1500	drill cuttings	0.87
c-75-A	172	core	1.40
c-75-A	1174	core	no data
c-75-A	1178	core	1.71
d-94-G	150-170	drill cuttings	0.95
d-94-G	355-370	drill cuttings	1.18
d-94-G	530-550	drill cuttings	1.36
d-94-G	615-625	drill cuttings	1.32
d-94-G	684	drill cuttings	1.45
d-94-G	760-765	drill cuttings	1.60
d-94-G	1030-1040	drill cuttings	1.51
d-94-G	1275-1285	drill cuttings	1.49
d-94-G	1500-1515	drill cuttings	1.52
d-94-G	1710-1715	drill cuttings	1.65
d-94-G	1970-1975	drill cuttings	1.71
d-96-E	913	core	0.78
d-96-E	920	core	0.97
d-96-E	963.5	core	0.93
d-96-E	1399	core	n/a
d-96-E	1554	core	0.88
d-96-E	1727	core	0.91
d-96-E	1884	core	0.73
d-96-E	1894	core	1.11
d-96-E	2115-2180	drill cuttings	0.82
d-96-E	2175-2180	drill cuttings	0.70
d-96-E	2342.5-2350	drill cuttings	0.73
d-96-E	2575-2580	drill cuttings	0.82
d-96-E	2780-2785	drill cuttings	0.93
d-96-E	2855-2860	drill cuttings	1.00
d-96-E	2980-2990	drill cuttings	0.94
d-96-E	3045	drill cuttings	0.93

Palynology work by Hunt (1992) suggests an Aptian-age and a terrestrial environment for well d-96-E rocks. We question the suggested non-marine environment for these fine clastic rocks because the type of kerogen present (Type II) is typical of a marine origin. The age of these rocks overlaps that of Jackass Mountain Group and possibly the lower parts of the Paradise Formation, both of which have thick sections of dark grey marine shale and siltstone in the lower parts. Resampling of these horizons is planned, together with examination of well logs, to further characterize these zones.

During the 2005 field season, surface samples for Rock-Eval analysis were obtained from shaly parts of the Last Creek Formation and Relay Mountain, Taylor Creek, and Jackass Mountain Groups for determination of source rock potential (Table 2). Black shales and siltstones of the Last Creek Formation are part of a regional blanket of dark fine clastics deposited during a major Early to Middle Jurassic anoxic event (Ferri and Boddy, 2005). In the Bowser Basin and Ashcroft areas, time-equivalent strata (Spatsizi and Ashcroft Formations, respectively) have high TOC contents and, although over-mature, may originally have been

TABLE 5. MAGNETIC SUSCEPTIBILITY READINGS FROM 2005 FIELD STATIONS.

Station	UTM east	UTM north	Location name	Formation or Group	Rock type	MS reading ($X 10^{-3}$ SI)
	All stations UTM Zone 10					
FF05-30	451542	5713086	Taseko River	Jackass Mountain Group	conglomerate	14.50
FF05-34a	455527	5714305	Taseko River	Chilcotin Group	basalt	2.50
FF05-35	459682	5722908	Taseko River	Chilcotin Group	basalt	11.10
FF05-36	476234	5744941	Taseko River	Eocene sedimentary	sandstone	0.75
FF05-37	475007	5745605	Taseko River	Cretaceous or Tertiary pluton	granodiorite	9.74
FF05-38	475060	5745563	Taseko River	Eocene sedimentary	granule conglomerate	9.47
FF05-39	491015	5710508	Big Ck.	Eocene volcanic	dacite	12.40
FF05-40	481831	5701760	Big Ck.	Spences Bridge?	volcanic breccia	0.42
FF05-41	481520	5702027	Big Ck.	Spences Bridge?	volcanic breccia	14.90
FF05-41	481520	5702027	Big Ck.	Spences Bridge?	tuff	30.50
FF05-42	481482	5702563	Big Ck.	Spences Bridge?	volcanic breccia	0.35
FF05-43	482468	5702776	Big Ck.	Spences Bridge?	volcanic breccia	0.73
FF05-44	473928	5714838	Big Ck.	Cretaceous pluton	granite	5.68
FF05-45	470911	5719402	Big Ck.	Spences Bridge?	andesite	15.60
FF05-46	470143	5723642	Big Ck.	Spences Bridge?	andesite	23.80
FF05-47	473983	5719816	Big Ck.	Spences Bridge?	andesite	14.50
FF05-48	486174	5724102	Big Ck.	Eocene volcanic	dacite	25.10
FF05-49	479689	5719593	Big Ck.	Cretaceous or Tertiary pluton	granite	11.00
FF05-50	487778	5724316	Big Ck.	Chilcotin Group	basalt	4.33
FF05-51	492762	5722331	Big Ck.	Eocene volcanic	rhyolite	1.08
FF05-52	506063	5723902	Big Ck.	Cretaceous pluton	granite	0.31
FF05-53	504383	5722776	Big Ck.	Spences Bridge?	amphibolite	56.10
FF05-54	510496	5715757	Big Ck.	Cretaceous pluton	quartz diorite	1.24
FF05-55	501888	5704608	Big Ck.	Piltz Peak plutonic complex	diorite	0.34
FF05-56	501319	5704419	Big Ck.	Piltz Peak plutonic complex	gneiss	0.14
FF05-57	493405	5746187	Big Ck.	Eocene volcanic	volcanic breccia	9.27
FF05-58	496349	5742551	Big Ck.	Eocene volcanic	volcanic breccia	16.40
FF05-60	437930	5869933	Baezaeko River	Hazelton	conglomerate	0.32
FF05-61	437572	5870194	Baezaeko River	Hazelton	gabbro	8.15
FF05-62	438840	5871012	Baezaeko River	Hazelton Group	basalt	2.34
FF05-63	442117	5865727	Baezaeko River	Eocene volcanic	basalt	7.64
FF05-64	434844	5870204	Baezaeko River	Hazelton	siltstone	0.36
FF05-65	435193	5870555	Baezaeko River	Pluton, unknown age	diorite	0.42
FF05-66	441154	5864344	Baezaeko River	Eocene volcanic	andesite	4.80
FF05-67	443575	5867884	Baezaeko River	Eocene volcanic	basalt	2.87
FF05-68	471631	5836686	Nazko River	Taylor Ck-Dash?SQ?	sandstone	0.05
FF05-69	471496	5836820	Nazko River	Taylor Ck-Dash?SQ?	siltstone	0.15
FF05-69	471496	5836820	Nazko River	Taylor Ck-Dash?SQ?	conglomerate	0.02
FF05-71	470252	5835011	Nazko River	Taylor Creek-Lizard?	sandstone	0.04
FF05-72	471246	5832206	Nazko River	Taylor Creek.	sandstone	0.06
FF05-73	471588	5834194	Nazko River	Taylor Creek	conglomerate	0.02
FF05-73	471588	5834194	Nazko River	Taylor Creek	sandstone	0.03
FF05-74	469584	5842179	Nazko River	Taylor Creek	conglomerate	0.22
FF05-74	469584	5842179	Nazko River	Taylor Creek	sandstone	0.32
FF05-76	469775	5846631	Nazko River	Taylor Creek	conglomerate	0.05
FF05-77	455689	5866203	Baezaeko River	Taylor Creek	conglomerate	0.02
FF05-78	455908	5866539	Baezaeko River	Taylor Creek	sandstone	0.07
FF05-79	456567	5870427	Baezaeko River	Taylor Creek	conglomerate	0.03
FF05-81	451001	5783484	Redstone	Taylor Creek	sandstone	0.15
FF05-82	462976	5768349	Redstone	Taylor Ck - Silverquick?	sandstone	0.23
FF05-83	430949	5785280	Puntzi Lake	Hazelton Group	tuff	0.12
FF05-84	431276	5785280	Puntzi Lake	Powell Creek?	volcanic bx	28.30
FF05-85	434471	5785920	Puntzi Lake	Powell Creek?	volcanic bx	28.30

high-quality source rocks (Ferri and Boddy, 2005). Only 4 samples from the Last Creek Formation were obtained, and these had TOC values up to 1.72% and low HI values (<50 mg HC/g TOC).

Samples from the Relay Mountain Group returned low TOC values; the single sample of the Jackass Mountain Group and all of the time-equivalent Paradise Formation (of the Taylor Creek Group) samples produced TOC and HI values that are not promising for source bed potential. The dark grey to black shale and siltstone of the Paradise Formation and the base of the Jackass Mountain Group are regional in extent, however, so further sampling is required to adequately characterize them. The presence of bituminous shale in time-equivalent strata of wells d-96-E and a-4-L indicates that these horizons warrant further investigation, and they will be targeted for sampling during the 2006 field season.

THERMAL MATURATION

Vitrinite reflectance data for surface and subsurface sections are shown in Tables 3 and 4 and Figures 13, 15, 17, 18, and 19. In the subsurface, maturation levels from vitrinite reflectance are similar to those indicated by T_{max} values from Rock-Eval analysis of cuttings. Maturation levels could not be determined within the bulk of wells b-22-K and b-16-J due to low organic contents. Vitrinite reflectance data were obtained from only the upper part of the Tertiary strata of well b-22-K and indicate that the sediments are undermature. One sample from near the bottom of the well is in the dry gas zone. No samples could be obtained from the b-16-J well for reflectance determination. Furthermore, the low organic contents for this and the b-22-K well rendered the bulk of the T_{max} data as unreliable for thermal maturation determination. Apatite fission track analysis of samples of cuttings from these holes may provide better information on the thermal maturation history of these rocks.

Taylor Creek Group and Silverquick Formation(?) rocks from wells a-4-L, d-96-E, and b-82-C returned vitrinite reflectance and T_{max} values bracketing the oil window (Table 4; Figures 13, 14, and 17). The only suitable sample from the upper Tertiary(?) part of well b-82-C yielded results within the top of the oil window. The section below this, starting at approximately 1200 m, contains material suggesting oil window conditions. Again, we anticipate that apatite fission track samples within the upper 1200 m of this well will provide more precise constraints on the thermal maturation of these rocks.

Much higher thermal maturation values have been obtained from wells c-75-A and d-94-G (Table 4; Figures 18 and 19). Reliable data from well c-75-A is lacking due to low TOC, but the available vitrinite reflectance data suggest dry gas conditions. Although the d-94-G well contains lithologies of low organic content, they are distributed evenly throughout the section and of sufficient organic content to allow thermal maturation determination. Thermal maturation data suggest conditions within the well straddled the oil and gas windows. Furthermore, both T_{max} and vitrinite reflectance data show a decrease below the 900 m and a change in thermal maturation gradient; the decrease in thermal maturation values below 900 m could be the result of a thrust repetition.

CONCLUSIONS

- Gravity and surface geological data suggest that the southern Nechako Basin is composed of several smaller sub-basins.
- Biostratigraphy and interpretation of subsurface sections suggest most wells in the southern Nechako area penetrated Cretaceous sections correlative with the Taylor Creek and Jackass Mountain Groups, Silverquick conglomerate and Powell Creek volcanics. In addition, several wells penetrated thick sections of Tertiary clastics and volcanics. No rocks of the Relay Mountain Group have been recognized in the subsurface.
- Rock-Eval data indicate the potential for source bed horizons at several intervals, although further work is needed to properly characterize these horizons. No regionally persistent rich source bed horizon has yet been recognized.
- Oil inclusions occur at several horizons in the d-96-E well. These have been extracted for analysis.
- The following studies are underway: apatite fission track thermochronology, subsurface pollen biostratigraphy, reservoir porosity, and surface and subsurface radiometric dating. Results will be published as they become available.

ACKNOWLEDGEMENTS

We are grateful to Veera Bonner of Fletcher Lake and the Class family of Nemaiah Valley for hospitable accommodation in the field. Les Rolston of Cariboo-Chilcotin Helicopters provided safe transportation in the Chilcotin Mountains. We are grateful to Paul Schiarizza for providing ongoing tutoring on the complexities of the geology of the Chilcotin Mountains and for suggesting improvements to an earlier manuscript. We would like to thank Carmel Lowe and Mel Best for allowing us to use material from a 2004 CSPG oral presentation. Vern Stasiuk of GSC Calgary provided prompt processing and analysis of Rock-Eval and vitrinite reflectance samples. Mike Fournier's reliable and patient help with the production of maps and figures is invaluable.

REFERENCES

A report on Hudson's Bay Redstone c-75-A well in c-75-A/93-B-4; *B.C. Ministry of Energy, Mines and Petroleum Resources*, Well File 630.

A report on the Texalta Punchaw c-38-J/93-G-06 well; *B.C. Ministry of Energy, Mines and Petroleum Resources,* Well File 3149.

Archibald, D.A., Glover, J.K. and Schiarizza, P. (1989): Preliminary report on 40Ar/39Ar geochronology of the Warner Pass, Noaxe Creek and Bridge River map areas (92O/3, 2; 92J/16); *B.C. Ministry of Energy, Mines and Petroleum Resources,* Geological Fieldwork 1988, Paper 1989-1, pages 145-151.

Best, M. (2004a): Gravity and Magnetic Survey, Nechako Basin Study, acquisition and processing phase; *B.C. Ministry of Energy and Mines;* Petroleum Geology Open File 2004-1.

Best, M. (2004b): Qualitative Interpretation of Potential Field Profiles: Southern Nechako Basin; *in* Summary of Activities 2004, Resource Development and Geoscience Branch, *B.C. Ministry of Energy and Mines,* pages 73-78.

Cosgrove, D.T. (1981a): Well history report on Canadian Hunter *et al.* Nazko d-96-E/93-B-11; *B.C. Ministry of Energy, Mines and Petroleum Resources,* Well File 5439.

Cosgrove, D.T. (1981b): Well history report on Canadian Hunter *et al.* Redstone b-82-C/92-O-14; *B.C. Ministry of Energy, Mines and Petroleum Resources,* Well File 5680.

Cosgrove, D.T. (1982): Well history report on Canadian Hunter *et al.* Chilcotin b-22-K/93-C-9; *B.C. Ministry of Energy, Mines and Petroleum Resources,* Well File 5702.

Cosgrove, D.T. (1986a): Well history report on Canadian Hunter Esso Nazko b-16-J/93-B-11; *B.C. Ministry of Energy, Mines and Petroleum Resources,* Well File 5544.

Cosgrove, D.T. (1986b): Well history report on Canadian Hunter Redstone d-94-G/92-O-12; *B.C. Ministry of Energy, Mines and Petroleum Resources,* Well File 6438.

Engebretson, D.C., Cox, A., and Gordon, R.G. (1985): Relative motions between oceanic and continental plates in the Pacific basin*; Geological Society of America,* Special Paper 206, 59 pages.

Enkin, R. J., Mahoney, J. B. and Baker, J. (*in preparation*): Paleomagnetic signature of the Silverquick/Powell Creek succession, south-central British Columbia: Reaffirmation of Late Cretaceous large-scale terrane translation; *in Geological Association of Canada*, Special Volume on Major Displacements in the Cordillera.

Ferri, F. and Boddy, M. (2005): Geochemistry of Early to Middle Jurassic Organic-Rich Shales, Intermontane Basins, British Columbia; *in* Summary of Activities 2004, *B.C. Ministry of Energy and Mines, Resource Development and Geoscience Branch,* pages 132-151.

Ferri, F., Lowe, L. and Best, M. (2004): Possible Late Cretaceous to Tertiary Structural Control on Basin Configuration, southern Nechako area; *Canadian Society of Petroleum Geologists* Annual Convention, Calgary, AB, Program with Abstracts, Conference Abstract Archive CD.

Focht, G. (1982a): Nechako Basin, B.C. Project #81-152, Final Operations Report; *B.C. Ministry of Energy, Mines and Petroleum Resources,* Geological Report 2378.

Focht, G. (1982b): Nechako Basin, B.C. Project #81-147, Final Operations Report; *B.C. Ministry of Energy, Mines and Petroleum Resources,* Geological Report 2379.

Focht, G. (1982c): Nechako Basin, B.C. Project #81-111, Final Operations Report; *B.C. Ministry of Energy, Mines and Petroleum Resources,* Geological Report 2380.

Focht, G. (1982d): Nechako Basin, B.C. Project #81-162, Final Operations Report; *B.C. Ministry of Energy, Mines and Petroleum Resources,* Geological Report 2381.

Focht, G. (1982e): Nechako Basin, B.C. Project #81-235, Final Operations Report; *B.C. Ministry of Energy, Mines and Petroleum Resources,* Geological Report 2382.

Focht, G. (1982f): Nechako Basin, B.C. Project #80-223, Final Operations Report; *B.C. Ministry of Energy, Mines and Petroleum Resources,* Geological Report 2383.

Focht, G. (1982g): Nechako Basin, B.C. Project #80-155, Final Operations Report; *B.C. Ministry of Energy, Mines and Petroleum Resources,* Geological Report 2384.

Focht, G. (1982h): Nechako Basin, B.C. Project #81-46, Final Operations Report; *B.C. Ministry of Energy, Mines and Petroleum Resources,* Geological Report 2386.

Focht, G. (1982i): Nechako Basin, B.C. Project #80-254, Final Operations Report; *B.C. Ministry of Energy, Mines and Petroleum Resources,* Geological Report 2387.

Friedman, R.M. and Armstrong, R.L. (1988): Tatla Lake Metamorphic complex: an Eocene metamorphic core complex on the southwestern edge of the Intermontane Belt of British Columbia; *Tectonics*, Vol. 7, No. 6, pages 1141-1166.

Friedman, R.M., Mahoney, J.B. and Cui, Y. (1995): Magmatic evolution of the southern Coast Belt: constraints from Nd-Sr isotopic systematics and geochronology of the southern Coast Plutonic Complex; *Canadian Journal of Earth Sciences,* Vol. 32, pages 1681-1698.

Garver, J.I. (1989): Basin evolution and source terranes of Albian-Cenomanian rocks in the Tyaughton basin, southern British Columbia; implications for mid-Cretaceous tectonics in the Canadian Cordillera; unpublished PhD thesis, *University of Washington*, Seattle, 228 pages.

Garver, J.I. (1992): Provenance of Albian – Cenomanian rocks of the Methow and Tyaughton basins, southern British Columbia: a mid-Cretaceous link between North America and the Insular terrane; *Canadian Journal of Earth Sciences,* Vol. 29, No. 6, pages 1274-1295.

Gradstein, F.M. and Ogg, J.G. and Smith, A.G. (2005): Geologic Time Scale 2004, *Cambridge University Press,* New York.

Halliday, I.R. (1969): Structure and stratigraphy of the Quesnel Basin, B.C.; Amoco Canada Report, *B.C. Petroleum Resources Branch* Assessment Report 1465, 9 pages.

Hannigan, P., Lee, P.J., Osadetz, K.G., Dietrich, J.R. and Olsen-Heise, K. (1994): Oil and Gas Resource Potential of the Nechako-Chilcotin Area of British Columbia; *B.C. Ministry of Energy and Mines*, Geofile 2001-6.

Hayes, B. (2002): Petroleum Exploration Potential of the Nechako Basin, British Columbia; *B.C. Ministry of Energy and Mines*, Petroleum Geology Special Paper 2002-3.

Hayes, Mark, Ferri, Filippo and Morii, Sachie (2004): Interior Basins strategy; *in* Summary of Activities 2004, *B.C. Ministry of Energy and Mines*, Resource Development and Geoscience Branch, pp. 69-71.

Hickson, C.J. (1992): An update on the Chilcotin-Nechako project and mapping in the Taseko Lakes area, west-central British Columbia; in Current Research, Part A; *Geological Survey of Canada,* Paper 92-1A, pages 129-135.

Hickson, C.J. (1993): Geology of the northwest quadrant, Taseko Lakes map area (92O), west-central British Columbia; 1:50,000 maps, *Geological Survey of Canada,* Open File 2695.

Holland, S.S. (1964): Landforms of British Columbia: a physiographic outline; *British Columbia Department of Mines Petroleum Resources,* Bulletin No. 48, 138 pages.

Hunt, J.A. (1992): Stratigraphy, Maturation and Source Rock Potential of Cretaceous Strata in the Chilcotin-Nechako Region of British Columbia, unpublished M.Sc. thesis, *University of British Columbia,* Vancouver, British Columbia, 448 pages.

Hunt, J.A. and Bustin, R.M. (1997): Thermal maturation and source rock potential of Cretaceous strata in the Chilcotin-Nechako region, south-central British Columbia, Geological Note *in Bulletin of Canadian Petroleum Geology*, Volume 45, Number 2, p. 239-248.

Kleinspehn, Karen L. (1985): Cretaceous sedimentation and tectonics, Tyaughton-Methow Basin, southwestern British Columbia, *Canadian Journal of Earth Sciences*, Vol. 22, pages 154-174.

Koch, N. G. (1970): The Central Cordilleran Region; *in* the Future Petroleum Provinces of Canada, R.G. McCrossan (ed.); *Canadian Society of Petroleum Geologists*, Memoir 1, p. 37-71.

Lafargue, E., Marquis, F. and Pillot, D. (1998): Rock-Eval 6 applications in hydrocarbon exploration, production, and soil contamination studies; *Revue de l'Institut Français Du Petrole,* Volume 53, No. 4, pages 421-437.

Landreth, T.C. (1961): Well history report on Honolulu Nazko a-4-L/93-B-11; *B.C. Ministry of Energy, Mines and Petroleum Resources,* Well File 634.

Lowe, C., Enkin, R.J. and Struik, L.C. (2001): Tertiary extension in the central British Columbia Intermontane Belt: magnetic and paleomagnetic evidence from the Endako region; *Canadian Journal of Earth Sciences,* Vol. 38, pages 657-678.

Mahoney, J.B., Hickson, C.J., van der Heyden, P. and Hunt, J.A. (1992): The Late Albian-Early Cenomanian Silverquick conglomerate, Gang Ranch area: evidence for active basin tectonism, *in* Current Research, Part A; *Geological Survey of Canada*, Paper 92-1A, p. 249-260.

Mahoney, J. B. (1993): Facies reconstructions in the Lower to Middle Jurassic Ladner Group, southern British Columbia, *in* Current Research, Part A; *Geological Survey of Canada,* Paper 93-1A, pages 173-182.

Majorowicz, J. A., Osadetz, K.G., Evenchick, C.A., Ferri, F. and Hayes, M. (2004): Temperature and thermotectonic histories from the Intermontane Superterrane in British Columbia; *Canadian Society of Petroleum Geologists* Annual Convention, Calgary, AB, Program with Abstracts, Conference Abstract Archive CD.

Maxson, J. A. (1996): A sedimentary record of Late Cretaceous Tectonic Restructuring of the North American Cordillera: The Tyaughton-Methow Basin, Southwest British Columbia, unpublished Ph.D. thesis, *University of Minnesota,* 190 pages.

Mustard, P. S. and van der Heyden, P. (1997): Geology of the Tatla Lake (92N/15) and the east half of Bussel Creek (92N/14) map areas; *in* Interior Plateau geoscience project: summary of geological, geochemical and geophysical studies, *B.C. Ministry of Employment and Investment,* Paper 1997-2, pages 103-118.

Osadetz, K.G., Snowdon, L.R. and Obermajer, M. (2003): Rock-Eval/TOC results for eleven Northern British Columbia boreholes; *Geological Survey of Canada,* Open File 1550.

Perry, R.G. and Bullock B.D. (1960): Preliminary Geological Report, Permit 1192, BC Report; *B.C. Ministry of Energy, Mines and Petroleum Resources,* Geological Report 904.

Ramsay, T.B. (1972): Sample descriptions for Vieco Texacal Punchaw c-38-J/93-G-6; *B.C. Ministry of Energy, Mines and Petroleum Resources,* Well File 3149.

Rusmore, M. and Woodsworth, G.J. (1994): Evolution of the eastern Waddington thrust belt and its relation to the mid-Cretaceous Coast Mountains arc, western British Columbia; *Tectonics*, Vol. 13, No.5, pages 1052-1067.

Rusmore, M. and Woodsworth, G.J (1991): Coast Plutonic Complex: A mid-Cretaceous contractional orogen; *Geology*, Vol. 19, pages 941-944.

Salt, W.T. (1980a): Gravity Survey detailing the Honolulu Oil - Nazko Wellsite area and Reconnaissance lines in the North Chezacut area of the Nechako basin; *B.C. Ministry of Energy, Mines and Petroleum Resources,* Geological Report 2394.

Salt, W.T. (1980b): Gravity Survey of the Big Creek area of the Nechako Basin; *B.C. Ministry of Energy, Mines and Petroleum Resources,* Geological Report 2393.

Salt, W.T. (1981a): Gravity Survey detailing the North Chezacut area and Reconnaissance of an area north of the West Road River of the Nechako basin; *B.C. Ministry of Energy, Mines and Petroleum Resources,* Geological Report 2396.

Salt, W.T. (1981b): Gravity Survey of the Chezacut - Chilanko Forks - Chilko River area of the Nechako Basin; *B.C. Ministry of Energy, Mines and Petroleum Resources,* Geological Report 2395.

Salt, W.T. (1982a): Detailed Gravity Survey of the Chezacut Area of the Nechako Basin Project Number 81-156; *B.C. Ministry of Energy, Mines and Petroleum Resources,* Geological Report 2397.

Salt, W.T. (1982b): Gravity Survey of the South Big Creek area of the Nechako Basin Project Number 81-164; *B.C. Ministry of Energy, Mines and Petroleum Resources,* Geological Report 2398.

Schiarizza, P. (1996): Tatlayoko Project update (92N/8, 9. 10; 92O/5, 6, 12): *in* Geological Fieldwork 1995, *B.C. Ministry of Energy, Mines and Petroleum Resources,* Paper 1996-1, p. 77-91.

Schiarizza, P., Gaba, R.G., Glover, J.K., Garver, J.I. and Umhoefer, P.J. (1997): Geology and mineral occurrences of the Taseko-Bridge River area; *B.C. Ministry of Employment and Investment,* Bulletin 100, 292 pages.

Struik, L.C. (1993): Intersecting intracontinental Tertiary transform fault systems in the North American Cordillera; *Canadian Journal of Earth Sciences,* Vol. 30, pages 1262-1274.

Taylor, N.W. (1960): Report of Photogeological Survey and Surface Geological Study, The Nazko River Permit Area- Interior Plateau, Central British Columbia; Honolulu Oil Corporation Report, *B.C. Ministry of Energy, Mines and Petroleum Resources* Geological Report 850, 17 pages.

Taylor, N.W. (1961): A Report on the Nazko River and Puntzi Permit Areas - Interior Plateau, central British Columbia; Honolulu Oil Corporation Report, *B.C. Ministry of Energy, Mines and Petroleum Resources* Geological Report 935, 32 pages, 8 maps, and well log for a-4-L/93B-11.

Thomson, R.C., Smith, P.L. and Tipper, H.W. (1986): Lower to Middle Jurassic (Pliensbachian to Bajocian) stratigraphy of the northern Spatzizi area, north-central British Columbia, *Canadian Journal of Earth Science,* Volume 23, pages 1963-1973.

Thornsteinsson, E. (*in preparation*): Well descriptions from the Interior Basins of British Columbia; Geological Survey of Canada, Open File; *B.C. Ministry of Energy, Mines and Petroleum Resources*, Petroleum Geology Open File.

Tipper, H.W. (1959): Geology, Quesnel map area; *Geological Survey of Canada,* Map 12-1959, 1:253,440 scale (1 inch to Four Miles).

Tipper, H.W. (1963): Geology, Taseko Lakes, British Columbia, 92O; *Geological Survey of Canada,* Map 29-1963, 1:253,440 scale (1 inch to Four Miles).

Tipper, H.W. (1962): Nechako River map area, British Columbia; *Geological Survey of Canada,* Map 1131A, 1:253,440 scale (1 inch to Four Miles).

Tipper, H.W. (1963): Nechako River map-area, British Columbia; *Geological Survey of Canada*, Memoir 324, 59 pages.

Tipper, H.W. (1969): Geology, Anahim Lake, British Columbia, *Geological Survey of Canada,* Map 1202A, 1:253,440 scale (1 inch to Four Miles).

Tipper, H.W. (1978): Taseko Lakes (92O) map area; *Geological Survey of Canada,* Open File 534, 1:125,000 scale.

Travers, W.H. (1978): Overturned Nicola and Ashcroft Strata and their relation to the Cache Creek Group, Southwestern Intermontane Belt, British Columbia; *Canadian Journal of Earth Science,* Volume 15, pages 99-116.

Umhoefer, P.J. and Tipper, H.W. (1998): Stratigraphy, depositional environment, and tectonic setting of the Upper Triassic to Middle Jurassic rocks of the Chilcotin Ranges, southwestern British Columbia; *Geological Survey of Canada*, Bulletin 519, 58 pages.

Umhoefer, P. J., Schiarizza, P. and Robinson, M. (2002): Relay Mountain Group, Tyaughton-Methow basin, southwest British Columbia: a major Middle Jurassic to Early Cretaceous terrane overlap assemblage; *Canadian Journal of Earth Sciences*, Vol. 39, pages 1143-1167.

Williams, E.P. (1959): Geological Investigations, Redstone Project, British Columbia, Hudson's Bay Oil and Gas Company Limited, *B.C. Ministry of Energy, Mines and Petroleum Resources* Geological Report 828, 5 pages.

SUPPORTING EVIDENCE FOR A CONFORMABLE SOUTHERN CONTACT OF THE BOWSER LAKE AND SKEENA GROUPS

Gareth T. Smith[1] and Peter S. Mustard[1]

ABSTRACT

New geological mapping in the Hazelton and immediately adjacent map areas has clarified both Bowser Lake Group (BLG) stratigraphy in this area and the relationship of this strata to the overlying Early Cretaceous Skeena Group. The upper unit of the BLG in this area comprises a sandstone-dominated, shallow-marine succession, which can be lithostratigraphically correlated to the well-documented Muskaboo Creek assemblage in the central and northern Bowser Basin. In three widely separate geographic locations, this shallow-marine succession gradationally changes upward into a non-marine unit that has previously been considered to be a stratigraphic unit either of the Cretaceous Skeena Group or undivided Bowser/Skeena strata. These new sections confirm our previous hypothesis that the Skeena Group gradationally overlies the Bowser Lake Group and represents a southern non-marine component of an originally contiguous Jura-Cretaceous Bowser Basin.

KEYWORDS: Sedimentology, stratigraphy, Muskaboo Creek Assemblage, Skeena Group, Bowser Lake Group, Cretaceous, Jurassic

INTRODUCTION

Recent efforts have been made by the BC Ministry of Energy and Mines (BCMEM) and the Geological Survey of Canada (GSC) to improve the structural and geological knowledge of the Jurassic-Cretaceous Bowser Basin of northeast BC (Figure 1) as well as to assess its integrated petroleum resource potential (Hayes *et al*., 2004, Evenchick *et al*., 2003). During the summers of 2004 and 2005, this research focused on the southern and central parts of the extensive Bowser Basin NTS map sheets 93M and 104A (summarized in Ferri *et al*., 2005, Evenchick *et al*., 2005, 2006 respectively).

The Bowser Lake Group (BLG) consists of sedimentary rocks of late Middle Jurassic to "mid" Cretaceous age and is the oldest of the three major stratigraphic successions that comprise the Bowser Basin and related sedimentary rocks (Figure 2). The southernmost region of the BLG in the Hazelton map sheet (NTS sheet 93M) is dominated by shallow-marine siliciclastics, which on extant geological maps are defined as "undivided Bowser Lake Group" (*e.g*., Richards, 1990). Outcropping south of the BLG, a second stratigraphic succession of Lower to Upper Cretaceous rocks is generally termed the Skeena Group (SG). This unit has been interpreted to record predominantly non-marine fluvial/floodplain and shallow-marine environments with localized volcanic influence (*e.g*., Basset, 1995; Bassett and Kleinspehn 1997). The stratigraphic relationship between the undivided BLG and the non-marine sedimentary rocks of the Skeena Group in the southernmost region of the Bowser Basin remains unclear. Previous workers have suggested that the contact is unconformable or a fault contact (Tipper and Richards, 1976) or that the Skeena Group sediments represent the Cretaceous continuation of Bowser Basin deposition (Bassett and Kleinspehn 1997). Ferri *et al*. (2005) summarize previous studies in this area and the complex evolution of stratigraphic terms involving the stratigraphy now termed "Skeena Group" and "Bowser Lake Group" in this region.

PROJECT GOALS

This project characterizes the shallow-marine siliciclastic unit, which appears to be the uppermost stratigraphic unit of the BLG within the Hazelton map area and immediately adjacent regions. The project's aim is to describe this unit in terms of its sedimentological make-up and depositional history. Ultimately this unit will be compared to previous studies of similar lithostratigraphic units in the BLG and Skeena Group in order to discern whether they are correlative. A second major goal of this project is to more clearly define and differentiate the nature of the BLG contact with the overlying Skeena Group.

WORK TO DATE

Much of the initial part of this project involved assisting in the regional mapping of the west half of the Hazelton map area to define local and regional stratigraphic relationships as well as to view the lateral variance of the undivided BLG and their regional interrelationships (summarized in Ferri *et al.*, 2005).

[1]Department of Earth Sciences, Simon Fraser University, Burnaby, BC, V5A 1S6

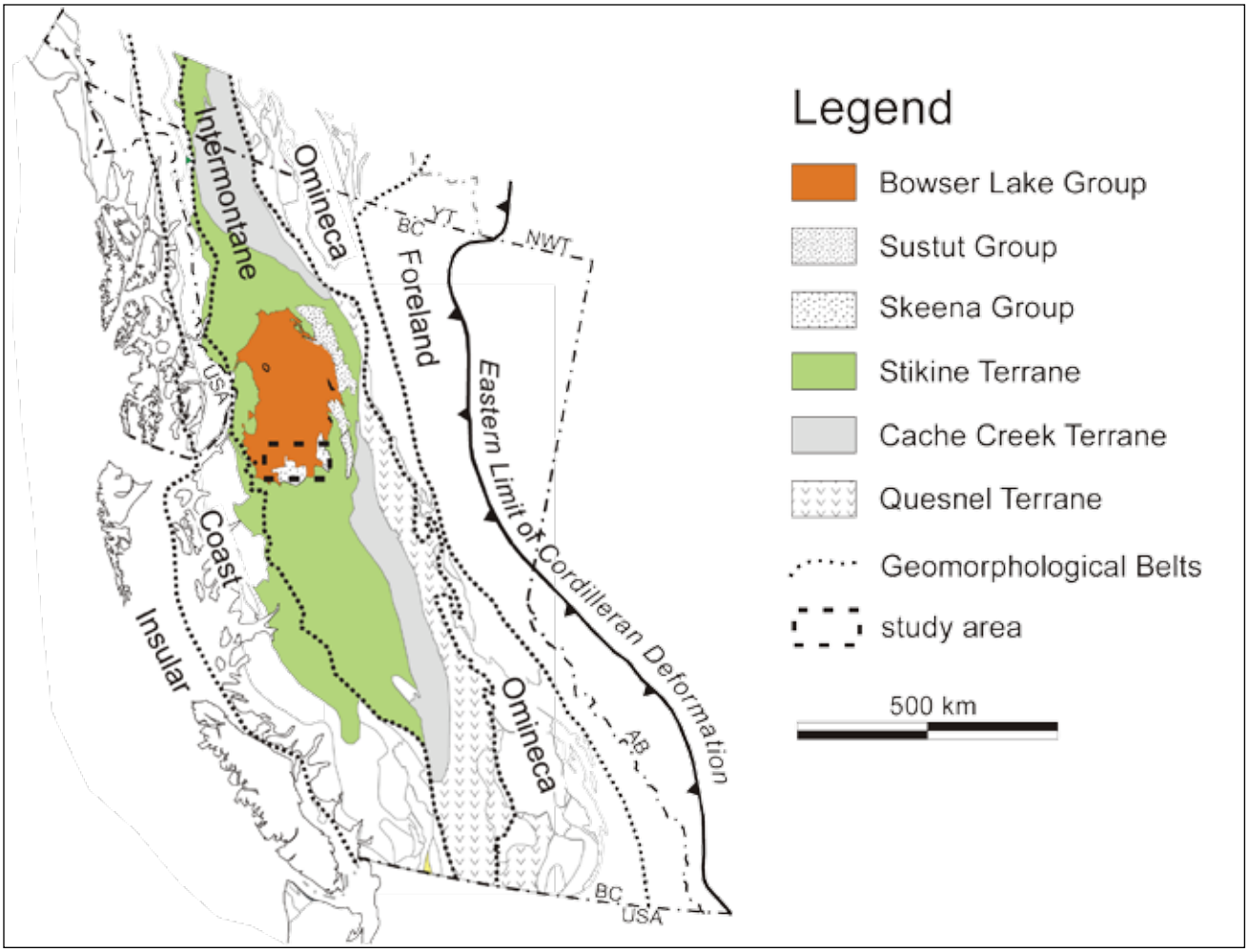

Figure 1. Location of the Bowser, Sustut, and Skeena groups within the geological framework of the Canadian Cordillera. Outlined box represents area of investigation during the 2005 field season (modified from Ferri *et al.,* 2005 and Evenchick *et al.*, 2003).

Mapping in the summer of 2005 continued into the eastern Hazelton map area (93M topographic sheet), with regional examinations extending west into the Nass River map area (103P topographic sheet). New results are summarized in Evenchick *et al.*, 2006).

In conjunction with (and, in part, as a result of) the geological mapping, eight stratigraphic section localities were chosen in 2004 (see Smith and Mustard, 2005), and two new sections identified in 2005. Our selection of the localities was limited to areas that were previously mapped as undivided Bowser Lake Group or Skeena Group or that have been mapped to show transitional characteristics from possible BLG into Skeena Group. These selections were made as a result of the new geological mapping and with reference to previous work documented by Bassett (1995) and Tipper and Richards (1976).

In like manner for the 2004 sections, each 2005 location entailed the construction of a detailed measured stratigraphic section. In the majority of cases, a basal contact was not identified, and therefore measurement began from the clearest exposed surface; thus these sections do not represent the total thickness of the stratigraphic unit. Each measured section comprises a detailed lithostratigraphic description, identification of primary sedimentary structures and internal gradational relationships, and inference of depositional nature. Suitable hand samples were taken at each site to permit petrographic identification and thin-section analysis; also taken were maturation and palynology samples from the more carbonaceous layers to assist in age determinations and reservoir potential.

Smith and Mustard (2005) concluded that shallow-marine strata of the Hazelton map area correspond to the Muskaboo Creek assemblage of the Bowser Lake Group, as described in more northern occurrences. It was also determined that at one locality the shallow-marine succession changes upward across a transitional contact into non-marine strata typical of lower Skeena Group as described by previous workers. It was suggested that this conformable relationship might be typical for much of this southern margin of the known extent of the Bowser Lake Group. During

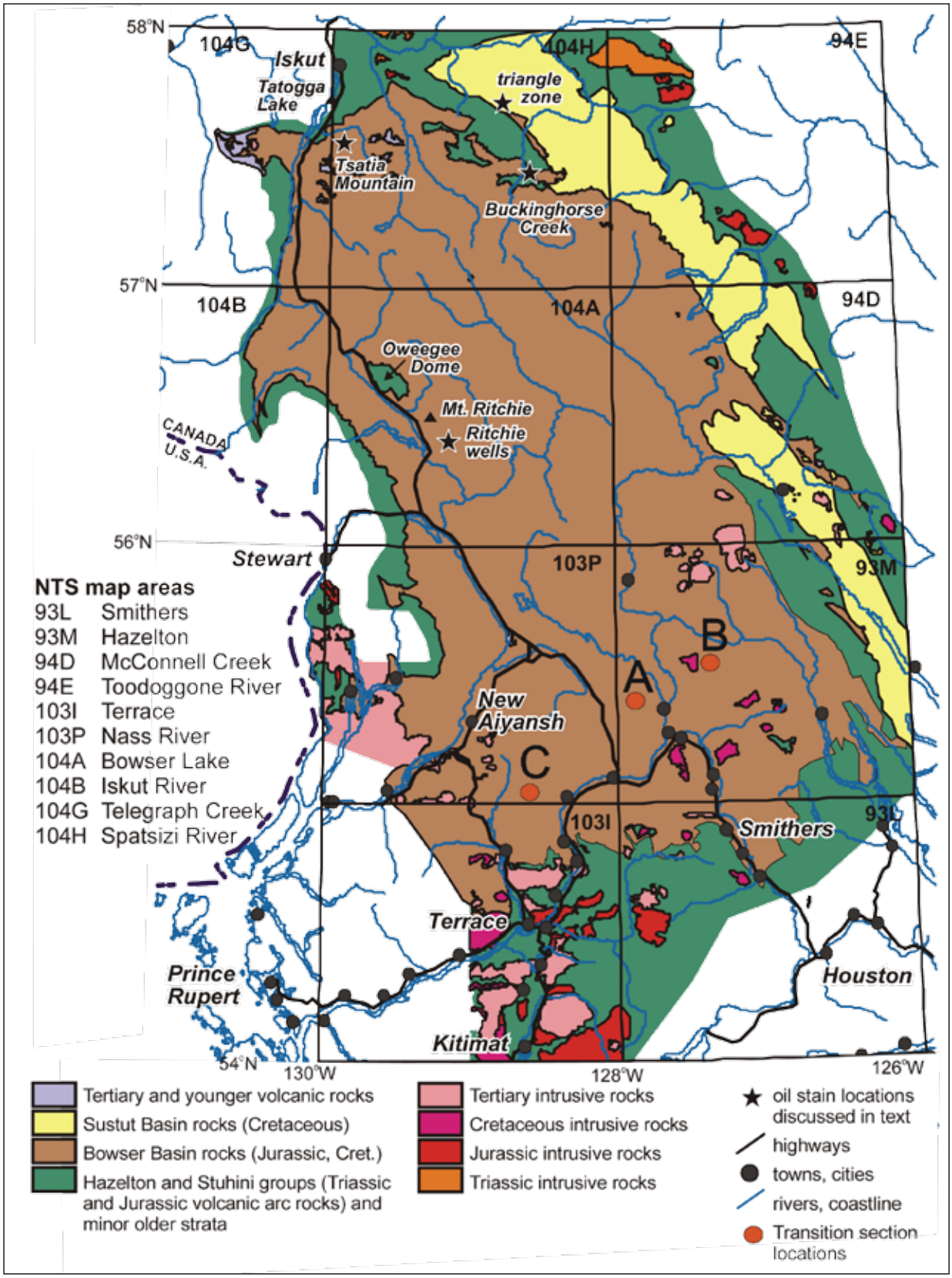

Figure 2. General geology of the Bowser Basin region, showing the location of measured sections B and C, described in this paper. Section A was described in Smith and Mustard (2005). Main figure modified from Ferri *et al*. (2005) and Evenchick *et al*. (2003).

2005, examination of both shallow-marine BLG and lower Skeena Group strata continued in eastern Hazelton map area and southeast Nass River map area. Two new examples of a gradational contact between these units were identified and measured in detail, as described below and located on Figure 2.

NEW EXAMPLES OF GRADATIONAL BOWSER-SKEENA TRANSITION

As part of general field mapping during the summer of 2005, two new examples of a marine to non-marine transition were identified from lithofacies of the Muskaboo Creek assemblage that are overlain by typical lower Skeena Group (Figure 2, localities B and C). Detailed measured sections characterize these contact relationships (Figures 4 and 5, with a common legend shown in Figure 3). These stratigraphic sections are significant not only because they provide additional examples of what appears to be a conformable BLG– Skeena Group contact but also because they suggest that this contact is geographically widespread. They also illustrate slightly different shoreline depositional environments along this transition compared to that documented in 2004 (Smith and Mustard, 2005).

At the eastern example of this transitional contact (Figure 4 and locality B on Figure 2), the lowest part of the stratigraphy consists of sandstone and mudstone, generally typical of the Muskaboo Creek assemblage. This includes both trough and hummocky cross-stratified, medium-grained sandstone bedsets up to 2 m thick (Figure 4B, D.). Stacked repetitions of these bedsets are intercalated with wavy rippled sandstone and mudstone, in some places including heterolithic sandstone-mudstone flaser or lenticular composite bedsets. Trace fossils are somewhat rare in this succession but include vertical and horizontal simple ichnogenera including *Skolithos* and *Ophiomorpa* and possibly some poorly preserved *Diplocrateron*. In addition, the lower part of the section includes a few metres of repeated intervals of normally graded, fine-grained sandstone to mudstone couplets, each a few centimetres to, at most, 5 cm thick (Figure 4C). These appear to be stacked, thin turbidites (mostly Bouma ABE divisions) and are somewhat unusual compared to typical Muskaboo Creek assemblage lithofacies.

The transitional zone identified at this section occurs over approximately 60 m of vertical section. Characteristic cycles within this transition consist of wave-dominated sandstone units, intercalated with laminated marine siltstone and periodically truncated by trough cross-stratified sandstone with abundant rip-up clasts and large plant and wood fragments. These latter channelized units appear to progressively fine upwards into silty mudstone and plant-rich sandstone packages, gradationally overlain by ever-thinning units of interlaminated sandstone and siltstone.

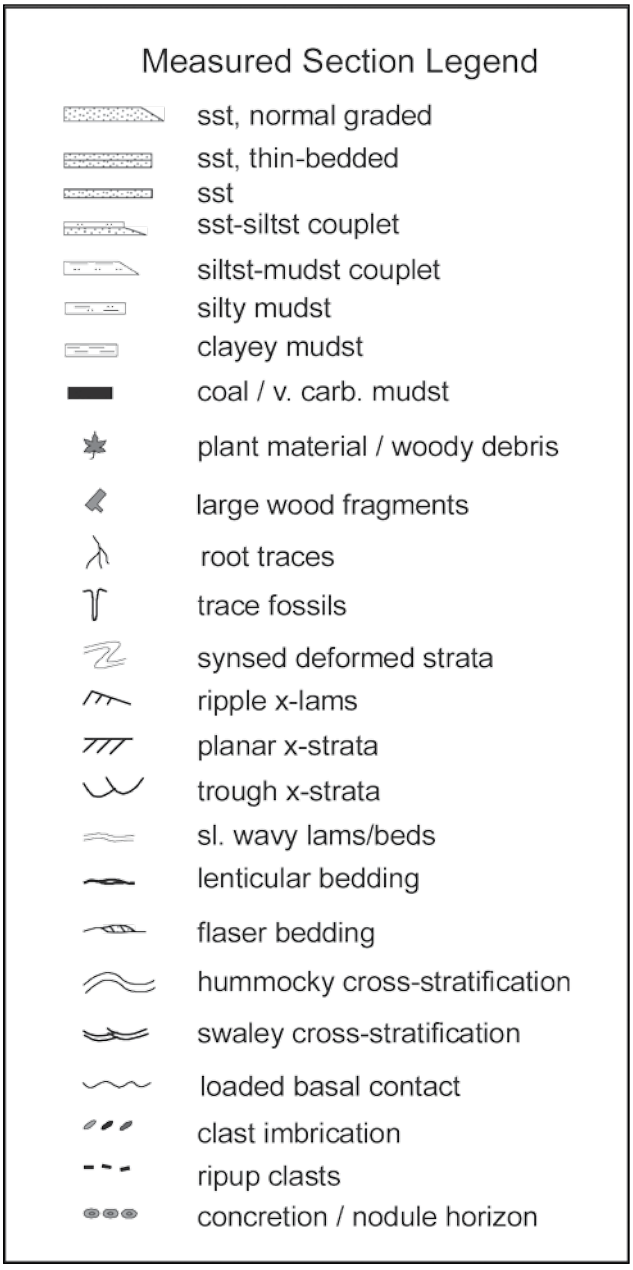

Figure 3. Legend of rock patterns and sedimentary structures common for the measured sections of Figures 4 and 5.

In the upper part of this transitional zone is an uncharacteristically thick (approximately 6 m) section of heavily reworked, wave-rippled, heterolithic sandstone-siltstone. This package, possibly indicative of reworked deltaic bottomset turbidites, marks the last visible, marine-dominated cycle in this transitional zone.

At approximately 134 m in the measured section, a very coarse granular sandstone body, rich in woody debris and rip-up clasts, is preserved—a lithofacies typical of the lower Skeena Group Buckley Canyon Formation as defined by Bassett and Kleinspehn (1997). Above this succession, four repeated cycles of fining-upward, clast-rich channel

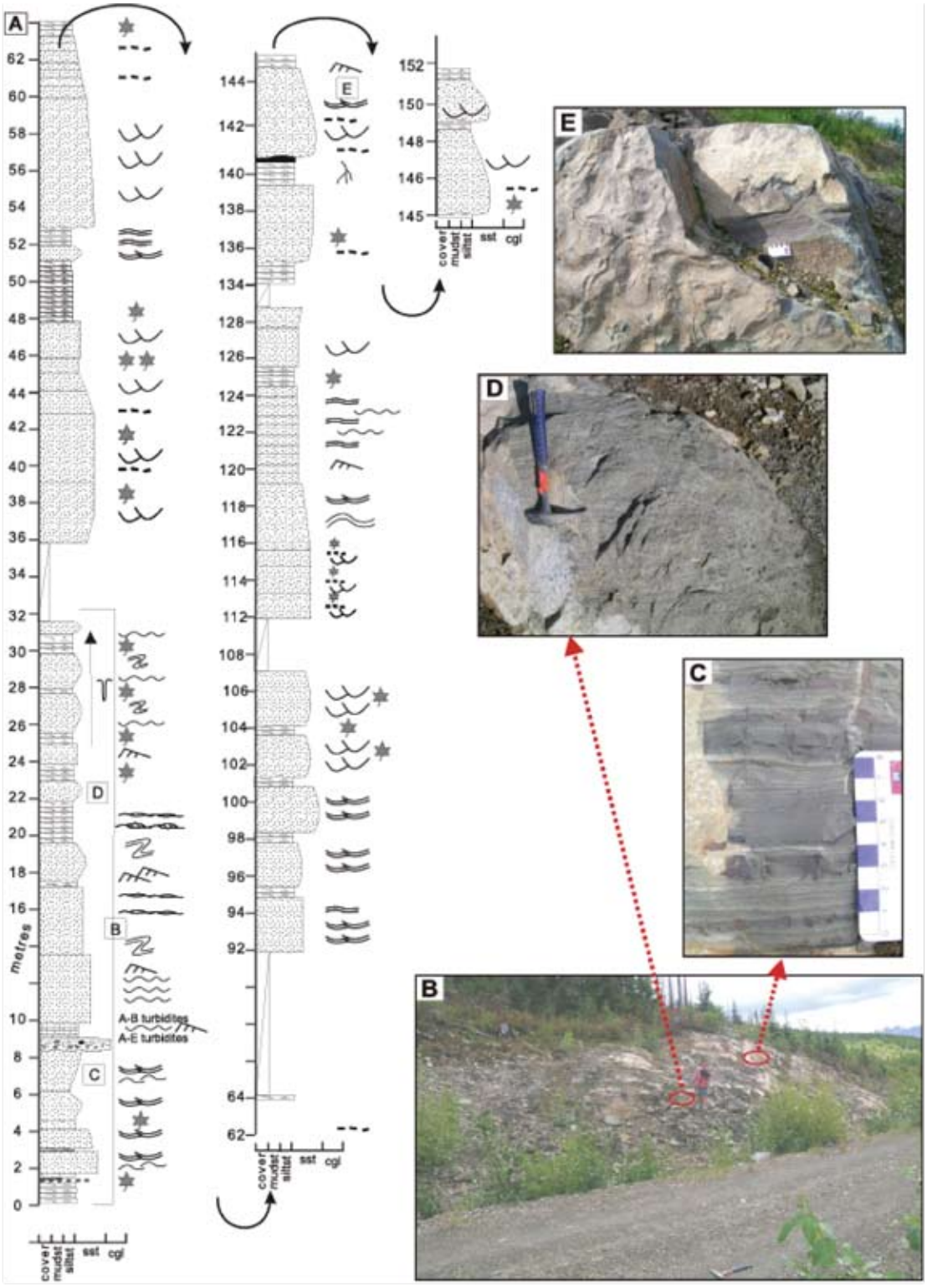

Figure 4. A. Measured section C in the east Hazelton map area; located on Figure 2. Photos B to E are located on the measured section. B. Overview of lower 30+ m of section, dominated by cross-stratified sandstone typical of Muskaboo Creek assemblage C. Rare repeated thinly bedded sandstones and mudstones showing good normal grading, are interpreted as delta bottomset turbidites in areas not reworked by high-energy shoreface waves. D. Cross-stratified sandstone typical of much of the lower part of this section. E. Thick sandstone bedset with irregular basal contact erosive into underlying coaly sandstones, contains common mudstone rip-up clasts and plant fragments, including large wood fragments (directly above scale bar), passing upward into current rippled sandstone (highest bed plane on left side of photo).

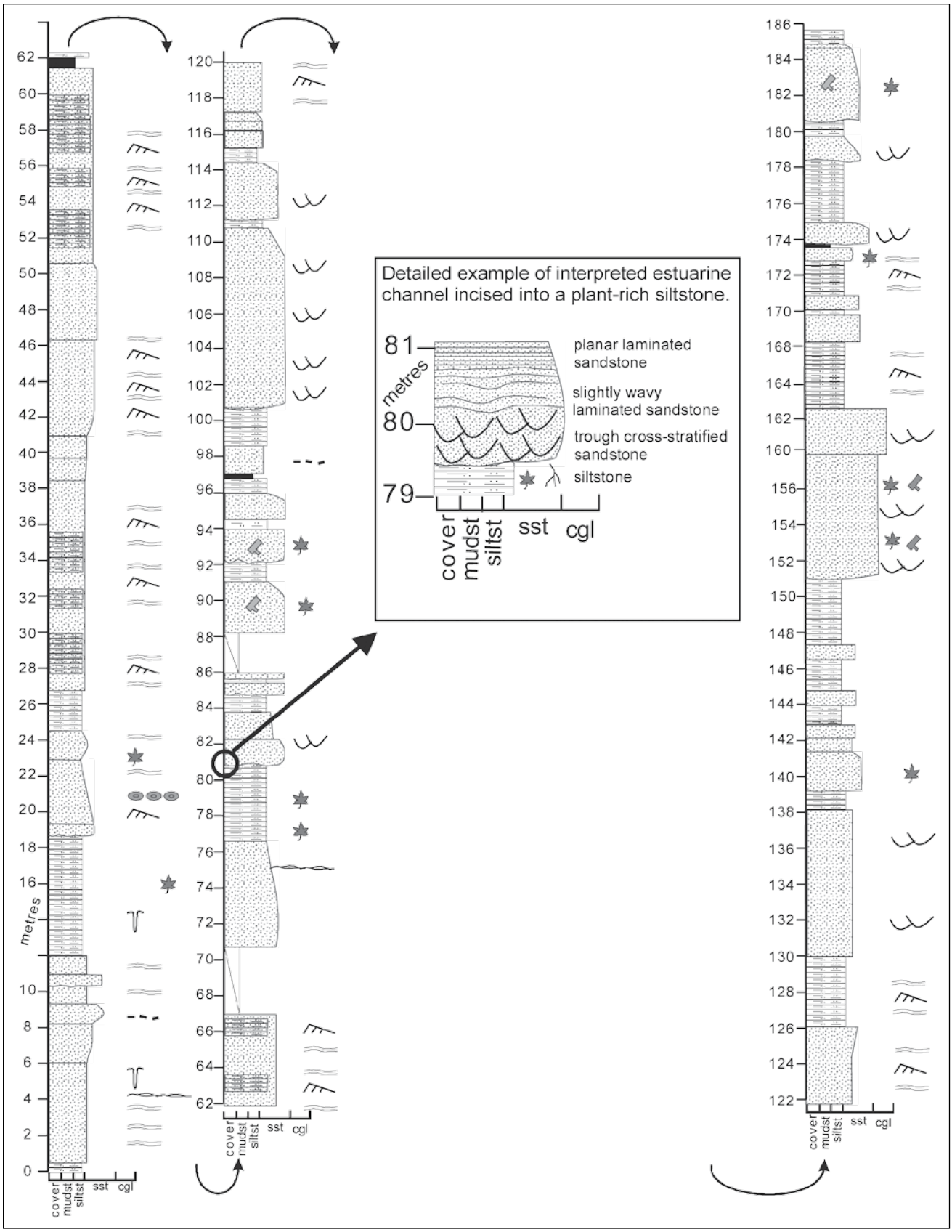

Figure 5. Measured section A in Nass River map area; located on Figure 2. Photographs from this measured section are shown in Figure 6.

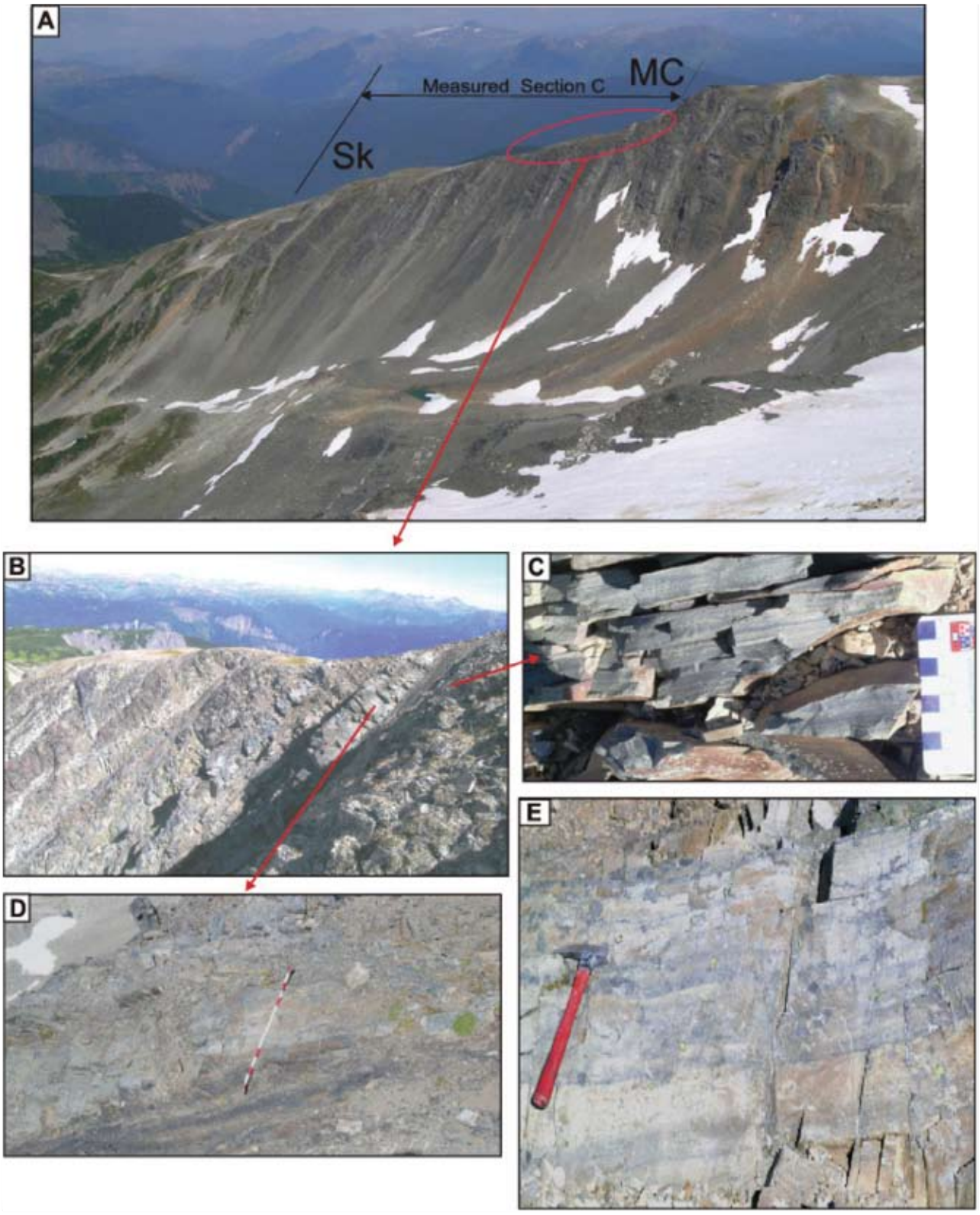

Figure 6. Measured section C photographs: A. Overview of the entire measured section from right to left (south to north). MC = Muskaboo Creek assemblage; Sk = lower Skeena Group strata. B. Approximately lower 50 m of section, dominated by sandstone bedsets with marine indicators, which we interpret as the upper part of the Muskaboo Creek assemblage. C. Fine-grained, laminated wavy sandstone to heterolithic sandstones and mudstones of the Muskaboo Creek assemblage. D. Plant-rich silty mudstones overlain across an erosive contact by fining upward sandstones, as shown in expanded part of section C at 79-81 metres. E. Wavy- to current-rippled sandstone within the transitional interval of the section.

sandstones fine into mudstones and carbonaceous coal horizons. The initiation of each cycle is marked by extensive incision into the uppermost carbonaceous unit. These cyclic events are indicative of the repeated meanderings of a fluvial channel. More of these fluvial cycles are preserved in outcrops overlying the top of the 152 m thick measured section, and no further evidence of marine conditions are preserved in this area. This suggests that the transitional marine to non-marine change documented in this section represents a regional gradational contact between the two lithostratigraphic units.

The depositional environments represented by this section appear to be indicative of a marine shoreline with high energy, wave-dominated shoreface successions with minor deltaic input, passing upward to a non-marine setting dominated by small river channel systems. In the lower part of the section the dominance of higher energy open shoreface structures (trough and hummocky cross-stratified sandstone) is typical of Muskaboo Creek assemblage elsewhere in the Bowser Lake Group. Less typical of the Muskaboo Creek is the presence of a few examples of fine-grained sandstone to mudstone turbidites, in some examples well-preserved over a few metres thickness (Figure 4C) but in others slightly reworked into more heterolithic thinly bedded sandstone-mudstone composite bedsets. We interpret these as remnants of small deltaic bottomset deposits (perhaps representing small protruding fluvial-dominated delta successions) that have been largely reworked by strong wave action into shoreface sand bodies, which by definition typically suggests a wave-dominated shoreline.

At the western example of this contact (Figure 5 and locality C on Figure 2), the lowest part of the stratigraphy consists of sandstone and siltstone, typical of the Muskaboo Creek assemblage. A thick succession of heterogeneous, laminated siltstones-sandstones and mudstones, exhibiting abundant wave ripples and lenticular stratification with little bioturbation, dominates the first 30 m of this section. This unit is overlain by an asymmetrical current-rippled, fining-upward sandstone body, with two large concretionary horizons, all capped by heavily rooted, muddy siltstone. This fining cycle occurs commonly within the Muskaboo Creek assemblage elsewhere and may be explained by the possible influence of an estuarine channel within an otherwise high-energy, shoreline-dominated succession. This typical mixed marine facies succession remains sedimentologically consistent for a considerable thickness (approximately 60 m).

The interval encompassing the transitional contact is poorly exposed in this section, occurring over a considerable vertical thickness (approximately 60 m) and with the unfortunate presence of abundant covered intervals. The general transitional nature is characterized by the first occurrence of repeated fining-upward successions, each a few metres thick, with bases of coarse-grained to granular, trough cross-stratified sandstones rich with plant and woody debris. These initial cycles are, in turn, overlain by wave-rippled sandstones and siltstones, locally including flaser bedding, with only minor bioturbation. Further upsection, these apparently cyclic fining-upward sandstone successions occur more commonly and as thicker bedsets (up to 10 m). Cycles are characterized by coarse-grained, debris-rich basal channel sandstones passing upward into rootlet-rich siltstones.

The depositional environment represented by this section appears to be one of a lower-energy marine shoreline succession (characterized by abundant heterolithic flaser-bedded and wave-rippled, fine- to medium-grained sandstone with a high silt percentage and a low abundance of trace fossils) grading upward into a non-marine area dominated by fluvial successions. Atypical of the upper Muskaboo Creek assemblage is the distinct lack of high-energy shoreface deposits, which could be explained by an estuarine influence in this area.

The progressive interfingering of marine to marginal-marine and fluvial successions is unusual, compared to the other examples of this transitional contact. Only in the top 30 m of the section do the strata consistently represent the typical lower Skeena Group fluvial successions. Stratigraphically above this section are several tens of metres of similar repeated, stacked fluvial cycles (not measured), suggesting the transitional change of the measured section does represent a regional contact from the upper Muskaboo Creek assemblage through a thick gradational transition into typical lower Skeena Group.

CONCLUSIONS AND CONTINUED STUDY

The evidence from the 2005 field season provides strong additional support to the preliminary conclusions summarized in Smith and Mustard (2005). Shallow marine facies of typical Bowser Lake Group Muskaboo Creek assemblage are widespread in the study area, including both the eastern Hazelton map area and southeast Nass River map area. In addition, two new examples of a gradational contact from the marine Muskaboo Creek assemblage upward into non-marine strata typical of the lower Skeena Group were identified. These transitions are geographically widely separated both from each other and from the original example documented in Smith and Mustard (2005). This suggests that a conformable Bowser-Skeena contact exists across an extensive area of the southern limit of strata, previously interpreted as Bowser Lake Group or a Bowser-Skeena undivided map unit. Age controls that will support this conclusion may be provided by analysis of abundant palynology samples and several isotope geochemistry samples from above and below the suggested transitional contact. If the widely separated contacts prove to be of similar age, this suggests a geographically extensive south-

ern shoreline for the Bowser Basin at this time, and one in which major river systems do not appear to be dominating the sedimentation patterns.

ACKNOWLEDGEMENTS

Logistical support and advice during the 2005 field season was provided by Carol Evenchick of the Geological Survey of Canada. Filippo Ferri of the BC Resource Development and Geoscience Branch also provided helpful advice. We are grateful to John Waldron from the University of Alberta, who during regional mapping first recognized the significance of the transitional change in lithofacies in the east part of the Hazelton map area, which we later measured as section B. We thank James MacEachern for a constructive review of the manuscript. This project was directly supported by grants to Mustard from the B.C. Ministry of Energy and Mines (Grant ca80405002) and NSERC (Grant 184290).

REFERENCES

Bassett, K.N. (1995): A basin analysis of the Lower to mid-Cretaceous Skeena Group, west-central British Columbia: implications for regional tectonics and terrane accretion; *Ph.D. Thesis,* Volume 1, pages 1-200.

Bassett, K.N. and Kleinspehn, K.L. (1997): Early to middle Cretaceous paleogeography of north-central British Columbia: stratigraphy and basin analysis of the Skeena Group; *Canadian Journal of Earth Sciences,* Volume 34, pages 164–1669.

Evenchick, C.A. and the Bowser Project Team (2006): The Bowser / Sustut project: Introduction, overview of project status, and highlights of recent research; Bowser Project workshop (BC Intermontane workshop), Feb.21, 2006, Calgary, AB.

Evenchick, C.A. and Thorkelson, D.J. (2005): Geology of the Spatsizi River map area, north-central British Columbia; *Geological Survey of Canada*, Bulletin 577, 288 pages, includes A-series maps 2028A - 2039A.

Evenchick, C.A., Ferri, F., Mustard, P.S., McMechan, M., Osadetz, K.G., Stasuik, L., Wilson, N.S.F., Hadlari, T. and McNicoll, V.J. (2003): Recent results and activities of the integrated petroleum resource potential and geoscience studies of the Bowser and Sustut basins project, British Columbia; Current Research*, Geological Survey of Canada,* Volume 2003-A13, pages 1-11.

Ferri, F., Mustard, P., McMechean, M., Ritcey, D., Smith, G., Evenchick, C. and Boddy, M. (2005): Skeena and Bowser Lake groups, west half Hazelton map area (93M): Resource Development and Geoscience Branch*, British Columbia Ministry of Energy and Mines,* Summary of Activities 2005, pages 113 – 131.

Hayes, M., Ferri, F. and Morii, S. (2004): Interior Basins Strategy; Resource Development and Geoscience Branch, *British Columbia Ministry of Energy and Mines,* Summary of Activities 2004, pages 69-71.

Richards, T.A. (1990): Geology of Hazleton map area (93M); *Geological Survey of Canada,* Open File 2322.

Smith, G.T. and Mustard, P.S. (2005): The Southern Contact of the Bowser Lake and Skeena Groups: Unconformity or Transition? Resource Development and Geoscience Branch*, British Columbia Ministry of Energy and Mines*, Summary of Activities 2005, pages 152-156.

Tipper, H.W. and Richards, T.A. (1976): Jurassic stratigraphy and history of North-central British Columbia; *Geological Survey of Canada,* Bulletin 270, pages 1-73.

A DISCUSSION ON CORRECTION OF GAS CONTENTS TO MINERAL–MATTER-FREE BASIS USING SPECIFIC GRAVITY DATA

Barry Ryan[1]

ABSTRACT

This note discusses an alternative way of correcting gas content data to a uniform base. Often data are corrected to a dry ash-free base, but this introduces errors proportional to the ash content of the original sample. It is much better to correct data to a mineral-matter-free basis (mmfb), however this is perceived as being more difficult or costly in terms of analyses. The use of density data or an ash-versus-gas plot can provide the basis for making the mmf correction.

KEYWORDS: Specific gravity, coal, mineral-matter-free, gas content, air-dried basis, coalbed gas

INTRODUCTION

Coalbed gas, CBG (also referred to as coalbed methane, CBM) resource and reserve calculations are usually made using gas content and in situ density values (or specific gravity, SG). The SG values are calculated using the as-received ash contents and by making the assumption that the measured equilibrium moisture value is the same as in situ moisture. There are a number of papers that discuss methodology and pitfalls of this approach (Mavor *et al.,* 1996). However, for comparative purposes, gas content data are often normalized to a constant base, being either dry ash-free (daf) or dry mineral-matter-free (dmmf), before plotting onto a depth- or pressure-versus-gas-ontent diagram. This allows data to be compared to a single isotherm and estimates made of the relative degree of gas saturation of the various samples. However, correcting samples with varying ash contents to a common base often introduces errors that may make the plot misleading.

The daf calculation is simple, requiring only ash and moisture analyses, but it can be deceptive if it is applied to samples with a wide range of ash contents. Ash content is not the same as mineral matter content and usually the weight loss (WTLOS) ratio of "weight of original mineral matter" / "weight of ash after combustion" varies from 1 (mineral matter = 100% quartz) to over 1.2 (high carbonate content in mineral matter). If the WTLOS ratio is known, then it is a simple matter to calculate the theoretical value of gas content for a mineral-matter-free sample. The underlying assumption that WTLOS is constant for samples of varying ash and maceral content is probably not valid and represents an approximation. If base/acid ratios (obtained from an oxide analysis of the ash) correlate with ash content then this probably means that the WTLOS ratio is also changing with ash content.

If the mineral-matter-free (mmfb) correction uses the Parr Equation (mineral matter = 1.08* ash+0.55* sulphur), then it requires ash and sulphur analyses. This correction is better than the daf correction but assumes constant mineral matter chemistry and consequently does not reflect changes from sample to sample nor project to project. Many laboratories measure sulphur contents and use the Parr Equation to derive gas contents on a mineral-matter-free basis. The equation actually assumes that a constant amount of pyritic sulphur in coal is converted to ferric oxide (remains in ash) and a constant amount of sulphur dioxide is lost to the atmosphere.

It is possible to use an alternative approach in some situations. This requires a data suite with a range of ash contents and measurement of the air-dried specific gravity (ASG) of each sample. The relationship of ASG to ash has the form

ASG=1/(A-B*ash) (1) (Ryan, 1991),

which can also be expressed as

1/ASG=A-B*ash (2)

The constant A= 1/(density for zero-ash coal, DC)

The constant B incorporates the density of rock (DMM) and the WTLOS ratio

B slope=(DMM-DC)/(DMM*DC)*WTLOS

It is not possible using the constants A and B to derive a unique solution for WTLOS but it is possible to derive a number of possible pair solution of WTLOS and DMM from which the most realistic pair can be selected.

Data (Figure 1) from a project provide an estimate of WTLOS of 1.15. Using this value, it is simple to correct all the ash adb values to equivalent mineral-matter-content values and then to derive gas contents on a mineral-matter-free basis (gas mmfb = gas db/[1-ash db*WTLOS]).

[1]Resource Development and Geoscience Branch, BC Ministry of Energy, Mines and Petroleum Resources, PO Box 9323, Stn Prov Govt, Victoria, BC, V8W 9N3

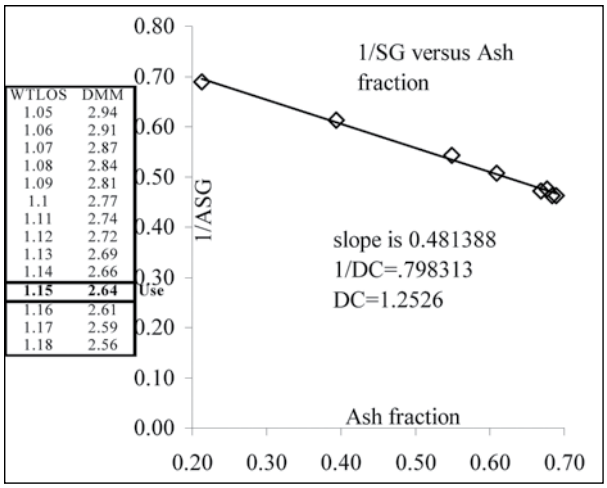

Figure 1. Plot of actual data to determine SG pure coal (DC), SG mineral matter (DMM), and WTLOS ratio.

If all samples from a project are gas-saturated, then after correcting gas contents to a mmf basis, all samples should have the same gas content. This will not be the case if the samples are corrected to a daf basis. As a demonstration, a theoretical sample suite, with samples all having a gas content of 10 cc/g mmfb and ash having a WTLOS ratio of 1.15, is plotted in Figure 2.

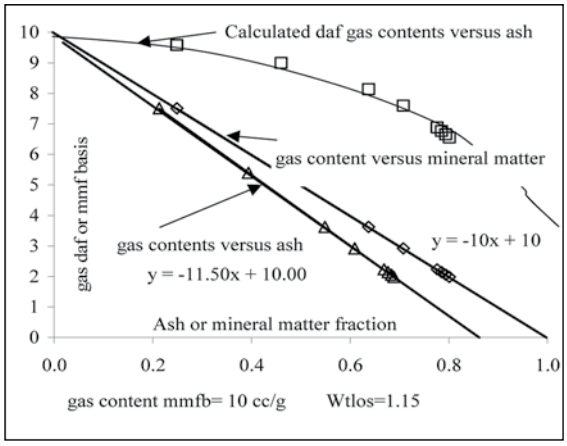

Figure 2. Theoretical data plot of gas content daf *versus* ash and gas content *versus* mineral matter.

The plot of gas content daf basis *versus* ash content indicates that the error introduced increases as one corrects for higher ash contents. Samples with higher ash contents after correction to a daf basis will appear to be under-saturated compared to samples with lower ash contents. The line *gas content versus mineral matter* projects to 100% mineral matter at zero gas content and has a slope of (- gas content mmfb). The slope of the line *gas content versus ash* is (- gas content mmfb x WTLOS) and the line intersects the x axis at 1/WTLOS * 100. This may provide another way of deriving the value of WTLOS and making mmf corrections to gas-content data.

Often, variation in petrography with increased vitrinite content in low-ash samples causes an increase in gas content mmfb for low-ash samples, and the line *gas content versus ash* has a bend at low ash contents with an increase in slope for low-ash samples.

The SG equation (Figure 3**)** can provide values of in situ SG if a suite of ASG data is used to solve for DC, DMM, and WTLOS. This is most easily done using the 1/ASG=A-B*ash relationship and the linear plot. It is then possible to estimate in situ SG based on assumptions of free-water content and void porosity. Varying free-water contents and void porosity volumes can provide better estimates of in situ SG to be used in CBM resource or reserve calculations.

The measurement of ASG on coal particles, crushed to 60 mesh and air-dried, provides a measure of SG for samples with all free water and fracture porosity removed. On the other hand, measurements of in situ SG using geophysical logs provide estimates of SG with free moisture and fracture porosity present. The difference between the two measurements provides information about the fracture porosity based on assumptions of water content (Figure 4).

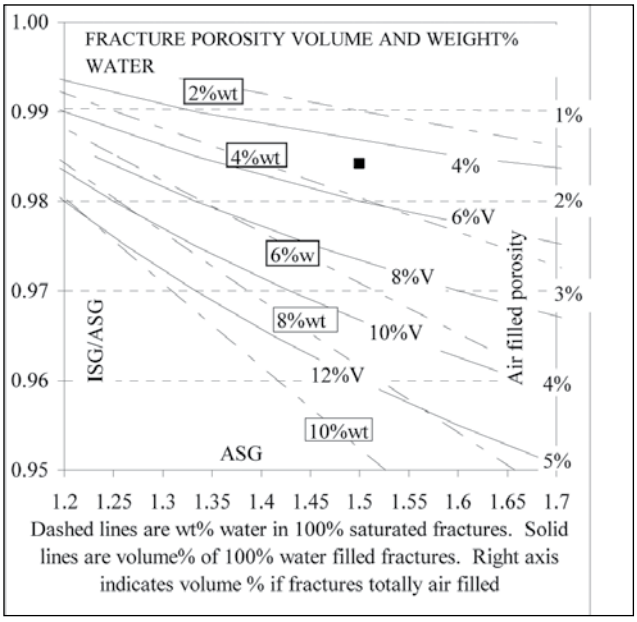

Figure 4. Calculation of fracture porosity using in situ and air-dried specific gravity.

Coal and gas-content data are calculated to various bases such as as-received, air-dried, and dry. Table 1 illustrates the way the various bases are calculated.

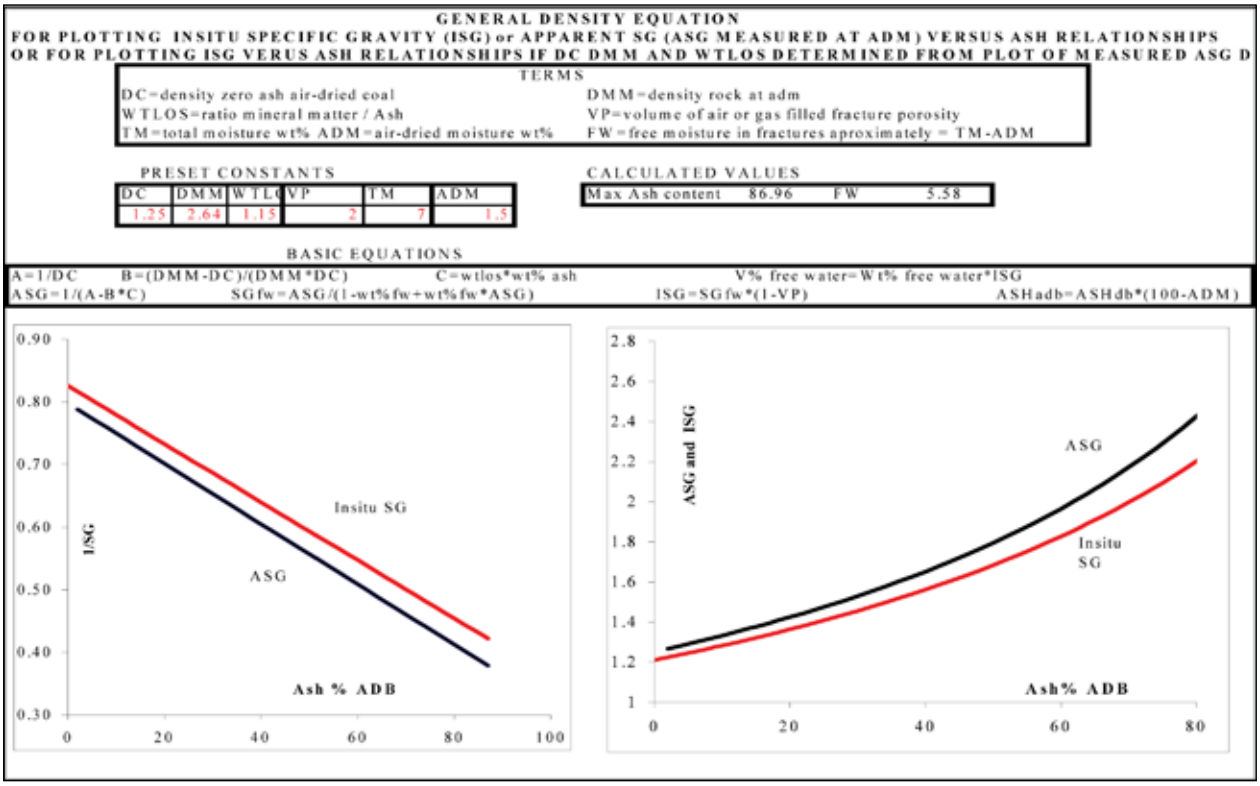

Figure 3. Equation for calculating SG at various water and porosity levels.

TABLE 1. CALCULATION OF MOISTURE CONTENTS AT DIFFERENT BASES.

It is very important to know how various water contents are calculated

Example calculations		enter	
Enter as-received weight	W1	115	
Enter weight after air drying	W2	102	
Enter weight after drying at 110 °C	W3	100	
Weight after heating air-dried sample to 750°C	W4	25	
Gas cc stp total	V	1000	
		result	**formula**
As-received moisture	ARM	**13.04**	(W1-W3)/W1
Air-dried loss	ADL	**11.30**	(W1-W2)/W1
Air-dried moisture	ADM	**1.96**	(W2-W3)/W2
Free moisture as % of total sample	FM	**11.30**	(W1-W2)/W1
Free moisture	FM	**11.30**	1-(1-ARM)/(1-ADM)
Ash content, air-dried basis (adb) %	A adb	**24.51**	W4/W2*100
Gas content, as-received basis (arb)	G arb	**8.70**	V/W1
Gas content, air-dried basis (adb)	G adb	**9.80**	V/W2
Gas content, dry basis (db)	G db	**10.00**	V/W3
Gas content, dry air-free (daf) basis	G daf	**13.33**	V/W3/(1-Aadb/(100-(W2-W3)/W2*100))
Gas content, dry air-free (daf) basis	G daf	**13.33**	Gadb/(100-Aadb-ADM)*100

CONCLUSIONS

When comparing gas-content data, it is important to understand how the data were normalized to a common base. Comparing gas data corrected to a daf basis when samples have a range of ash contents can be misleading. It is better to compare data on a mineral-matter-free basis, and there are various ways of making the calculation. One that is not regularly used involves measuring apparent specific gravity. This information is also very useful for estimating in situ SG when calculating reserves or resources.

If in situ and air-dried SG data are available, then it is possible to make some estimates of in situ fracture porosity, which is key to permeability.

REFERENCES

Mavor, M.J., Pratt, T.J., Nelson, C.R. and Casey, T.A. (1996): Improved gas-in-place determination for coal gas reservoirs; Paper SPE 35623, *Proceedings of SPE Gas Technology Symposium*.

Ryan, B.D. (1991): Density of Coals from the Telkwa Coal Property, Northwestern British Columbia (93L/11); *in* Geological Fieldwork 1990, *British Columbia Ministry of Energy, Mines and Petroleum Resources*, Paper 1991-1, pages 399-406.

Ryan, B.D. (1992): An Equation for Estimation of Maximum Coalbed Methane Resource Potential; *in* Geological Fieldwork 1991, *British Columbia Ministry of Energy, Mines and Petroleum Resources*, Paper 1992-1, pages 393-396.

Ryan, B.D. and Dawson, F.M. (1993): Coalbed Methane Canister Desorption Techniques; *in* Geological Fieldwork 1993, Grant, B. and Newell, J.M., Editors, *British Columbia Ministry of Energy, Mines and Petroleum Resources*, Paper 1994-1, pages 245-256.

Ryan, B.D. and Takkinen, M. (1999): In situ fracture porosity and specific gravity of highly sheared coals from southeast British Columbia (82G/7); *in* Geological Fieldwork 1999, *British Columbia Ministry of Energy and Mines*, Paper 2000-1, pages 359-372.

A DISCUSSION ON MOISTURE IN COAL: IMPLICATIONS FOR COALBED GAS AND COAL UTILIZATION

Barry Ryan[1]

ABSTRACT

There is a profusion of terms describing water in coal. The terms do not necessarily help in understanding the association of coal and water. Water isotherms provide the best way of indicating what component of total water in coal may interfere with gas adsorption. Most coals are saturated with water, but for coals that are under-saturated with water it is important to understand the interplay of water and gas adsorption within the coal.

KEYWORDS: Coal, equilibrium moisture, water isotherms, methane adsorption, fracture porosity, coal density

INTRODUCTION

This note summarizes existing data on moisture in coal and may make some new connections but does not add any new data; as such, it has no pretensions to be anything more than a useful summary.

Coal as an industry and as a science appears to alternately shine and fade over time rather than develop consistently and this has implications for those with persistent or long memories. There is a wealth of coal science literature, almost forgotten, that predates the development of the coal export market and the coalbed gas industry (coalbed methane, CBM). Much of the science, though conducted to answer questions of interest of the day, is still very useful today. This is true for a lot of the studies on coal moisture and coal surface characteristics, an understanding of which helps, for example, in attaining an in-depth understanding of methane isotherms. There are many other examples where this resource of older literature is very useful to understanding today's challenges.

MOISTURE, FRACTURE POROSITY, AND IN SITU SPECIFIC GRAVITY

Before discussing moisture in coal, it is important to make sure that the reader and writer are on the same page. There is a profusion of moisture terms, some of which are conceptual and some measurable. Some of these terms overlap and are probably redundant (Table 1). Total moisture in coal is broken down into a number of components with different significance (Figure 1).

The first moisture measurement made in a laboratory is the as-received moisture (ARM). This value can provide interesting information, based on how the fresh outcrop or core samples were collected and handled prior to arriving at the laboratory. Samples should be collected and placed in a sealed bag so that none of the as-received moisture is lost. Laboratories report as-received moisture and air-dried moisture; the percent difference of the two is nearly equivalent to the volume of water that was removed from the sample by air-drying (air-dried moisture loss). Because of the way as-received and air-dried moisture measurements are calculated in the laboratory, the percent of air-dried moisture loss (free moisture) is slightly more than the difference of the two measurements (Table 2). In some situations where the sample is not finely crushed coal, the free moisture is an estimate of water that fills fractures in the sample and can be expressed as fracture porosity, if the air-dried specific gravity (SG adb) of the sample is measured. Also it is possible to calculate the in situ SG using the SG adb and free-moisture content. The relationship between the moisture terms (as-received, air-dried moisture and air-dried moisture loss, fracture porosity, SG air-dried basis, and in situ SG) are depicted in Figure 2. In situ SG is essential for calculating in situ coal and gas resources.

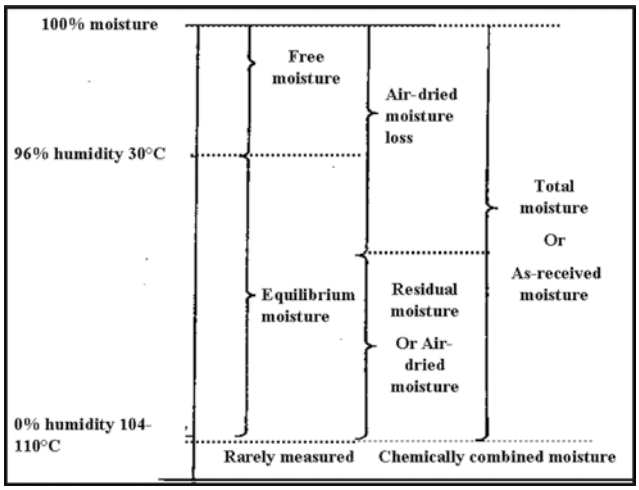

Figure 1. Moisture components in coal.

[1]Resource Development and Geoscience Branch, BC Ministry of Energy, Mines and Petroleum Resources, PO Box 9323, Stn Prov Govt, Victoria, BC, V8W 9N3

TABLE 1. SOME MOISTURE TERMS.

Name	Reality		Preferred or equivalent term
Equilibrium moisture	measured in lab	EQ	
Air-dried moisture	measured in lab	ADM	
Air-dried moisture loss	measured in lab	ADL	
As-received moisture	measured in lab	ARM	
Free moisture	conceptual	?	Surface moisture
Surface moisture	conceptual	?	
Total moisture	measured in lab	TM	As-received moisture
Inherent moisture	conceptual	IM	Air-dried moisture ?
Bed moisture	conceptual	?	Equilibrium moisture ?
Residual moisture	conceptual	RM	Air-dried moisture ?

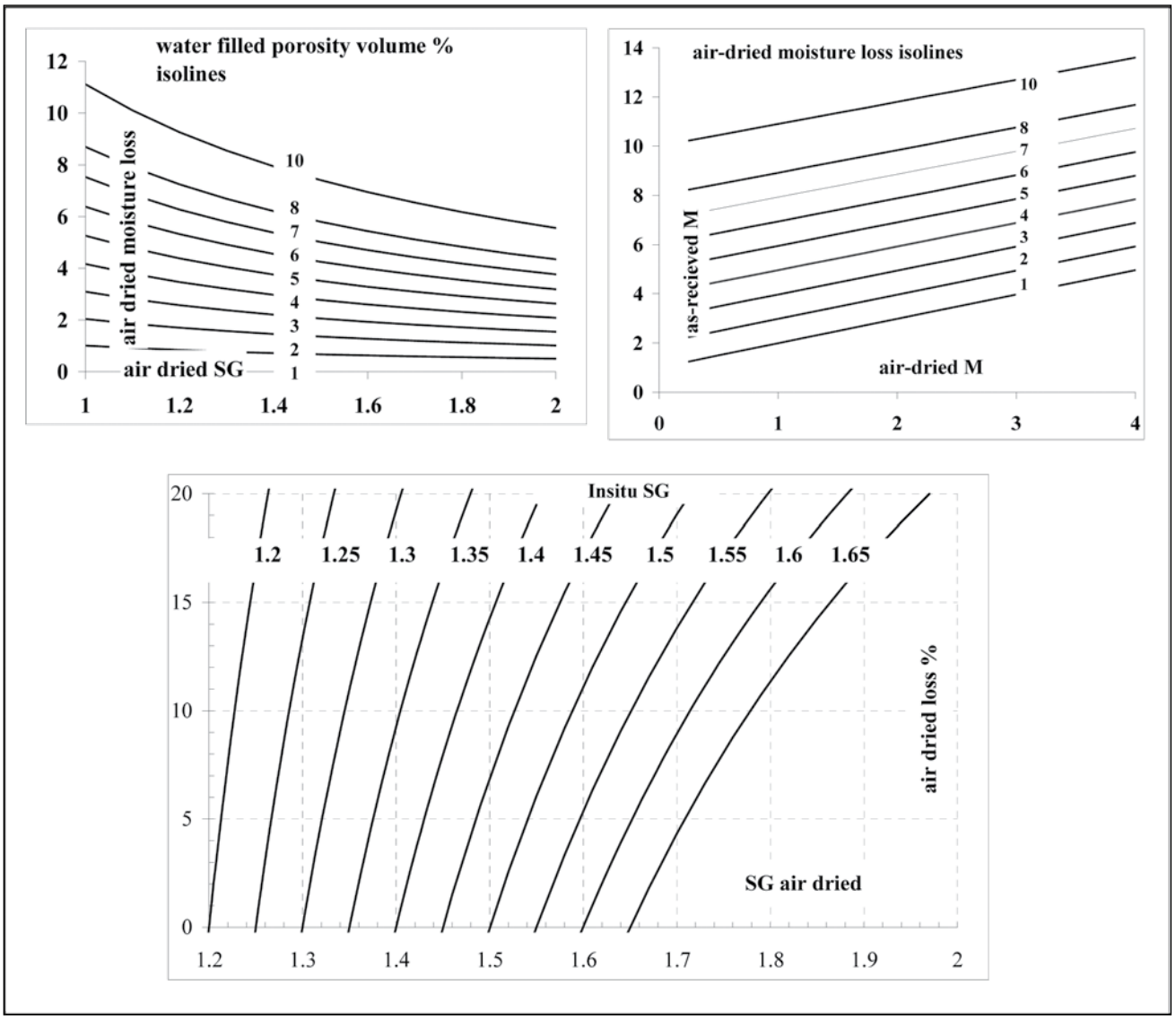

Figure 2. Relationship between measured moisture contents, SG air-dried basis, and in situ fracture porosity.

TABLE 2. CALCULATION OF GAS AND MOISTURE CONTENTS AT DIFFERENT BASES.

It is very important to know how various water contents are calculated.			
Example calculations		**enter**	
Enter as-received weight	W1	115	
Enter weight after air drying	W2	102	
Enter weight after drying at 110 °C	W3	100	
Weight after heating air-dried sample to 750°C	W4	25	
Gas cc stp total	V	1000	
		result	**formula**
As-received moisture	ARM	**13.04**	(W1-W3)/W1
Air-dried loss	ADL	**11.30**	(W1-W2)/W1
Air-dried moisture	ADM	**1.96**	(W2-W3)/W2
Free moisture as % of total sample	FM	**11.30**	(W1-W2)/W1
Free moisture	FM	**11.30**	1-(1-ARM)/(1-ADM)
Ash content, air-dried basis (adb) %	A adb	**24.51**	W4/W2*100
Gas content, as-received basis (arb)	G arb	**8.70**	V/W1
Gas content, air-dried basis (adb)	G adb	**9.80**	V/W2
Gas content, dry basis (db)	G db	**10.00**	V/W3
Gas content, dry ash-free (daf) basis	G daf	**13.33**	V/W3/{1-Aadb/[100-(W2-W3)/W2*100]}
Gas content, dry ash-free (daf) basis	G daf	**13.33**	Gadb/(100-Aadb-ADM)*100

The water that is dried off samples before measuring air-dried moisture contains total dissolved solids (TDS) that are precipitated onto coal surfaces during drying. It is possible to calculate the chemistry of TDS in the free water associated with the coal if a sample is weighed, air-dried to calculate weight of free water, and then soaked in a known volume of distilled water to re-dissolve the TDS. This may indicate the quality of water that might drain into an open-pit coal mine and may flag possible handling procedures. Based on sulphate contents, it can indicate the degree of oxidation of the associated coal. If samples are collected from depth, then the water chemistry may indicate CBM potential (Van Voast, 2003), based on the chemical fingerprint of the TDS in the water.

MOISTURE *VERSUS* ASH RELATIONSHIPS

Moisture content is generally considered to decrease as the amount of ash (or mineral matter) increases. For equilibrium moisture (EQ) or air-dried moisture (adm or inherited moisture), which are high for low-rank coals, the negative correlation is strong. The plot indicates that at the equivalent of 100% mineral matter, there is still some moisture in the sample. The amount can only be determined once the mineral-matter-to-ash ratio is know, as this defines the 100% mineral matter point on the $X = ash$ axis. For example, if the ratio is 1.15, then 100% mineral matter is equivalent to 87% ash. Results indicate that EQ moisture ranges from 1% to 4% at 100% mineral matter (Roberts, 1991). This is the moisture in the sample that is lost once it is dried to 110 °C and must represent capillary and/or adsorbed moisture, because the EQ measurement is conducted at 96% humidity in order to remove surface moisture. Roberts (1991) estimates adm of mud rocks to be in the range 0.4% to 3.2% (this is not structural water). This value should vary somewhat with rank, because of increased maturity of the mineral matter (clays), and with changes in composition. It provides information about the composition of the mineral matter and possibly about gas adsorption potential, if shale gas potential is being considered.

There are a lot of data sets of air-dried moisture (adm) *versus* ash for different rank coals (Figure 3). The adm of zero-ash coal is rank-dependent and varies from over 6% for low-rank coals to a minimum of less than 1% for medium-rank coals, increasing to about 2% for high-rank coals. The moisture content at 100% mineral matter (87% ash assuming a 1.15 mineral-matter-to-ash ratio) is an indication of the moisture remaining in the mineral matter after air-drying that is subsequently lost when the sample is dried at 110 °C. This probably represents adsorbed moisture. Plots of adm *versus* ash for low-rank coals (Rmax 0.67%) have negative slopes, indicating that the zero-ash coal adsorbs water more strongly than the included mineral matter does. Plots for higher-rank coals (Rmax 1.3% to 1.8%) indicate very little change in adm with increasing ash content. They also have lower adm contents for the full range of ash contents. It appears that these ranks of coal have the same amount of tightly adsorbed water as mineral matter and generally

lower adsorption than low-rank coals. The adm for zero-ash anthracite is higher than that for medium-rank coals. Surprisingly, the adm for 100% mineral matter is also high, and this may reflect changes in the types of clays that make up the ash present in high-rank coals.

Drying coal samples to 110 °C does not remove structural water from clays. This water is only apparent in the volatile matter content of mineral matter. In fact the slope of a line on an ash *versus* volatile matter (VM) plot gives information about the volatility of the ash, and a line on a CV *versus* ash plot gives information about the heat-stealing or heat-generating capacity of the ash, which is related to its composition.

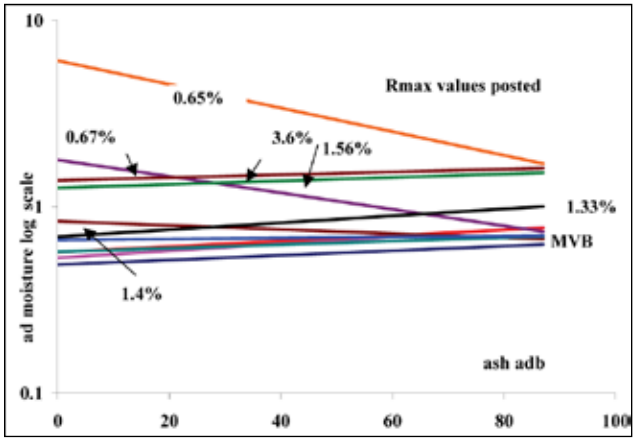

Figure 3. Plots of air-dried moisture *versus* ash for different rank coals.

MOISTURE AND PETROGRAPHY

Air-dried and EQ moisture contents vary based on maceral composition of samples. Generally, vitrinite contains the most moisture, and inert macerals the least (Figure 4). This is not always the case, and Roberts (1991) found a weak positive correlation of inertinite content with "inherent moisture", which, based on the way he sampled, is an estimate of bed moisture. The variation in EQ and adm contents probably mimics the ability of macerals to adsorb methane. For fresh, low-ash samples of the same rank, higher adm probably correlates with greater methane adsorption ability.

EQUILIBRIUM MOISTURE AND GAS ADSORPTION

Equilibrium moisture (EQ) is a laboratory-measured property of coal that is an approximation of immobile water in coal at in situ conditions; it is often referred to as bed moisture. In that EQ moisture is the moisture coal can hold in a humid atmosphere, it is effectively the sum of adsorbed moisture filling micropores and moisture filling large pores by capillary action. The test is performed on wetted 16-mesh (1 mm diameter) coal fragments held at 30 °C, 96% humidity, and a pressure of 30 mm mercury (atmospheric pressure is 760 mm mercury). There are a number of concerns with this procedure: EQ moisture may be influenced by grain size; the temperature of 30 °C does not necessarily reflect the in situ temperature of all samples; and the low pressure may cause complete degassing of methane and carbon dioxide and aid infusion of water into pores (this would increase EQ moisture above the equivalent in situ EQ moisture).

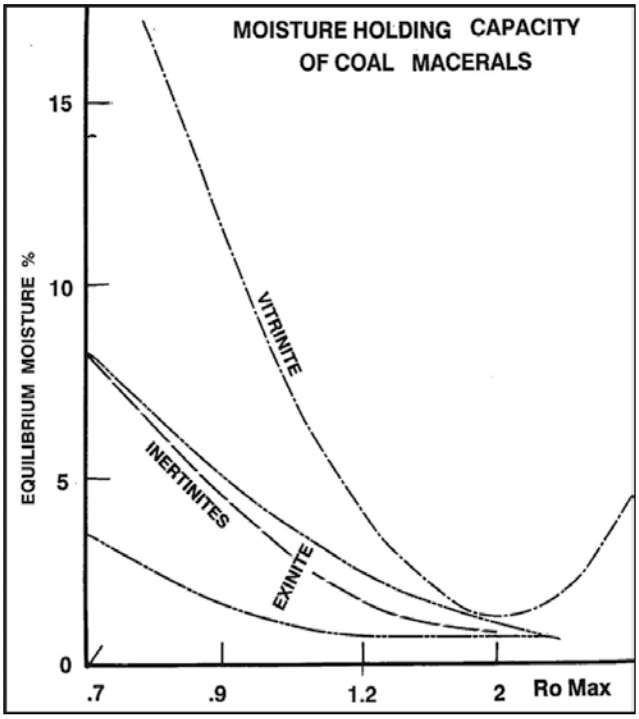

Figure 4. Variation in EQ moisture with rank and maceral content; plot from Shell internal publication.

The reason for equilibrating samples at EQ moisture (especially when the temperature is changed from 30 °C to in situ temperature) is to mimic during isotherm experiments the in situ moisture content of coal; this enables prediction of the true saturated gas capacity of coal at in situ conditions or at conditions that match in situ temperature (but not necessarily pressure). If isotherm experiments are run on coal with inappropriate moisture contents, it is difficult to determine whether desorbed coal samples are saturated or under-saturated. If EQ moisture is higher than in situ moisture, then under-saturated samples will appear to be saturated and some samples may appear to be over-saturated. If the EQ moisture is too low, compared to in situ conditions, then adsorption ability is increased and desorbed samples will appear to be under-saturated. It is important to have the correct estimate of the degree of gas saturation of samples because it has a major influence on production economics.

Many papers, for example Joubert *et al*. (1973) and Bustin and Clarkson (1998), indicate that gas capacity is very dependent on water content and can increase by 30% for low-rank coals if they are dried below EQ moisture. However, the difference in adsorption based on moisture content is much less for medium-rank coals. It is obviously very important to perform isotherm measurements at the correct moisture content. It is not clear that the EQ moisture value, even if modified for different temperatures, provides a sufficiently good estimate of the in situ moisture content to be used to model in situ gas capacity.

Bed moisture probably decreases with increasing depth of burial for iso-rank coals because of increasing temperature, but also possibly because of increasing pressure. Increasing effective stress will cause compaction of the coal based on its compressibility, which can be calculated using Poisson's Ratio and Young's Modulus. Based on average values, coal will compress (decrease volume) by about 0.3% for a 1000 m equivalent increase in effective stress. This would decrease the volume available for capillary moisture, but the effect is not large enough to cause large changes in EQ moisture. Equilibrium moisture decreases with increasing temperature (Figure 5). In that part of EQ moisture is adsorbed moisture, this is not unexpected because the Langmuir pressure is temperature-sensitive, increasing as temperature increases.

Low-rank coals with larger pores may experience evaporation from pores at humidities greater than 96%, and therefore EQ moisture may be considerably less than bed moisture (Luppens, 1988). This may result in isotherms over-estimating gas-saturated capacity if this evaporate moisture is occupying adsorption sites also available for methane. The problem extends to medium-volatile bituminous coals—the percent difference between bed moisture and EQ moisture is actually larger for medium-volatile coals, despite the fact that the actual difference is much lower than it is for low-rank coals (Figure 6).

If increasing temperature is the major factor decreasing EQ, then it is probably accompanied by a decrease in methane adsorption ability, rather than an increase that would be expected if the sample were dried below its EQ moisture without increasing temperature. If bed moisture varies with effective stress because of compression, and if this variation changes the saturated-gas capacity of coal, then saturation

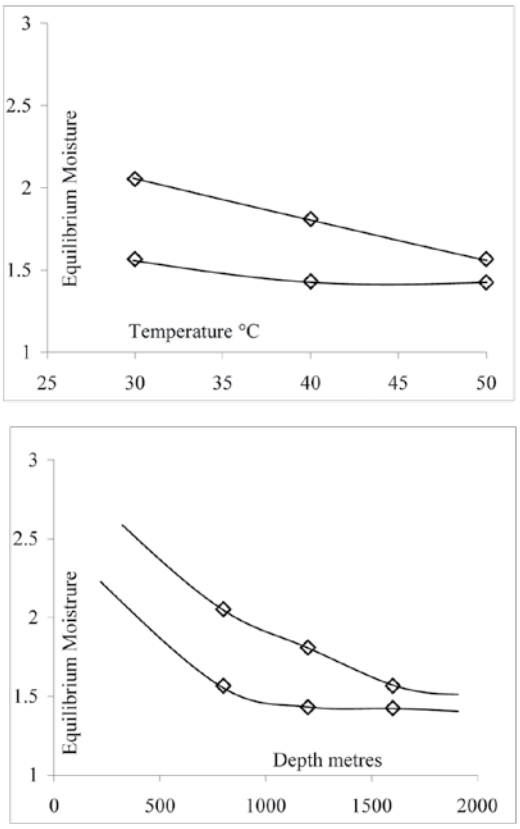

Figure 5. Changes in EQ moisture with increasing temperature (data from Bustin and Clarkson, 1998). Data calculated to indicate depth based on a geothermal gradient of 25 °C; surface temperature 10 °C.

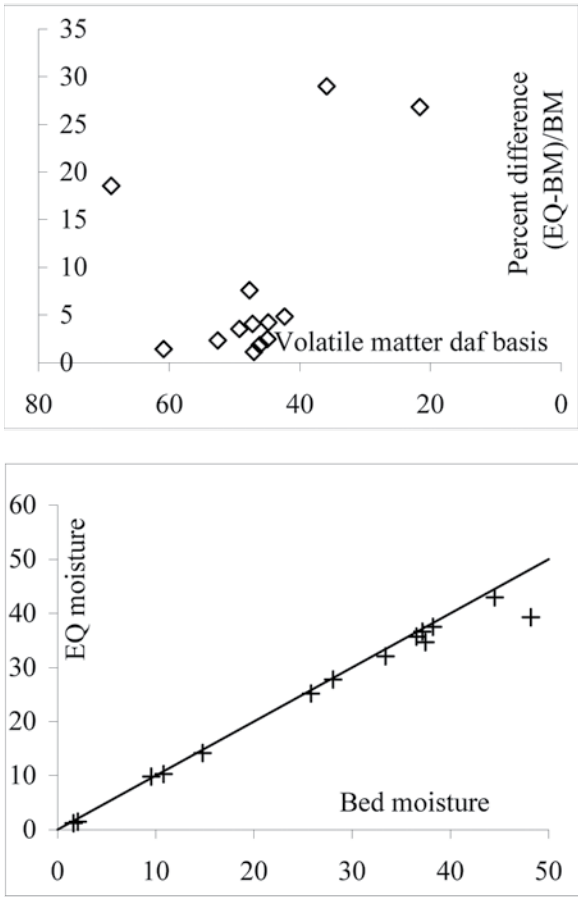

Figure 6. Relationship between bed moisture and equilibrium moisture; data from Luppens, (1988).

conditions will change during de-pressuring caused by production. As production proceeds, effective stress increases and the coal becomes more compressed. This may decrease saturated-gas capacity and initiate or stimulate desorption but slow diffusion.

WATER ISOTHERMS

Allardice and Evans (1978) provide an in-depth discussion of water adsorption in coal as well as an example of a water isotherm for a low-rank coal. The steep part of the curve of a water isotherm (Figure 7) at high humidities indicates loss of surface moisture. For this reason, EQ moisture is measured at 96 to 97% humidity because this ensures that surface moisture is evaporated and not included in the measurement. The amount of surface moisture on in situ coal is in part related to the amount of fracturing (amount of surface area available). However, this moisture will have minimal effect on gas adsorption (it may be significant in adsorption of gas on clays).

It is possible to measure a water isotherm by measuring the amount of water lost as the relative humidity decreases (Allardice and Evans, 1978). The shape of the resulting water sorption isotherm indicates at what relative humidity the various forms of water evaporate from coal. These include capillary water (steeper part of the curve, Figure 7), water in macropores (central, flatter part of the curve), multilayer adsorbed moisture, and monolayer adsorbed water (steep part of the curve close to the origin). Capillary and macropore moisture are removed at vapour pressures that range from 0.96 P/P_o to 0.5 P/P_o (Figure 7). From 0.5 P/P_o to about 0.1 P/P_o (i.e., the flat part of the curve), water from multilayer adsorption sites is lost, and monolayer adsorbed water is lost below 0.1 P/P_o.

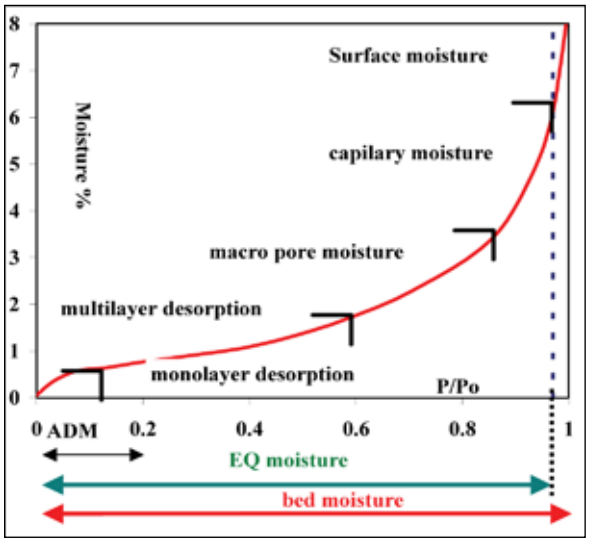

Figure 7. Water isotherm for a low-rank coal. Figure adapted from Allardice and Evans (1978).

The energy released during adsorption or required for desorption of various gases is important in situations where various gases are competing for adsorption sites. Allardice and Evans (1978) document the isoteric heat of adsorption of the various forms of water. The energy released or required to evaporate water in capillaries is 2.43 Mj/kg (580 cal/g or 10.4 Kcal/mole). The energy increases by 1 to 2.43 Mj/kg for water adsorbed as mono-layers (Allardice and Evans, 1978); i.e., in the range 3.43 to 4.86 Mj/Kg (14.7 to 20.8 Kcal/mole). When comparing gases, it is better to use units of Kcal/mole as this compares similar numbers of molecules. The heat of adsorption of water is similar to the heat of condensation (10.6 Kcal/mole); this compares to the heat of adsorption of methane, which is 4 to 6 Kcal/mole (Anderson *et al.,* 1964). The heat of adsorption of CO_2 (5.5 to 6.5 Kcal/mole; Ozdemir, 2004) is slightly higher than it is for methane and this in part explains its stronger adsorption.

Water isotherms are constructed by decreasing relative pressure (desorption isotherm) or by increasing relative pressure (adsorption isotherm). The two curves do not overlap; i.e., there is marked hysteresis, suggesting that the process of desorption from mono- and multilayer adsorption sites is not the same as adsorption. The desorption curve is always higher (Figure 8) than the adsorption curve, indicating that for a fixed relative pressure more water remains during desorption than is adsorbed during adsorption. The two curves do not always meet at the end points, indicating that sometimes shrinkage during desorption and drying causes permanent damage to the coal; the swelling resulting from adsorption does not overcome this damage. The amount of hysteresis for coals, which increases as rank decreases, indicates the degree of risk resulting from handling coals prior to conducting methane isotherm analysis. If a sample is over-dried prior to conducting an EQ measurement then the value will be too low, especially for low-rank coals.

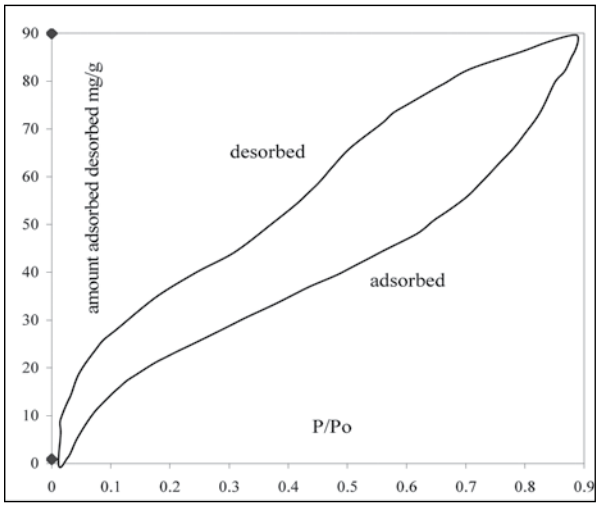

Figure 8. Hysteresis effect for desorption and adsorption; data from Mahajan and Walker (1971).

Water isotherms vary based on rank (Figure 9). The total amount of water adsorbed is high for low- and high-rank coals and low for medium-rank coals. However, sub-bituminous and bituminous coals adsorb more water at relatively low vapour pressures (multi- and monolayer adsorption) than do high-rank coals. Increasing temperature causes evaporation of capillary moisture because the saturated partial pressure of water vapour in air increases and water will evaporate to try to reach the new partial pressure. The adsorbed moisture content decreases, but the form of water sorption isotherms stay the same for samples (Mahajan and Walker, 1971).

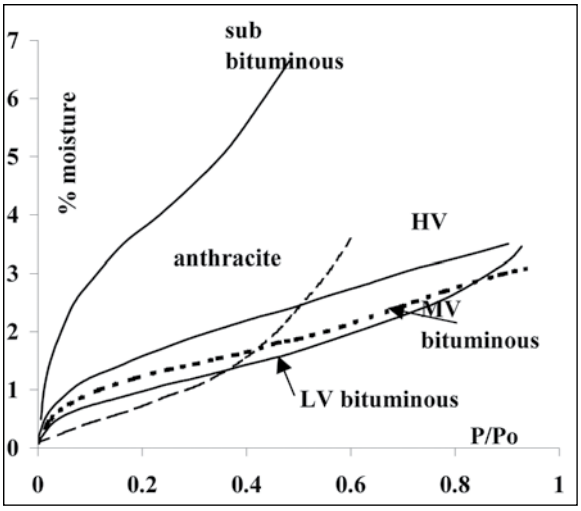

Figure 9. Water isotherms for different rank coals; data from Mahajan and Walker (1971).

Water molecules held by multi- or monolayer adsorption are attracted to hydrophilic sites on the coal surface that are oxygen-containing functional groups (Allardice and Evans, 1978). Mahajan and Walker (1971) found that the proportion of the surface area of coal that contains these sites varies from 60% in low-rank coals to 12% in low-volatile bituminous coals. These sites have a preference for adsorbing water rather than methane or other gases. Mahajan and Walker (1971) measured CO_2 surface areas of coals and used water isotherms to measure the amount of monolayer adsorbed water. They then calculated the surface area occupied by this water and were able to estimate the percentage of surface area occupied by monolayer adsorbed water in coals of different rank (Figure 10).

Their data indicate that the absolute surface area that appears to be hydrophilic is high for low-rank coals, decreases for medium-rank coals, and increases slightly for high-rank coals. Subtracting the area saturated by monolayer adsorbed water from the total surface area provides the area available for methane adsorption on water-saturated coals. The area increases with rank but goes through a minimum at intermediate ranks (Figure 10). The plot is

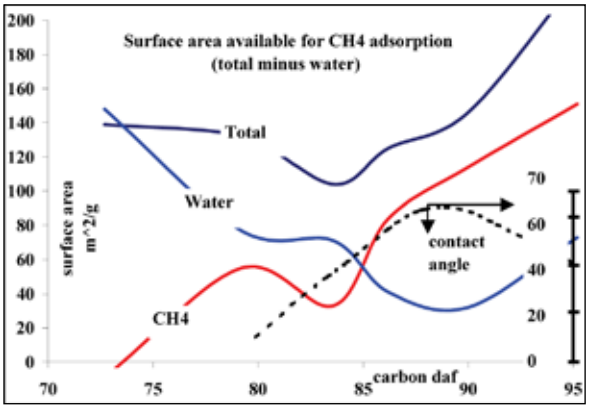

Figure 10. Percent surface area in coal occupied by monolayer adsorbed water; data from Mahajan and Walker (1971).

very important because it provides the basis for understanding the influence of water on methane adsorption on coals of different rank and different degrees of drying below EQ moisture.

There is no direct relationship between any component of a water isotherm and air-dried moisture content. However, adm may well be an estimate of the amount of multi- and monolayer adsorbed water. A curve of air-dried moisture *versus* rank is similar in form to the curve of adsorbed water *versus* rank (Figure 11).

The minimum adsorbed water saturation outlined (Figure 10) is mirrored by the behavior of the water contact angle to a coal surface (an inverse measure of wettability) that also goes though a maximum for medium-rank coals (i.e., beading). Large contact angles indicate a resistance to wetting for medium-rank coals, and this has implications for relative permeability and the ability to approach absolute permeability during production and dewatering. The results also agree with the data from Joubert *et al.* (1973) that indicate the high degree of sensitivity of gas adsorption to moisture content in low-rank coals.

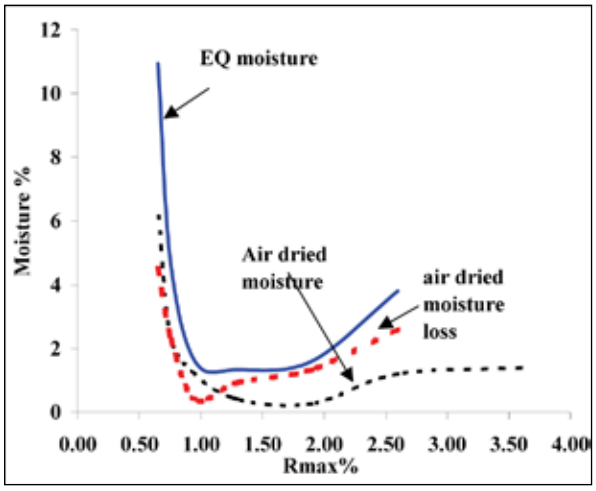

Figure 11. Air-dried and EQ moisture *versus* rank.

SURFACE AREA OF WATER IN COALS

The concept of surface area of coals should be treated with caution, as Marsh (1987) pointed out. It is a calculated rather than a physical property and may be misleading; for example, if pores are slit-shaped with widths approaching that of the diameter of one molecule, then the surface area will be two times the area covered by adsorbed molecules (Figure 12)**.** In comparison to larger pores, these molecules are bonded to two surfaces and this will increase heat of adsorption and decrease diffusivity.

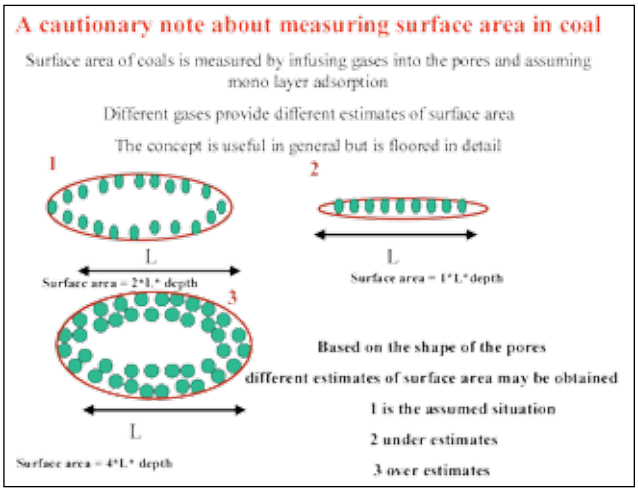

Figure 12. Schematic figure indicating relationship between surface area and adsorption.

It is possible to, very roughly, estimate the minimum surface area occupied by adsorbed water. For example, if 1% water is adsorbed, then this is equivalent to 0.01 cc/gm. Using Avogadro's number ($6*10^{23}$), this is $3.3*10^{20}$ molecules of water. If the water molecules, which have a diameter of about 4 angstroms, are arranged one layer deep in a square packing pattern, then the length of one side is

$(3.3*10^{20})^{1/2}*(4*10^{-8})$ cm = 7.3 m

so that the surface area covered is 53 square metres. Mahajan and Walker (1971) used a surface area for molecular water of 10.6 angstroms squared, which would result in a smaller surface area. These surface areas are less than but in the same order of magnitude as surface areas calculated using CO_2 adsorption.

A number of authors have measured surface area of coals (one of the earliest studies was by Walker and Kini, 1965). Surface area of coals ranges from 200m^2/g for low-rank coals to 100m^2/g for medium-rank coals to 250m^2/g for high-rank coals. It is easy to see that for low-rank coals with 60% hydrophilic surface area and high equilibrium moisture contents, there is the potential for none to nearly all of the surface area to be occupied by adsorbed water. This will result in a wide range in adsorbed gas concentrations based on how much the coal is dried below EQ moisture.

For high-rank coals with 12% of the surface area hydrophilic and lower EQ moisture contents, there is much less potential for the degree of water saturation to change adsorbed gas concentrations. The EQ moisture content of anthracites is higher than that of medium-rank coals (Figure 11). However, based on the shape of water isotherms, the increased moisture is capillary moisture (not monolayer adsorbed water) and therefore it will not affect the gas adsorption capacity. This means that drying anthracite below EQ moisture may not produce a marked increase in gas adsorption. The increase in capillary moisture in some situations may be related to macropores or vesicles produced by rapid de-volatilization related to a thermal event that affected the anthracite.

INFLUENCE OF WATER ON METHANE ADSORPTION

The relationship between water content below EQ moisture and Langmuir volume for methane is close to linear (Figure 13) (Joubert *et al.*, 1974). It appears that as water vacates sites, they are occupied by methane, and that water does not block access to additional sites. However, the replacement is not one-for-one. A 1% loss of water is equivalent to a loss of 0.01/18 moles of water; the weight of the same number of methane molecules is 16*0.01/18, and this mass of methane as a gas (at standard temperature and pressure) occupies 12.45 cc. Therefore for a one-to-one replacement of methane for evaporated water, the gradient on a cc/g *versus* moisture plot should be 12.45; in fact the gradient is much less and is rank-dependent (Figure 13). This means that for low-rank coals, approximately 1 methane molecule replaces 3 water molecule sites, but for medium-rank coals the ratio has decreased to 1 methane molecule replacing 11 water molecule sites.

The relationship of Langmuir pressure (Pl) to moisture content is ambiguous; for low-rank coals it appears to decrease as moisture decreases; for higher-rank coals there is no consistent change. A decrease in Pl implies easier adsorption of methane as moisture contents decrease.

Joubert *et al.* (1974) provide an equation

(Vd/Vw=Co*M+1)

where M is moisture content below EQ moisture and Co is a constant; Vw is adsorption on wet coal (the variable with M<EQ moisture); and Vd (a constant) is adsorption on dry coal. The ratio Vd/Vw is linearly related to moisture, not to the value Vw as implied by Killingley *et al.* (1995). Their data, re-plotted, provides a value of Co of 0.58, which is higher than the value 0.2 for the same pressure as predicted by Joubert *et al.* (1974). The term Co is pressure-dependent and decreases slightly as pressure increases.

The equation (Vd/Vw=Co*M+1) implies that the gradient of cc/g *versus* moisture varies and increases as

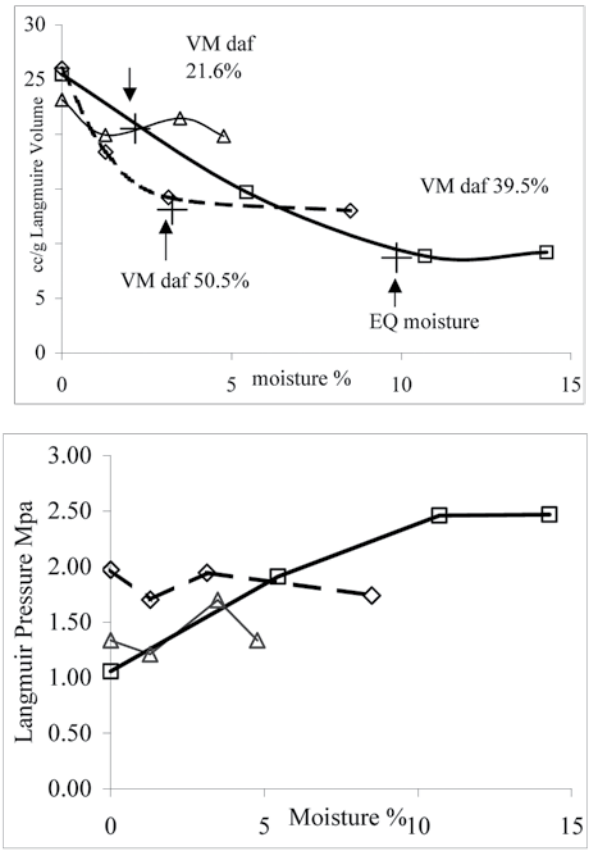

Figure 13. Langmuir volume and Langmuir pressure *versus* moisture content below EQ moisture; data from Joubert *et al.* (1974).

moisture decreases but does not increase to 12.45, even at very low water contents. This can be interpreted in terms of the location of water in coal as defined by water isotherms. At moisture levels a little below EQ, water is held by multilayer adsorption. Methane, with less polarity than water, tends not to occupy multilayer adsorption sites and therefore methane does not occupy many vacated water sites; i.e., the gradient is low. At low moisture levels where water is vacating monolayer adsorption sites, methane replacement is closer to one-to-one; i.e., the gradient is steeper. The gradient (Figure 13) is steeper for low-rank coals indicating, in agreement with water isotherms, that there is more replacement of monolayer adsorbed water by methane than in higher-rank coals. Because the interchange between water and methane molecules is not one-to-one, there will be a shrinkage as coal is dried below EQ moisture and water is replaced by methane, and there will be a swelling when methane-saturated dry coal is wetted and methane is released and water adsorbed. This may in part explain the hysteresis seen in water isotherms (Figure 8).

Based on the difference in heats of adsorption, in a situation where coal is dried below EQ moisture, if water and methane become available then coal will re-adsorb water in preference to methane until the water adsorption sites are filled. Coal with less than EQ moisture in a dry environment will contain more gas than if it contained EQ moisture. If the environment becomes water-saturated, then coal will re-attain EQ moisture and in the process will release methane, even if there is no decrease in pressure. This sequence of events may take place where a coal zone is subjected to regional or local temporary heating caused by intrusions. Heating decreases both EQ moisture and adsorbed gas content and, based on heats of adsorption, may reduce gas adsorption more than it does water adsorption. However, the expelled gas may, if a trap situation exists, produce a particular level in a coal-bearing section where the coal is gas-saturated and a lower level where the coal is water-saturated. On cooling, the gas-saturated area will have a moisture content below EQ moisture and an adsorbed gas content that recognizes this. Under normal conditions of increasing temperature, saturation of water and methane will both decrease, and methane will not have the opportunity to occupy vacated water adsorption sites.

OXYGEN CONTENT AND COAL PETROGRAPHY

Joubert *et al.* (1974) introduce an equation that relates Vw/Vd to oxygen content, to EQ moisture, and to three constants that are pressure-dependent. The equation does not predict how absolute gas-adsorption levels change with rank, it only predicts how EQ moisture and oxygen content (maceral- or rank-dependent) influence relative adsorption behavior (Vw/Vd) below EQ or critical moisture contents. The equations do not incorporate temperature, because the experiments were all done at the same temperature.

A number of authors provide plots of oxygen *versus* carbon content of coal and of EQ moisture *versus* carbon content (Berkowitz, 1979). These diagrams are rearranged to provide EQ moisture ranges *versus* carbon content with the EQ moisture prediction of Joubert *et al.* (1974) (Figure 14). The equations predict that EQ moisture increases slightly as pressure increases (no change in temperature) and that, as depth and rank increase, the difference between adsorption on dry and water-saturated coal decreases; i.e., Vw/Vd$\rightarrow$ 1 (Figure 15).

Water molecules bond to the coal on oxygen functional groups (OH and COOH) using oxygen in the coal and hydrogen bonds in the water molecules (Allardice and Evans, 1978). Analyses by Ladner and Stacey (1962) and Mastalerz and Bustin (1993) indicate that vitrinite has higher O/C ratios than do inert macerals of the same rank. This explains the positive correlation of EQ moisture with vitrinite content in coal. Data from both papers plotted into a Krevelen diagram (Figure 16) indicate the deceptive way macerals of the same rank plot into the diagram. Oxygen/carbon ratios are high for low-rank coals and decrease for high-rank coals, and for most ranks the O/C ratio is greater for vitrinite than for inert macerals (Figure 17). Despite an

increase in EQ moisture, the O/C ratio for anthracite does not increase, and this is the reason that for high-rank coals there is not a decrease in methane adsorption. The increase in EQ moisture is related to an increase in capillary moisture, not in monolayer adsorbed water, as indicated by the shape of anthracite water isotherms (Figure 9).

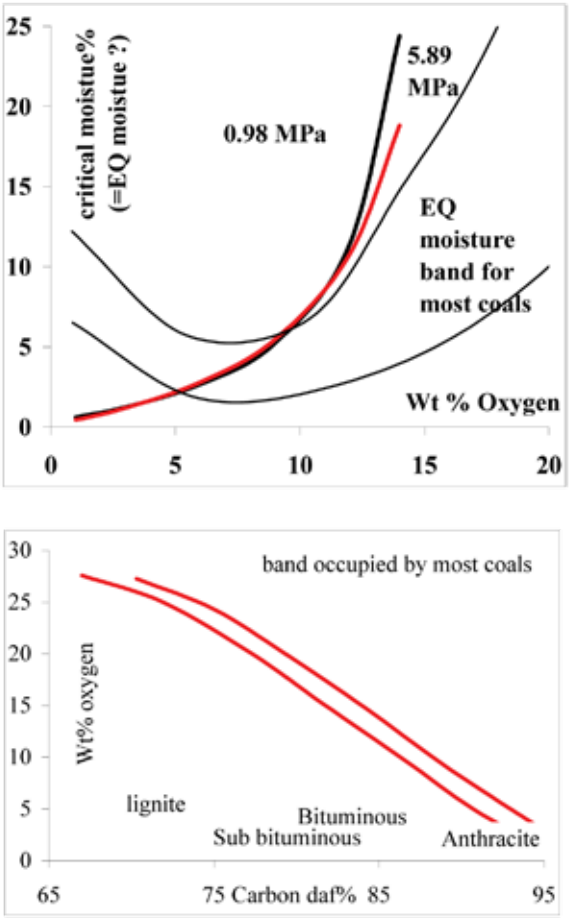

Figure 14. EQ moisture *versus* oxygen content (modified from Berkowitz, 1979) with the relationships developed by Joubert *et al.* (1974).

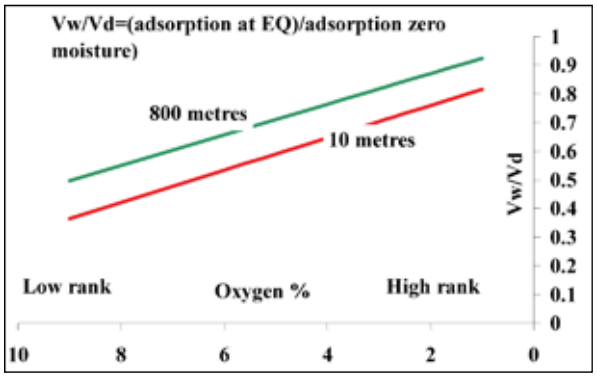

Figure 15. Variation of Vw/Vd with depth and rank as represented by oxygen content. Data from Joubert, *et al.* (1974).

The importance of available adsorption sites for water in influencing gas adsorption is indicated by a comparison of Australian Permian coals and Gates Cretaceous coals (Bustin and Clarkson, 1998). These coals have similar ranks and CO_2 surface areas, yet the Gates coals have 20% lower adsorption capacities. They have higher EQ moistures than Bulli coals for similar vitrinite contents (Figure 18). They also have a positive correlation of vitrinite content to EQ moisture content. The EQ moisture content of Bulli coals does not change much with changes in vitrinite content and has a weak negative correlation with EQ moisture.

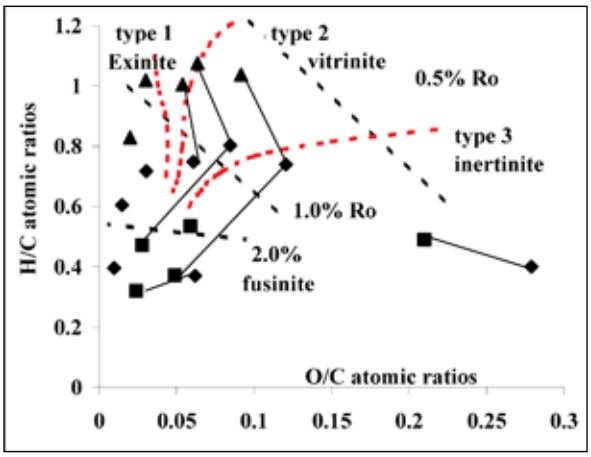

Figure 16. Maceral data from Mastalerz and Bustin (1993) and Ladner and Stacey (1962) plotted into a Van Krevelen diagram. Square=fusinite or semifusinite, diamonds=vitrinite and triangle=exinite. Lines join macerals from same coal sample.

The explanation for the lower gas contents in Gates coals may be related to lower O/C ratios for vitrinite from Bulli coals compared to vitrinite from Gates coals, indicating fewer adsorption sites stolen by monolayer adsorbed water. Part of the explanation may also lie in different shapes of water isotherms for inert macerals from the two areas. For South African coals, Roberts (1991) found a negative correlation of EQ moisture with vitrinite content, similar to the Bulli results (Figure 18). In this situation vitrinite probably has more sites for multi- or monolayer adsorption than do semi-fusinite and fusinite, but fusinite and semi-fusinite have more macropore and capillary moisture, so on balance they have greater EQ moisture contents than does vitrinite. This emphasizes the importance of the shape of water isotherms for different coals or macerals. In the Bulli coals with similar vitrinite and EQ moisture contents to Gates coals, less of the moisture in the Bulli coal is occupying multi- or monolayer adsorption sites, and therefore less methane is displaced by water. The difference in EQ moisture contents may also be related to a difference in overburden pressure. Roberts (1991) found that some Permian South African coals have lower inherent moisture contents than do northern hemisphere coals of similar rank and petrographic composition.

MULTIGAS COMPETITION FOR ADSORPTION SITES

Much of the discussion above considers the competition between methane and water for adsorption sites in the coal. There is very little information in the literature that sheds light on the situation where there are a number of gases (for example, CH_4, CO_2, and water) competing for adsorption sites. No papers were located that investigate adsorption of CO_2 on partially dried coals.

A study by Busch *et al.* (2006) measured selective adsorption of CO_2 from a CO_2/CH_4 gas mixture on wet and dry coal; their results indicate that compared to CH_4, CO_2 is preferentially adsorbed on dry coal. This may indicate that, in contrast to CH_4, CO_2 can compete with water for sites not available to CH_4. Coals in contact with a gas rich in CO_2 may in fact have lower EQ moistures than coals in contact with air.

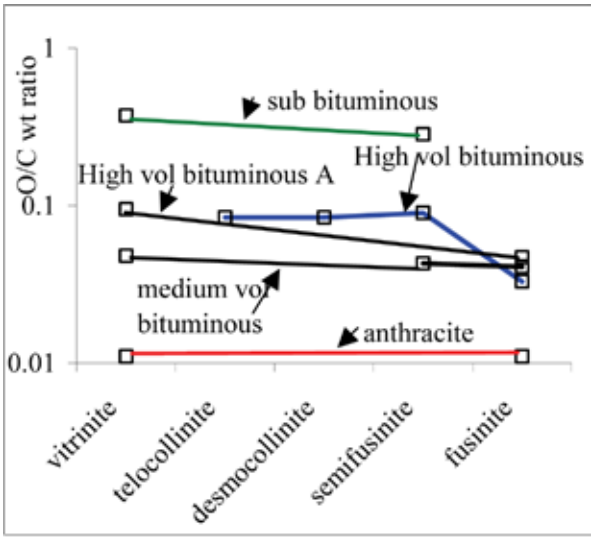

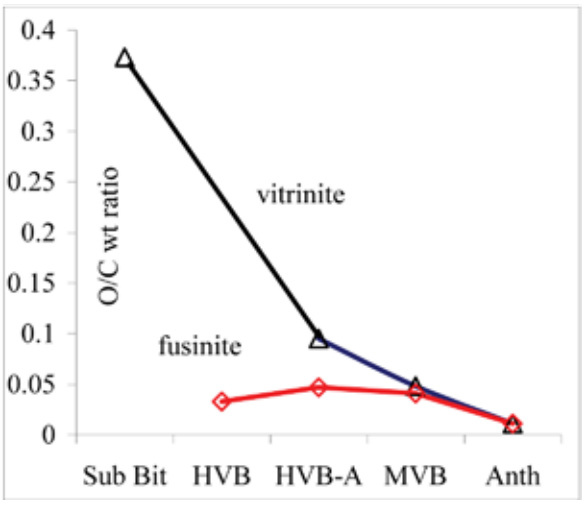

Figure 17. Variation of O/C wt ratio by rank and maceral type; data from Mastalerz and Bustin (1993).

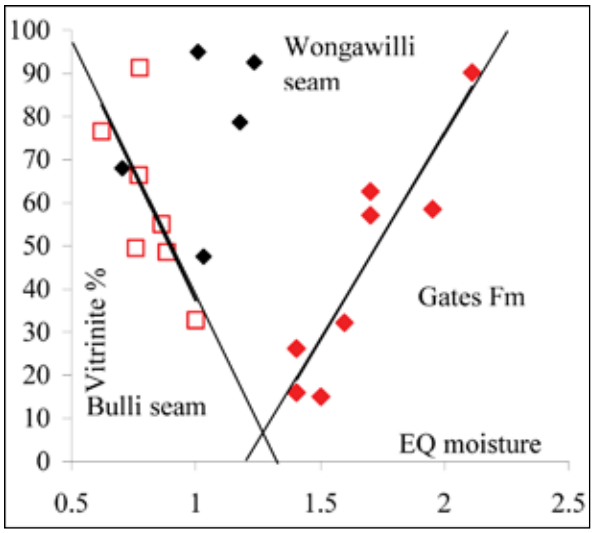

Figure 18. Variation of EQ moisture *versus* vitrinite content for Bulli (Australian) and Gates (British Columbia) coals; data from Bustin and Clarkson (1998).

CONCLUSIONS

The intricacies of moisture in coal are not well understood by many people apart from a few intimately involved in coal analysis. There is a profusion of terms with interchangeable definitions. But even before considering the interrelationship of coal moisture and gas adsorption, there is useful information buried in moisture analyses. With some careful sampling, water analyses can provide information on coal fracture porosity and in situ SG. In some cases it is possible to estimate the quality of interstitial water using a process of drying and leaching coal samples.

There is generally a poor understanding of the effect of water on gas adsorption. Some papers not directly dealing with CBM provide valuable insights. Water isotherms provide information on the various ways water is held in coal, and this indicates how the water will affect gas adsorption.

The weight of EQ water can be roughly expressed as the equivalent area of adsorbed water; comparing this to the surface area predicted by CO_2 adsorption indicates that water can only adsorb on a limited percentage of adsorption sites and that the percentage varies with rank. An understanding of both how water is adsorbed and the percentage area it occupies provides a better understanding of the way water adsorption influences gas adsorption.

Non-surface water (EQ moisture) occupies capillaries, multilayer adsorption sites, and monolayer adsorption sites all with different heats of adsorption, as indicated by the changing slope of water isotherms. The sites that are available for water or gas adsorption correlate with the oxygen content of the coal, which varies by rank and maceral content. These sites are oxygen functional groups such as COOH.

Methane molecules do not replace water molecules on a one-to-one basis. They prefer monolayer adsorption sites to multilayer adsorption sites, but even there the ratio of replacing methane molecules to water molecules is less than 1 to 3.

REFERENCES

Allardice, D.J. and Evans, D.G. (1978): Moisture in Coal; *in* Analytical Methods for Coal and Coal Products, Volume 1, Academic Press New York 1978.

Anderson, R.B., Bayer, J. and Hofer, L.J.E. (1964): Equilibrium sorption studies of methane on Pittsburgh Seam and Pocahontas No.3 Seam coal; pages 386-399.

Berkowitz, N. (1979): An Introduction to coal technology; Academic Press.

Busch, A., Gensterblum, Y., Kroos, B.M. and Siemons, N. (2006): Investigation of high pressure selective adsorption/desorption behavior of CO_2 and CH_4 on coals: an Experimental study; International Journal of Coal Geology, Volume 66, pages 53-68.

Bustin, R.M. and Clarkson, C.R. (1998): Geological controls on coalbed methane reservoir capacity and gas content; International Journal of Coal Geology, Volume 38, pages 3-26.

Diessel, C.F.K. (1992): Coal-bearing depositional systems; Springer-Verlag.

Joubert, J.I., Grein, C.T. and Bienstock, D. (1974): Effect of moisture on the methane capacity of American coals; Fuel, Volume 53, pages 186-191.

Killingley, J., Levy, J. and Day, S. (1995): Methane adsorption on coals of the Bowen Basin, Queensland Australia; Intergas 95 Conference, May 14-20, University of Alabama, pages 401-412.

Ladner, W.R. and Stacey, A.E. (1962): The hydrogen distribution in macerals; Fuel, pages 75-83.

Luppens, J.A. (1988): The Equilibrium moisture problem; Journal of coal Quality, Volume 7, pages 39-44.

Luppens, J.A. and Hoeft, A.P. (1991): Relationship between inherent and equilibrium moisture contents in coals by rank; Journal of Coal Quality, Volume 10, pages 133-141.

Mahajan O.P. and Walker Pl, Jr. (1971): Water adsorption on coals; Fuel, Volume 50, page 308.

Marsh, H. (1987): Adsorption methods of study micro porosity in coals and carbons - a critique; Carbon, Volume 25, Number 1, pages 49-58.

Mastalerz, M. and Bustin, R.M. (1993): Variation in elemental composition of macerals an example of application of electron microprobe to coal studies; International Journal of Coal Geology, Volume 22, pages 83-99.

Ozdemir, E (2004): Chemistry of the adsorption of carbon dioxide by Argonne premium coals and a model to simulate CO2 sequestration in coal seams; Ph.D. University of Pittsburgh.

Roberts, D.L. (1991): The inherent moisture content of South African Permian coals; International Journal of Coal Geology, Volume 17, pages 297-311.

Van Voast, W.A. (2003): Geochemical signature of formation waters associated with formation water; American Association of Petroleum Geologists, Bulletin 87, pages 667-676.

Walker, P.L. and Kini, K.A. (1965): Measurement of the Ultrafine surface area of coals; Fuel, Volume 44, pages 453-459.